A

ACID RAIN

Acid rain is one of the major environmental issues confronting industrialized countries, and is a wet form of acid deposition. Acid deposition is composed of sulfuric acid, nitric acid and ammonium, and occurs as wet deposition (rain, snow, sleet, hail), dry deposition (particles, gases and vapor), and cloud or fog deposition. Understanding the nature of acid rain and its impact requires a working knowledge of the concept of acidity and means by which atmospheric processes affect the potential for acid deposition.

Acidity

The acidity of a material is associated with the relative abundance of free hydrogen ions (H^+) when that substance is in a water solution. The pH scale is a logarithmic scale, where a value of 7 indicates neutrality; decreasing values on the scale indicate an increase in acidity and increasing values represent alkalinity. A pH scale with representative examples is shown in Figure A1.

Absolutely pure water (distilled) has a pH of 7, but if it is allowed to react with clean air its pH will decrease to near 5.6. This is a result of the absorption of carbon dioxide in the atmosphere to form weak carbonic acid. Most rainwater will have this pH; acid rain occurs when the pH is less than 5.6. For this reaction to occur, the atmosphere must be composed of chemicals that provide an acidic source. The atmosphere must also be able to deposit the material at the surface. This deposition is accomplished through the process of atmospheric cleansing.

Atmospheric cleansing

Acid deposition is a result of the "wet deposition" process, which involves the removal of chemicals through precipitation. Impurities in the atmosphere are incorporated in the entire precipitation process, beginning with cloud droplet formation, and are deposited as part of the resulting precipitation. Cleansing can also happen via "dry deposition", which implies that substances in the atmosphere are deposited through gravitational settling. Large particles settle under their own weight; very small particles may be transported far from their source to eventually polymerize until they are large enough to fall under their own weight. These particles generally are returned to earth through the wet deposition process.

Wet and dry depositional processes do not include all aspects of deposition. Other forms include fog droplet interception (especially prevalent in high-altitude forests), dew, frost, and rime icing.

The current distribution of wet-deposition acid in the United States is shown in Figure A2. The eastern part of the country, centered on the northeastern states, clearly has higher acidity than the remainder of the area. In part, this distribution reflects the conditions in the drier west where the chemistry of precipitation is altered by alkaline substances contributed to the atmosphere.

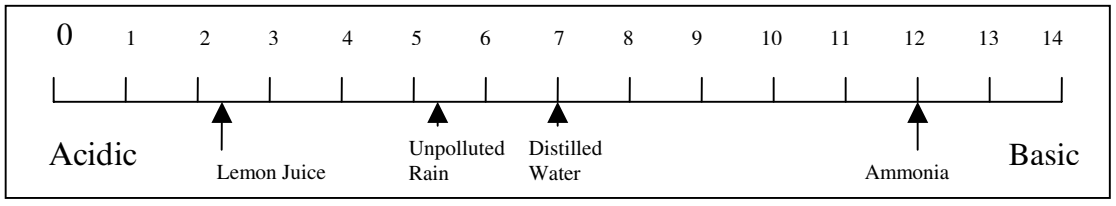

Figure A1 The pH scale denoting examples of some common substances.

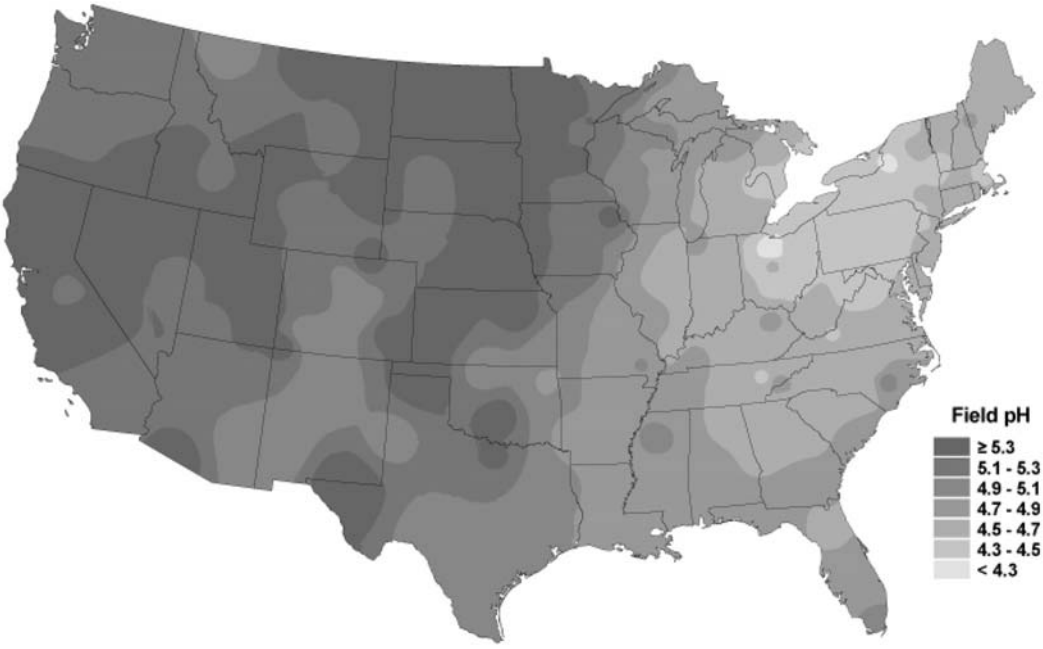

Figure A2 Distribution of acidity in the United States (National Atmospheric Deposition Program/NTN). Hydrogen ion concentration as pH from measurements made at the field laboratories, 2002.

Acid rain sources

Acid rain is primarily a result of the release of sulfur oxides (SO_2) and nitrogen oxides (NO_x) into the air by industrial and transportation sources. These oxides are transformed into sulfuric acid and nitric acid through oxidation and hydrolysis. Oxidants play a major role in several of these acid-forming processes. Rates of transformation are controlled by environmental conditions such as temperature, humidity, clouds, sunlight, and the presence of other select chemicals.

Table A1 summarizes all the major chemicals that influence the acidity of rain, with both natural and man-made sources identified. As noted above, man-made sources of SO_2 and NO_x contribute significantly to the development of acid rain. It is important to note that 95% of the elevated levels of NO_x are the result of human activities, including transportation sources (50%), electric utilities (26%), and industrial combustion (14%). The major sources of sulfur dioxide emissions were electric utilities (60%), industrial combustion (17%), and industrial processes (8%), measured in 1997.

Central to this conclusion is the question of a transport mechanism for air pollutants responsible for acid rain and the location of the source to areas that are currently experiencing acid deposition. Given that pollutants can return to earth instantaneously or remain airborne for a week or longer, then atmospheric circulation patterns and prevailing winds are significant. Examination of continental air currents demonstrates that seven states in the Midwest comprise the dominant source area for sulfur dioxide emissions that travel downwind to the Northeast (Driscoll et al., 2001). These states contributed 41% of the total national emissions of SO_2 in 1997. Furthermore, five of these states accounted for 20% of the total national emissions of NO_x.

Defining the location of actual sources contributing chemicals to acid rain is compounded by both political and economic circumstances. As mentioned above, there has been much controversy over the role of Midwestern industries and power plants using high-sulfur coal, thereby advancing acid rain in the northeastern United States. However, Phase I of the Clean Air Acts Amendment, Title IV (1995) has resulted in lower sulfate concentrations in precipitation in both the Eastern US and along the Ohio River Valley.

In 1980 the US Congress established the National Acid Precipitation Assessment Program to research the effects of acid deposition. Studies identified electric power generation as responsible for two-thirds of SO_2 emissions and one-third of NO_x emissions. Utilizing findings from these studies, Congress created the Acid Rain Program under Title IV (Acid Deposition Control) of the Clean Air Act Amendments (CAAA) of 1995. The Acid Rain Program set a goal of reducing NO_x by two million tons from 1980 levels, and requires a 50% decrease in SO_2 emissions from electric-generating facilities by 2010. By 2001, SO_2 levels have been reduced by 30% in the United States. However, nitrogen oxide emissions were not significantly affected. Research in the northeast United States has shown that acid rain is still a significant issue.

Effects of acid rain

In the 1960s and 1970s researchers in Scandinavia and the United States found that there was an increase in acidity and decrease in fish population in certain lakes and streams. Although acid rain can degrade water quality by lowering pH levels, the relationship is much more complex. Surrounding soils and vegetation contribute chemical ions that also modify acidity. Acid rain can also decrease the acid-neutralizing capacity and increase the aluminum concentrations of surface water.

Table A1 Chemicals that influence the acidity of rainfall

Ions in deposition	Source	Type	Significance
Sulfate (SO_4)	Swamps	Natural	
	Volcanoes	Natural	Minor
	Oceans	Natural	
	Power plants	Human activities	
	Industrial processes	Human activities	Major
	Smelters	Human activities	
Nitrate (NO_3)	Lightning	Natural	
	Soil biologic activity	Natural	Minor
	Industrial processes	Human activities	
	Transportation	Human activities	Major
Chloride (Cl)	Oceans	Natural	Minor
	Land surface	Natural	
	Industrial processes	Human activities	Minor
	Road salt	Human activities	
Ammonium (NH_4)	Biologic processes	Natural	
	Animals	Natural	Moderate
	Industrial processes	Human activities	
	Agriculture	Human activities	Minor
Calcium (Ca)	Land surface	Natural	Moderate
	Industrial processes	Human activities	Minor
	Agriculture	Human activities	
Sodium (Na)	Oceans	Natural	
	Land surface	Natural	Minor
	Road salt	Human activities	Minor
Magnesium (Mg)	Industrial processes	Human activities	
Potassium (K)	Land surface	Natural	Minor
	Agriculture	Human activities	

Acid rain is also thought to have a detrimental effect on forests. Trees may be injured by the direct action of acid on leaves or needles, or by changes in soil chemistry caused by the acid solution. By the early 1980s 20–25% of European forests were classified as moderately or severely damaged by acid rain. The decline of red spruce and sugar maple trees in the northeast United States has been occurring for the past four decades and has been linked to acid rain. Agricultural productivity may also be adversely impacted by acid rain.

Scientists have determined that, in soils impacted by acid rain, nutrients such as potassium, magnesium, and calcium are displaced by excess hydrogen ions, and that plant growth is retarded. Aluminum may also be released by excess hydrogen. Aluminum can be toxic to plants and, when released, can compromise the plant's ability to absorb water and nutrients. Acid rain also increases the accumulation of sulfur and nitrogen in the soil.

Buildings and monuments are also impacted by acid rain. Chemical reactions resulting from both wet and dry deposition have been recognized as a cause of extensive damage to historical buildings. Monuments such as the Acropolis in Athens and Jefferson Memorial in Washington DC show signs of damage from acid rain. Marble and limestone are susceptible due to the acids attacking the calcium carbonate in these materials. In addition to stone structures, acid rain also damages other building materials, particularly iron, steel, zinc, paint, and wood, and can cause the lifetimes of these structures to be shortened noticeably.

The chemicals comprising acid rain can also have an impact on human health, among other things. EPA has associated NO_x with photochemical smog, respiratory illness, ecosystem changes, visibility impairment, acidification of fresh-water bodies, eutrophication of estuarine and coastal waters, and increasing levels of toxins harmful to fish and other aquatic life. Likewise, high levels of SO_2 concentrations have been associated with increased respiratory difficulties.

The future

There are still many unanswered questions concerning acid rain. If acid rain proves to be as destructive as suggested by many writers, then it is certainly one of the major environmental concerns that must be dealt with in the near future.

Climatology will play an integral role in deriving many of the answers. Of importance is the transport of pollutants in the atmosphere, a problem that is associated with both meso- and macro-circulation patterns; a complete understanding of the chemistry involved in the wet deposition process; and comprehension of dry deposition processes. Additionally, politics, both national and international, will also play a role.

Melissa L. Kemling

Bibliography

Driscoll, C.T., Lawrence, G.B., and Bulger, A.J., et al., 2001. *Acid Rain Revisited: advances in scientific understanding since the passage of the 1970 and 1990 Clean Air Act Amendments*. Hubbard Brook Research Foundation. Science Links Publication, Vol. 1, no. 1.

Lynch, J.A., Bowersox, V.C., and Grimm, J.W., 1996. *Trends in Precipitation Chemistry in the United States, 1983–94: an analysis of the effects in 1995 of phase I of the Clean Air Act Amendments of 1990*, Title IV, US Geological Survey, Open File Report 96-0346.

National Atmospheric Deposition Program (NRSP-3)/National Trends Network, 2002. NADP Program Office, Illinois State Water Survey, 2204 Griffith Dr., Champaign, IL 61820.

Silver, C.S., and DeFries, R.S., 1990. *One Earth, One Future: our changing global environment*. Washington, DC: National Academy Press, pp. 131–144.

US EPA, 1999. *Progress Report on the EPA Acid Rain Program*. EPA 430-R-99-011.

US EPA, 2002. *Clearing the Air: the facts about capping and trading emissions*. EPA 430-F-02-009. Office of Air and Radiation. Clean Air Markets Division (6204N).

Cross-references

Aerosols
Air Pollution Climatology
Atmospheric Nuclei and Dust
Climatic Hazards
Precipitation

ADIABATIC PHENOMENA

An adiabatic process is one in which the system being considered does not exchange heat with its environment. The most common atmospheric adiabatic phenomena are those involving the change of air temperature due to change of pressure. If an air mass has its pressure decreased, it will expand and do mechanical work on the surrounding air. If no heat is taken from the surroundings, the energy required to do work is taken from the heat energy of the air mass, resulting in a temperature decrease. When pressure is increased, the work done on the air mass appears as heat, causing its temperature to rise.

The rates of adiabatic heating and cooling in the atmosphere are described as lapse rates and are expressed as the change of temperature with height. The adiabatic lapse rate for dry air is very nearly 1°C per 100 m. If condensation occurs in the air parcel, latent heat is released, thereby modifying the rate of temperature change. This retarded rate is called the pseudo-adiabatic lapse rate; it is not a constant for its value depends on the temperature at which the process takes place and the amount of water vapor in the air mass. However, for general descriptive purposes it is assumed as 0.5°C per 100 m.

The usefulness of the adiabatic approximation has led to the development of special thermodynamic diagrams that enable the results of adiabatic processes to be determined graphically. These charts are characterized by having two thermodynamic variables as coordinates and the values of various others represented by isopleths. Well-known examples of these "adiabatic diagrams" are the Tephigram, Stuve diagram, and Skew-T diagram.

Large-scale atmospheric motions are approximately adiabatic, and clouds and snow or rain associated with them are primarily adiabatic phenomena in that they result from cooling air associated with decreasing pressure of upward air motion. Simpler adiabatic phenomena occur on a smaller scale. A common example is that of rising "bubbles" of air on a warm day, leading to cumulus cloud forms. The growth of such cumulus clouds into thunderclouds is more complex but still a largely adiabatic phenomenon.

An example of the reverse effect, heating due to an increase in pressure, is the warm Foehn or Chinook wind that results from the descent of air from higher levels.

Rhodes W. Fairbridge

Bibliography

Cole, F.W., 1980. *Introduction to Meteorology*, 3rd edn. New York: Wiley.

McIlveen, R., 1992. *Fundamentals of Weather and Climate.* London: Chapman & Hall.

Cross-references

Boundary Layer Climatology
Cloud Climatology
Lapse Rate
Local Winds

AEROSOLS

Aerosols are technically defined as a relatively stable dispersion of solid or liquid particles in a gas. However, in common usage in the atmospheric sciences the term refers to the particles themselves. Aerosols are involved in a number of important atmospheric processes. These include atmospheric electricity; visibility; cloud and precipitation formation, including acidity of the precipitation; atmospheric biogeochemical cycles; and the radiative properties of the atmosphere. In all of these processes the size distribution of the aerosols is particularly important, as is their chemical composition.

Atmospheric aerosols are generated by a number of natural processes and as a result of human activities. Aerosols may be classified as "primary" or "secondary", depending on their production process. Primary aerosols are particles that are injected into the air directly, often by some mechanical process such as wind erosion of land surfaces (mineral aerosol), or wave breaking (sea salt aerosol). Secondary aerosols result from gas-to-particle conversion processes within the atmosphere that generate new particles. Table A2 presents the estimated source strengths for different types of primary and secondary aerosols. In terms of mass, sea salt and mineral aerosols (or dust) dominate the primary aerosols and also total global aerosol production. Industrial dust, various combustion processes and direct injection of particles from vegetation are also significant primary aerosol sources. The most significant secondary aerosols include sulfate, nitrate and organic particles, all resulting from the reaction of gaseous precursors in the atmosphere.

Table A2 Sources and radiative forcing of aerosols[a]

Aerosol type	Source strength (Tg/year)	Anthropogenic fraction (%)	Fine fraction (%)	Global mean direct radiative forcing[b] ($W m^{-2}$)
Primary				
Sea salt	3300	0	<1	—
Mineral dust	2200	~50	20	−0.60 to +0.40
Biomass burning	60	>90	~100	−0.20
Fossil fuel burning	35	100	~100	−0.10 or +0.20[c]
Biogenic	55	0	small	—
Industrial dust	100	100	~100	—
Total Primary	*~5800*	*~20*	*~10*	
Secondary				
Sulfate	200	~60	~100	−0.40
Nitrate	18	~80	~100	—
Organic compounds	17	~4	~100	—
Total Secondary	*~235*	*~60*	*~100*	
Global total	*~6000*	*~25*	*~15*	

[a] Numbers are derived from Houghton et al. (2001); 1 Tg = 1×10^{12} g.
[b] Values have uncertainties of a factor of 2 to 3. The global mean total *indirect* aerosol radiative forcing is estimated at 0 to $-2.0\,W m^{-2}$.
[c] Organic carbon is −0.10 and black carbon is +0.20.

Table A2 also provides information on the size of the particles from each of these sources. Typically aerosols are categorized according to size as "coarse (generally greater than ~1 μm radius) and "fine" (generally less than ~1 μm radius). Essentially all of the aerosol mass for secondary aerosols is in the fine category, whereas most of the mass of the primary aerosols is in the "coarse" category. The "fine" particles in turn have two components: the nuclei mode, from about 0.005 to 0.1 μm radius; and the accumulation mode, from about 0.1 to 1.0 μm radius. Particles in the nuclei mode are formed from the nucleation of atmospheric gases. The accumulation mode particles result from the coagulation of nuclei mode particles as well as from some condensation of gases onto existing particle surfaces.

The "fine" and "coarse" aerosols not only have very different sources, they are transformed differently, they have different chemical composition and optical properties, and they are removed from the atmosphere by different processes. For example, size has a significant impact on the atmospheric lifetimes of "coarse" and "fine" aerosols. The nuclei mode fraction of the "fine" aerosols has relatively short lifetimes (roughly hours or less) within that size range due to their rapid growth via coagulation with themselves or other particles into the larger accumulation mode aerosols. Accumulation mode aerosols can have atmospheric lifetimes of days to a week or more and can thus be transported great distances in the atmosphere. The primary removal mechanism for the accumulation mode aerosols is by precipitation. The "coarse" aerosols generally have atmospheric lifetimes of from hours to a day or two, with the lifetime decreasing as the particle size increases. Direct dry deposition is important for the coarse aerosol, and this becomes increasingly important as the particle size increases. Even "coarse" aerosols can be transported great distances, however. There have been numerous occasions when mineral dust from the Chinese deserts has been transported in the atmosphere to the east across the Pacific Ocean and North America to the Atlantic Ocean. Similarly, mineral dust from the Sahara Desert in Africa is often carried west across the tropical North Atlantic Ocean and Caribbean Sea to the eastern Pacific Ocean. Similar transoceanic transport of pollution-derived aerosols has also been observed on numerous occasions. Atmospheric sea salt aerosols from oceanic regions are also often observed in mid-continent locations.

The data in Table A2 indicate that about 20% of the primary aerosols and 60% of the secondary aerosols are derived from human-related, or anthropogenic, sources. This is particularly important for sulfate aerosols, which are often primarily responsible for visibility degradation and precipitation acidity in urban and near-urban regions. The predominant sources for the gaseous precursors for the secondary sulfate aerosols are industrial emissions and the combustion of fossil fuels. Similarly, fossil fuel combustion is the major source for the gaseous precursors of nitrate aerosols. Contrary to earlier estimates, anthropogenic sources do not appear to be a significant source of organic aerosols.

Table A3 provides information on typical number and mass concentrations of aerosols in different regions. In urban areas particle number concentrations of millions per cubic centimeter are common, whereas in the remote marine atmosphere concentrations can be less than 100 particles per cubic centimeter. In urban areas the mass concentrations can range up to several hundred micrograms per cubic meter, whereas under some

Table A3 Typical properties of aerosols in different regions*

Region	Total number (cm^{-3})	Mass	
		$<1\,\mu m$ ($\mu g\,m^{-3}$)	$1–10\,\mu m$ ($\mu g\,m^{-3}$)
Urban (pollution)	1×10^5–4×10^6	30–150	70–150
Rural	2×10^3–1×10^4	3–8	5–30
Remote continental	1×10^2–1×10^4	0.5–3	1.5–7
Remote marine	1×10^2–4×10^2	1–4	10–35

* Derived from Seinfeld and Pandis (1998).

conditions in remote continental regions the mass concentrations can be as low as one microgram per cubic meter or less. In areas near major dust storms concentrations of 1 gram per cubic meter or more have been observed.

Aerosols have both a direct and an indirect role in the radiative forcing of climate. The direct forcing results because they can absorb and scatter both infrared and solar radiation in the atmosphere. Indirect forcing occurs because aerosols can affect and change the processes that control cloud and precipitation formation, which in turn can affect the radiative properties of the atmosphere. There has been strong interest in aerosol forcing. This is because the forcing is negative for most aerosol types, rather than the positive forcing associated with the major radiatively active trace gases, such as carbon dioxide, methane, nitrous oxide, halocarbons and tropospheric ozone. Once again, size distribution and chemical composition are critical factors in the efficiency of aerosols in affecting these forcings. While significant progress has been made in recent years in determining the importance of aerosols of various types in radiative forcing, the uncertainties are still quite large. The most recent Intergovernmental Panel on Climate Change (IPCC, Houghton et al., 2001) report has developed new estimates of aerosol forcing, and some of their results are shown in Table A2. Note that the numbers given represent the mean direct radiative forcing for the aerosols described (except for mineral dust, where only a range was given), but the uncertainties in these estimates range from a factor of 2 to 3. Aerosol types where the evidence shows negative forcing include sulfate aerosols, organic carbon aerosols, and aerosols from biomass burning. The sign of the net forcing for mineral aerosols is still uncertain. Black carbon aerosols appear to cause a positive forcing. Note also that the indirect forcing is estimated to be from 0 to $-2.0\,W\,m^{-2}$. The values for aerosol forcing in Table A2 can be compared with the best estimate for carbon dioxide forcing of $+1.46\,W\,m^{-2}$.

Robert A. Duce

Bibliography

Arimoto, R., 2000. Eolian dust and climate: relationships to sources, tropospheric chemistry, transport and deposition. *Earth Science Review*, **54**: 29–42.

Charlson, R. and Heintzenberg, J., eds., 1995. *Aerosol Forcing of Climate.* London: John Wiley & Sons.

Houghton, J.T., Ding, Y., Griggs, D.J., et al., 2001. *Climate Change 2001: the scientific basis* (The IPCC Third Assessment Report). Cambridge: Cambridge University Press.

Murphy, D.M., Anderson, J.R. et al., 1998. Influence of sea-salt on aerosol radiative properties in the Southern Ocean marine boundary layer, *Nature*, **392**: 62–65.

National Research Council, 1993. *Protecting Visibility in National Parks and Wilderness Areas*. Washington: NRC Press.

Seinfeld, J.H., and Pandis, S.N. 1998. *Atmospheric Chemistry and Physics.* New York: John Wiley & Sons.

Cross-references

Air Pollution Climatology
Albedo and Reflectivity
Cloud Climatology

AFRICA: CLIMATE OF

Africa covers an area of more than 30 million km^2 and is second in size only to Asia. Of all continents it is the most symmetrically located with regard to the equator, and this is reflected in its climatic zonation. The coastline is remarkably smooth and the continent has been called a giant plateau, since there is a relative absence of very pronounced topography, although some high mountains exist, especially in the East African region (Kilimanjaro, 5894 m; Mount Kenya, 5199 m; and the Ruwenzoris, 5120 m). Lake Victoria, astride the equator, covers an area of 70 000 km^2 and is exceeded in size only by Lake Superior among the world's fresh water lakes.

We will note below how certain evidence can be used to reconstruct the early climate of Africa, but climatic observations really only began with the European explorers of the late eighteenth and nineteenth centuries. Then, in the last few decades of the nineteenth century, meteorological services were formed that began systematic observations at a network of stations. In most cases the meteorological service followed the meteorological practices of the colonial or governing power and this characteristic has tended to persist, even after independence was obtained. A number of the countries have suffered from internal disturbance since independence, a fact often leading to a hiatus in the records. Nevertheless, the standard of observation generally has remained high at the first-order or synoptic stations, but care must be taken when using data from many of the cooperative or second-order stations.

Weather controls

As in other regions of the globe, the pattern of solar radiation is the major control of climate. However, the nature of the air–surface interface and topography also play important roles. Although ocean currents help to determine the climate of some narrow bands of land, it is by appreciating the nature of the air masses reaching a region that one can begin to understand the observed climatic pattern.

Most of the time the continent is affected by tropical air masses, often maritime (moist) in nature, but in certain areas and during certain months they can be of continental (dry) origin. At the extreme latitudinal boundaries of the continent, in the littoral region of the Mediterranean Sea, and in the area around and east of Cape Town, the effects of polar air masses cannot be ignored at the time of low sun. The terms high sun (summer) and low sun (winter) are often used when discussing reasonal variation in the topics.

Temperature, at a particular station, is a rather conservative element with a relatively small annual range, and wind speeds are normally low compared to areas in higher latitudes. Precipitation, mostly rainfall, is the significant feature of the African climate. For rainfall to occur two criteria must be met – an adequate amount of water vapor within the atmosphere and the initiation of a cooling mechanism.

The cooling mechanism is usually obtained through the ascent of a large parcel of air. Such uplifting is generally due either to topography or to horizontal convergence of the air, which is simply the coming together of air parcels or masses. The ways in which such horizontal convergence can occur over Africa are detailed in Johnson and Morth (1960).

There are four important phenomena that determine rainfall amounts and patterns over the tropical continents: (1) the intertropical convergence zone (ITCZ), (2) the equatorial trough (ET), (3) easterly waves, and (4) tropical cyclones. The latter two play relatively minor roles over Africa.

The ITCZ, defined as a surface discontinuity separating the trade winds of the two hemispheres, can be identified readily on climatic charts, but it is not easily found on daily weather maps. The confluence of convergence of the usually relatively moist air masses leads to rainfall patterns that reflect the seasonal migration of the sun, with a time lag.

The equatorial trough (ET), the zonal pressure minimum, is detected up to an average height of 500 mbar (5500 m) with a mean position near the equator at that height. At lower levels there is evidence of a pronounced shift in location with season.

Weather situations

To set the stage for an appreciation of the various climatic patterns experienced, it is helpful to understand the weather situations dominant during certain months.

January

A broad low-pressure region is noted north of the equator with only light winds in evidence. In the upper air the divergent northeasterlies act to suppress rainfall. The surface position of the ET is north of the rain belt in Central Africa whereas, in the southern sector, upper-level troughs cause heavy rains over the Angolan plateau. Frontal activity brings rain to the North African coast.

April

There has been a movement of the ET northward from the January situation. In West Africa the ET becomes identified more easily on the daily surface charts. Thompson (1965) considers the rainfall now to be the result of many complex interplays among synoptic processes and dismisses the concept of a continuous zonal belt of rainfall moving northward.

July

The position of the surface ET is now at about its furthest north, near 20°N. There is a meridional (longitudinal) pressure gradient extending from the high-pressure belt of the southern hemisphere to the intense heat lows of Arabia and North Africa. In East Africa the topography leads to periods of convergence above the 700 mbar (3000 m) level, giving rise to the wettest month, while there is subsidence at 850 mbar (1500 m), where little rainfall is reported.

October

The rain belt is now moving southward, while a new trough begins to develop over Somalia and the Arabian Sea. Like April, this is a transitional month between the extremes of January and July.

Continental patterns of important climatic elements

The best method of identifying analogous climatic zones is to consider aspects of each of the important elements separately and then to combine them to obtain the overall picture. The elements selected here are temperature, precipitation, humidity and radiation.

Temperature

The mean annual temperature range (MATR), the difference between the mean temperatures of the hottest and coldest months, is of small magnitude over most of the continent, being less than 6°C over about half the continent. Its minimum value is 1.4°C at Barumbu in northernmost Zaire whereas the greatest is 23–24°C in parts of the Algerian Sahara. The dependence of the MATR on the continentality of the station, as well as its latitude, is shown in Table A4.

The mean annual diurnal temperature range is extremely dependent on continentality, as shown in Figure A3. Nearly all the coastal regions exhibit values of below 10°C, whereas in the central Sahara the range reaches 20°C, one of the highest values for any region of the world.

Actually, the best measure of the temperature variation is the highest mean monthly maximum temperature (H) and the lowest mean monthly minimum temperature (L). The patterns of these two variables are given in Figures A4 and A5. Figure A4 shows that it is only north of the equator where values exceeded 35°C and only in parts of the foggy coastal strip of southwestern Africa where values less than 20°C were reported. In Figure A5 the effects of elevation and latitude are more evident than those of continentality. Values below 5°C are unusual and only at high altitudes (over 1000–1500 m) in Algeria, Morocco

Table A4 Mean annual temperature range (MATR)

	Latitude E	Longitude N	MATR (°C)
Port Harcourt	7°01′	4°46′	2.5
Lokoja	6°44′	7°48′	3.6
Kano	8°32′	12°32′	5.8
Zinder	9°00′	13°48′	9.4
Agadez	7°59′	16°59′	13.3
Tamanrasset	5°31′	22°42′	16.7
Ourgla	5°20′	31°54′	23.3
Biskra	5°44′	34°51′	22.7
Constantine	6°37′	36°22′	18.3
Philippeville	6°54′	36°52′	14.2

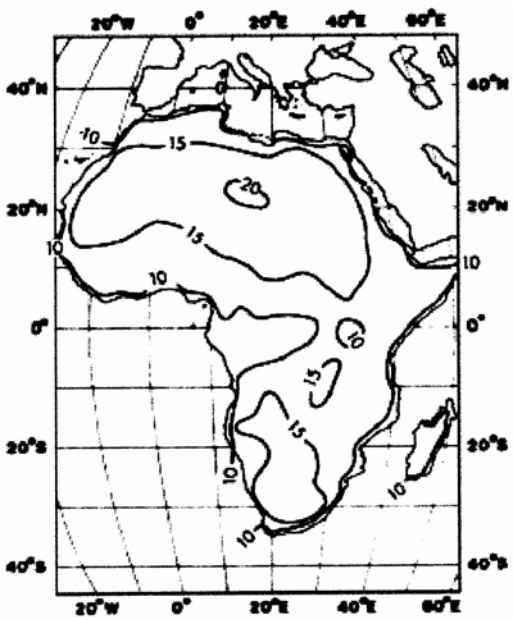

Figure A3 The mean diurnal temperature range (°C).

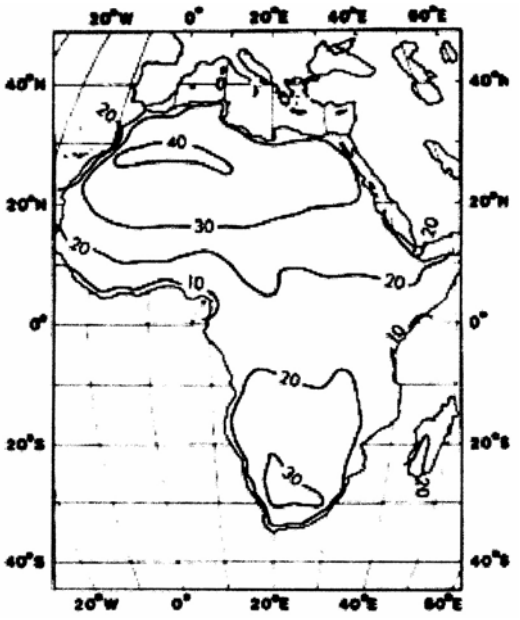

Figure A5 The lowest mean monthly temperature (°C).

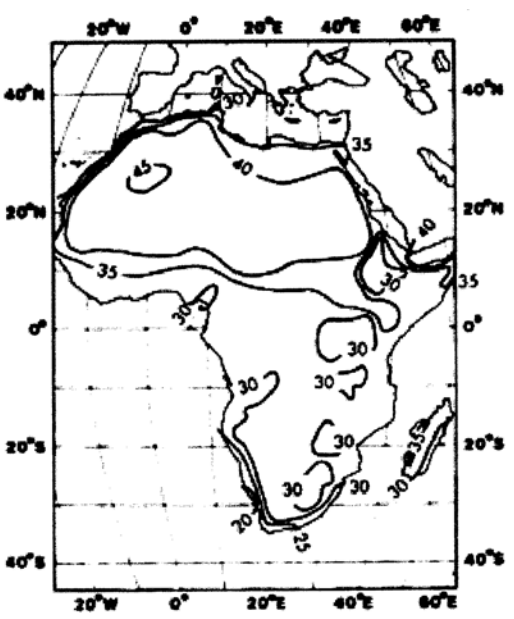

Figure A4 The highest mean monthly temperature (°C).

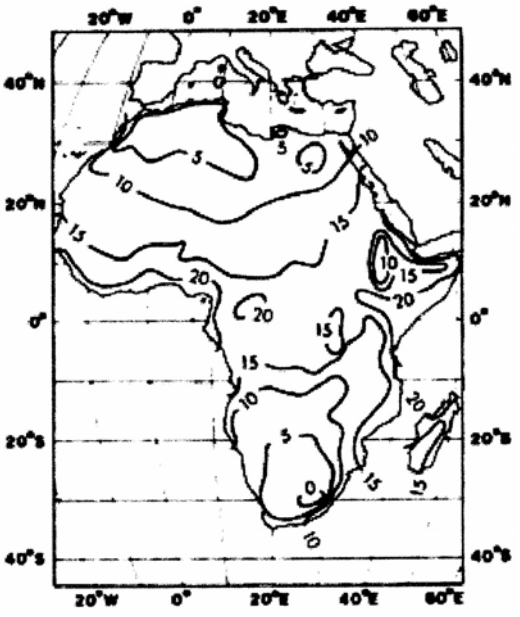

Figure A6 The difference between the highest mean monthly maximum temperature and the lowest mean monthly temperature.

and South Africa does L go below 0°C. The largest value is 26°C noted at Dallol, Ethiopia. The mean annual temperature variation (MATV), defined as H − L, which is depicted in Figure A6, is a combined measure of both annual and diurnal range and shows a relationship with both latitude and continentality. Again, the maximum values (above 30°C) occur in drier areas, the greatest being at Adrar in western Algeria, with 42°C. As would be expected, the equatorial littoral yields the lowest values, reaching only 8°C in Liberia and Sierra Leone.

Precipitation

Because both the ITCZ and the polar front lows exhibit large spatial movements, a basic seasonal pattern of precipitation can be identified on the continent. However, the complexities introduced by topography, upper-air conditions, ocean currents and inland lakes, among others, make the detailed pattern extremely complicated. An example of this is given by Griffiths (1972) for East Africa, whereby overlaying the spatial patterns of mean

monthly precipitation, 52 separate regions with 30 different rainfall seasons evolve.

Over most of the continent the seasonal distribution of precipitation exhibits the single significant maximum pattern, such as shown in Table A5. The season of maximum amount is generally around the time of high sun. In Figure A6 those regions in which three consecutive months receive at least 50% of the annual rainfall are shown. Only in the eastern sector of the Mediterranean coast is there a maximum at the time of low sun, but amounts involved are very small.

In the central belt of the continent most stations exhibit some degree of double maxima. However, the areas in which there is a really significant double swing during the year are quite small (Figure A7). For this illustration, significance is defined as occurring when the difference between the secondary maximum and secondary minimum exceeds 5% of the annual mean (see example of Lagos in Table A5), and this criterion limits the regions to just two. The sector in the Horn of Africa is mostly semiarid, except around Nairobi, Kenya. For stations with annual mean rainfall of over 1000 mm, Kitui, Kenya, is unique; its mean monthly totals (mm) being 41, 24, 118, 244, 56, 5, 3, 5, 0, 82, 304 and 143, giving a 22% swing.

The average annual rainfall totals show a wide range (roughly 0–10 000 mm), exhibiting a decrease away from the equatorial regions to reach a minimum around 20–30° latitude, then showing a slight increase (Figure A8). Since snow and hail amounts are generally small, all precipitation can be considered as rain. Nevertheless, snowfalls have been recorded in the Sahara, as far south as 15°N. Some falls have been quite heavy and reference to Dubief (1959, 1963) will give fuller details and some interesting photographs.

A distinctive feature of tropical rainfall is its large variability, interpreted as the difference within monthly, seasonal and annual totals. The station of Makindu, Kenya, is outstanding in this respect. Although its mean annual value is 610 mm, it has recorded as low as 67 mm and as high as 1964 mm of precipitation. On the other hand, April, its wettest month (111 mm average), has had amounts ranging from 822 mm, which exceeds the annual mean, to 0 mm. In Figure A9 a measure of annual rainfall fluctuations is depicted. Use is made of the relative variability statistic, V_r, defined as mean deviation/mean:

$$V_r = \Sigma(X_i - \overline{X})/\Sigma X_i$$

where X_i is individual yearly amounts and $\overline{X}$ is the yearly mean. Values of V_r show dependence on the mean, $\overline{X}$, so data for 500 stations were used to compute the expected value of V_r as a function of $\overline{X}$, called $V_r(\overline{X})$, and comparing V_r for the station with its corresponding $V_r(\overline{X})$. Differences are given as a percentage of $V_r(\overline{X})$.

The great variability in certain areas of the continent can be illustrated further by two examples. Quseir, Egypt, has received 33 mm in a day – 11 times its average annual total; Lobito, Angola, had 536 mm of rain in one day – over 1.5 times its annual average fall of 330 mm.

Hail is not a common phenomenon on the continent, especially on the coast of the tropical regions. However, Maputo, Mozambique, experienced a very heavy fall in October 1977 that did considerable damage. Few places have more than five incidences annually, but a region around Kericho, Kenya, reports as many as 80 hailstorms per year. (Fresby and Sansom, 1967)

Thunderstorm days are frequent with over 20% of the continent reporting in excess of 100 annually. This band of 100 occurrences stretches from about Sierra Leone across the central area as far as Lakes Victoria and Malawi. There are a few locations where convective instability leads to annual values of more than 200, with Kampala, Uganda, 242; Bukavu, Zaire Republic, 221; and Calabar, Nigeria, 216 holding the top places.

Humidity

Relative humidity, as an expression of the atmospheric moisture condition, can be rather misleading because its impact on human comfort is dependent on the air temperature occurring at the same time. For this reason it is preferable to use the dew point temperature as an indicator since this shows little diurnal variation and can be related more readily to human comfort. Values in excess of around 21°C can be considered very sultry, and this isopleth is indicated by a thick line in Figures A10 and A11. Some scientists consider dew points above 18°C uncomfortable. With this threshold about 30% of the continent falls into this category in January and 25% in July.

Along the humid and hot coastal regions of Africa the trade winds and/or sea breezes provide reasonably comfortable conditions, contrary to most people's concepts of the humid tropics. When there is little wind, as is often the case inland, in cities or in wooded areas, the situation is quite enervating. For a good discussion of and information on human comfort conditions consult Terjung (1967).

Table A5 Seasonal distribution of precipitation

	Jan.	Feb.	Mar.	Apr.	May	June	July	Aug.	Sept.	Oct.	Nov.	Dec.	Annual
Single maximum													
Algiers, Algeria	116	76	57	65	36	14	2	4	27	84	93	117	641
Kano, Nigeria	0	1	2	8	71	119	209	311	137	14	1	0	873
Mbeya, Tanzania	199	165	161	116	17	1	1	1	3	15	52	152	883
Pretoria, South Africa	117	101	78	46	25	9	8	6	25	63	110	120	708
Wau, Sudan	0	4	20	69	132	170	199	234	179	130	8	0	1145
Double maxima													
Lagos, Nigeria	40	57	100	115	215	336	150	59	214	222	77	41	1625

Note: Double maxima significance (222 − 59)/1625 = 10%. See text.

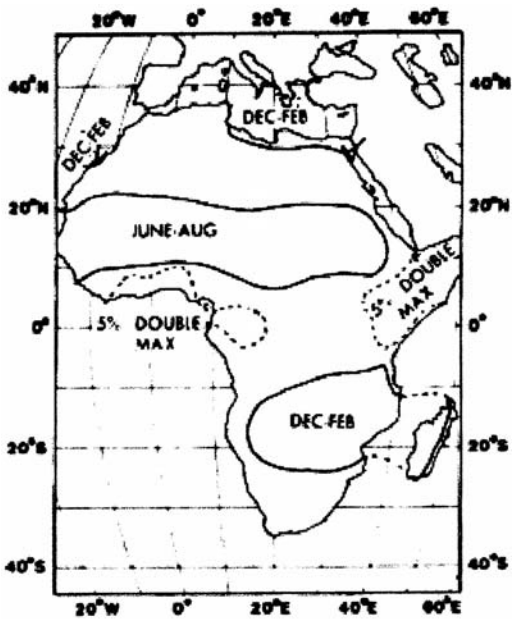

Figure A7 The 3-month period of maximum precipitation and those areas with a significant double maximum distribution.

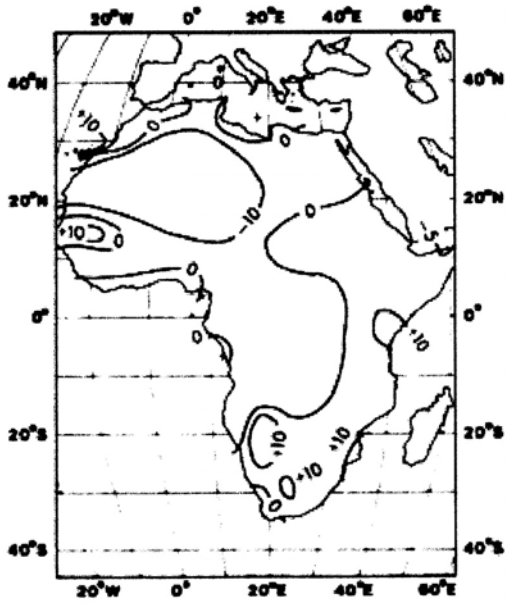

Figure A9 Variation of annual precipitation values in per cent (see text for details).

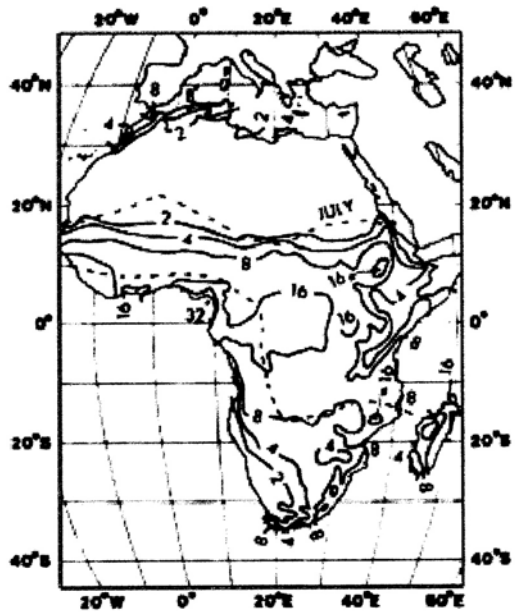

Figure A8 Mean annual precipitation (mm).

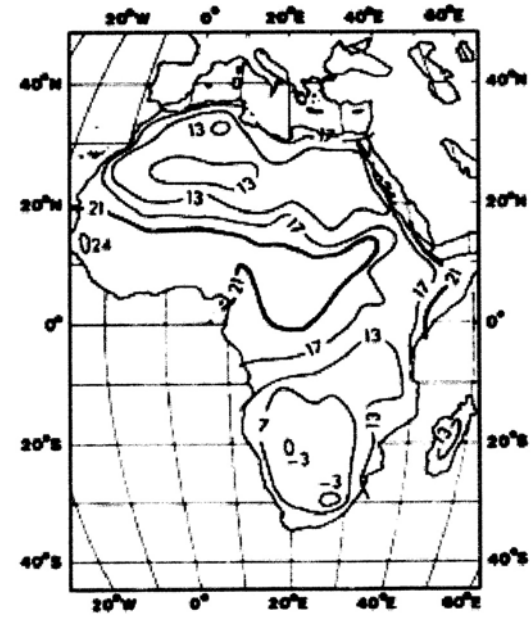

Figure A10 Mean January dewpoint temperature (°C).

Radiation

Africa extends from 38°N to 35°S, so that the annual fluctuation of solar radiation at the top of the atmosphere is small compared with that in higher latitudes. Mean annual global radiation (solar radiation measured on a horizontal plane at the surface) varies from nearly 600 ly day^{-1} in the Sahara–Nubia area to something less than 400 ly day^{-1} around Gabon, the Algerian coast and East London, South Africa.

Climatic zones

Using the findings of the earlier sections, it is possible to identify eight important climatic zones in Africa: (1) tropical wet; (2) tropical, short dry spell; (3) tropical, long dry spell; (4) tropical desert; (5) tropical highland; (6) subtropical desert; (7) subtropical, summer rain; and (8) subtropical, winter rain.

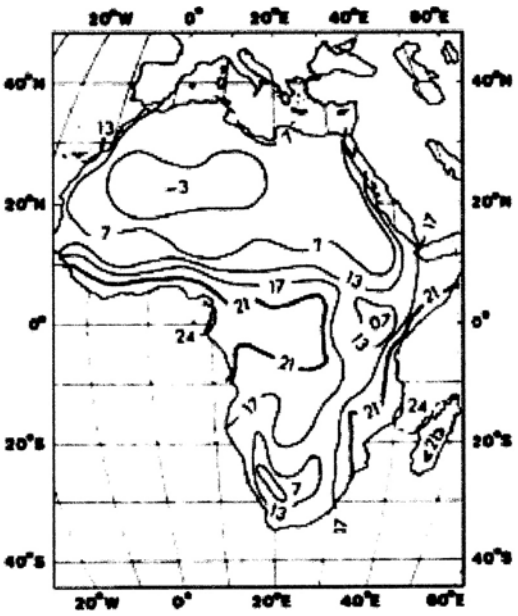

Figure A11 Mean July dewpoint temperature (°C).

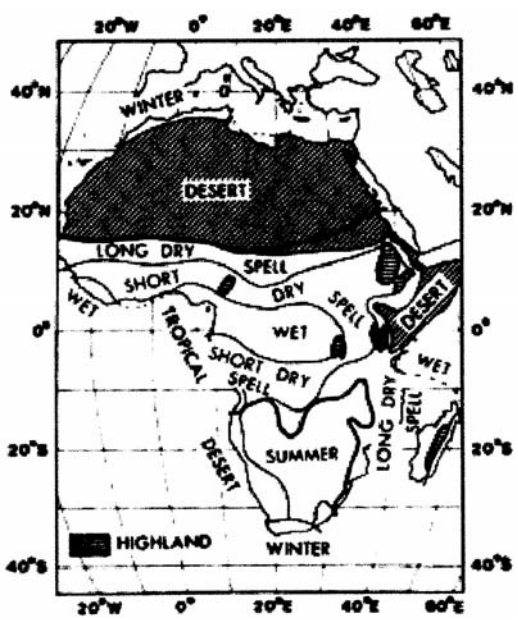

Figure A12 A simple climatic classification. Thick lines (N and S) indicate tropical boundaries (see text for details).

In addition, smaller zones of subtropical, uniform rain and subtropical highland can be found. The eight major zones are shown in Figure A12. For these purposes "tropical" designates that the mean temperature of each month is 18°C or greater; "desert" occurs when the mean annual rainfall (cm) is less than $16 + 0.9\overline{T}$, where $\overline{T}$ is the mean annual temperature (°C), and "highland" is where the altitude causes the region to be classified in a different thermal zone from what it would be if at sea level.

The tropical wet climate (Kisangani, Table A6) exhibits some rain in all months. Temperatures are uniformly high all year round and the conditions are very enervating, although sea breezes and/or trade winds can reduce the stress along the coast. The tropical rainforest is found in abundance in this zone.

Surrounding the first zone is the tropical, short dry spell climate (Kinshasa, Table A6). Here a period of 3–5 dry months is experienced. Precipitation and temperature are still high, but the annual temperature range tends to be larger than in the wet climate. Vegetation changes from forest near the boundary with the previous zone to deciduous woodland on the drier side although, because this is an important climate for agriculture, much clearing has taken place.

The tropical, long dry spell climate (Niamey, Table A6) is on the equatorial side of the desert regions and has low rainfall for at least 6 months. Rainfall amounts are less than in the two zones discussed above and temperatures show a much larger seasonal swing. The area is susceptible to drought and at such times the often marginal agriculture suffers tremendously. Vegetation is normally savanna and scrubland. The northern belt is referred to as the Sahel, a region in which famine has afflicted millions of inhabitants. The extreme variability of rainfall amount and frequency is a characteristic of the zone (Todorov, 1984).

Tropical desert climates (Obbia, Table A6) are not common, the biggest region being in the Horn of Africa where the prevailing winds, NE at low sun and SW at high sun, ensure that very few moist air masses reach the area.

The tropical highlands climate (Nairobi, Table A6) offers relief from the tropical heat, as well as a decrease in absolute humidity. Precipitation amounts can change quite rapidly in short distances as exposure to prevailing winds plays a dominant role. Generally, there is an increase in annual amount with height up to a belt of maximum rainfall, often around 2000 m or more, but changing according to the direction of slope. If the elevation is high enough (over about 5500 m) the region is permanently snowcapped. This transition from sea level to snowfield means that many vegetation belts are identifiable on the slopes.

The subtropical desert climate (Wadi Halfa, Table A6) is the most extensive of all zones on the continent. Summer temperatures in the Sahara are among the highest in the world, although they are not quite as great as in Namibia. Due to the low relative humidity and clear skies, diurnal temperature ranges can be extreme, with values in excess of 20°C often being reported. As may be expected, radiation and sunshine amounts are extremely large. Vegetation, while sparse, springs to life after any brief shower.

The subtropical, summer rain climate (Harare, Table A6) is found mainly in the southern plateau. Precipitation usually is so concentrated that about half the annual total falls in 3 months. Winters are generally very pleasant and comfortable.

The subtropical winter rain (or Mediterranean) climate (Cape Town, Table A6) is found at the extremities of the continent. These areas can experience extremely hot and dusty winds in summer from their adjacent deserts, but from fall to spring conditions are ideal. Vegetation is xerophytic, able to withstand the long dry spell.

Table A7 lists some climatic extremes for the continent. It is interesting to note how many of these are also world record extremes. Even in the precipitation class only two stations, Waialeale, Hawaii, with 1455 mm and Cherrapunji, India, with 10 820 mm, exceed Ureka's total. At another site near Cherrapunji a 5-year mean of 12 650 mm has been reported.

Table A6 Monthly temperature and precipitation data for representative stations

	Jan.	Feb.	Mar.	Apr.	May	June	July	Aug.	Sept.	Oct.	Nov.	Dec.	Average temperature or total precipitation for year
Kisangani, Congo, D.R.: 0°26′N, 25°14′E, 410 m													
Mean maximum temperature (°C)	31.1	31.1	31.1	31.1	30.6	30.0	28.9	28.3	29.4	30.0	29.4	30.0	30.0
Mean minimum temperature (°C)	20.6	20.6	20.6	21.1	20.6	20.6	19.4	20.0	20.0	20.0	20.0	20.0	20.6
Precipitation (mm)	53	84	178	157	137	114	132	165	183	218	198	84	1703
Kinshasa, Congo, D.R.: 4°20′S, 15°18′E, 324 m													
Mean maximum temperature (°C)	30.6	31.1	31.7	31.7	31.1	28.9	27.2	28.9	30.6	31.1	30.6	30.0	30.0
Mean minimum temperature (°C)	21.1	21.7	21.7	21.7	21.7	19.4	17.8	18.4	20.0	21.1	21.7	21.1	20.6
Precipitation (mm)	135	145	196	196	157	8	3	3	30	119	221	142	1355
Niamey, Niger: 13°31′N, 2°06′E, 215 m													
Mean maximum temperature (°C)	33.9	36.7	40.6	42.2	41.1	38.3	34.4	31.7	33.9	38.3	38.3	34.4	36.7
Mean minimum temperature (°C)	14.4	17.2	21.7	25.0	26.7	25.0	23.3	22.8	22.8	23.3	18.3	15.0	21.1
Precipitation (mm)	0	2	5	8	33	81	132	183	91	13	1	0	549
Obbia, Somalia: 5°20′N, 48°31′E, 15 m													
Mean maximum temperature (°C)	29.4	30.6	32.2	33.9	31.7	29.4	28.3	28.9	39.4	30.0	31.7	30.6	30.6
Mean minimum temperature (°C)	22.2	23.3	24.4	25.5	25.0	23.9	22.2	22.2	22.8	23.3	23.3	22.8	23.3
Precipitation (mm)	12	0	8	21	33	0	1	1	2	38	25	25	166
Nairobi, Kenya: 1°16′S, 36°48′E, 1820 m													
Mean maximum temperature (°C)	25.0	26.1	25.0	23.9	22.2	21.1	20.6	21.1	23.9	24.4	23.3	23.3	23.3
Mean minimum temperature (°C)	12.2	12.8	13.9	14.4	13.3	11.7	10.6	11.1	11.1	12.8	13.3	12.8	12.8
Precipitation (mm)	38	64	124	410	157	46	15	23	30	53	109	86	1155
Wadi Halfa, Sudan: 21°55′N, 31°20′E, 125 m													
Mean maximum temperature (°C)	23.9	26.1	31.1	36.7	40.0	41.1	41.1	40.6	38.3	36.7	30.6	25.6	34.4
Mean minimum temperature (°C)	7.8	8.9	12.2	16.7	21.1	23.3	23.3	23.9	22.2	19.4	14.4	9.4	16.7
Precipitation (mm)	T[a]	T	T	T	T	0	T	T	T	T	T	0	1
Harare, Zimbabwe: 17°50′S, 31°08′E, 1403 m													
Mean maximum temperature (°C)	25.6	25.6	25.6	25.6	23.3	21.1	21.1	23.3	26.1	28.3	27.2	26.1	25.0
Mean minimum temperature (°C)	15.6	15.6	14.4	12.8	9.4	6.7	6.7	8.3	11.7	14.4	15.6	15.6	12.2
Precipitation (mm)	196	178	117	28	13	2	1	2	5	28	97	163	828
Cape Town, South Africa: 33°54′S, 18°32′E, 17 m													
Mean maximum temperature (°C)	25.6	26.1	25.0	22.2	19.4	18.3	17.2	17.8	18.3	21.1	22.8	24.4	21.7
Mean minimum temperature (°C)	15.6	15.6	14.4	11.7	9.4	7.8	7.2	7.8	9.4	11.1	12.8	14.4	11.7
Precipitation (mm)	15	8	18	48	79	84	89	66	43	30	18	10	508

[a] Trace.

Table A7 Some climatic extremes for Africa

Temperature		
Absolute maximum	58°C[a]	Azizia, Libya (13 Sept. 1922)
Highest mean monthly maximum	47°C[a]	Bou-Bernous, Algeria (July)
Highest mean monthly	39°C[a]	Bou-Bernous, Algeria (July)
Highest mean annual	35°C[a]	Dallol, Ethiopia
Highest mean monthly minimum	32°C[a]	Dallol, Ethiopia
Highest mean of coldest month	31°C[a]	Dallol, Ethiopia
Highest absolute minimum	21°C[a]	Dallol, Ethiopia
Absolute minimum	−24°C (11°F)	Ifrane, Morocco (11 February 1935)
Precipitation		
Highest mean annual	10 450 mm	Ureka, Equat, Guinea
	10 300 mm	Debundscha, Cameroons
Lowest mean annual	0.5 mm	Wadi Halfa, Sudan
Miscellaneous		
Highest average dewpoint	29°C	Assab, Ethiopia (June afternoons)
Highest mean annual sunshine	4300 + h	Wadi Halfa, Sudan
Highest hourly radiation	113 langleys[a]	Malange, Angola
	112 langleys[a]	Windhoek, Namibia

[a] World record.

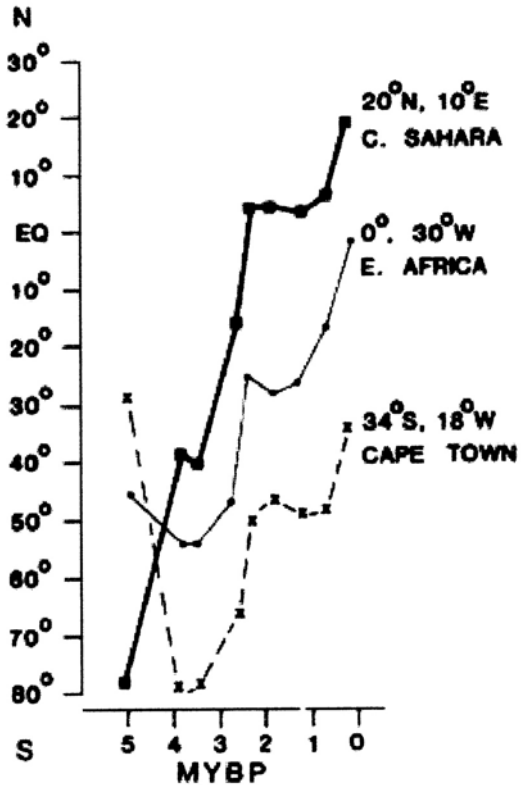

Figure A13 Latitudinal changes at three locations during the past 500 million years. (After Newell, 1974.)

Past climates

There has been relatively little study of past climates in Africa compared with studies of Europe and North America. However, it is known that the continent has occupied very different latitudes from that in which it is presently situated due to tectonic plate movements. In Figure A13 the latitudinal changes in the positions of three points on the continent are shown. From this alone it can be appreciated that in the period 450–200 million years before present (Ma BP) the Cape Town site, occupying a position within the Antarctic Circle, must have had a very cold climate, whereas now it is in relatively the same latitude as it was 500 Ma BP. The Central Saharan site has shown an almost steady progression from 80°S and it is likely that around 300 Ma BP it was also semiarid to arid, but from 200 to 50 Ma BP it was quite wet and humid. The East African location has not shown such extreme latitudinal variation but, nevertheless, must have experienced midlatitude and subtropical climates before reaching its present equatorial situation.

Some remark must be made concerning climate changes in the Saharan area. There have been many papers on this subject and the consensus of opinion is that from 20 000 to 12 000 years ago there was great aridity and the desert advanced southward. Following this period there were some very moist periods, while over the past 2000 years the rainfall has declined sufficiently to make the agriculture practiced in the time of Roman occupation no longer feasible (Carpenter, 1969). Murphey (1951) claimed that the cause is basically artificial and, even today, the growth of the desert must be attributed in great measure to anthropogenic influences. It is interesting to note that there are reports of ice on the Nile in the ninth and eleventh centuries (Oliver and Fairbridge, 1987).

For eastern Africa a more recent study (Hastenrath, 1984) suggests that there was a distinct retreat or disappearance of glaciers around 11 000–15 000 years ago, the deglaciation beginning at lower altitudes (*ca*. 3000 m). The most detailed studies of the historical climatology of Africa have been published by Nicholson (1976, 1978) and Nicholson and Flohn (1980). Nicholson finds, in the times of anomalous climate and climatic discontinuities, reasonable correlation between the sub-Saharan area and that of southern Africa. She identifies anomalous weather patterns in the 1680s and 1830s and a major rainfall change around 1800. Apparently the nineteenth century had greater snowfall than the twentieth century.

In the period 1870–1895, both the Sahara and eastern Africa had above-average rainfall, after which drier conditions set in and by the mid-1910s severe droughts were common in much of the tropics and subtropics. In the 1920s and 1930s there were indications of wetter conditions – Nile discharge up 35%, Lake Chad depth up 50%, and Sierra Leone reporting a third more rainfall than in the late nineteenth century.

Studies of African climate during the last 100 years or so are made problematic because of the vast areas for which the periods of record are very short. It is true that some temperature and precipitation measurements exist from the first half of the nineteenth century, such as in Tripoli and western Africa, but in general few reliable records exist before about 1890. Exceptions to this would include the island of Mauritius which has an almost unbroken record since around 1851.

A special project of the Global Climate Laboratory, part of the National Climatic Data Center, located in Asheville, North Carolina, is concerned with locating, extracting and digitizing data of monthly mean maximum and minimum temperatures and precipitation amount. In a few countries, including Egypt,

Nigeria and South Africa, there are enough stations to allow a regional investigation.

John F. Griffiths

Bibliography

Carpenter, R., 1969. Climate and history, *Horizon*, **11**(2): 48.

Desanker, P.V., and Justice, C.O., 2001. Africa and global climate change: critical issues and suggestions for further research and integrated assessment modeling. *Climate Research*, **17** (this issue is devoted to this topic).

Dubief, J., 1959. *Le Climat du Sahara*, Vol. 1. Algiers: University of Algeria.

Dubief, J., 1963. *Le Climat du Sahara*, Vol. 2. Algiers: University of Algeria.

Griffiths, J.F. (ed.), 1972. Climates of Africa, in *World Survey of Climatology*, Vol. 10. Amsterdam: Elsevier.

Hastenrath, S., 1984. *The Glaciers of Equatorial East Africa.* Dordrecht: Reidel.

Johnson, D.H., and Morth, H.T., 1960. Forecasting research in East Africa. In Bargman, D.J., ed., *Tropical Meteorology in Africa.* Nairobi: Munitalp Foundation, pp. 56–137.

Leroux, M., 2002. *The Meteorology and Climate of Tropical Africa*. Berlin: Springer Praxis Books.

Murphey, R., 1951. The decline of North Africa since the Roman occupation, *Association of American Geographers Annals*, **41**(2): 116–132.

Newell, R.E., 1974. The Earth's climate history, *Technol. Rev.,* pp. 30–45.

Nicholson, S.E., 1976. A climatic chronology for Africa: synthesis of geological, historical, and meteorological information and data. Unpublished PhD dissertation. Madison: University of Wisconsin.

Nicholson, S.E., 1978. Climatic variations in the Sahel and other African regions during the past five centuries, Journal of Arid Environments, **1**: 3–24.

Nicholson, S.E., and Flohn, H., 1980. African environmental and climatic changes and the general atmospheric circulation in Late Pleistocene and Holocene, *Climate Change*, **2**: 313–348.

Oliver, J.E., and Fairbridge, R.W., 1987. *The Encyclopedia of Climatology*. New York: Van Nostrand Reinhold, pp. 305–323.

Preston-Whyte, R.A., and Daughtrey Tyson, P., 2003. *The Weather and Climate of South Africa*. Oxford: Oxford University Press.

Terjung, W.H., 1967. The geographical application of some physioclimatic indices to Africa, *International Journal of Biometeorology*, **11**(1): 5–19.

Thompson, B.W., 1965. *The Climate of Africa*. London: Oxford University Press.

Todorov, A.V., 1984. The changing rainfall regions and the "normals" used for its assessment, *Journal of Climate and Applied Meteorology*, **24**: 97–107.

Cross-references

Airmass Climatology
Atmospheric Circulation, Global
Intertropical Convergence Zone
Mediterranean Climates
Rainforest Climates
Savanna Climate

AGROCLIMATOLOGY

Agroclimatology, often also referred to as agricultural climatology, is a field in the interdisciplinary science of agrometeorology, in which principles of climatology are applied to agricultural systems. Its origins relate to the foremost role that climate plays in plant and animal production. Formal references to the terms "agrometeorology" and "agroclimatology" date to the beginning of the twentieth century, but use of empirical knowledge can be traced back at least 2000 years (Monteith, 2000). Agroclimatology is sometimes used interchangeably with agrometeorology, but the former refers specifically to the interaction between long-term meteorological variables (i.e. climate) and agriculture. As such, they share common fundamental principles, methods and tools, but specific concepts are applied as described here.

Fundamental principles

Understanding the interactions between atmospheric variables and biological systems in agriculture, and applying this knowledge to increase food production and improve food quality, are the main goals of agrometeorology. Biological systems in agriculture are comprised of crops and forests, including the soil in which these grow; animals; and associated weeds, pests and diseases. Atmospheric variables that may affect these systems range from physical variables, such as solar radiation, precipitation, wind speed and direction, temperature, and humidity, to chemical variables, such as trace gas concentrations (e.g. CO_2, O_3). Agrometeorology is concerned with the characterization of these variables not only in the natural environment, but also in modified environments (e.g. irrigated areas, greenhouses, and animal shelters).

The fundamental principles used in the study of interaction between the atmosphere and agricultural systems are: (1) conservation of mass and energy, (2) radiation exchange, and (3) molecular and turbulent diffusion. The response of biological systems to these interactions draws on principles of soil physics, hydrology, plant and animal physiology, plant and animal pathology, entomology and ecology. Topics of research include water and radiation use efficiency by crops, animal comfort levels as affected by the physical environment, air pollution damage to crops, disease and pest development as a function of environmental conditions, and greenhouse gas emission by agricultural activities.

Methods and tools

Spatial scales in agroclimatology cover a wide range, from <0.1 m (e.g. response of fungi to leaf wetness) to regional and global scales (e.g. drought monitoring). Temporal scales may span past, present or future climate. Choice of instrumentation and measurement methods for weather and biological variables occurs according to the spatial and temporal scales of interest. Most often, agroclimatologists rely on long-term climate data provided by national meteorological services. In some countries weather stations originally were established in association with agricultural research institutes, attesting to the importance of weather and climate to agricultural production. Expertise in instrumentation, typically sensors for air temperature and humidity, solar radiation, precipitation, and wind measurement, is required from agroclimatologists in some applications, particularly those involving smaller spatial scales than provided by weather stations (i.e. microclimatological scales).

In all cases data describing the condition of the biological system are also needed. These include observations of developmental stages in crops, weeds, or insects; crop, milk or meat yield; grain or forage quality; and other physical and

physiological measurements. Increasingly, remote sensing measurement techniques are being used to obtain regional and global scale estimates of variables, such as vegetation indices, or surface temperature.

Data handling, management, and processing procedures, spatial and temporal interpolation, statistical analyses, mathematical models that simulate the response of biological systems, and geographical information systems (GIS), decision support systems (DSS) are examples of tools used by agroclimatologists.

Concepts

A few concepts widely used in agroclimatology are presented here. The reader is referred to Griffith (1994) for additional background and examples of applications.

Degree-days and length of growing season

The concept of thermal time, or degree-days, was one of the earliest concepts developed, with wide application in agroclimatology. Climate records are matched to cardinal temperatures of crops, and daily mean temperatures above a minimum threshold, but below a maximum threshold, are accumulated over phenological phases. Stages in development for specific species or varieties occur once a certain degree-day value has been reached. Degree-day requirements for crops to reach maturity are then used to select suitable climatic regions for each crop or variety. Conversely, climatic records are used to calculate degree-days during the growing season. Provided water is available, length of growing season has its starting date defined by last mean spring frost date and ending date defined by first mean fall frost date. Probability distributions of historical degree-day records allow for selection of adequate crops and cultivars, those that will reach maturity for an accepted risk level.

The same concept can be applied to predict probability of occurrence of damaging development phases of pests in crops during certain times of the year, guiding the application of control measures.

Evapotranspiration and water balance

Water loss from the soil–plant system, through soil evaporation and plant transpiration, is termed evapotranspiration (ET). This is an energy-consuming process fueled mostly by net radiation absorption by the soil–plant surface. Soil water availability also determines the ET rate, with additional control provided by plant stomata. Under optimum water conditions plants do not need to control water loss, and carbon dioxide uptake also proceeds without restriction. Hence, crop yields are optimum under non-limiting water conditions. Numerous models have been developed for prediction of ET from crops given optimal and limiting soil water conditions. The Penman–Monteith equation, and the use of crop coefficients are commonly used (Allen et al., 1998) in agroclimatology to predict seasonal crop water requirements, and to determine irrigation needs of crops. This is accomplished through a soil water budget, where losses due to ET, runoff and deep percolation are compared to inputs such as precipitation and irrigation. Water stored, as determined by soil characteristics and rooting depth, decreases if outputs exceed inputs, and vice-versa. Limiting growth conditions, and reductions in yields, occur if soil water available to crops falls below a critical level, signaling the need for irrigation. A water budget applied using climatic data determines crop water requirements for optimal yields, and irrigation viability, contributing to long-range planning of land and water resource use.

Agroclimatic zoning

In contrast to climatic classifications, which are usually based on temperature and precipitation, agroclimatic classifications also take soil type, crop potential productivity and moisture deficiency, among other variables, into consideration (Bishnoi, 1989). Agroclimatic zoning allows for assessment of resources for agriculture, crop planning, and improvement in crop productivity. This concept was expanded to include environmental impact, resulting in the concept of agroecological zoning (AEZ) by the United Nations Food and Agriculture Organization (FAO). Recently, AEZ has been used to establish a global environmental resource database, including climatic, soil, terrain, and land cover, assessing the agricultural potential of 28 crops at three levels of farming technology (Fischer et al., 2001).

Animal comfort

The energy budget of homeothermic animals determines the level of comfort experienced, and if additional energy needs to be expended in keeping the body in a thermally comfortable zone. Excessive energy spent in thermal regulation results in reduced productivity, and may affect survival in extreme cases. Different livestock species and breeds have contrasting climatic requirements, and resistance to diseases typical to each environment. Consequently, climatic factors play a role in determining the level of success of the livestock enterprise. For example, a temperature–humidity index (THI), calculated from climate normals, has been used to indicate when temperate-evolved Holstein cows become less productive in various climate zones (Johnson, 1994).

Importance

Understanding of interactions between weather and agriculture leads to opportunities to use this knowledge for increased agricultural production, and also for minimizing agriculture's risks and impact on the environment. Thus, agrometeorology can play an important role in promoting sustainable development, through protection of the atmosphere and fresh water resources, desertification and drought control, sustainable agriculture, and education and training (Sivakumar et al., 2000). Knowledge obtained through research in agrometeorology is applied to guide: (1) strategic decisions in long-range planning; (2) tactical decisions in short-term planning, and (3) agrometeorological forecasts (WMO, 1981). Agroclimatology addresses needs in long-range planning, with typical examples of strategic decisions being selection of crops, livestock or forest species that match the existing climatic environment (agroclimatic characterization); and scheduling of agricultural operations (planting, pest control, etc.) that take into account long-term records and minimize risks. Hence, agroclimatology also provides tools needed in assessing the impact of climate change on agriculture, and strategies for farmers to adapt to a changing climate.

Claudia Wagner-Riddle

Bibliography

Allen, R.G., Pereira, L.S., Raes, D., and Smith, M., 1998. *Crop Evapotranspiration*. Food and Agriculture Organization, Irrigation and Drainage Paper No. 56.
Bishnoi, O.P., 1989. *Agroclimatic Zoning*. Commission of Agricultural Meteorology Report No. 30.
Fischer, G., Shah, M., van Velthuizen, H., and Nachtergaele, F.O., 2001. *Global Agro-ecological Assessment for Agriculture in the 21st Century*. Laxenburg, Austria: International Institute for Applied Systems Analysis.
Food and Agriculture Organization, 1993. *Agro-ecological Zoning Guidelines*. FAO Soil Bulletin 73.
Griffiths, J.F., 1994. *Handbook of Agricultural Meteorology*. Oxford: Oxford University Press.
Johnson, H.D., 1994. Animal physiology. In Griffiths, J.F., ed., *Handbook of Agricultural Meteorology*. Oxford: Oxford University Press, pp. 44–58.
Monteith, J.L., 2000. Agricultural meteorology: evolution and application. *Agricultural and Forest Meteorology*, **103**: 5–9.
Sivakumar, M.V.K., Gommes, R., and Baier, W., 2000. Agrometeorology and sustainable agriculture. *Agricultural and Forest Meteorology*, **103**: 11–26.
World Meteorological Organization, 1981. *Guide to Agricultural Meteorological Practices*. Geneva: WMO No. 143.

Cross-references

Applied Climatology
Climate Comfort Indices
Degree Days
Drought
Evapotranspiration
Spring Green Wave
Water Budget Analysis

AIRMASS CLIMATOLOGY

An airmass is a large body of air with relatively uniform temperature, humidity, and lapse rate characteristics across its horizontal extent. Especially in the midlatitudes, large seasonal and daily changes of weather commonly result from alternating dominance by airmasses derived from a variety of source regions. Specific types of these airmasses, typically covering hundreds of kilometers, are also responsible for stretches of days with similar weather, such as a cold polar outbreak in winter, or a hot–humid string of days in summer. Airmass climatology generally will describe the types of airmasses found in an area, will classify them according to their temperature and moisture characteristics, and will determine their seasonal or annual frequency of occurrence. This focus on temperature and moisture characteristics contrasts with weather-typing schemes that typically concentrate on pressure patterns and circulation features.

Airmass climatology grew out of the so-called "Norwegian" school of synoptic weather analysis. Bergeron (1928) formulated the concept of the airmass in the 1920s and proposed that a study be made of airmass characteristics and frequencies as a means of explaining recurring weather patterns (see Willet, 1931, for an English-language discussion). Petterssen (1940) first put together a northern hemisphere summary of airmasses. Strahler (1951) presented a worldwide synthesis showing general source regions and areas of dominance. Although too general for application to specific locations or during specific seasons, Strahler's model served well as a framework for other more detailed climatologies. Growing as it did out of midlatitude weather analysis, airmass climatology is most applicable where weather changes are frequent and airmasses numerous. The weather and climate of the tropics, poles, or other areas having a relative constancy of a single airmass type are generally less amenable to analysis by airmasses, since the significant weather patterns are caused by other mechanisms.

Classical airmass analysis is a manual exercise that requires subjective interpretations by the researcher that can be difficult to replicate, and often lack the precision necessary for successful applications. The availability of upper-air data and rise of numerical techniques, overshadowed the utility of the airmass as a weather forecasting tool by the late 1950s. Starting in the 1960s, dissatisfaction with the limitations of all manual classifications, coupled with increasing computer power, led to a dramatic reduction in their use. They were replaced by experimentation with many automated weather-typing techniques. None was widely adopted, nor did these schemes match the elegant simplicity and utility of the airmass concept for explaining midlatitude weather phenomena. However, neither did it appear possible to make classical-style airmass climatologies sufficiently rigorous for modern use.

Starting in the early 1990s, a new body of airmass work has grown from a commitment to a hybrid approach, combining manual and automated classification techniques to rehabilitate airmass climatology as a modern research tool (Schwartz, 1991; Kalkstein et al., 1996; Sheridan, 2002). Applications of the new approach have been successfully demonstrated in many areas, including describing the seasonal climate of an area, showing coherent upper-level circulation relationships to surface airmass distributions, interpreting precipitation intensity, assessing climate change, characterizing urban heat islands, identifying excessive heat-stress conditions, and even evaluating GCM output. Airmass climatology is again a fertile ground for discussion and research.

Airmasses

Formation

The critical properties of airmasses are temperature, humidity, and lapse rate. Of these, temperature and humidity are largely determined by the surface over which an airmass originates, whereas lapse rate is controlled by a number of factors. Usually, the geographic origin of an airmass within features of the general circulation (such as subtropical high pressure system or intertropical convergence zone) determines the lapse rate of the airmass.

In order for an extensive portion of the atmosphere to become recognizable as an airmass, it must reside for a time over a surface that is rather homogeneous across large expanses. The most effective way for this to occur is for a large anticyclone (high-pressure system) to remain stationary over an area for a number of days or weeks. Within the anticyclone, pressure gradients are weak, winds are light and slow subsidence induces radial drainage of air away from the center, which assures little mixing of foreign airstreams into the anticyclone. As the system stagnates, the atmosphere is slowly modified through radiative and convective processes to take on the temperature and humidity characteristics of the surface. For

example, within a wintertime polar anticyclone the resident air will lose heat through radiative transfer to the surface, and the airmass will become cold and dry as water-holding capacity decreases with temperature. This airmass will have a relatively stable lapse rate because of cooling in the lower layers and adiabatic warming of subsiding air aloft.

Oceans, deserts, and extensive continental plains at high and low latitudes are the usual birthing places of the classical airmasses, as it is in these locations that large pieces of the atmosphere can reside for a long time over a relatively homogeneous surface. Mountainous areas and continental plains at midlatitudes are usually not considered source regions of airmasses, since the surface conditions of mountains are too heterogeneous, and midlatitudes continents do not often experience the stable weather conditions necessary for the formation of airmasses. On the other hand, midlatitude oceans typically are source regions for airmasses, since horizontal temperature variation in the oceans is usually rather small. The damp foggy conditions of midlatitude, west coast locations (marine type climate) are attributed to continual dominance by marine airmasses.

The subtropical high pressure systems (STH) near 30° latitude illustrate the complex interaction between general circulation features and surface conditions in influencing lapse rates of airmasses. These semipermanent high-pressure systems are strongest over subtropical oceans, and they are stronger to the east and weaker to the west. In addition, subtropical oceans usually have a relatively cold ocean current along their eastern portion and a warm ocean current in their western part. Airmasses formed within the strongly subsident eastern portion of a STH therefore have a very stable lapse rate aloft resulting from subsidence and adiabatic warming, and they also experience a slight cooling in the lower layers from contact with the cold ocean water. These airmasses are extremely stable; they typically have a surface temperature inversion and may also have a middle-level temperature inversion. With such a stable lapse rate it is almost impossible for these airmasses to produce rain. The aridity of coastal areas in eastern Australia, western North America, the Atacama Desert (South America) and the Kalahari Desert (Africa) is the result of the continual dominance by these stable airmasses that originate over oceans. Airmasses formed in the less strongly subsident western portion of a subtropical high originate over a warm water surface and are usually rather unstable. They often contain thunderstorms and are responsible for much of the precipitation received by the east coast of continents at subtropical latitudes (for example, southeastern United States or Japan).

Airmass types

Airmasses are traditionally classified based on temperature and humidity, although the location or latitude of the source region and lapse rate or stability are also important variables in classification. A typical qualitative air mass classification is shown in Table A8 (a good treatment of traditional manual airmass classification and weather patterns is provided in Trewartha and Horn, 1980; see also Pettersen, 1956). The temperature symbols in Table A8 (A, P, T, E) reflect both the midlatitude origin and evolution of airmass analysis since the original airmass meteorological work in Scandinavia, Canada, and the United States emphasized the role of cA, mP, cP, and mT airmasses in midlatitude weather systems. The gradual evolution of this terminology has caused some confusion, since polar airmasses, in reality, originate at latitude 45–66° and are more properly termed subpolar airmasses (James, 1970). The extremely frigid air originating in polar latitudes has come be called Arctic (or Antarctic) air. A symbol for equatorial airmasses (E) has also joined the list, primarily because airmasses originating from the unstable western limb of subtropical anticyclones near 30° latitude are usually classified as maritime tropical (mT) air, although their origin may not have been strictly in tropical latitudes. The mE classification, then, refers to actual tropical airmasses and mT air refers to the hot, moist, subtropical air experienced in summer by midlatitude locations.

In addition, other letters can be added to manual classifications to provide information on the lapse rate or the temperature of the airmass relative to the surface across which it moves. For

Table A8 Classical airmass types

Variable	Abbreviation	Source	Airmass characteristics
Temperature	A (Arctic)	Arctic	Frigid
	P (polar)	50°–70° Latitude	Cold
	T (tropical)	Subtropical	Hot
	E (equatorial)	Equatorial	Hot
Humidity	m (maritime)	Over water	Moist
	c (continental)	Over land	Dry
Symbol	Airmass name	Airmass characteristics	
mE	Maritime equatorial	Hot, moist	
mT	Maritime tropical	Hot, moist	
mP	Maritime polar	Cool, moist	
cT	Continental tropical	Hot, dry	
cP	Continental polar	Cold, dry	
cA	Continental Arctic	Frigid, dry	

The abbreviations in the upper part of the table are usually combined to give a specific airmass a two-letter identification symbol as shown in the lower part of the table.

Table A9 Integrated method airmass types (Schwartz, 1991)

Symbol	Airmass name	Airmass source
C	Continental	Central Canada
Pa	Pacific	Pacific, via Rocky Mountains
Po	Polar	C + Pa (summer only)
D	Dry tropical	SW USA (mostly summer)
dT	Dilute tropical	Modified T (non-summer)
T	Tropical	Gulf of Mexico
U	Unclassed	Transition and mixing

Table A10 Spatial synoptic classification airmass/weather types (Kalkstein et al., 1996)

Symbol	Airmass name	Airmass characteristics
DP	Dry polar	Similar to cP
DM	Dry moderate	No traditional source region
DT	Dry tropical	Analogous to cT
MP	Moist polar	Large subset of mP
MM	Moist moderate	Warmer, more humid than MP
MT	Moist tropical	Analogous to mT
TR	Transitional	Days one type yields to another

example, a cP airmass moving over a warm surface is colder than the surface, receives fluxes of energy and moisture, and is therefore unstable. This airmass would be given the classification cPku, where the k stands for cold (relative to the surface), and u stands for unstable. This type of airmass would be typical of conditions along the east coast of a midlatitude continent in winter, with cold, polar airmasses being advected across warmer ocean water, resulting in fog and frequent cyclogenesis.

Recent airmass climatologies using hybrid manual-automated techniques have started to move away from the classical definitions. Schwartz's (1991) methodology was not directly comparable to previous work, but tried to use generic names similar to the classical ones to recognize major airmass types in the north central United States (Table A9). Kalkstein et al. (1996) decided that the classical definitions were too limited for application to environmental problems, and developed a revised set of airmass/weather types for the spatial synoptic classification (SSC), for use in the conterminous USA (Table A10).

Airmass modification

One of the major difficulties in identifying and classifying particular airmasses is that their properties change over space and time. Schwartz (1991) and Kalkstein et al. (1996) employed differential station airmass criteria and new types to account for these effects. Central North America provides two excellent examples of these problems of identification, modification, and classification of airmasses. In the summertime, mT air from the Gulf of Mexico frequently streams northward across central North America, but convection and mixing with other non-mT air modifies the properties of these airmasses. Air that had a temperature of 32°C and a dewpoint temperature of 21°C over the Gulf may have a temperature of 28°C and a dewpoint temperature of 17°C by the time it reaches the Great Lakes. In the interim, midtropospheric dry air from the Rocky Mountains, subsiding beneath a ridge (or high-pressure system) in the upper air westerlies, has significantly diluted the mT air flowing northward at the surface.

Central North America also provides another example of a different style of airmass modification. Borchert (1950) found that, for over 6 months of the year, the central Great Plains are occupied by airmasses that originate over the Pacific Ocean and that are then advected over the western North American cordillera. In the process these Pacific airmasses lose most of their moisture over the mountains and gain latent heat. As these airmasses subside over the Great Plains they are much warmer and drier than when they originated. Borchert classified these airmasses as mP air, but he referred to them as modified mP air, recognizing that they are relatively warm and dry; in fact, mP would better refer to "mild Pacific" rather than "maritime Polar" air. Schwartz (1991) recognized this mP air as "Pacific" and Kalkstein et al. (1996) as "moist polar". These examples illustrate several of the problems associated with attempting a rigorous manual classification based solely on the origin of airmasses, and demonstrates some reasons why the new hybrid classification techniques are desirable.

Methods of airmass analysis

One of the central problems in airmass climatology is identification of particular airmasses. Classical airmass identification techniques may be grouped into two broad categories: those aimed at determining some characteristic of an airmass, and those that trace the path of movement of an airmass. Airmasses originate in core areas, and a single airmass ought to resemble closely the characteristics of the core area. Airmass identification for a given station usually begins, therefore, with an identification of the major airmass core areas and airmass types that might be expected to influence the study area. Further identification and classification of a single airmass occurring away from its core area is usually accomplished by comparing airmass characteristics such as temperature, relative humidity, dewpoint temperature, or lapse rate with characteristics of source regions. The weak link in this type of analysis is identification of source region characteristics; although these core areas are usually located based on widely agreed upon features of the general circulation, it is still a subjective judgement by the analyst who determines their temperature and moisture values. In North America, Brunnschweiler (1952) first attempted to classify climate based on airmass patterns, but his technique was not considered rigorous and remains unused. Other regional climatologies of note include Borisov (1965) for the USSR, Arakawa (1937) for Japan, Belasco (1952) for the British Isles, and Tu (1939) for China.

For rigorous scientific analysis some automated methods of airmass identification are desirable to reduce the possible bias introduced by analyst's assumptions. The partial collective method has been used to identify airmass dominance based on some property such as temperature. In the partial collective method, airmasses from a single source region are theorized to have temperatures that tend toward a modal value, and the deviation of the temperature of a specific airmass away from the mode is apparently caused by longer or shorter residence time in the source area. Theoretically, the daily temperature distribution at any weather station can be decomposed into a group of normal distributions (partial collectives of the whole distribution), each of which has a separate modal temperature representing multiple occurrences of a certain airmass. Bryson

(1966) used this method to determine North American airmass regions, but some of his airmass boundaries did not coincide with boundaries determined by Barry (1967), using frontal analysis methods. Ozorai (1963) did not find this method particularly useful for Hungary, since the temperature histogram of Budapest displayed many more partial collectives than existing airmass categories.

Taljaard (1969) attempted a southern hemisphere synthesis of airmass dominance, while Oliver (1970) concentrated on classifying Australia's climate based on airmass dominance. These two studies are notable since airmass literature concentrates strongly on northern hemisphere topics, and southern hemisphere climatologies are few in number. Oliver (1970) offered an alternative to the partial collective method. He assigned characteristics to airmasses in Australia based on thermohygric diagrams showing temperature, specific humidity, and relative humidity, as well as through theoretical identification of the presumed source areas. Monthly data were plotted and clusters of points were identified as airmass types. Oliver was able to generalize the analysis so that temperature and precipitation data could be used to identify regions of airmass dominance in Australia. His scheme for identifying the airmass dominance at a station (called monthly airmass identification, MAMI) remains largely untested for the rest of the world.

Trajectory analyses trace the path of an airmass as it moves and is modified. Again, the use of a trajectory method usually presupposes that source regions for airmasses are already known. An alternative type of this analysis attempts to trace airmass trajectories back to the source region. Wendland and Bryson (1981) determined such "airstream" regions for the northern hemisphere by tracing mean resultant near-surface wind flow, under the assumption that airmass trajectories follow wind flow. Source regions were identified as areas where mean wind flow diverged in many directions from a single point. Several areas were shown to be dominated by airstreams of relatively consistent and conservative properties, and these regions are analogous to airmass regions identified in other ways.

Schwartz (1991) explored the airmass classification problem with a hybrid manual – automated methodology, in order to benefit from the inherent advantages of each approach. The new scheme addressed the nonreplicability problem of manual classifications, the boundary identification problem of automated methods, and the difficulty in quantifying misclassification error common to all techniques. The manual portion of Schwartz's "integrated method" analysis identified maxima and minima of 850-hPa temperature and dewpoint values for each airmass type, at every station in the north central USA (NCUS) study area, during the four seasons (represented by the months of January, April, July, and October). The 850-hPa level was chosen because it is close enough to the ground to reflect surface conditions, but enough removed to be free of diurnal boundary layer processes, and fairly conservative of temperature and moisture characteristics. Trajectory analysis was used on a number of airmasses of known origin, until the accuracy of the specific numerical limits defining each airmass was ensured.

The automated portion of the integrated method used the partial collective technique to identify normal curve components in the temperature and dewpoint frequency distributions for each station-month, starting from initial estimates of each components' mean, standard deviation, and weight (percent of the total distribution), and the number of different air mass types present, based on the results of the manual analysis. The manual and automated analyses were combined to produce the final numerical limits and transition zones for each airmass type in the four seasons (Figure A14). Ideally, the transition zones were centered on the values where the component normal distributions crossed (had the same Z-score probability). In order to assess classification error, each airmass limit was assigned a probability value based on its relationship to the component normal distributions.

The results supported the validity of the normal component theory of airmasses, as average Z-score probabilities of the numerical limits were largest in the west-central portion of the NCUS. They then decreased consistently toward the outer edges of the study area, indicating stronger single airmass dominance and more distinct separation in airmass characteristics when moving closer to the respective Continental, Pacific, Dry

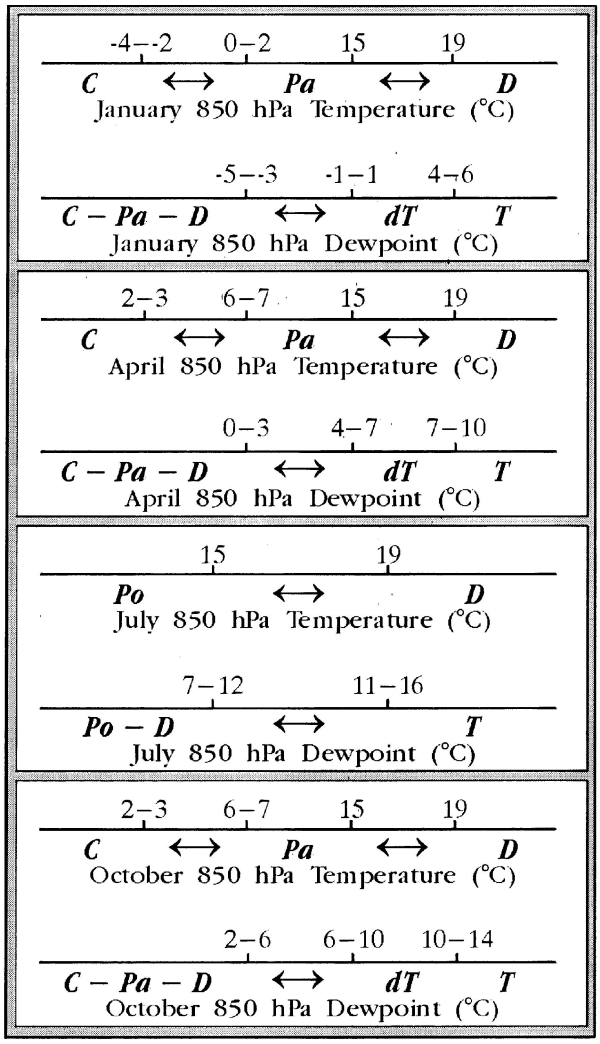

Figure A14 Integrated-method airmass criteria in January, April, July, and October for the north central United States (NCUS). Each airmass is defined by a range of temperature and dewpoint values except for dT and T airmasses which are distinguished by dewpoint alone. Double-ended arrow symbols show the U areas. A range of values indicates that limits vary depending on location within the NCUS. See Table A9 for names associated with airmass symbols (source: Schwartz, 1995).

Tropical, and Tropical air source regions (Table A9). Thus, the integrated method scheme is an easily interpreted approach to major airmass type classification that is numerically precise and allows assessment of misclassification error.

Kalkstein et al. (1996) continued development of hybrid techniques, by introducing the spatial synoptic classification (SSC) system, for the conterminous USA. Surface air temperature and dewpoint criteria were still central to the approach, but integration of multiple measurements each day, and the additions of other variables such as cloud cover, sea level pressure, and diurnal ranges of temperature and dewpoint, allowed for more detailed airmass definitions (Table A10). SSC's core was the manual selection of seed days for each airmass at every station location. A seed day is an actual day that displays the typical conditions for the given airmass at a selected station. Care was taken to ensure that adjacent stations have similar criteria for the same airmasses in order to create spatial continuity.

SSC used simultaneous discriminant analysis of all input variables to automate determination of the appropriate airmass type. Additionally, a parallel procedure identified and reassigned selected days as transitional situations (when one airmass yields to another). The result was a generally robust and replicable airmass classification scheme that has proven useful for many applications. However, an important limitation of SSC was its availability for only the winter and summer seasons.

Sheridan (2002) introduced enhancements to the SSC technique, with a revised approach labeled SSC2. Most notable were the creation of a new "sliding seed day" method that allowed the classification to be applied throughout the entire year, improvement in the spatial cohesiveness among stations, and expansion of the areas covered to include Canada, Alaska, and Hawaii, in addition to the conterminous USA.

Applications

One of the interesting applications of airmass climatology is ecology and paleoecology. Bryson (1966) showed that major vegetation boundaries in North America correlated very well with transition zones between major airmass types. He concluded that the location of each major vegetation regime was controlled by the dominance of a single airmass for more than 50% of a mean year. Barry (1967) questioned some of Bryson's methods and data, but Krebs and Barry (1970) found significant correspondence between vegetation transitions and mean frontal positions between airmass types in Eurasia. The implication that certain airmass types, through their influence on weather patterns, influence plant ecology, provides an exciting means of inquiry into the dynamics of plant distributions and the reasons behind the location of major natural regions.

Other researchers have used the correspondence between mean airmass dominance and vegetation regions to construct paleoairmass climatologies that describe the airmass climate of an area thousands of years ago. In this extremely complex analysis, researchers begin by making assumptions that climate (airmass dominance) largely determines the type of vegetation in a region, and the "pollen rain" from plants onto the surface of the earth is a reflection of the type of vegetation in an area. Although relatively few geologic deposits contain identifiable plants, certain ideal locations (peat bogs, lakes, ponds) have preserved a sediment accumulation for thousands of years, and from these sediments pollen found in ancient sediments presumably mirrors the types of vegetation grown in the area some time in the past and, from the pollen and radiocarbon dating of organic remains in the sediments, it is possible to reconstruct the type of vegetation that grew in an area thousands of years ago. It is assumed that vegetation regions are controlled by airmass dominance (for example, tundra vegetation exists in areas experiencing dominance by Arctic air for over 6 months of the year), then, from the records of many peat bogs or ponds across the continent, it is possible to piece together airmass climatologies for periods in Earth history from which we have no climatic records. For example, a profusion of grassland types of pollen found in 5000–7000-year-old sediments of peat bogs in currently forested areas of the eastern United States apparently records an expansion of the prairies of North America eastward as a result of expanded dominance by dry "mP" airmasses from the Pacific Ocean and Rocky Mountains (Wright, 1968). From today's correspondence between vegetation, pollen, and airmasses, along with the paleopollen record, it is possible to reconstruct a paleoclimatology of airmasses. These airmass paleoclimatologies provide an efficient means of understanding the character of past climates. (For example, see Bryson and Wendland, 1967; Webb and Bryson, 1972; Moran, 1973; and Sorenson and Knox, 1973.) However, these questions still need to be explored in greater detail.

A large number of applications have been undertaken in the broader field of synoptic climatology using automated "synoptic indices" that are similar to airmass climatologies. For example, the temporal synoptic index (TSI) developed by Kalkstein et al. (1987) has been applied to many problems, such as air pollution monitoring, glacier energy balance, and climate change detection (summarized in Kalkstein et al., 1990). Yarnal et al. (2001) provide an overview of developments in this and other areas of synoptic climatological research during the 1990s.

Applications have also been explored with modern hybrid airmass classification schemes since the mid-1990s. Schwartz and Skeeter (1994) showed that specific NCUS airmass distributions can be related to a small number of meaningful North American 500-hPa height and surface pressure patterns in all seasons, and also that key transects within these patterns can be used to describe changes in monthly airmass dominance from one year to another. Schwartz (1995) explored the use of airmass analysis as a tool for detecting structural climate change in the NCUS. Examinations of airmass temperature, dewpoint, and frequency changes over time, are superior to simple analyses of changes in monthly mean temperatures, as they may point to potential causes of change. Schwartz found increasing amounts of tropical air, coupled with decreasing polar air in summer over the 1958–1992 period, which suggested increases in the number of 500-hPa troughs over the western USA.

Schwartz (1996) used airmass analysis to assess the accuracy of a GCM control run. The results suggested that seasonal GCM performance was promising, but that substantial differences may exist between the control runs and observed climate data at the daily time scale. Greene (1996) used SSC to assess summertime precipitation intensity, and Sheridan et al. (2000) examined the urban heat island effect. Lastly, another important application of modern hybrid airmass analysis has been to identify excessive heat-stress conditions, and the development of health watch/warning systems (Sheridan and Kalkstein, 1998; Kalkstein, 1999). Sheridan (2002) summarized earlier work in this area, and recent studies incorporating SSC2 into systems designed for a number of cities in North America, Europe, and China.

Mark D. Schwartz and William T. Corcoran

Bibliography

Arakawa, H., 1937. Die Luftmassen in den Japanischen, *Am. Meteorol. Soc. Bull*., **18**: 407–410.

Barry, R.G., 1967. Seasonal location of the Arctic front over North America. *Geog. Bull*., **9**: 79–95.

Belasco, J.E., 1952. Characteristics of air masses over the British Isles. *Geophys. Mem*., **11**.

Bergeron, T., 1928. Uber die dreidimensional veknupfende Wetteranalyse, Part 1: Prinzipelle Einfuhurung in das Problem der Luftmassen-und Frontenbildung, *Geofys. Publ*. (Oslo), **5**: 1–111.

Borchert, J.R., 1950. The climate of the central North American grasslands. *Assoc. Am. Geog. Ann.*, **40**: 1–39.

Borisov, A.A., 1965. *Climates of the U.S.S.R.*, 2nd edn. A. Ledwood (trans.), C.A. Halstead, (ed.). Edinburgh: Oliver & Boyd.

Brunnschweiler, D.H., 1952. The geographic distribution of airmasses of North America, *Naturf. Gesell. Zurich Viertel*., **97**: 42–48.

Bryson, R.A., 1966. Airmasses, streamlines, and the boreal forest. *Geog. Bull*., **8**: 228–269.

Bryson, R.A., and Wendland, W.M., 1967. Tentative climatic patterns for some late glacial and post glacial episodes in central North America. In Mayer-Oakes, W.J., ed., *Life, Land, and Water*. Winnipeg: University of Manitoba Press, pp. 271–299.

Greene, J.S., 1996. A synoptic climatological analysis of the summertime precipitation intensity in the eastern United States. *Phys. Geog.,* **17**: 401–418.

James, R.W., 1970. Air mass climatology. *Met. Rund*., **23**: 65–70.

Kalkstein, L.S., 1999. Heat-health watch systems for cities. *World Meteor. Org. Bull.*, **48**: 69.

Kalkstein, L.S., Tan, G., and Skindlov, J., 1987. An evaluation of three clustering procedures for use in synoptic climatological classificiation. *J. Climate Appl. Meteorol.*, **26**: 717–730.

Kalkstein, L.S., Dunne, P.C., and Vose, R.S., 1990. Detection of climatic change in the western North American Arctic using a synoptic climatological approach. *J. Climate*, **3**: 1153–1167.

Kalkstein, L.S., Nichols, M.C., Barthel, C.D., and Greene, J.S., 1996. A new spatial synoptic classification: application to air-mass analysis, *Int. J. Climatol.*, **16**: 983–1004.

Krebs, J.S., and Barry, R.G., 1970. The Arctic front and the tundra–taiga boundary in Eurasia, *Geog. Rev*., **60**: 548–554.

Moran, J.M., 1973. The late-glacial retreat of "Arctic" air as suggested by onset of *Picea* decline. *Prof. Geogr*., **25**: 373–376.

Oliver, J.E., 1970. A genetic approach to climate classification, *Assoc. Am. Geogr. Ann.,* **60**: 615–637.

Ozorai, Z., 1963. An assessment of ideas in relation to airmasses. *Idojara*, **67**: 193–203.

Petterssen, S., 1940. *Weather Analysis and Forecasting*. New York: McGraw-Hill.

Petterssen, S., 1956. *Weather Analysis and Forecasting*, 2nd edn. New York: McGraw-Hill.

Schwartz, M.D., 1991. An integrated approach to air mass classification in the North Central United States. *Prof. Geogr.*, **43**: 77–91.

Schwartz, M.D., 1995. Detecting structural climate change: an air mass-based approach in the North Central United States, 1958–1992. *Assoc. Am. Geogr. Ann.*, **85**: 553–568.

Schwartz, M.D., 1996. An air mass-based approach to GCM validation. *Climate Res.*, **6**: 227–235.

Schwartz, M.D., and Skeeter, B.R., 1994. Linking air mass analysis to daily and monthly mid-tropospheric flow patterns. *Int. J. Climatol.*, **14**: 439–464.

Sheridan, S.C., 2002. The redevelopment of a weather-type classification scheme for North America. *Int. J. Climatol.*, **22**: 51–68.

Sheridan, S.C., and Kalkstein, L.S., 1998. Heat watch-warning systems in urban areas, *World Resource Rev.*, **10**: 375–383.

Sheridan, S.C., Kalkstein, L.S., and Scott, J.M., 2000. An evaluation of the variability of air mass character between urban and rural areas. In *Biometeorology and Urban Meteorology at the Turn of the Millennium*. World Meteorological Organization, pp. 487–490.

Sorenson, C.J., and Knox, J.C., 1973. Paleosols and paleoclimates related to Late Holocene forest/tundra border migrations: MacKenzie and Keewatin, N.W.T., Canada. In Raymond, S., and Schlederman, P., eds., *International Conference on the Prehistory and Paleoecology of Western North Arctic and Subarctic*. Calgary: University of Calgary Archeology Association, pp. 187–204.

Strahler, A.N., 1951. *Physical Geography*. New York: Wiley.

Taljaard, J.J., 1969. Airmasses of the southern hemisphere, *Notos*, pp. 79–104.

Trewartha, G.T., and Horn, L.H., 1980. *An Introduction to Climate*. New York: McGraw-Hill.

Tu, C.W., 1939. Chinese air mass properties, *Q. J. Roy. Meteorol. Soc*., **65**: 33–51.

Webb, T., III, and Bryson, R.A., 1972. Late and post-glacial climatic change in the Northern Midwest, U.S.A. *Quatern. Res.*, **2**: 70–115.

Wendland, W.M., and Bryson, R.A., 1981. Northern hemisphere airstream regions. *Monthly Weather Rev*., **109**: 255–270.

Willett, H.C., 1931. Ground plan for a dynamic climatology. *Monthly Weather Rev*., **59**: 219–223.

Wright, H.E., 1968. History of the prairie peninsula. In Bergstrom, R.E., ed., *The Quaternary of Illinois*. Special Publication No. 14, University of Illinois College of Agriculture.

Yarnal, B., Comrie, A.C., Frakes, B., and Brown, D.P., 2001. Developments and prospects in synoptic climatology. *Int. J. Climatol.*, **21**: 1923–1950.

Cross-references

Atmospheric Circulation Global
Climatic Classification
Lakes, Effects on Climate
Local Winds

AIR POLLUTION CLIMATOLOGY

Air pollution is defined as an atmospheric condition in which substances (air pollutants) are present at concentrations higher than their normal ambient (clean atmosphere) levels to produce measurable adverse effects on humans, animals, vegetation, or materials (Seinfeld, 1986). Polluting substances can be noxious or benign, and can be released by natural and anthropogenic (human-made) sources. According to the World Health Organization an estimated 3 million people die each year because of exposure to air pollution (WHO, 2000). Air pollution climatology is concerned with the study of atmospheric phenomena and conditions that lead to occurrence of large concentrations of air pollutants and with their effects on the environment.

Air pollutants are typically classified into three categories: suspended particulate matter (SPM), gaseous pollutants (gases and vapors) and odors. SPM in the air includes PM_{10} (particulate matter with median diameter less than 10 μm), $PM_{2.5}$ (particulate matter with median diameter less than 2.5 μm), diesel exhaust, coal fly-ash, mineral dusts (e.g. asbestos, limestone, cement), paint pigments, carbon black and many others. Gaseous pollutants include sulfur compounds (e.g. sulfur dioxide (SO_2)), nitrogen compounds (e.g. nitric oxide (NO), ammonia (NH_3)), organic compounds (e.g. hydrocarbons (HC), volatile organic compounds (VOC) and polycyclic aromatic compounds (PAH), etc.). Known odorous agents are generally sulfur compounds such as hydrogen sulfide (H_2S), carbon disulfide (CS_2) and mercaptans.

The past few decades have seen much progress in the understanding of air pollution climatology and meteorology, due to rapid progress in pollutant measurement techniques, increased understanding of atmospheric dynamics, and computational capabilities, particularly for areas with complex terrain. At the time of the last edition of this *Encyclopaedia* (1986), the processes of air pollution dispersion were well understood for

Table A11 Typical spatial and temporal scales of air pollution problems

Air pollution type	Horizontal scale	Vertical scale	Temporal scale
Indoor	10–100 m	Up to 100 m	Minutes–hour
Local	100 m–10 km	Up to 3 km	Minutes–hours
Urban	10–100 km	Up to 3 km	Hours–days
Regional	100–1000 km	Up to 15 km	Hours–months
Global	40 000 km	Up to 50 km	Months–decades

Source: Modified after Stern et al. (1984).

urban areas over relatively simple terrain. However, knowledge gaps existed regarding the dispersion of pollutants in cities near coastlines or lake shores, or in areas of complex topography such as mountainous areas – all of which may be considered as "complex terrain". In addition, air pollution climatology now considers not only localized issues, but also global problems such as stratospheric ozone reduction. The role of long-range transport of pollutants in degradation of air quality in remote/distant regions has also been recognized. Over the past few decades a combination of field observational studies – such as the European Tracer Experiment (ETEX; Girardi et al., 1998) and the Across North America Tracer Experiment (ANATEX; Draxler et al., 1991) – in conjunction with different modeling approaches – has added to a growing knowledge base concerning the complexities of air pollution dispersion.

Natural air pollution has always occurred throughout Earth's history. Volcanic eruptions, natural fires and wind-blown dust are examples of natural phenomena that introduce pollutants into the atmosphere. Anthropogenic sources have only become a serious problem during the past 200 years with the growing population, increased urbanization and accelerating industrialization. It is estimated that 2 billion metric tons of air pollutants are released into the atmosphere world-wide (Arya, 1999). Air quality is affected not only by emissions into the atmosphere, but also by the pollution potential of air. Stern et al. (1984) provide a useful classification for the types and scales of air pollution problems (Table A11).

Earlier examples of important literature on air pollution climatology include Slade (1968), Williamson (1972), Stern (1976), Holzworth (1974) and Pasquill (1974). However, several introductory books that contain in-depth information on recent developments in this discipline are now available. Arya (1999) is an invaluable book that covers the physics of meteorology and dispersion, while Jacobson (2002) includes perspectives on history and science. The book by Seinfeld and Pandis (1998) also contains a wide range of topics on the physics and chemistry of air pollution. Those who require an extensive treatment of atmospheric chemistry (ambient and polluted) are encouraged to consult Finlayson-Pitts and Pitts (1986). A concise literature review is provided by Sturman (2000).

This account will focus on air pollution climatology by first introducing contemporary air pollution problems and issues; then by considering the components of air pollution, including emissions, atmospheric conditions and receptor response. The item continues by discussing air pollution dispersion models and air quality guidelines and standards.

Contemporary air pollution problems and issues

Air quality issues came to the forefront of scientific and societal attention during the 1950s. In 1952 London's "killer fog" caused a great increase in human fatality (4000 excess deaths), especially in people with a history of cardiopulmonary problems. The episode resulted in the implementation of air pollution mitigation measures by the authorities (Brimblecombe, 1987). The air pollution in London was due to the emission of smoke from the burning of coal and other raw materials into the foggy atmosphere; this type of pollution is known as the London-type smog (smoke plus fog). In the same decade another type of smog, which is formed by chemical reactions in the atmosphere – the Los Angeles photochemical smog – also gained notoriety. During the 1970s acid rain emerged as the top environmental concern. A decade later the reduction of stratospheric ozone due to emission of anthropogenic compounds became the top international concern.

Major air pollution problems facing humanity in the 21st century include urban smog, acid deposition, indoor air pollution, Antarctic stratospheric ozone depletion (global stratospheric ozone reduction), and the highly contentious issue of global warming due to alteration of the global longwave (infrared) radiation balance caused by emission of greenhouse gases (GHG) such as carbon dioxide, methane, and nitrous oxide. Table A12 lists some of the polluting substances present in the atmosphere.

Urban smog

This is characterized by build-up of harmful gases and particulates emitted from vehicles, industry, or other sources (primary pollutants) – that cause the London-type smog, or is formed chemically in the air from emitted precursors (producing *secondary* pollutants) – that cause the Los Angeles-type smog. London-type smog events have been observed in various places around the world, such as the Meuse Valley in Belgium, Pittsburgh in the United States, and Christchurch in New Zealand, to name just a few. Photochemical smog has been observed in most cities around the world; the problem is particularly severe in mega-cities such as Mexico City, Tokyo, Beijing and Tehran.

Transboundary pollution

This is characterized by transport of pollutants across political boundaries and/or vast distances. Examples of such pollution include acid deposition (also known as acid rain – a term introduced by Robert Angus Smith in the nineteenth century) and regional haze caused by forest fires. Acid deposition happens when sulfuric acid (H_2SO_4), hydrochloric acid (HCl), or nitric acid (HNO_3) is deposited on the ground in vapor form or dissolved in rainwater, fogwater, or particulates. This increased acidity in turn harms soils, lakes, vegetation and materials. Cowling (1982) provides an historical perspective on the discovery of and mitigation measures used to deal with acid rain. Natural examples of transboundary pollution include the 1998 dust clouds caused by intense storm events in western China, which carried vast quantities of particulate matter across the Pacific Ocean, contributing to increased concentrations in Vancouver, Canada (McKendry et al., 2001).

Indoor air pollution

Most people spend a large amount of time indoors where they are constantly exposed to indoor air pollution. This is caused from either the emission of gases and particulates in enclosed

Table A12 Gases and particulate matter components in air pollution

Outdoor urban air pollution	Indoor air pollution	Acid deposition	Stratospheric ozone depletion	Global climate change
Gases				
Ozone (O_3)	Nitrogen dioxide (NO_2)	Sulfur dioxide (SO_2)	Ozone (O_3)	Water vapor
Nitric oxide (NO)	Carbon monoxide (CO)	Sulfuric acid (H_2SO_4)	Nitric oxide (NO)	Carbon dioxide (CO_2)
Nitrogen dioxide (NO_2)	Formaldehyde (HCHO)	Nitrogen dioxide (NO_2)	Nitric acid (HNO_3)	Methane (CH_4)
Carbon monoxide (CO)	Sulfur dioxide (SO_2)	Nitric acid (HNO_3)	Hydrochloric acid (HCl)	Nitrous oxide (N_2O)
Ethene (C_2H_4)	Organic gases	Hydrochloric acid (HCl)	Chlorine nitrate ($ClONO_2$)	Ozone (O_3)
Toluene ($C_6H_5CH_3$)	Radon (Rn)	Carbon dioxide (CO_2)	CFC-11 ($CFCl_3$)	CFC-11 ($CFCl_3$)
Xylene ($C_6H_5CH_3$)			CFC-12 (CF_2Cl_2)	CFC-12 (CF_2Cl_2)
PAN ($CH_3C(=O)O_2NO_2$)				
Aerosol particle components				
Black carbon	Black carbon	Sulfate (SO_4)	Sulfate (SO_4)	Black carbon
Organic matter	Organic matter	Nitrate (NO_3)	Nitrate (NO_3)	Organic matter
Sulfate (SO_4)	Sulfate (SO_4)	Chloride (Cl)	Chloride (Cl)	Sulfate (SO_4)
Nitrate (NO_3)	Nitrate (NO_3)			Nitrate (NO_3)
Ammonium (NH_4)	Ammonium (NH_4)			Ammonium (NH_4)
Soil dust	Allergens			Soil dust
Sea spray	Asbestos			Sea spray
Tyre particles	Fungal spores			
Lead (Pb)	Pollens			
	Tobacco smoke			

Source: Modified after Jacobson (2002).

buildings or transport of pollutants from outdoors; but it is not as extensively researched as outdoor air pollution (Wanner, 1993). Health effects of indoor air pollutants can be severe and directly affect the respiratory and cardiovascular systems. Indoor air pollutants include radon gas, ammonia, volatile organic compounds (VOC), polycyclic aromatic hydrocarbons (PAH) and second-hand cigarette smoke. Radon gas has a long-term health effect and is naturally released by soil due to radioactive decay of radium (Bridgman et al., 2000). Indoor exposure to particulate matter increases the risk of acute respiratory infections, leading to an increase in infant and child mortality rates in developing countries. WHO reports that such exposure is responsible for between half and one million excess deaths in Asia, and 300 000–500 000 excess deaths in sub-Saharan Africa (WHO, 2000).

Antarctic ozone depletion

Antarctic ozone depletion and the reduction of global stratospheric ozone are due to emission of chlorine and bromine compounds such as chlorofluorocarbons (CFC). CFC break down by photolysis reaction (breakdown of molecules by solar radiation) after they have traveled to the upper atmosphere. The reduction of ozone increases the amount of ultraviolet (UV) radiation that reaches Earth's surface. UV radiation can damage genetic material of organisms and in humans it is known to cause skin cancer.

Scientific consensus supports the theory that human emission of carbon dioxide, methane, nitrous oxide and other gases may play a significant role in the cause of global warming (IPCC, 2001). Therefore global warming is also an air pollution issue.

Components of an air pollution problem

Air pollution problems usually have three components: (1) emission of polluting substances into the air; (2) the pollution potential of the atmosphere characterized by its ability to transport, diffuse, chemically transform and remove the pollutants; and (3) response of the receptors (e.g. people, animals, vegetation) to the exposed concentration. Each of these components is considered in this section.

Pollution emissions

Emission sources can be categorized as follows:

1. Urban and industrial. Industrial sources include power generation plants that use fossil fuel, mining, manufacturing, smelting, pulp and paper plants, and chemical industries. Major gaseous pollutants emitted are carbon monoxide (CO), carbon dioxide (CO_2), sulfur dioxide (SO_2) and volatile organic compounds.
2. Agricultural and rural. Agricultural areas can be sources of air contaminants due to decaying waste from animals and plants which can release ammonia, methane (CH_4, a powerful greenhouse gas) and other noxious gases. In addition, windblown dust due to plowing, tilting, and harvesting, and smoke and haze due to slash burning can lead to severe degradation in air quality. An interesting example of air pollution caused by agricultural practices is the regional haze and smog events that plagued the Southeast Asian countries in 1997 due to forest fires in Indonesia (Davies and Unam, 1999; Khandekar et al., 2000). Burning forests is a traditional way of clearing land for agricultural purposes in Indonesia (and indeed in many other parts of the world), but the fires became unmanageable due to prolonged drought and the delayed onset of the monsoon rains caused by the 1997 El Niño episode. A strong increase in tropospheric ozone concentrations occurred over tropical Southeast Asia, reaching as far as Hong Kong (Chan et al., 2001).
3. Natural. In addition to anthropogenic sources, many natural sources can contribute to air pollution. These include: volcanic

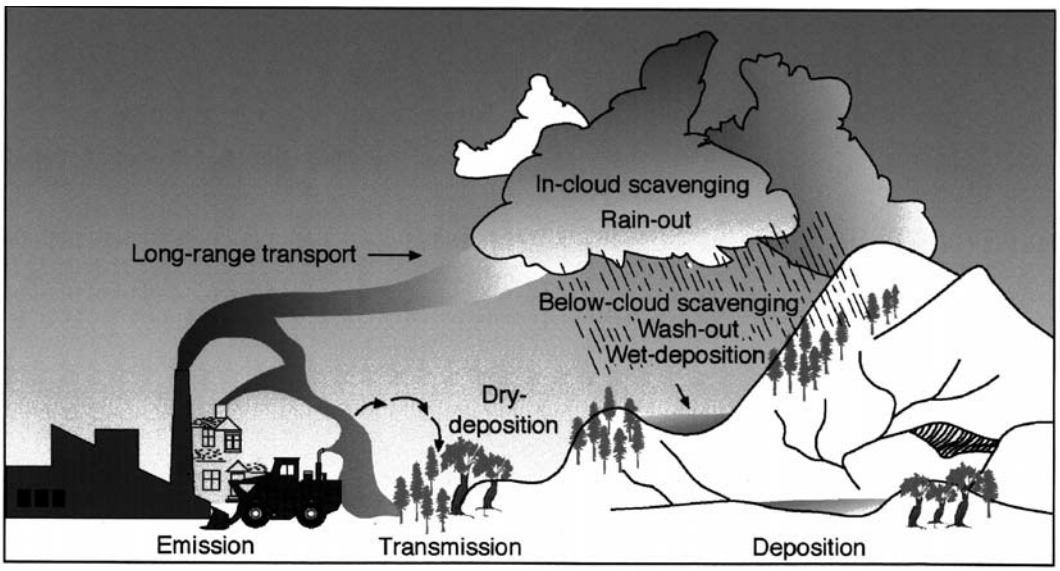

Figure A15 Schematic illustration of emission, transmission and deposition of air pollution.

eruptions that release vast quantities of particulate matter, CO_2, SO_2, and other gases, into the atmosphere; *biogenic* (from biological sources) emissions from forests and marshlands of compounds such as hydrocarbons (terpenes and isoprenes; Guenther et al., 1995), methane and ammonia; and soil microbial processes which contribute NO, CH_4 and H_2S.

Atmospheric conditions

The state of the atmosphere determines its pollution potential, which is affected by three important processes: *dispersion* which is the horizontal and vertical spread and movement of pollutants; *transformation* which involves chemical reactions that occur between pollutants or to pollutants under certain temperature and sunlight conditions; and *removal* of pollutants through such mechanisms as dry and wet deposition (Figure A15). Each of these processes will be considered in turn, but first the overriding control of synoptic conditions will be considered.

Synoptic controls

"Synoptic conditions" refers to an intermediate scale of atmospheric activity between global and regional scales and includes circulation systems such as anticyclones and cyclones. Synoptic circulation features have a spatial dimension of the order of thousands of kilometers and may last about a week on average. Atmospheric circulation at this scale has an important control on air pollution since it influences cloud (amount, thickness, height and type), temperature and relative humidity of the airmass, the type and amount of precipitation, and the wind speed and direction. These parameters in turn influence the vertical temperature structure of the atmosphere which determines the atmospheric stability. If the air temperature decreases rapidly with height (i.e. at a rate greater than the dry adiabatic lapse rate of 9.8°C km^{-1}) then the atmosphere is unstable. This means that vertical motion is promoted and any emissions will mix well into the boundary layer (the lowest layer of the atmosphere that is affected by the diurnal cycle of temperature, humidity, wind, and pollution). However, in stable conditions, which occur when temperature either decreases slowly with height (at a rate less than the dry adiabatic lapse rate) or increases with height (which is known as a temperature inversion), pollution may become trapped close to the emission source, resulting in increased concentrations. The layer through which the mixing of pollutants occurs is known as the mixed layer, and the height to which pollutants mix is called the mixing depth or mixing height.

Anticyclonic circulation is more conducive to pollution episodes since it usually involves weaker synoptic winds and clear skies. In summer, stronger surface heating under anticyclonic flow results in warmer temperatures in the boundary layer, and this warmth, together with high solar radiation levels and generally calm or light airflow, can lead to the formation of photochemical smog (discussed in more detail later). Since anticyclonic circulation involves subsidence of air towards the surface (and hence warming), this results in elevated inversions which can trap pollutants in a shallow mixed layer (Figure A16a).

In winter, clear skies and light winds during anticyclonic conditions lead to strong nocturnal radiative cooling of the surface which results in surface or radiative inversions (Figure A16b). During such conditions any pollutants emitted at the surface (e.g. through industrial emissions, domestic heating or traffic) become trapped very close to the surface and may result in high pollutant concentrations. This is the typical scenario that produces classic smog as a combination of smoke and fog. Figure A17 shows the severe degradation in air quality in Christchurch, New Zealand, as a result of emission of smoke from solid-fuel burning (wood) into a shallow surface inversion layer.

Dispersion

The dispersal of air pollutants is governed mainly by the mean wind speed and the characteristics of atmospheric turbulence. Together these factors determine the stability characteristics of the atmosphere. Turbulence consists of horizontal and vertical eddies that mix pollution with the surrounding air. As turbulence increases, so too does mixing, which results in good dispersion

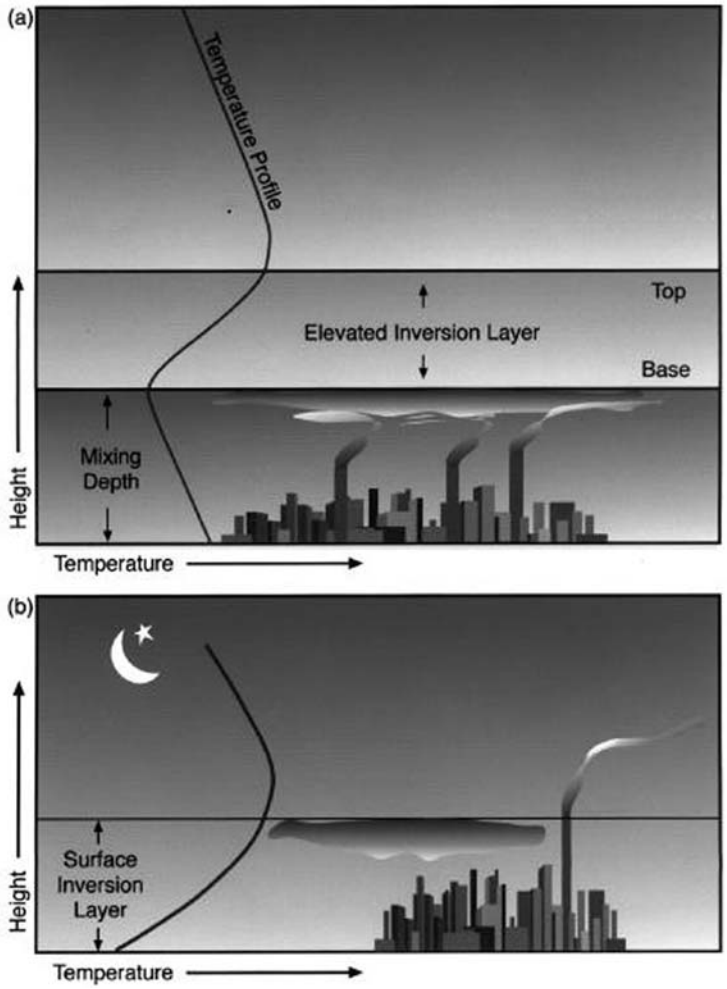

Figure A16 Air pollutants emitted at the surface can become trapped by (**a**) an elevated inversion layer and (**b**) a surface inversion layer (modified after Whiteman, 2000).

and lowered pollutant concentrations. Strong turbulence occurs in an unstable atmosphere in which vertical motion is enhanced. Conversely, when turbulence is weak, there is little propensity for mixing to occur and pollutant levels may increase. Conditions of weak turbulence are often typical of clear mornings in winter.

Turbulence can be generated through both thermal and mechanical means. Thermally generated turbulence results from heating of the surface, which leads to buoyancy-induced convective motion (i.e. vertical transport of heat away from the surface). With stronger heating of the surface, thermal turbulence will increase. Mechanically generated turbulence can result from wind shear as the wind blows across the Earth's surface. Mechanical turbulence increases with increasing wind speed and is greater over rougher surfaces (e.g. cities and forests). For a more in-depth explanation of the theory and mathematical representation of turbulence in the boundary layer refer to Stull (1998) or Garratt (1992).

A typical diurnal cycle of radiative heating and cooling in cloud-free conditions results in varying stability conditions throughout the day (Figure A18). In the early morning, before sunrise, the nocturnal temperature inversion is still present. Any pollutants emitted close to the ground may be trapped in this inversion, if the chimney stacks are lower than the inversion top, smoke plumes will take on a fanning shape (Figure A18a). After sunrise, surface heating results in the generation of convection which mixes the air close to the surface within the layer beneath the remains of the nocturnal inversion. This situation is one of the worst for pollutant concentrations at ground level as *fumigation* occurs (downward movement of pollutants from aloft because of a growing mixed layer), resulting in pollution originally emitted and trapped aloft being mixed to ground level, often in quite high concentrations (Figure A18b). As daytime heating continues the nocturnal inversion is completely eroded and replaced by a *lapse* profile (decrease of temperature with height; Figure A18c). This is typical of an unstable atmosphere which promotes vertical mixing. This mixing is evident in the behavior of smoke plumes which may take on looping behavior (Figure A18c). In late afternoon the atmosphere may become neutral, in which the environmental lapse rate equals the dry adiabatic lapse rate (Figure A18d). This results in coning of smoke plumes (Figure A18d). As the sun sets the surface begins

Figure A17 Christchurch, New Zealand, on a winter morning. The thick smoke at the surface is the result of poor ventilation due to a surface inversion layer that formed overnight. Smoke and particulate matter is emitted from home heating with solid-fuel burners (courtesy of The Christchurch Press).

to cool and the nocturnal inversion is again established (Figure A18e). If the smoke stack is above the inversion height, then lofting of the plume is observed (Figure A18e).

A common and relatively simple estimate of stability is the Pasquil–Gifford stability classification (Table A13). This scheme assumes that stability in the layers near the ground depends on net radiation as an indication of convective eddies, and on wind speed as an indication of mechanical eddies. At low wind speeds and with strong daytime insolation (i.e. radiative heating from the sun), the atmosphere will be extremely unstable (class A). As both cloud and wind speed increase, the atmosphere becomes less unstable (B, C) and may become neutral (D). Under light winds and clear skies at night the atmosphere may become stable (E and F).

Air pollution episodes are typically worse during stable atmospheric conditions since these restrict or limit the amount of vertical mixing. Temperature inversions, which are characteristic of a moderate to strongly stable atmosphere, can occur through several different mechanisms including surface cooling, warming of air aloft and *advection* (mean horizontal movement of air). Surface or radiation inversions occur during clear, calm nights as the ground cools rapidly due to the loss of longwave radiation to the outer atmosphere. Their strength and depth may be locally increased by cold air drainage. Surface cooling can also occur through evaporative cooling as water evaporates from a moist surface during the day in fine weather.

Inversions due to warming can occur through subsidence during anticyclones (as described earlier) or in the lee of mountains. In both cases the descending air warms adiabatically and creates elevated inversions which can effectively cap any mixing of pollution from below. In the lee of the Rocky Mountains in winter, radiative cooling over the interior of North America creates a very cold air mass which ponds against the mountains. Descending warm air spreads over the top of this stagnant pool and severely inhibits any upward dispersion (Oke, 1992).

Advection inversions can occur when warm air blows across a cooler surface such as a cold land surface, water body or snow cover. In this situation the cooling of the underside of the air mass creates an inversion with its base at the surface (Figure A19a). Existing inversion structures can also be modified during advection. For example, when a cool sea breeze (or rural air) flows over warmer land (or urban) areas, the inversion becomes elevated, and this can lead to serious fumigation problems if chimney stacks are located in the coastal zone (Figure A19b, c).

Complex terrain such as in coastal or alpine regions, or indeed anywhere that has significant variation in topography, can lead to complex airflows. In such areas under clear skies and light synoptic winds, local circulation systems often develop, such as land–sea breezes or mountain–valley winds. These circulation systems are not good pollution ventilators since they tend to have low wind speeds, are often closed systems and have a diurnal reversal of flow. Thus the pollution can be recirculated over the source area and may build up to high levels.

Pollutant transformation

Air pollutants may often undergo chemical transformations in the air to produce what are termed secondary pollutants. The damaging London smogs of 1952, which killed thousands of people, involved sulfuric acid fogs which remained stagnant for 4–5 days. These fogs occur when SO_2 (which is generated by the combustion of fuels – particularly from coal with high sulfur content) is oxidized in the air to sulfur trioxide (SO_3) which then reacts with water vapor (H_2O) in the presence of catalysts to form sulfuric acid mist. If the meteorological conditions are such that dispersion is poor, these toxic mists can have deadly consequences.

More common in recent decades is the formation of photochemical smog. There is a naturally occurring NO_2 photolytic cycle in which solar radiation results in the photo-dissociation

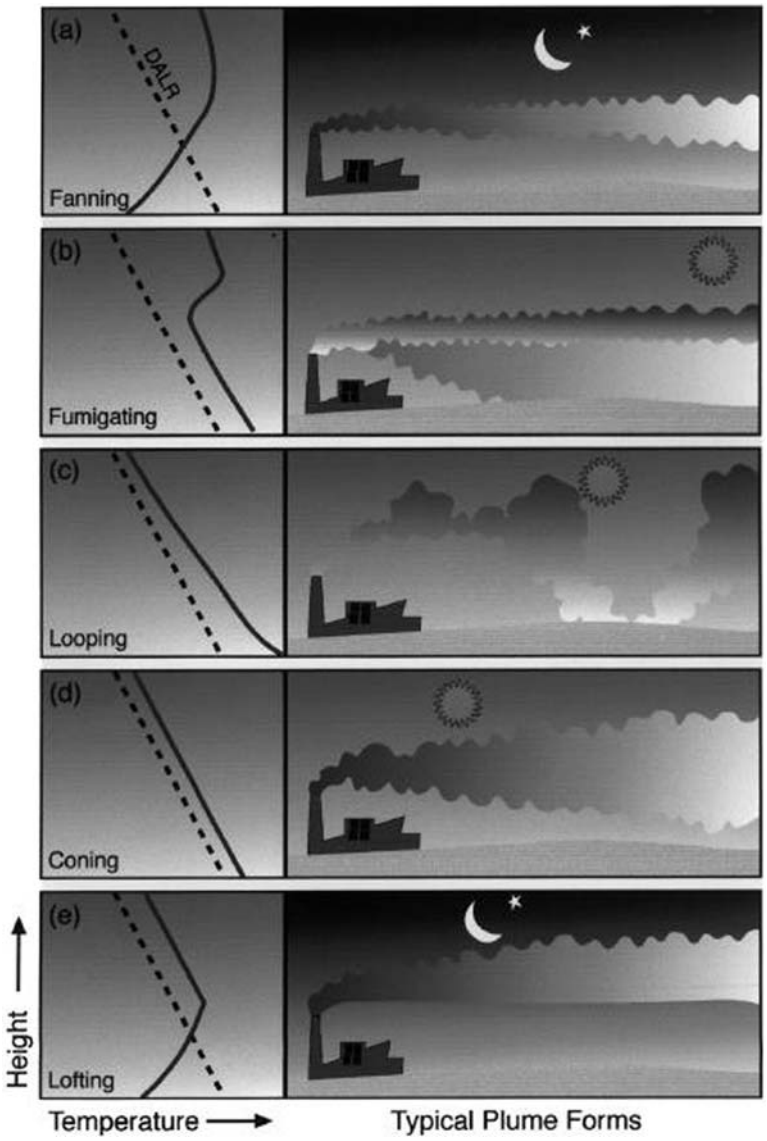

Figure A18 Stability changes throughout the day and effects on smoke plumes (modified after Whiteman, 2000). The dashed line (DALR) is the dry adiabatic lapse rate and the solid line is the environmental lapse rate.

Table A13 Pasquil–Gifford stability class

	Day-time insolation			Night-time cloudiness	
Wind speed at 10 m (ms^{-1})	Strong	Moderate	Slight	≥4/8 Cloudiness	≤3/8 Cloudiness
<2	A	A–B	B	—	—
2–3	A–B	B	C	E	F
3–5	B	B–C	C	D	E
5–6	C	C–D	D	D	D
>6	C	D	D	D	D

A, extremely unstable; B, moderately stable; C, slightly unstable; D, neutral, E, slightly stable; F, moderately stable. Insolation is the rate of solar radiation received per unit of Earth's surface and cloudiness is defined as the fraction (in octas) of sky above the local apparent horizon that is covered by clouds.

of NO_2 into NO and O (Figure A20). The oxygen atom (O) is highly reactive and combines with an oxygen molecule (O_2) to produce ozone (O_3). The ozone then reacts with NO to give NO_2 and O_2. However, the presence of reactive organic gases (ROG – which may be sourced from vehicles, but also naturally from vegetation) disrupts the cycle and can accelerate the production of ozone and other chemicals, such as aldehydes and ketones and peroxyacetyl nitrates (PAN) and even some particulates. Photochemical smog has a characteristic odor (partly due to the aldehydes), a brownish haze (due to NO_2 and light scattering by particulates) and may cause eye and throat irritation and plant damage. Figure A20 illustrates the sequence of chemical reactions that lead to formation of ozone as a by-product of photochemical smog following the emission of NO and ROG (the primary pollutants) into the atmosphere.

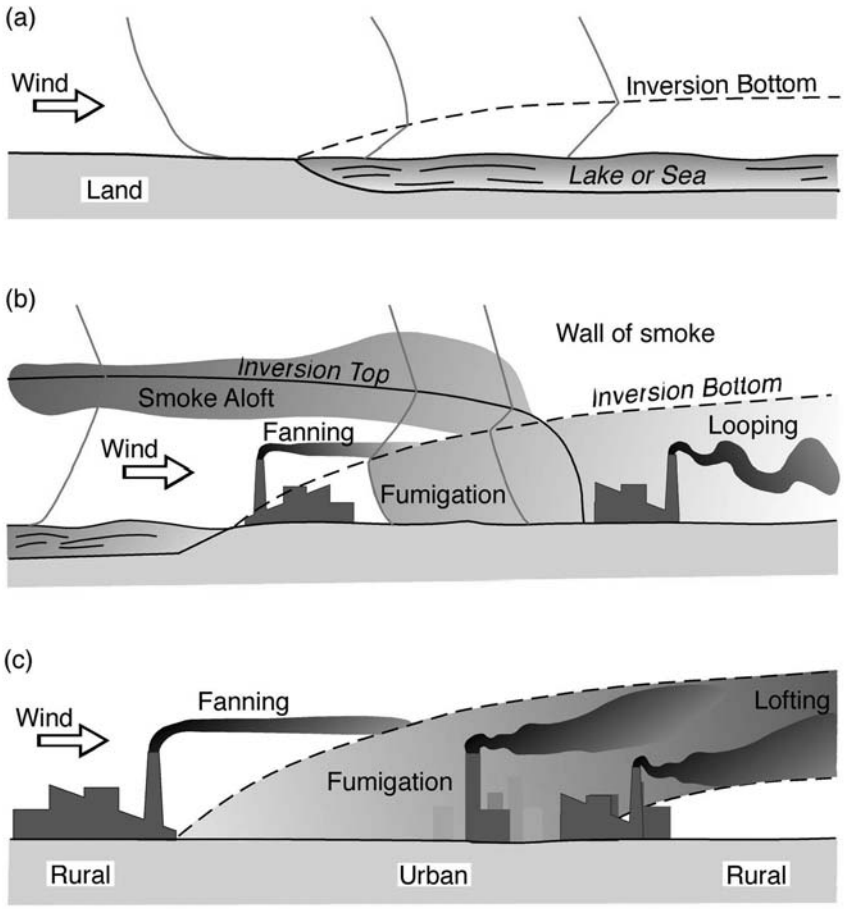

Figure A19 Examples of advection inversions. (**a**) Warm air flowing over cooler water, (**b**) sea breeze fumigation on a clear day and (**c**) fumigation over an urban area (modified after Oke, 1992 and Karl et al., 2000).

Organic peroxy radicals (RO_2) are formed by the break-up of ROG, which by reaction with NO form ozone. This type of smog has been reported from many cities around the world, including cities in Australia, Brazil, Britain, Canada, Greece, Netherlands, Iran, Israel, Japan and the United States.

Pollutant removal

As well as through chemical reaction, pollutants can be removed from the atmosphere by other processes, such as gravitational settling, and dry and wet deposition (Figure A15). Gravitational settling removes larger particulates, with the rate of removal related to the size and density of the particles and the strength of the wind. This process removes most particulates larger than 1 micrometer (μm) in diameter, but smaller particles become influenced by turbulence and may remain aloft for long periods. Dry deposition is a turbulent process in which there is a downward flux of pollutants to the underlying surface. The amount of deposition depends on the characteristics of turbulence, with increased rates under stronger turbulence.

Wet deposition involves the removal of air pollutants through absorption by precipitation elements (water droplets, ice particles and snowflakes) and consequent deposition to the Earth's surface during precipitation. This removal process includes the attachment of pollutants to cloud droplets during cloud formation, incloud scavenging (also known as *washout*), and through coalescence of rain drops with material below the cloud (*rainout*; Arya, 1999). Slin (1984) provides a comprehensive review of precipitation scavenging processes.

Receptor response

Air pollution is a concern due to its adverse effects on organisms and damage to materials. Research has demonstrated that air pollution can affect the health of humans and animals, damage plants, reduce visibility and solar radiation, and affect weather and global climate.

Effects on humans, animals and vegetation

During extreme air pollution episodes in urban areas the concentration of air pollutants can reach high levels for several hours or days. This can cause extreme discomfort, exacerbate illnesses and increase mortality rates among the most vulnerable part of the population (children, the elderly and the sick). Health-effect studies have revealed a number of adverse effects associated with common air pollutants. Peroxyacetyl nitrates (PAN), which are a

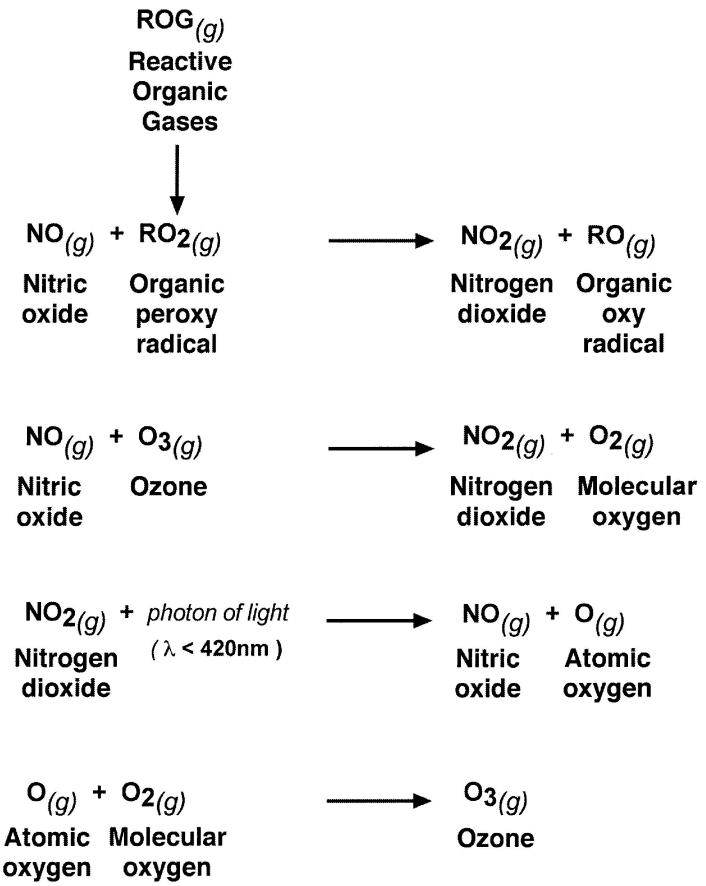

Figure A20 Chemical reactions in a polluted troposphere leading to photochemical ozone formation.

component of photochemical smog, can cause eye and throat irritation. Other health hazards of air pollutants include chronic bronchitis, pulmonary emphysema, lung cancer and respiratory infections. Even short-term exposure to particulate matter can cause an increase in the rate of asthma attacks.

Adverse effects of air pollution on vegetation include leaf damage, stunting of growth, decrease in size and yield of fruit, and severe damage to flowers. Domesticated animals such as cattle and dogs cannot only breathe in toxic air, but may also ingest pollution-contaminated feeds. The air pollutants that are of major concern are fluoride, lead, and other heavy metals and particulate matter.

Effects on materials

Air pollutants affect materials by chemical reactions and soiling. Extensive damage can occur to structural metals, building stones, fabrics, rubber, leather, paper, and other materials. For example, a well-known effect of photochemically produced ozone in the troposphere is cracking of rubber products. The number of cracks in automobile tyres, as well as their depth, has been related to ambient ozone concentrations.

Air pollution dispersion models

During the past two decades advances in computer technology have allowed the use of increasingly sophisticated air pollution dispersion models (also known as air quality models). Numerous books are now available that give an in-depth explanation of the theory and derivation behind the mathematical formulations used in air pollution models. For example, Zannetti (1990) provides information on a wide spectrum of dispersion models, while Jacobson (2000) offers an excellent and exhaustive treatise on the theory, the numerical techniques and chemistry of air pollution models. Arya (1999) also describes the diffusion/dispersion theories behind the modeling systems including detailed mathematical formulation. These models are used for both regulatory and research purposes.

Box models

The simplest air pollution models are single- and multi-box models (Lettau, 1970). Box models predict the concentration of primary pollutants inside a box using mass conservation principles, where the box represents a large volume of air over a city. A box model considers the emission source at the surface (lower boundary), advective inflow and outflow at the sides (lateral boundaries), and the evolution of the mixing depth and subsequent entrainment of pollutants from aloft. More complicated box models include chemical and photochemical transformations to predict concentrations of secondary pollutants like ozone (Demerjian and Schere, 1979; Dodge, 1977).

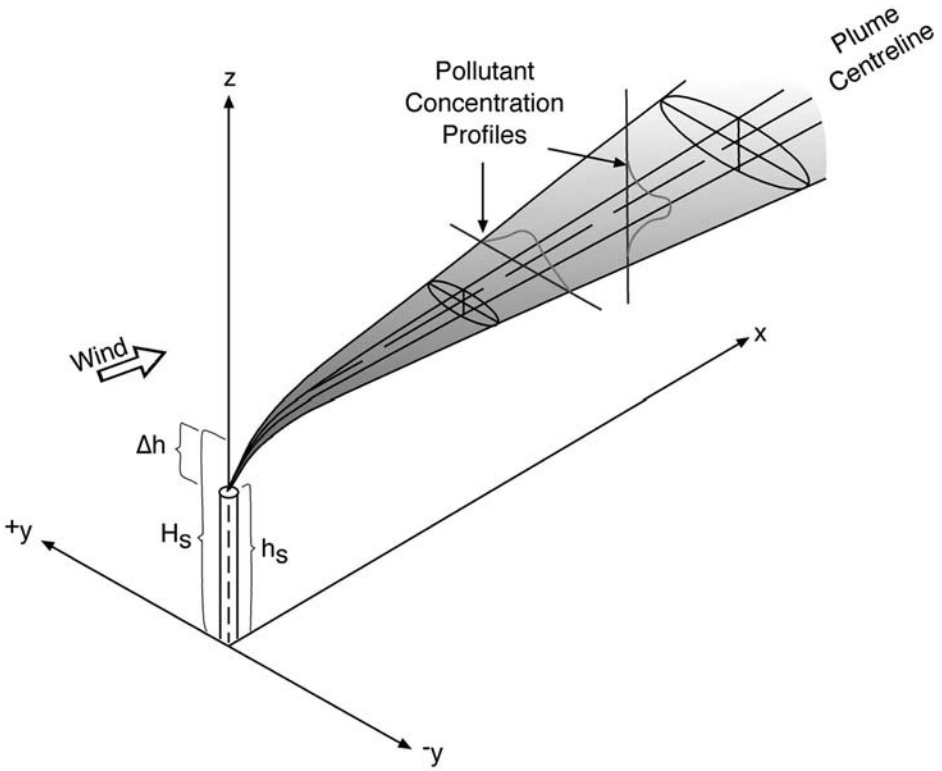

Figure A21 Schematic of plume dispersion from a stack with Gaussian distribution in horizontal and vertical (H_s is the height of the plume centerline and h_s is the stack height) (modified from Arya, 1999).

Gaussian plume models

Gaussian plume and puff models are used to estimate three-dimensional pollutant concentrations resulting from emissions generated at a point source, under stationary (unchanging) meteorological situations (Gifford and Hanna, 1973; Turner, 1964), although some models also incorporate non-stationary conditions. The underlying assumption in the Gaussian model is that with sufficiently long averaging periods (e.g. 1 hour) a bell-shaped (Gaussian) concentration distribution is produced in both horizontal and vertical directions (Figure A20). A plume model assumes a continuous point source with a uniform strong background flow, where release time and sampling time are longer than travel time. Puff models are used in cases where emission from a source is almost instantaneous and much shorter than travel time of the plume, such as accidental releases of hazardous material into the atmosphere. Gaussian models are commonly used in a regulatory framework because of their simplicity and cheap computational demands (relative to three-dimensional numerical models, which are described below). The severe limitation of the Gaussian models is that they generally do not work in calm conditions; in addition, the complexity of local terrain and variation of atmospheric conditions with time is ignored.

Numerical meteorological models

The most sophisticated and hence computationally demanding way of calculating pollutant concentrations is by simulating detailed meteorology (three-dimensional fields of wind, turbulence, temperature and water content) and coupling these fields to emission scenarios. The role of the meteorological component of the model is to provide input for the pollutant diffusion component. A numerical meteorological model uses numerical techniques to approximate meteorological equations that describe fluid flow – collectively known as the Navier-Stokes equations. These are highly complex and non-linear, and at present, no analytic solution is known for them. Stull (1998) and Pielke (2002) describe the numerical techniques and turbulence parameterizations behind these types of models. The Navier–Stokes equations take into account conservation of mass, heat, momentum and water. Air pollution scientists use many names for numerical models, but they are frequently referred to as grid-based and mesoscale.

Diagnostic models

Diagnostic models by definition do not provide a forecast for the state of the atmosphere. Diagnostic outputs are three-dimensional fields of meteorological variables obtained by interpolation and extrapolation of available meteorological measurements. They are computationally economical and appear to be effective analysis tools when the dominant factor driving the boundary layer airflow is the terrain. A major drawback is the requirement for sufficient observational data as input for the analysis. A three-dimensional diagnostic model such as CALMET – which is the meteorological component of the CALPUFF modeling system (Scire et al., 1990) – is widely used by regulatory/environmental organizations such as the US Environmental Protection Agency. The Earth Tech Corporation

Table A14 Summary of air quality standards from Canada, United States, New Zealand, and United Kingdom

Pollutant	Canada Air Quality Objectives and Standards[a]	United States Federal Primary Standards (NAAQS)	New Zealand Air Quality Guidelines[c]	United Kingdom National Standards
Carbon monoxide (CO)				
8-hour average	15 mg/m^3	10.5 mg/m^3	10 mg/m^3	11.6 mg/m^3 [d]
1-hour average	35 mg/m^3	40 mg/m^3	30 mg/m^3	—
Nitrogen dioxide (NO_2)				
Annual	100 μg/m^3	100 μg/m^3	—	—
24-hour average	200 μg/m^3	—	100 μg/m^3	—
1-hour average	400 μg/m^3	470 μg/m^3 [b]	200 μg/m^3	287 μg/m^3
Ozone (O_3)				
Annual average	30 μg/m^3	—	—	—
24-hour average	50 μg/m^3	—	—	—
8-hour average	—	160 μg/m^3	100 μg/m^3	100 μg/m^3 [e]
1-hour average	160 μg/m^3	235 μg/m^3	150 μg/m^3	—
Sulfur dioxide (SO_2)				
Annual average	60 μg/m^3	80 μg/m^3	—	—
24-hour average	300 μg/m^3	365 μg/m^3	120 μg/m^3	—
15 minute average	—	—	—	266 μg/m^3
PM_{10}				
Annual average		50 μg/m^3	20 μg/m^3	—
24-hour average		150 μg/m^3	50 μg/m^3	50 μg/m^3

[a] Values are maximum acceptable.
[b] California Standard.
[c] New Zealand has not legislated air quality standards yet.
[d] Running average.

freely distributes the code for the CALPUFF modeling system at http://www.calgrid.net/calpuff/calpuff1.htm.

Prognostic models

Prognostic models are able to forecast the evolution of the state of the atmosphere by numerically solving (both in time and space) the detailed set of approximations to the Navier–Stokes equations. Prognostic models take into account the evolution of synoptic scale winds and allow the formation of diurnally reversing local scale circulations such as sea/land breezes and valley/mountain flows (Whiteman, 2000). A great appeal of prognostic models, aside from their research applications, is that they can be the core of real-time air quality forecasting systems in case of accidental or intentional release of pollutants into the atmosphere. The forecast for the meteorological variables, in conjunction with appropriate turbulence statistics, is used to determine the probable spread and diffusion of the plume. Scientific centers that generate such forecasts and issue warnings use supercomputers, since expediency is important and prognostic models are computationally demanding. Examples of such organizations include the Atmospheric Research Division at the Commonwealth Scientific and Industrial Research Organization (CSIRO), which has implemented the Australian Air Quality Forecasting System (AAQFS), and the Lawrence Livermore National Laboratory in the United States which has the National Atmospheric Release Advisory Centre (NARAC). AAQFS routinely predicts daily levels of photochemical smog, atmospheric particles and haze, whereas NARAC is generally designed for emergency response purposes in case of accidental emissions of hazardous pollutants (e.g. radiological, chemical and biological substances).

Air quality guidelines and standards

Good health is (should be) a fundamental human right. The primary aim of air quality guidelines is to protect public health from the harmful effects of air pollution, and to eliminate or substantially reduce exposure to hazardous air pollutants. To achieve these aims, many countries use regulatory control through legislation to set legally enforceable air quality standards (AQS). These represent values that are the maximum average ground-level concentration allowed by law. AQS values are derived from air quality guidelines (AQG) determined purely from epidemiological/toxicological analysis. AQS have to consider technological feasibility; cost of compliance; and social, economic and cultural conditions. The maximum concentrations allowed are categorized by averaging periods, the most commonly used being hourly, daily and yearly. The air quality standards are different in each country. For example, in the United States they are referred to as National Ambient Air Quality Standards (NAAQS), while in Canada they are known as National Air Quality Objectives. Currently, the maximum allowable concentration for each pollutant (and for each averaging period) is prescribed differently in each standard. Table A14 shows maximum allowable concentrations for some common pollutants.

Peyman Zawar-Reza and Rachel Spronken-Smith

Bibliography

Arya, S.P., 1999. *Air Pollution Meteorology and Dispersion*. New York: Oxford University Press.

Bridgman, H., Warner, R., and Dodson, J., 2000. *Urban Biophysical Environment*. Melbourne: Oxford University Press.

Brimblecombe, P., 1987. *The Big Smoke*. London: Methuen.
Chan, C.Y., Chan, L.Y., Zheng, Y.G., Harris, J.M., Oltmans, S.J., and Christopher, S., 2001. Effects of 1997 Indonesian forest fires on tropospheric ozone enhancement, radiative forcing, and temperature change over Hong Kong Region. *Journal of Geophysical Research (D) Atmospheres*, **106**(14): 14875–14885.
Cowling, E.B., 1982. Acid precipitation in historical perspectives, *Environmental Science and Technology*, **16**: 110A–123A.
Davies, S.J. and Unam, L., 1999. Dec06 smoke-haze from the 1997 Indonesian forest fires: effects on pollution levels, local climate, atmospheric CO concentrations, and tree photosynthesis. *Forest Ecology and Management*, **124**(2–3): 137–144.
Demerjian, K.L. and Schere, K.L., 1979. Applications of a photochemical box model for O_3 air quality in Houston, Texas. *Proceedings of specialty conference on ozone\oxidants: interactions with the total environment*. Research Triangle Park, NC: US Environmental Protection Agency.
Dodge, M.C., 1977. Combined use of modelling techniques and smog chamber data to derive ozone precursor relationships. *Proceedings of the international conference on photochemical oxidant pollution and its control, Vol. II*. Research Triangle Park, NC: US Environmental Protection Agency, pp. 881–889.
Draxler, R.R., Dietz, R., Lagomarsino, R.J., and Start, G., 1991. Across North America Tracer Experiment (ANATEX): sampling and analysis. *Atmospheric Environment*, **25A**: 2815–2836.
Finlayson-Pitts B.J. and Pitts, J.N., 1986. *Atmospheric Chemistry: Fundamentals and Experimental Techniques*. New York: Wiley.
Garratt J.R., 1992. *The Atmospheric Boundary Layer*. Cambridge: Cambridge University Press.
Gifford, F.A. and Hanna, S.R. 1973. Modelling urban air pollution. *Atmospheric Environment*, **7**: 131–136.
Girardi, F., Graziani, G., van Velzen, D., et al., 1998. *ETEX – The European Tracer Experiment.* Luxembourg: EUR 18143 EN, Office for the official publications of the European communities.
Guenther, A., et al., 1995. A global model of natural volatile organic compound emissions. *Journal of Geophysical Research*, **100**: 8873–8892.
Holzworth, G.C., 1974. *Climatological Aspects of the Composition and Pollution of the Atmosphere*. Technical Note No.139. Geneva: World Meteorological Organization.
Intergovernmental Panel on Climate Change (IPCC), 2001. *Third Assessment Report. Climate Change 2001: The Scientific Basis.* (Houghton, J. et al., eds.) New York: Cambridge University Press.
Khandekar, M.L., Murty, T.S., Scott, D., and Baird, W., 2000. The 1997 El Niño, Indonesian forest fires and the Malaysian smoke problem: a deadly combination of natural and man-made hazards. *Natural Hazards*, **21**(2–3): 131–144.
Jacobson, M.Z., 2000. *Fundamentals of Atmospheric Modelling.* Cambridge: Cambridge University Press.
Jacobson, M.Z., 2002. *Atmospheric Pollution: History, Science and Regulation.* Cambridge: Cambridge University Press.
Lettau, H., 1970. Physical and meteorological basis for mathematical models of urban diffusion. *Proceedings of symposium on multiple source urban diffusion models*. Air pollution control official publication No. AP86, US Environmental Protection Agency.
McKendry, I.G., Hacker, J.P., Stull, R., Sakiyama, S., Mignacca, D., and Reid, K., 2001. Long-range transport of Asian dust to the lower Fraser Valley, British Columbia, Canada. *Journal of Geophysical Research – Atmosphere*, **106**(D16): 18361–18370.
Oke, T.R., 1992. *Boundary Layer Climates.* Canada: Routledge.
Pasquill, F., 1974. *Atmospheric Diffusion,* 2nd ed., Ellis Horwood Ltd., England: Chichester.
Pielke, R.A., 2002. *Mesoscale Meteorological Modelling.* San Diego: Academic Press.
Schnelle, K.B. and Dey, P.R., 2000. *Atmospheric Dispersion Modeling Compliance Guide.* New York: McGraw-Hill.
Scire, J.S., Insley, E.M., and Yamartino, R.J., 1990. *Model Formulations and User's Guide for the CALMET Meteorological Model.* Concord, MA: Sigma Research Corp.
Seinfeld, J.H., 1986. *Atmospheric Chemistry and Physics of Air Pollution.* New York: Wiley-Interscience.
Seinfeld, J.H. and Pandis, S.N., 1998. *Atmospheric Chemistry and Physics: From Air Pollution to Climate Change.* New York: Wiley-Interscience.
Slade, D.H., 1968. *Meteorolgy and Atomic Energy 1968*. U.S. Department of Energy, Technical Information Centre, Oak Ridge, TN.
Stern, A.C., 1976. *Fundamentals of Air Pollution*. New York: Academic Press.
Stern, A.C., Boubel, R.W., Turner, D.B., and Fox, D.L., 1984. *Fundamentals of Air Pollution*. San Diego: Academic Press.
Stull, R.B., 1998. *An Introduction to Boundary Layer Meteorology*. Boston: Kluwer.
Sturman, A.P., 2000. Applied Climatology. *Progress in Physical Geography*, **24**: 129–139.
Turner, D.B., 1964. A diffusion model for an urban area. *Journal of Applied Meteorology,* **3**: 83–91.
Wanner, H.U., 1993. Sources of pollutants in indoor air. *IARC Science Publications,* **109**: 19–30.
Whiteman, C.D., 2000. *Mountain Meteorology*. New York: Oxford University Press.
Williamson, S.J., 1972. *Fundamentals of Air Pollution*. MA: Addison-Wesley, Reading.
World Health Organization (WHO) (2000) http://www.who.int.
Zannetti, P., 1990. *Air Pollution Modelling: Theories, Computational Methods and Available Software*. New York: Van Nostrand Reinhold.

Cross-references

Acid Rain
Aerosols
Inversion
Lapse Rate
Turbulence and Diffusion
Winds and Wind System

ALBEDO AND REFLECTIVITY

Albedo

Albedo is the percentage of solar radiation reflected by an object. The term is derived from the Latin *albus*, white. A pure white object would reflect all radiation that impinges on it and have an albedo of 100%. A pure black object would absorb all radiation and have an albedo of 0%. Bright Earth features such as clouds, fresh snow, and ice have albedos that range from 50% to 95%. Forests, fresh asphalt, and dark soils have albedos between 5% and 20%. Table A15 presents representative albedos for a variety of objects. Knowledge of albedo is important because absorbed solar radiation increases the amount of energy available to the Earth's surface and atmosphere, whereas reflected radiation returns to space.

Appreciation of the relation between albedo and climate extends historically to at least classical Greek times. P. Bouguer and J. Lambert first formulated the principles and theories by which albedo and reflectivity may be explained and measured in the eighteenth century, but accurate measurements did not begin until the early twentieth century (Fritz and Rigby, 1957). The work of early investigators, including A. Ångström, C. Dorno, N. Katlin, F. Götz, H. Kimball, and others, rapidly developed an extensive body of knowledge concerning albedos that is still drawn on today (see annotated bibliography by Fritz and Rigby, 1957). One of the more interesting approaches to early observations of the Earth's planetary albedo employed measurements of earthshine and sunshine on the moon (Danjon, 1936, cited in Fritz and Rigby, 1957). Similar efforts continue today (Goode et al., 2001). Use of aircraft and spacecraft as observing platforms has significantly expanded albedo studies in recent decades (Barrett, 1974; Brest and Goward, 1987; Schaaf et al., 2002).

Table A15 Albedos for selected objects

Water surfaces	
Winter:	
0° latitude	6
30° latitude	9
60° latitude	21
Summer:	
0° latitude	6
30° latitude	6
60° latitude	7
Bare areas and soils	
Snow, fresh-fallen	75–95
Snow, several days old	40–70
Ice, sea	30–40
Sand dune, dry	35–45
Sand dune, wet	20–30
Soil, dark	5–15
Soil, moist gray	10–20
Soil, dry clay or gray	20–35
Soil, dry light sand	25–45
Concrete, dry	17–27
Road, black top	5–10
Natural surfaces	
Desert	25–30
Savanna, dry season	25–30
Savanna, wet season	15–20
Chaparral	15–20
Meadows, green	10–20
Forest, deciduous	10–20
Forest, coniferous	5–15
Tundra	15–20
Crops	15–25
Cloud overcast	
Cumuliform	70–90
Stratus (500–1000 ft thick)	59–84
Altrostratus	39–59
Cirrostratus	44–50
Planets	
Earth	34–42
Jupiter	73
Mars	16
Mercury	5.6
Moon	6.7
Neptune	84
Pluto	14
Saturn	76
Uranus	93
Venus	76
Human skin	
Blond	43–45
Brunette	35
Dark	16–22

Source: After Sellers (1965).

Reflectivity

Reflectivity is the capacity of an object to reflect solar radiation. It is described as a function of radiation wavelength and is determined by the physical composition of the object. The adjective "spectral" is frequently used in conjunction with reflectivity to indicate that reflectivity varies as a function of solar wavelength.

Representative spectral reflectivity measurements for common Earth surface features are given in Figure A22. Soil reflectivity in general increases monotonically with increasing wavelength to about 1.3 μm and then decreases with sharp dips at 1.4 μm and 1.9 μm because of absorption by soil water. Living green vegetation reflectivity is low in the visible portion of the spectrum (0.4–0.7 μm) as a result of absorption by chlorophyll and related pigments, high in the near infrared (0.7–1.3 μm) because of light scattering by internal leaf cellular structures, and decreases past 1.3 μm in a manner similar to soils due to absorption by water within leaves. Snow is highly reflective in the visible and decreases to low values in the infrared, again as a result of water absorption. Water reflects little radiation in any portion of the spectrum when solar elevation is high.

Spectral reflectivity varies significantly for each surface type as a function of physical condition and composition. Soil reflectivity varies because of variations in moisture content, particle size, organic matter content, surface roughness and mineral composition. Figure A23 presents the variation of a silty loam soil reflectivity due to changes in moisture content. Vegetation reflectivity varies with percentage ground cover, canopy geometry, leaf size, and area and plant growth stage. Snow reflectivity varies with crystal size, compaction, age, and liquid water content. Water reflectivity is affected by turbidity, depth, and phytoplankton concentrations. Also, because water in its pure form is a dielectric, its albedo increases as the angle of incidence of radiation decreases. Water albedo is lowest when the sun is near zenith and increases to near 100% when the sun is near the horizon. (For further discussion see chapter 4, Kondrotyev, 1973; chapter 8, Miller, 1981). Other factors may affect the reflectivity of these surfaces, such as lichen crusts, and other materials such as rocks, and man-made materials (e.g. asphalt and concrete) also display unique spectral reflectivity patterns.

Relation of reflectivity to albedo

Albedo is the integrated product of incident solar radiation spectral composition and the spectral reflectivity of the object. Outside the atmosphere, solar radiation spectral composition is relatively constant, peaking at about 0.5 μm, decreasing rapidly at shorter wavelengths to small amounts at 0.2 μm, and decreasing less rapidly at longer wavelengths to small amounts at about 4.0 μm.

The atmosphere selectively absorbs and scatters solar radiation. As a result, at the Earth's surface the spectral composition of solar radiation varies significantly as a function of atmospheric conditions (e.g. clouds, water vapor, and dust) and solar elevation (Robinson, 1966; Dickinson, 1983). The majority of albedo measurements have been carried out under clear-sky, high-sun elevation conditions (Table A15). Under cloudy conditions radiation is predominantly in the visible spectrum. This decreases the albedos of soils and vegetation but increases snow albedo (Miller, 1981). When atmospheric turbidity is high, or the sun is low in the sky, the spectral distribution of solar radiation shifts to the red and infrared portion of the spectrum. Soil and vegetation albedos increase and snow albedo decreases (Kondrotyev, 1973). This variability points out the need to know both the spectral reflectivity of objects and the spectral composition of incident radiation in order to evaluate earth albedos.

Surface and planetary albedos

Two global albedo measurements are of general interest to climatologists: surface and planetary albedos. Surface albedo is

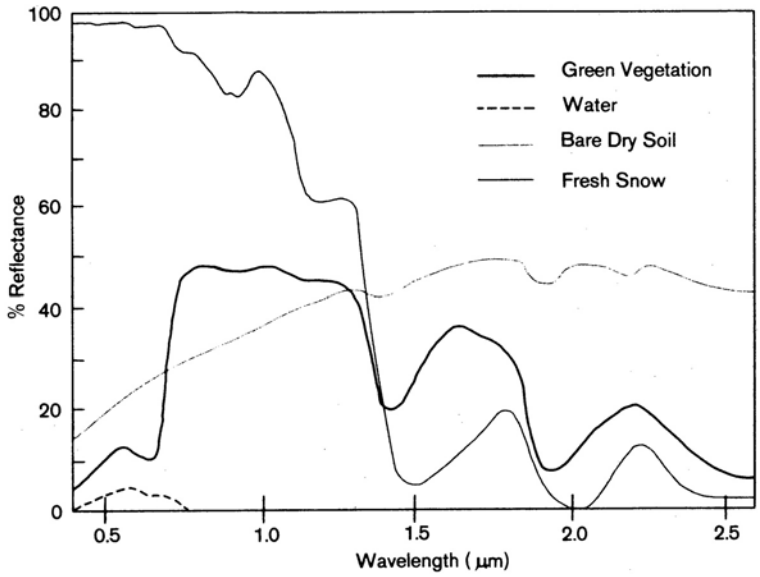

Figure A22 Spectral reflectance of selected Earth surface features.

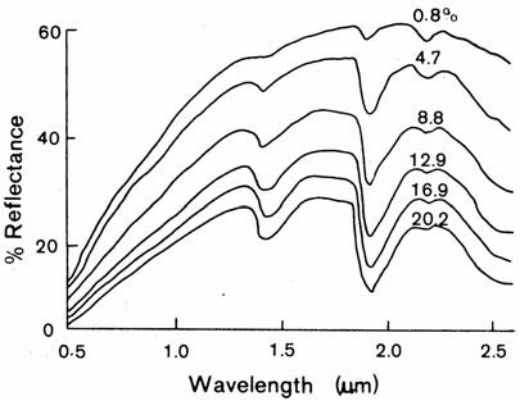

Figure A23 Variations of silty loam soil spectral reflectance as a function of water content (percentage water content shown by each plot) (after Kondrotyev, 1973).

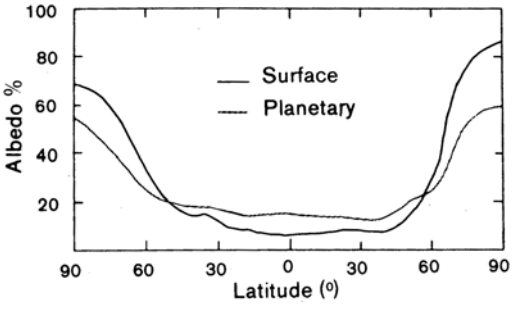

Figure A24 Latitudinal variations in surface and planetary albedo (after Hummel and Reck, 1979).

the ratio of incident to reflected radiation at the interface between the atmosphere and the Earth's land and water areas. Almost 75% of all solar energy absorbed by the Earth is absorbed at this interface; the remainder is absorbed in the atmosphere (Sellers, 1965). Any change in surface albedo will alter climate by significantly changing the amount of solar energy absorbed by the planet. Several studies have evaluated the Earth's surface albedo with resultant estimates ranging between 13% and 17% (Sellers, 1965; Kondrotyev, 1973; Hummel and Reck, 1979; Briegleb and Ramanathan, 1982). This range of results is suggestive of current limitations in knowledge of the distribution and reflectivity of Earth surface features.

Planetary albedo is the ratio between incident and reflected radiation at the top of the atmosphere, also referred to as "Bond" albedo, named after the astronomer who first described this metric. It includes the effects of reflection from the atmosphere, particularly clouds, and surface albedo. Only about 6% of the incident radiation is reflected by scattering in the atmosphere but, on average, 24% of incident radiation is reflected by clouds (Sellers, 1965). Changes in atmospheric turbidity or cloud cover can alter climate by changing the amount of solar radiation that reaches the Earth's surface. Studies of the Earth's planetary albedo have been carried out over the past 60 years (Barrett, 1974). Barrett notes that estimates have progressively decreased from 50% in early studies to current estimates between 30% and 35%, based on satellite estimates. He suggests that this trend is due to improved knowledge of global cloud cover. However, the possibility of inter-annual and longer-term variations in planetary albedo should not be overlooked (Rossow and Zhang, 1995).

Geographic patterns

Both surface and planetary albedos increase with distance from the equator (Figure A24). Surface albedo shows a slight minimum at the equator because of dense evergreen forest and a

secondary minimum at 40°S latitude because of the large extent of open ocean at this latitude. Increases at 25° to 30° north and south result from the presence of subtropical deserts with relatively high albedos (>40%). At higher latitudes the seasonal or permanent occurrence of snow cover and sea ice raise average albedos, which are in excess of 60% in the polar regions. The latitudinal patterns of planetary albedo are less extreme than the surface trends. Two factors affect this difference. Tropical and midlatitude land areas that are vegetated are in latitudes of frequent cloud occurrence. Contrasts between vegetated and desert latitudes are thus less apparent in the planetary figures. In addition, interactions between surface albedo and atmospheric scattering and absorption tend to reduce albedo differences between the tropics and the poles. Where surface albedo is high, the reflected radiation passes back and forth through the atmosphere many times, increasing absorption both at the surface and in the atmosphere. Over regions of low albedo, scattering in the atmosphere increases planetary reflectance when compared to surface albedos (Hummel and Reck, 1979).

Measurements

Traditionally, two pyranometers, one pointed toward the sky, the other toward the surface, have been used to measure albedos. Pyranometers are solar radiation measurement devices that respond thermally to record the amount of radiation incident on the device. They are designed to absorb all wavelengths of solar radiation equally (Sellers, 1965). In the late 1960s, photoelectric detectors, such as silicon cells, became widely used for albedo and spectral reflectance measurements (Dirnhirm, 1968). The advantage of photon detectors is that they respond quickly to changes in incident radiation and thus permit high-resolution measurements, particularly from aircraft and spacecraft (Barrett, 1974; Justice and Townshend, 2002). One limitation of photon detectors is that they are sensitive to restricted spectral ranges. Silicon, for example, senses only wavelengths between 0.5 μm and 1.0 μm. Measurements must be either compensated for in those portions of the solar spectrum not observed, or two or more different detectors must be used. However, ease of use in the field and in aircraft and spacecraft has significantly increased their use for albedo measurements.

Human effects on Earth's albedo

Recently investigators have suggested that human modifications of the Earth's surface, accompanying continued expansion of urbanization, agriculture and forestry, may be altering the planet's albedo. For example, Otterman (1977) showed that overgrazing in desert regions can increase surface albedo by as much as 20%. Charney (1975) estimated that such changes may suppress rainfall, which would enhance the process of "desertification" that is occurring in sub-Saharan Africa. Sagan et al. (1979) proposed that extensive deforestation in tropical rainforests may significantly increase surface albedo and result in major climate changes. Such change may influence local climatic conditions, but global assessment suggests that such human changes to the Earth's land area contribute only slightly to possible global albedo changes (Henderson-Sellers and Gornitz, 1984).

Samuel N. Goward

Bibliography

Barrrett, E.C., 1974. *Climatology from Satellites*. London: Methuen.

Brest, C.L., and Goward, S.N. 1987. Deriving surface albedo measurements from narrow band satellite data. *International Journal of Remote Sensing*, **8**(3): 351–367.

Briegleb, B., and Ramanathan, V., 1982. Spectral and diurnal variations in clear sky planetary albedo. *Journal of Applied Meteorology*, **21**: 1160–1171.

Charney, J., 1975. Dynamics of deserts and drought in the Sahel, *Quarterly. Journal of the Royal Meteorological Society*, **101**: 193–202.

Dickinson, R.E., 1983. Land surface processes and climate-surface albedos and energy balance. *Advances in Geophysics*, **25**: 305–353

Dirnhirm, I., 1968. On the use of silicon cells in meteorological radiation studies. *Journal of Applied Meteorology*, **7**: 702–707.

Fritz, S., and Rigby, M., 1957. Selective annotated bibliography on albedo. *Meteorological. Abstracts and Bibliographies*, **8**: 952–998.

Goode, P.R., Qui, J., Yurchyshyn, V., et al., 2001. Earthshine observations of the earth's reflectance. *Geophysical Research Letters*, **28**(9): 1671–1674.

Henderson–Sellers, A., and Gornitz, V., 1984. Possible climatic impacts of land cover transformations, with particular emphasis on tropical deforestation. *Climatic Change*, **6**: 231–257.

Hummel, J.R., and Reck, R.A., 1979. A global surface albedo model. *Journal of Applied Meteorology*, **18**: 239–253.

Justice, C.O., and Townshend, J.R.G., 2002. Special Issue: The moderate resolution imaging spectrometer (MODIS): a new generation of land surface monitoring. *Remote Sensing of Environment*, **83**(1-2): 1–359.

Kondrotyev, K. Ya., ed., 1973. *Radiation Characteristics of the Atmosphere and the Earth's Surface*, V. Pondit (trans.). New Delhi: Amerind.

Miller, D.H., 1981. *Energy at the Surface of the Earth.* International Geophysics Series, vol. 27. New York: Academic Press.

Otterman, J., 1977. Anthropogenic impact on albedo of the Earth. *Climatic Change*, **1**: 137–155.

Petzold, D.E., and Goward, S.N., (1988) Reflectance spectra of Subarctic lichens. Remote Sensing of Environment, **24**: 481–492.

Robinson, N., 1966. *Solar Radiation*, New York: Elsevier.

Rossow, W.B., and Zhang, Y.-C., 1995. Calculation of surface and top of atmosphere radiative fluxes from physical quantities based on ISCCP data sets: 2. Validation and first results. *Geophysical Research*, **100**: 1167–1197.

Sagan, C., Toon, O.B., and Pollock, J.B., 1979. Anthropogenic albedo changes and the Earth's climate. *Science*, **206**(4425): 1363–1368.

Schaaf, C.B., Gao, F., Strahler, A.H., et al., 2002. First operational BRDF, albedo and nadir reflectance products from MODIS. *Remote Sensing of Environment*, **83**: 135–138.

Sellers, W.D., 1965. *Physical Climatology*. Chicago: University of Chicago Press.

Cross-references

Cloud Climatology
Energy Budget Climatology
Snow and Snow Cover

ALEUTIAN LOW

This is a low-pressure area over the Pacific Ocean that reflects the average position of a depression that formed on the western side of the North Pacific, developed into maturity over the Aleutian Islands, and then decayed over North America. It is located in the central part of the North Pacific and is associated with the subpolar low-pressure belt.

The Aleutian Low, in conjunction with its changing relationship with the North Pacific (Hawaiian) High in the eastern part of the Pacific Ocean, is the major feature of the general circulation controlling the weather over parts of North America. It is

a semipermanent "center of action" of persistently lower pressure where barometric pressure of less than 1013 mb (29.92 in) prevails and where higher humidity and relatively higher temperatures for that latitude are common. In an analogous fashion to the Icelandic Low in the North Atlantic, the Aleutian Low is an area of average low pressure that reflects the frequent passage of cyclonic storms that migrate along the polar front from the continents that lie to the west (Akin, 1991). Consequently, the area is very stormy, with frequent strong winds, cloudy conditions, damp weather, and abundant precipitation.

The position of the Aleutian Low does change during the year. Beginning in November and continuing through February, the expanded low averages about 1002 mb (29.59 in). This causes migrating storms to move well into Mediterranean regions to the south more often as winter continues. In March the low diminishes slightly in intensity and migrating storms are less frequent by April. By July the low has virtually disappeared, showing up only as a trough extending from Kamchatka across central Alaska. By September the cycle starts again, as the low begins to form over the Bering Sea, leading to increasing disturbances.

Christoforou and Hameed (1997) studied the location of the Aleutian Low and found its location was highly correlated with mean annual sunspot numbers. When solar activity is at a minimum during its 11-year cycle the Aleutian Low migrates eastward.

Robert M. Hordon and Mark Binkley

Bibliography

Ahrens, C.D., 2003. *Meteorology Today: An Introduction to Weather, Climate, and the Environment*, 7th edn. Brooks/Cole (Thomson Learning).

Akin, W.E., 1991. *Global Patterns: Climate, Vegetation, and Soils.* Norman, Oklahoma: University of Oklahoma Press.

Barry, R.G., and Chorley, R.J., 2003. *Atmosphere, Weather, and Climate*, 8th edn. London: Routledge.

Christoforou, P., and Hameed, S., 1997. Solar cycle and the Pacific "centers of action". *Geophysical Research Letters*, Washington, DC: American Geophysical Union, **24**(3): 293–296.

Curry, J.A., and Webster, P.J., 1999. *Thermodynamics of Atmospheres and Oceans.* San Diego, California: Academic Press.

Graedel, T.E., and Crutzen, P.J., 1993. *Atmospheric Change: An Earth System Perspective.* New York: Freeman.

Hartmann, D.L., 1994. *Global Physical Climatology.* San Diego, California: Academic Press.

Lutgens, F.K., and Tarbuck, E.J., 2004. *The Atmosphere: An Introduction to Meteorology*, 9th edn. Upper Saddle River, New Jersey: Pearson Prentice Hall.

Nese, J.M., and Grenci, L.M., 1998. *A World of Weather: Fundamentals of Meteorology*, 2nd edn. Dubuque, Iowa: Kendall/Hunt.

Oliver, J.E., and Hidore, J.J., 2002. *Climatology: An Atmospheric Science,* 2nd edn. Upper Saddle River, New Jersey: Pearson Prentice Hall.

Robinson, P.J., and Henderson-Sellers, A., 1999. *Contemporary Climatology*, 2nd edn. Harlow, Longman.

Wallace, J.M., and Hobbs, P.V., 1997. *Atmospheric Science: An Introductory Survey.* San Diego, California: Academic Press.

Cross-references

Airmass Climatology
Atmospheric Circulation, Global
Centers of Action
Icelandic Low
Zonal Index

ANGULAR MOMENTUM, ANGULAR VELOCITY

An important physical concept appropriate to a rotating globe such as a planet, angular momentum is defined as the moment of the linear momentum of a particle about a point, thus:

$$M = \vec{r} \times m\vec{V}$$

where M is the angular momentum about a point 0, $\vec{r}$ the position vector from 0 to the particle, m the mass of the particle and $\vec{V}$ the velocity.

Angular momentum plays an important role in both the Earth's rotation and the coupling of the solid earth to the atmosphere. The speed of rotation (angular velocity) of the Earth varies only by small amounts, and these may be related in part to angular momentum lost to or received from the atmosphere. The atmospheric circulation patterns are modified by these energy transfers. The Earth's angular velocity is the speed of its rotation about the geographic pole, thus its pole of instantaneous rotation, and not with reference to a point in space. The angular velocity is approximately 2π/S or sidereal day of 86 164.09 seconds, roughly 24 hours, or 15.04106863 seconds of arc per second of time.

As Rossby (1940) explained it, the Earth's angular momentum can easily be visualized by taking a marble on the end of a string and rotating it on a smooth table. If the string is shortened the rate increases; if lengthened it slows. The speed is inversely proportional to radius, the product of the two remaining constant. This product, the angular momentum per unit mass, is a constant unless energy is added or subtracted (Newton's Law of Conservation of Momentum, his "first law of motion").

If part of the atmospheric envelope, rotating with the Earth at the equator at a speed of 465 m/s, moves poleward it will tend to speed up. At latitude 60° the radius (distance from axis of rotation) being reduced to half that at the equator, would indicate that the linear velocity of the Earth's surface would be reduced to 232 m/s. However, a frictionless atmosphere here (of the same mass, but halved radius) should be accelerated to double its original velocity, thus 930 m/s, but the relative speed would be higher, the Earth's surface linear velocity here being reduced by 232 m/s, the resultant relative ground speed of the atmosphere being 698 m/s (1560 mph); the direction would be easterly, since the Earth's sense of rotation is from west to east. The velocity would also be reduced owing to friction, etc. In the upper atmosphere high-velocity easterlies are often observed, but they are far from universal, being replaced by westerlies under the influence of frictional and differential heating, thermodynamic phenomena.

The easterlies have the effect of removing angular momentum from the Earth. If they were the only planetary winds they would cause a gradual deceleration of the Earth. The westerlies, however, compensate and, traveling faster than the Earth, impart angular momentum to it (through friction). The westerlies thus lose angular momentum to the Earth, and they would die out if they had no powerful source of energy. From one or possibly both sides of the westerly belts, large eddies such as cyclones and anticyclones set up by the shears of the westerlies, and in lesser degree by thermodynamic processes, bring in the necessary momentum to keep the westerlies in motion.

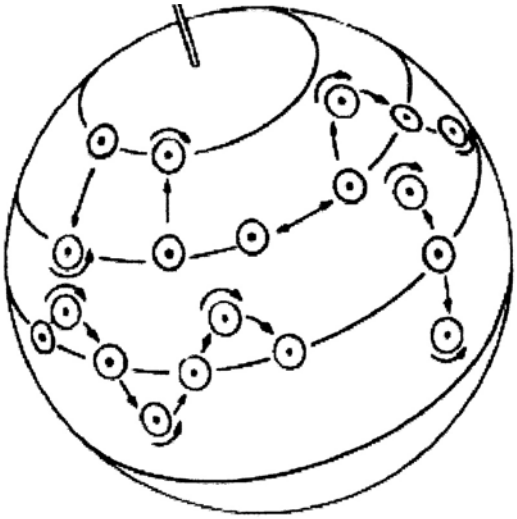

Figure A25 Planetary vorticity: angular momentum tends to be conserved in columns of constant height as they change latitude along different trajectories (from Von Arx, 1962; by permission of Addison-Wesley, Reading, MA).

An additional important principle, illustrated in Figure A25, is the conservation of angular momentum in any parcel of air (or water) as it changes latitude.

Rhodes W. Fairbridge

Bibliography

Barry, R.G. and Chorley, R.J., 1998. *Atmosphere, Weather, and Climate*, 7th edn. London: Routledge.

Clough, H.W., 1920. The principle of angular momentum as applied to atmospheric motion, *Monthly Weather Review*, **45**(8): 463.

Goody, R., 1995. *Principles of Atmospheric Physics and Chemistry.* New York: Oxford University Press.

McIlveen, R., 1992. *Fundamentals of Weather and Climate*. London: Chapman & Hall.

Nese, J.M., and Grenchi, L.M., 1998. *A World of Weather: Fundamentals of Meteorology*, 2nd edn. Dubuque, Iowa: Kendall Hunt.

Robinson, P.J., and Henderson-Sellers, A., 1999. *Contemporary Climatology*, 2nd edn. Harlow: Longman.

Rossby, C.G., 1940. Planetary flow patterns in the atmosphere. *Quarterly Journal Royal Meteorological Society*, **66**: 68–87.

Thompson, R.D., 1998. *Atmospheric Processes and Systems*. London: Routledge.

Von Arx, W.S., 1962. *An Introduction to Physical Oceanography.* Reading, MA: Addison-Wesley.

Wallace, J.M., and Hobbs, P.V., 1997. *Atmospheric Science: An Introductory Survey*. San Diego, CA: Academic Press.

Widger, W.K., 1949. A study of the flow of angular momentum in the atmosphere. *Journal of Meteorology*, **6**: 291.

Cross-references

Atmospheric Circulation, Global
Jet Streams
Vorticity
Zonal Index

ANTARCTIC CLIMATES

Introduction

Climate and the polar regions

Ice plays a critical role in polar climate (Bintanja, 2000). In contrast with lower latitudes, the high albedo and low thermal conductivity of snow cover and ice (sea ice, floating ice shelves, continental ice sheets) have associated negative values of the surface radiation budget (e.g. Nakamura and Oort, 1988). Accordingly, low temperatures occur at the surface and in the free atmosphere in polar regions, and the troposphere has low thickness and tends to be barotropic. The low average temperatures mean a low water-holding capacity of the air, realized as low precipitation amounts annually (i.e. "polar desert"). Because of the atmosphere's extreme static stability over ice-covered surfaces, clouds and precipitation tend not to be generated *in situ*; rather, they are advected in from lower latitudes by frontal cyclones. This poleward movement of moisture is a consequence of the inflow of energy into polar regions necessitated by the net-radiation deficit. Although these climatic characteristics are common to both polar regions on Earth, there are physical geographic major differences between the Arctic and Antarctic, manifest in their respective climates. Most notably, surface and free-air temperatures, along with cloud amounts, average lower in the Antarctic than the Arctic (Weller, 1982).

The Antarctic versus the Arctic

Whereas the Arctic is a landlocked ocean covered most of the year by sea ice, Antarctica is a polar continent upon which rests a thick ice sheet. The ice sheet rises to over 3000 m in East Antarctica (Figure A26), with a small area ("pole of inaccessibility") exceeding 4000 m. Moreover, Antarctica is surrounded by the Southern Ocean: the only interruption to the zonal configuration of the continent occurs in the Antarctic Peninsula (AP). The extreme continentality results from the high elevation of the ice sheet and the continent's isolation from other land masses (Carleton, 1992). In contrast, the Arctic is linked directly with middle latitudes via North America and Eurasia. The greater longitudinal variation of land and sea in boreal regions is expressed as a more meridional average pattern of the tropospheric waves and, accordingly, with enhanced transport of heat and momentum by the waves occurring between middle and high latitudes (van Loon, 1979). Over Antarctica the air is often poorly mixed, especially in austral winter and spring. This promotes a colder circumpolar vortex compared with that in the Arctic, and largely is responsible for the more extensive and intense stratospheric "ozone hole" of southern high latitudes.

Antarctica virtually doubles its own area between the early fall and spring because of the growth of sea ice (Figure A27). This large annual increase in sea ice occurs because, unlike the Arctic Ocean, the equatorward margin of Antarctica is unconstrained by land, and because atmospheric and oceanic mean circulations are relatively zonal (Carleton, 2003a). Interannual variations of Antarctic sea-ice conditions (its latitude extent, ice-water concentration) are most pronounced regionally (Parkinson, 1992), impacting the surface temperatures and precipitation. In addition to its negative feedback with surface

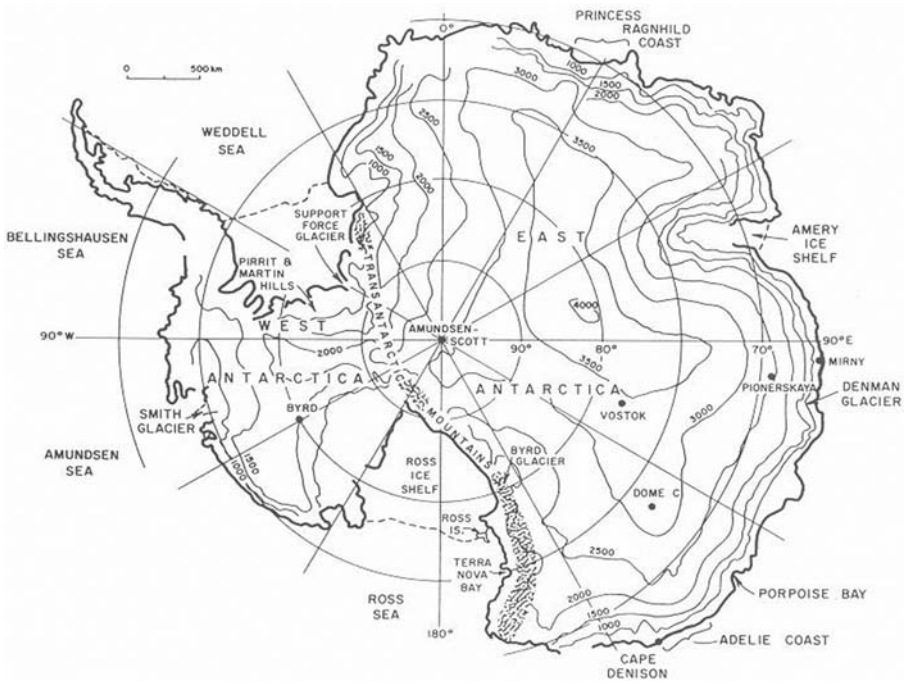

Figure A26 Map of Antarctica showing major physical geographic features (coastline, Antarctic seas, mountain ranges, ice-shelf margins, ice-sheet contours) and locations of selected permanent manned bases (named). (From Parish and Bromwich, 1991.)

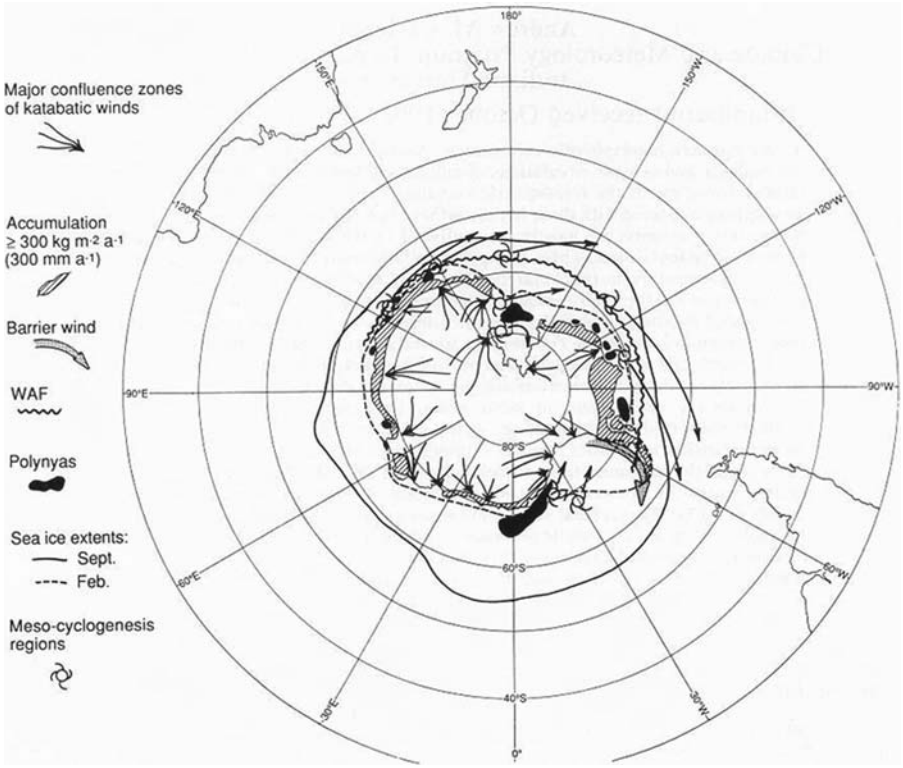

Figure A27 Schematic summarizing important features of Antarctic-region climate (side legend), as derived from multiple sources (map reoriented with respect to that appearing in Figure A26). (From Carleton, 1992.)

temperature, the sea ice extent influences snowfall in coastal areas: the increasing distance between the moisture source (Southern Ocean) and the coast that occurs as sea-ice extent increases during fall and winter, reduces snowfall amounts. Sea ice–climate interactions manifest fluctuations in atmospheric circulation that include shifts in the preferred "storm tracks" of synoptic cyclones, as modulated by lower-frequency climatic teleconnections. The latter involve particularly the "Antarctic Oscillation" (AAO) and El Niño Southern Oscillation (ENSO).

Developments in Antarctic climatology

Major advances have occurred in our understanding of Antarctic meteorology and climatology since the first *Encyclopedia of Climatology*, "Antarctic Climates" item was written 20 years ago. In that time the major developments have been as follows:

1. Improvements in the routine observational network. For the surface, automatic weather stations (AWS) provide data on pressure, temperature and winds, as frequently as every 15 minutes, and their spatial density has increased since 1980, especially in the Ross Sea area. AWS data have been used to improve the representation of 500 hPa height fields over the continent via the atmospheric thickness relationship (Phillpot, 1991); to characterize temperature–sea-ice extent associations locally (Carleton et al., 1998); and to better determine the surface energy balance (Reijmer and Oerlemans, 2002). Satellite retrievals of climate variables additional to those acquired by visible and infrared sensors, include scatterometer-derived near-surface winds over ice-free ocean, ice-sheet altitude and topography from radar altimetry, surface "skin" temperatures and sea ice extent and concentration, including open-water leads and polynyas, from microwave radiometers; stratospheric ozone from atmospheric sounders; and upper-ocean biological activity from shortwave narrow-band sensors. Crucial in these developments has been the establishment of satellite direct-readout facilities on the continent, and the ability to include Antarctic data in global real-time synoptic analyses. Thus, our understanding of Antarctic contemporary climates comes from an array of data sources; some conventional, some remotely sensed, yet with different lengths of record.
2. Advances in numerical modeling of Antarctic climates; not just using atmospheric General Circulation Models (GCM) but also coupled ocean-ice–atmosphere models (e.g. Hall and Visbeck, 2002). In particular, mesoscale meteorological models developed for middle-latitudes are now applied to polar environments (e.g. Polar MM5: Guo et al., 2003). More reliability can be placed in modeling the following features of Antarctic climate: the impacts of changes in sea-ice conditions on atmospheric circulations in the southern extratropics (Raphael, 2003a); the important role of ice-sheet topography and local sources of heat and moisture associated with coastal polynyas, for the surface katabatic winds and cold-air mesoscale cyclone systems (*mesocyclones*) generated in coastal regions of Antarctica (van den Broeke and van Lipzig, 2003); and understanding how the ENSO signal is expressed in Antarctica. These studies confirm that Antarctica interacts actively with lower latitudes, and even may influence climate in parts of the northern hemisphere at certain times of year (Hines and Bromwich, 2002).
3. Development of longer-term archives of daily synoptic analyses for higher southern latitudes, as compiled from operational analyses of the Australian Bureau of Meteorology (ABM) and the European Centre for Medium-Range Weather Forecasts (ECMWF), for studying the circulation climates of higher southern latitudes. More recently, the application of automated techniques for tracking cyclones and anticyclones in these data has greatly extended our understanding of Antarctic-region synoptic climatology (e.g. Simmonds et al., 2003). Reanalysis data sets – meteorological fields generated by an analysis/forecast model that is fixed rather than changing through time, and in which all available data are included – particularly are illuminating Antarctic-region circulation climate (Pezza and Ambrizzi, 2003). Composite studies of synoptic phenomena using reanalysis data have identified the typically occurring circulation environments of mesocyclones, explosively deepening cyclones, and extremely strong wind events (Carleton and Song, 1997; Murphy, 2003). However, reanalysis datasets are not equally reliable for climate change studies: the NCEP-NCAR reanalyses of SLP generally are considered inferior to those of the ERA (ECMWF reanalyses) over southern high latitudes.
4. Dedicated intensive observing periods and special monitoring programs to study Antarctic-region weather and climate. In the mid-1990s a concerted effort to better depict and understand Antarctic synoptic meteorology and climatology was realized with the FROST (First Regional Observing Study of the Troposphere) project (Turner et al., 1999). An outgrowth of FROST was the drive to develop an updated long-term climatology of surface and free-atmosphere conditions for the Antarctic manned stations as part of the SCAR (Scientific Committee for Antarctic Research) READER (Reference Antarctic Data for Environmental Research) project. Stringent quality control of the observation data acquired by the nations which are signatories to the Antarctic Treaty, is permitting the reliable determination of annual and seasonal trends and changes in climate. For longer time scales, recent scientific traverses, particularly the shallow ice cores drilled in West Antarctica as part of ITASE (International Trans-Antarctic Scientific Expedition), are permitting an assessment of climatic variability and changes over about the last two centuries at mesoscale spatial resolutions.
5. Improved determination of the variability (spatial, temporal) of Antarctic surface energy budgets, over both sea ice and continental ice. These have involved shipboard measurements in the sea ice zone, as well as satellite remote sensing (Wendler and Worby, 2001).
6. Refinements in depicting the spatial patterns and temporal variability of variables significant to the ice sheet mass balance (Vaughan et al., 1999); notably, precipitation and the near-surface katabatic winds (Guo et al., 2004).
7. Application of newer analytical and statistical techniques to determining the links between coarse-resolution climate data, such as mapped fields of geopotential height generated from reanalyses or GCM, and local climate conditions (i.e. "downscaling") (Reusch and Alley, 2002). These methods include artificial neural networks and "self-organizing maps".
8. Development of satellite-image based "climatologies" of mesocyclones for several genesis key regions around Antarctica. Moreover, there is a realization that these storms

are important for the snowfall and wind climatologies of coastal areas and embayments. Accordingly, attempts are being made to more accurately forecast these developments.

9. The addition of another 20 years' data has permitted identification of temporal trends and longer-term changes in Antarctic climate (atmospheric variables, sea ice conditions, ocean temperatures)). In particular, opposing trends of surface temperature between the AP and the rest of Antarctica have become evident (see "Antarctica and global change", below).
10. A realization that Antarctica is not isolated from the weather and climate processes of extratropical latitudes, or even the northern hemisphere. Rather, Antarctica is intimately connected with other places via atmospheric teleconnections, primarily the ENSO.
11. Identification and characterization of the dominant modes of variability (subseasonal, interannual, subdecadal) in the atmospheric circulation of higher southern latitudes, and links with the upper ocean circulation. These modes include particularly the ENSO, but also the AAO, the "Pacific–South America" (PSA) pattern, and an "Antarctic Circumpolar Wave" (ACW) that was discovered in the mid-1990s.

Accordingly, this revised item emphasizes particularly the above-noted developments in Antarctic climatology.

Antarctica and global climate change

Documenting Antarctic-region climate and its temporal variations has taken on increased urgency in recent decades, in the context of "global change". The following climate trends and changes, and their possible global associations, have spurred the increased monitoring of Antarctic weather, climate, biology, glaciology, and oceanography, particularly using satellites (e.g. Schneider and Steig, 2002).

1. "Global warming". This is likely to be evident earliest in polar regions, owing to "ice–albedo feedback". The latter involves a positive link between reduced snow/ice extent associated with warming, greater absorption of solar radiation by the surface, and continued warming. With respect to Antarctica, the following have been observed: a strong warming trend in the AP over the past several decades (Harangozo et al., 1997), especially in winter (van den Broeke, 2000a), that has been accompanied by reduced sea-ice extent west of the AP; the recent retreat and collapse of ice shelves such as Larsen-B on the eastern AP (Vaughan and Doake, 1996); an observed freshening of the upper ocean in the Ross Sea that suggests increased precipitation and/or melting from the West Antarctic ice sheet (Jacobs et al., 2002); and a subsurface warming concentrated within the Antarctic Circumpolar Current (ACC) (Gille, 2002). GCM studies (e.g. Wu et al., 1999) support a close link between recent climate warming and observed sea ice changes in Antarctica that mostly involve reduced ice–water concentration.
2. Stratospheric ozone depletion over the Antarctic in austral spring is a major contributor to global-scale reductions of ozone. Moreover, interannual variations in high-latitude circulation affect the configuration, spatial extent, intensity, and seasonal persistence of the ozone hole (e.g. Thompson and Solomon, 2002). The increased receipt of ultraviolet radiation in higher southern latitudes during spring and summer has deleterious consequences for organisms, including humans (e.g. Jones et al., 1998). In regions of Antarctica where cooling has occurred, a physical link with ozone depletion via the AAO has been proposed (e.g. Sexton, 2001).
3. The observed role of larger-scale atmospheric circulation patterns and their teleconnections for interannual variations and recent changes in climate over extrapolar as well as polar latitudes. These include surface temperature trends and summer melt periods linked to the AAO (Torinesi et al., 2003), and the sensitivity of the Antarctic ice sheet's mass balance to fluctuations in moisture transport, especially in the Pacific sector, where there is a strong ENSO signal (Bromwich et al., 2000).
4. Since the mid- to late-1970s the change in the dominant Semi-Annual Oscillation (SAO) of climate variables, especially SLP, temperature and precipitation in sub-Antarctic latitudes and coastal Antarctica, has been accompanied by warming in the tropical Pacific and cooling over large areas of the ice sheet (Hurrell and van Loon, 1994). For the same period the ozone hole worsened.
5. The strong interactions glimpsed between biological productivity in the Southern Ocean, and circulation–climate variations expressed as changes in sea surface temperature (SST), sea ice extent, and zonal wind speed.
6. The role of Antarctica in long-term global-scale climate changes (glaciations, deglaciations), via its influence on the deep-water ocean circulation. Moreover, contemporary climate processes in the Antarctic appear crucial influences on deep water formation; notably via the polynyas and leads of coastal and sea ice areas generated by strong offshore (katabatic) winds, and by the spin up of polar mesocyclones (see Figure A27). Mesocyclones extract large amounts of energy from the upper ocean, increasing the salinity and density of the water, which then sinks to great depths (Carleton, 1996).

Antarctic climate(s)

No single "Antarctic climate" can be identified (e.g. Bintanja, 2000). Regional ice–atmosphere interactions change markedly with latitude, elevation, season, and exposure to heat and moisture sources (either from open ocean or within the sea ice zone), and with the passage of synoptic systems (Schwerdtfeger, 1984). The seasonal sea ice zone (SSIZ) near maximum extent is considerably further equatorward than the Antarctic Circle, but it remains relatively close to the continent in longitudes south of Australia (Figure A27). The AP frequently exhibits a pattern of climate variability different to that of the rest of Antarctica (Rogers, 1983). The influence of the southern polar region in the global oceanic and climatic environment demands a broad definition, so here "Antarctica" is taken to include the continent and its ice shelves, the SSIZ, and the adjacent ocean area including the ACC (see Figure A26). A discussion of the radiation and energy climates of these higher southern latitudes, and their influence on the atmospheric circulation, is given below in the context of the general circulation, as well as synoptically and subsynoptically. Accordingly, regional variations in these climatic factors are also discussed.

Radiation climates and the energy balance

The radiation balance is the principal climate-causing factor (World Meteorological Organization, 1967) in the Antarctic,

where there are strong seasonal variations in solar radiation as well as variations in elevation and surface characteristics. The high reflectivity of the surface (i.e. surface albedo) means that very little insolation is absorbed; thus keeping surface temperatures low all year. Satellite monitoring (visible, infrared, microwave) provides synoptic information on variables crucial to an accurate determination of the radiation balance, such as the extent, thickness and concentration of sea ice; accurate albedo measurements, and cloudiness. For modeling the surface energy balance, these satellite data augment ground-level observations.

Surface energy balance equation

The energy balance equation for unit horizontal area at Earth's surface is:

$$Q^* = K\downarrow (1-\alpha) + L^* = Q_H + Q_E + Q_G$$

Where $K\downarrow$ = global (direct plus diffuse) solar radiation; α = albedo, or fraction of shortwave reflected; L^* = net longwave radiation ($L\downarrow - L\uparrow$) (where $L\downarrow$ = atmospheric downward and $L\uparrow$ the terrestrial upward); Q_H = turbulent transfer of sensible heat; Q_E = turbulent transfer of latent heat (E = evaporation); Q_G = subsurface heat flux through ice, soil, or water. The conductive flux (Q_G) approximates to zero on an annual basis. Over snow- or ice-covered surfaces the radiative fluxes dominate the turbulent convective terms of Q_H and Q_E. However, over ice-free ocean or areas of low sea-ice concentration or small ice thickness within the pack, the convective terms become important, at least locally.

Solar radiation ($K\downarrow$)

The global radiation ($K\downarrow$) varies from virtually zero in mid-winter south of the Antarctic Circle to values comparable to the highest on Earth over the ice sheet in December and January. The high summer insolation is due to lack of clouds, elevation of the Antarctic plateau, a highly transmissive (low aerosol and water vapor content) atmosphere, 24 hours of daylight, and the occurrence of perihelion. These high values are not reduced much even by periods of cloud cover; a decrease in the direct (clear-sky) component is more or less balanced by an increase in the diffuse radiation.

Annual total received solar radiation is relatively high over the continent, particularly for East Antarctica, but decreases over the pack ice zone to a minimum over the sub-Antarctic oceans. This gradient is due to the increasing cloudiness associated with traveling cyclonic systems and proximity to the Antarctic Circumpolar Trough, ACT (see "Climatic variables; Cloudiness", below).

Albedo

The Antarctic experiences an annual negative net radiation balance largely due to high surface albedo. Albedo values are highest over the permanent snow cover of the continental interior, where around 83% of the incident solar radiation is reflected, and lowest over the ocean (around 11%). Over the coastal sea ice and pack ice zones the albedo is strongly dependent on the presence of meltwater (low α), the presence of snowcover (increases α), and the amount of open water that includes substantial polynyas (Wendler and Worby, 2001). Wendler et al. (1997a) found that midsummer values of albedo for 10/10 ice cover averaged 59%, but with hourly values increasing to 76% where snow covered. Average values of albedo for 5/10 ice concentration were around 30%.

Although the surface albedo increases generally with latitude, the greater cloudiness over sub-Antarctic oceans modulates the effect of short-term variations in sea–ice concentrations on the planetary albedo. Over the continent, determination of cloud amount from space is difficult and leads to large discrepancies in computed solar radiation budget if not constrained using available surface observations (Hatzianastassiou and Vardavas, 2001). In summer the maximum variation in surface albedo occurs at about latitudes 60–70°S (78%), where it is dominated by the change from open water to ice cover. Seasonally, this constitutes about a 60% change in albedo. Between latitudes 80°S and 90°S the annual range does not exceed 10%.

Net longwave radiation (L^*) and the Antarctic inversion

The net longwave radiation (L^*) at the surface is a function of surface and atmospheric temperatures, and of the downward radiation from clouds, water vapor and aerosols. L^* is uniformly negative at the surface over southern high latitudes in winter. In summer there are large differences between the continent and peripheral oceans (50–60°S), due mainly to cloud cover effects. Increasing cloud cover tends to increase L^* over the ice sheet because $L\downarrow$ becomes more important over high albedo surfaces. Over sea ice, L^* varies due both to cloud amount and the ice–water concentration ($L\uparrow$ is reduced with increasing ice cover, Table A16). Satellite observations of the outgoing longwave radiation at the top of the Antarctic atmosphere show strong negative values in both summer and winter.

The intense radiational cooling and highly transmissive atmosphere produce a persistent low-level temperature inversion that reaches its greatest depth over the higher elevations of the ice sheet, where it is present almost the entire year (Schwerdtfeger, 1984). The inversion is no stronger at the end than at the beginning of the polar night, because an equilibrium is reached between $L\uparrow$ (decreases as surface temperature falls), and $L\downarrow$ from the atmosphere above the inversion layer, which changes relatively little with time. Combined with the slope of the ice surface, the semipermanent inversion is the source of the persistent katabatic winds (Connolley, 1996). A clearly defined time for the occurrence of the inversion maximum temperature is absent in the Antarctic, comprising the "coreless winter". This feature is evident for surface temperatures (T_s) at the Antarctic stations, including the AWS. This is because the rapid radiational cooling begun in the fall is arrested and, in many years, reversed in winter. Changes in the tropospheric longwave

Table A16 Mean outgoing longwave radiation ($L\uparrow$) and surface temperature (T_s) for different Antarctic sea-ice concentrations, from shipboard observations in the period 24 December, 1994 to 6 January, 1995

	Ice concentration in tenths		
	0–4	4–7	7–10
$L\uparrow$ (W m^{-2})	292	287	276
T_s (°C), for $\epsilon = 0.97$[a]	−3.2	−4.4	−7.0

[a] ϵ = emissivity.
Source: After Wendler et al. (1997a).

Table A17 Mean fluxes of energy budget (EB) components for interior Adélie Land, Antarctica, in the period 20 November–22 December 1985. Values are expressed in $W\,m^{-2}$ and percent, and are positive (negative) toward (away from) the surface. Q_B replaces Q_G and is the snow heat flux. I = imbalance (3.4%), resulting from measurement errors

	EB components					
	K^*	L^*	Q_H	Q_E	Q_B	I
Heat balance: ($W\,m^{-2}$)	+72	−70	+9	−9	−5	+3
Percent	86	84	10	10	6	3

Source: After Wendler et al. (1988).

pattern between early winter and midwinter, and the consequent poleward movement of warmer air, help explain this temperature feature, which comprises part of the Semi-Annual Oscillation (SAO) of SLP and tropospheric height (see "Climatic variables; Temperature").

Net (all-wave) radiation (Q^*) and energy balance

For the South Pole, Carroll (1982) estimated that 85–90% of the winter deficits of Q^* (i.e. the net "all-wave" radiation, or net shortwave minus net longwave) are made up of sensible heat (Q_H) losses. Table A17 summarizes the energy budget over Adelie Land in East Antarctica, for the period 20 November–22 December 1985, emphasizing the importance of the radiation terms. In the coastal ablation zone, Q^* is positive from late September through late February. Q^* becomes slightly positive over much of the Antarctic interior around the time of maximum solar elevation, due to increased cloud cover and a downward flux of Q_H.

The annual deficit of Q^* necessitates a net influx of energy to Antarctica. This occurs primarily as eddy sensible heat advected by frontal cyclone systems migrating into high latitudes. Because the amplitudes of southern hemisphere planetary waves are reduced, on average, compared with their northern hemisphere counterparts, the waves themselves transport relatively little sensible heat into the Antarctic. Instead, the remainder of the heat transport is carried out by the ocean, whereby divergence (convergence) of air in the near-surface wind field occurs on the western (eastern) side of a standing tropospheric trough, promoting upwelling of cold (downwelling of warm) water.

Turbulent exchange and the role of sea ice in the energy balance

Seasonal and interannual variations in sea ice conditions (areal extent, ice–water concentration, presence/absence of snow cover, ice-edge latitude) profoundly influence the surface energy budget and climate. The sea ice cover modulates the oceanic fluxes of heat to the atmosphere, and thereby its own thickness (Wu et al., 2001). The average thickness of Antarctic sea ice is around 1 m or so in late winter, except where deformation occurs and it reaches thicknesses of up to 4 m. During the 1990s, which was broadly representative of the longer period 1978–2000, a trend to increased Antarctic sea–ice extent accompanied reduced ice–water concentration.

Close to the continent the sea ice tends to have higher concentration and a longer seasonal duration than further out. Moreover, when sea ice is advected equatoward (poleward) by winds and the ocean circulation, it undergoes divergence (convergence), which leads to increasing ice extent and decreasing ice concentration (decreasing ice extent and increasing ice concentration). These associations are evident particularly in the major embayments, notably the Weddell Sea, and on interannual time scales (Carleton, 1988; Turner et al., 2002b). Anomalies of this type appear related to the AAO and the ENSO). Additionally, the presence of low ice-concentration areas and open-water leads and polynyas can significantly influence the local to regional-scale climate (e.g. as increased cloud cover and precipitation). This occurs owing to the enhanced oceanic heat losses to the atmosphere as Q_H and Q_E, especially in winter. Then these fluxes can be at least one order of magnitude greater than those of adjacent areas of higher sea ice concentration.

Table A18 summarizes the radiation and energy fluxes for a ship transect through variable sea ice conditions in Antarctic longitudes of the Tasman Sea during summer (Wendler et al., 1997a). In addition to showing the very strong contribution of the radiative fluxes to the surface energy balance, and of the ocean as a heat sink, these results reveal that the fluxes of Q_H and Q_E are of approximately similar magnitude but opposite sign: Q_H is a source of energy to the surface, Q_E is a sink. In late winter, as sea ice concentration decreases below about 50%, the convective fluxes change relatively little compared with those from open ocean (Worby and Allison, 1991).

Climatic variables

Temperature

Setting the surface energy balance to zero determines the equilibrium T_s. Mean winter T_s of −60°C to −70°C occurs on the highest areas of the ice sheet. Maps of mean T_s (Figure A28) indicate that the cold pole is displaced into East Antarctica, both in January and July (Borisenkov and Dolganov, 1982). There is a general decrease of temperature with latitude, especially evident in the AP. Considerable interannual variability of

Table A18 Summary of radiation and energy fluxes ($W\,m^{-2}$) through the Antarctic sea ice for the period 24 December, 1994 to 6 January, 1995 (variable ice concentrations). Note the dominance of the radiative fluxes. As in Table A17, the fluxes are positive (negative) toward (away from) the surface. Q_B = ocean or ice heat flux or phase changes

	EB components						
	$K\downarrow$	$K\uparrow$	$L\downarrow$	$L\uparrow$	Q_H	Q_E	Q_B
Average fluxes	241	−93	252	−285	11	−17	−109
			$Q^* = 115$				
Percent of sources (+) or sinks (−)		+91.3%			+8.7%	−13.5%	−86.5%

Source: After Wendler et al. (1997a).

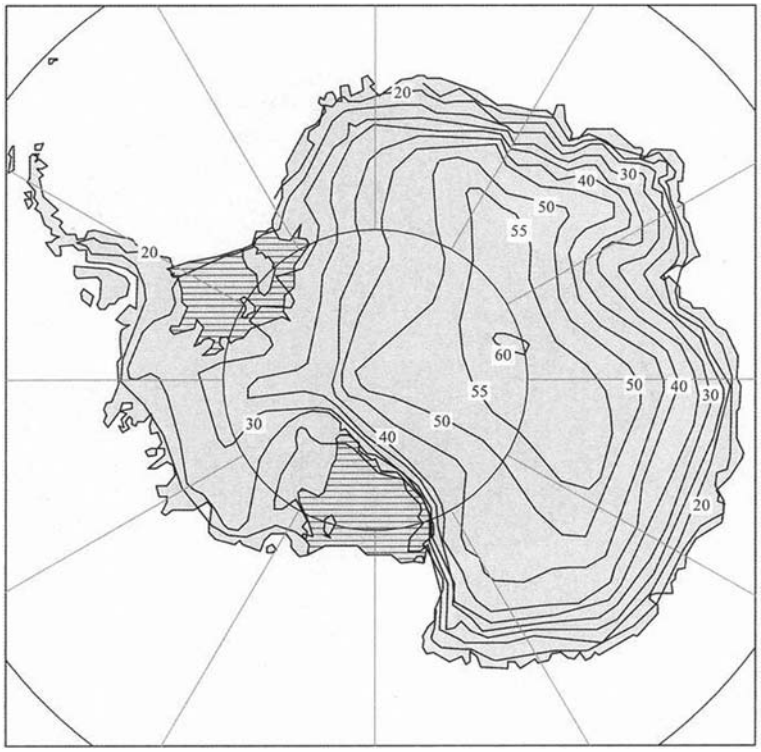

Figure A28 Map showing mean annual near-surface temperature field for Antarctica, synthesized from surface observations; isotherms in degrees below 0°C. (From Guo et al., 2004.)

T_s occurs, notably along the western AP and for stations south of the ACC (60–70°S) because of their position within the SSIZ (the temperature gradient in the latter zone increases to above 1°C/1° latitude in winter, compared with about 0.6°C/1° latitude between 30°S and 60°S). Some of the interannual variability of temperature is related to ENSO (Schneider and Steig, 2002). SST gradients are steepest in the vicinity of the ACC, comprising an Ocean Polar Front (OPF), but strong thermal gradients also border the continent, particularly in winter. On average the meridional strong gradients of temperature near the surface disappear in the mid-troposphere (van Loon et al., 1972).

Trends in Antarctic temperatures are evident over the past several decades. Although the sign and magnitude of recent temperature trends differ somewhat by study and the method of spatially extrapolating the sparse data (cf. Doran et al., 2002; Turner et al., 2002b), a strong warming of the AP region (winter on western side, summer on eastern side) is evident in many studies. The winter warming has been accompanied by decreases in sea ice extent and reduced concentration to the westward, suggesting the importance of ice–ocean–air positive feedbacks. Synoptically, warm (cold) winters in the AP are associated with a greater (reduced) frequency of northerly wind components as the Amundsen–Bellingshausen Sea mean low pressure intensifies (weakens). These SLP patterns also resemble those connected with the tropical ENSO and its teleconnection to higher southern latitudes occurring via the Pacific–South America (PSA) pattern (see "Circulation variations and climatic teleconnections; The El Niño Southern Oscillation (ENSO) in Antarctica").

In contrast to the recent warming of the AP, a cooling over much of the continent has coincided with lowering pressures in the ACT, strengthening westerlies over sub-Antarctic latitudes, and greater sea ice extent on average. These are associated with a trend toward more positive values of the AAO.

The dominant SAO in the annual march of temperature – and related changes in wind, pressure, geopotential height and precipitation – over sub-Antarctic latitudes and coastal Antarctica, produces gradient maxima in the equinoctial (March, September) months. The SAO results primarily from the tropospheric radiative imbalances between middle and high latitudes, which are at a maximum around the equinoxes. Also, a SAO has been detected in the latitude of the speed maximum of the ACC (Large and van Loon, 1989).

The atmospheric SAO is involved in the annual patterns of sea ice freeze-up and melt (Enomoto and Ohmura, 1990), as well as ice–water concentration (Watkins and Simmonds, 1999), via its interactions with the latitude location of the ACT and associated patterns of easterly (westerly) low-level winds occurring to the south (north) of this feature. In summer and early fall, when the ACT lies equatorward of the ice edge, easterly winds produce convergence of the pack, resulting in little increase in ice area despite the lowering surface temperatures. However, as the ACT shifts poleward of the ice edge in March, westerly winds to the north encourage ice divergence and a relatively rapid expansion of the pack through the winter and early spring. In December and January the ACT again lies north of the ice edge, which has melted back as temperatures have risen. The associated easterly winds encourage compaction of the ice pack and its retreat to higher latitudes.

There has been a climate change in the SAO since the mid-1970s to late 1970s (Hurrell and van Loon, 1994; Simmonds and Jones, 1998), involving primarily a shift in the springtime phase from September and early October into November. This change has coincided with strengthened latitude gradients of temperature originating mostly from a warming in the tropical Pacific, possibly associated with more frequent El Niño events (Mo, 2000); reduced sea-ice extent in the Amundsen–Bellingshausen seas (van den Broeke, 2000b), but significant cooling in coastal East Antarctica in early winter (van den Broeke, 2000a). At least part of the increased severity of the ozone hole over the past two decades likely is related to the longer isolation of the southern circumpolar vortex in austral spring, accompanying this change in the SAO.

Cloudiness

Satellite-observed cloud cover is at a maximum (80–100%) over ocean higher latitudes adjacent to the pack ice zone, varies little with the season, and is due to traveling cyclonic storms (see "Synoptic processes; Synoptic cyclone activity", below). Manned observing station data indicate a cloudiness minimum over the interior plateau (Figure A29 Borisenkov and Dolganov, 1982), especially in midwinter (less than about 25%), and generally low seasonal variability. Maximum cloud cover variability occurs at Antarctic coastal stations located between these two zones (van Loon et al., 1972), arising from higher rates of alternation of high- and low-pressure systems. The contribution of lower cloud to the total cloud amount reaches a maximum over coastal regions and the pack ice zone (cyclonic), and a minimum over interior East Antarctica where subsidence of air dominates. In recent decades, cloudiness in the spring and summer seasons has increased by about 15–20% at the South Pole. These increases appear to be associated with changes in the high-latitude circulation.

Precipitation

Snowfall dominates precipitation in the Antarctic. However, the contribution of clear-sky precipitation (e.g. "diamond dust") and blowing snow to the ice sheet mass balance, increases in importance over the higher, colder and dryer regions of the interior (Giovinetto et al., 1990). The mass balance is the result of precipitation, evaporation, direct deposition (rime, frost), drifting, and runoff from melting at low elevations (Figure A30). Snow drift represents a net loss from the continent to the coastal sea ice zone. Although our confidence in measurements of Antarctic continental T_s and pressure is reasonably high, it remains low for precipitation. This results from a lack of data and the difficulty of separating real precipitation from drifting snow, especially in katabatic wind-prone areas. Accordingly, indirect estimates of Antarctic precipitation have been more forthcoming. These compute the net surface mass balance as $P - E$, where P = precipitation and E = sublimation, from moisture fluxes directed toward the continent. Recently, model calculations of precipitation have been undertaken. The decrease of precipitable water, relative humidity, and precipitation with increasing latitude, together with increasing distance from the Southern Ocean moisture

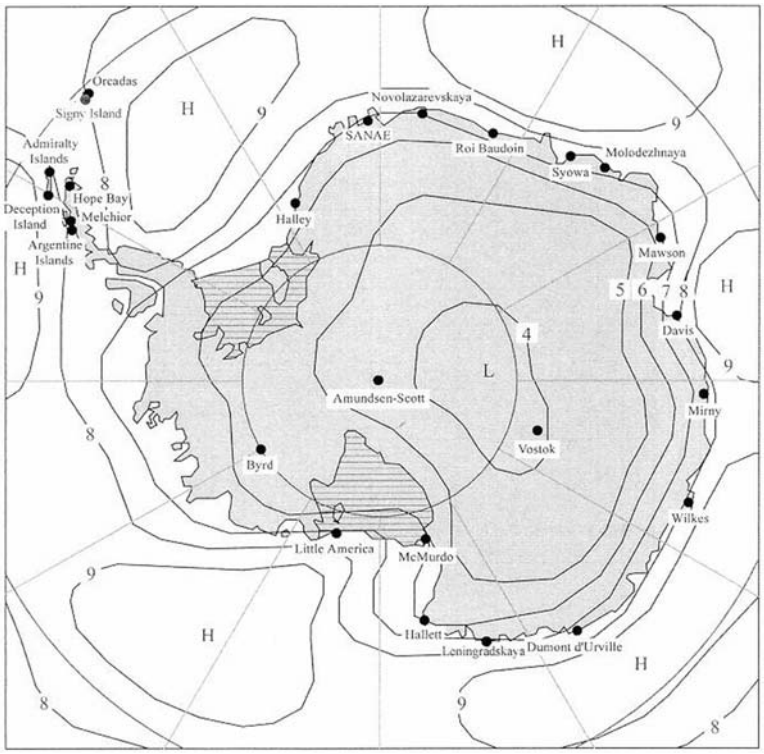

Figure A29 Map showing mean annual total cloud cover from station observations (dots show observation sites used for the compilation); cloud cover isopleths in tenths. (From Guo et al., 2004.)

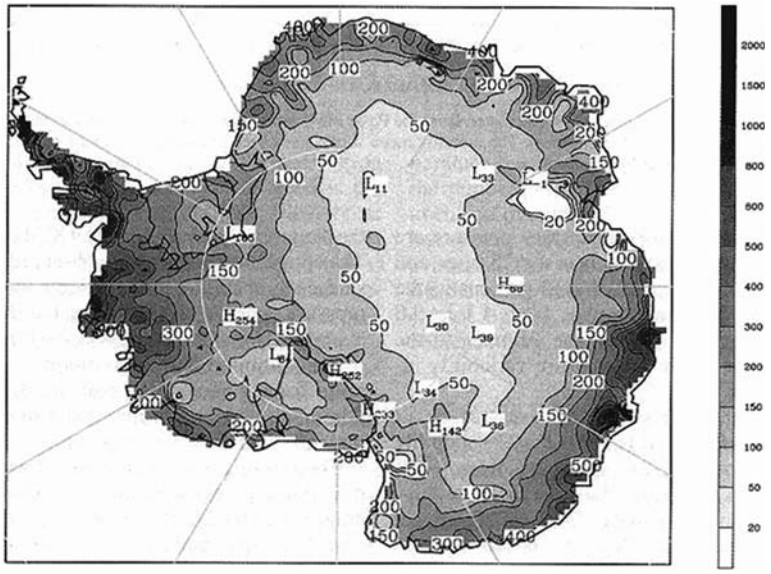

Figure A30 Map showing long-term accumulation distribution; units of mm yr^{-1}. (From Guo et al., 2004.)

source, means that annual precipitation on the high plateau is less than about 2 cm yr^{-1} water equivalent. This increases by up to at least 2 orders of magnitude at the coast (Figure A30). The lower elevations of West Antarctica facilitate moisture transport into the interior, mostly by synoptic cyclones.

Interannual variations of coastal precipitation are high, in response to high variability of cyclonic activity, especially along the western AP where they manifest fluctuations in the intensity of the Amundsen–Bellingshausen mean low pressure. The latter has an ENSO component (Guo et al., 2004). There has been a statistically significant upward trend in precipitation averaged over the continent between 1979 and 1999, although weakly downward trends are evident regionally and in the interior.

Surface winds

The surface wind is a persistent katabatic (downslope) flow that is gravitational and thermal in origin, relatively shallow (100–200 m deep), and essentially decoupled from the synoptic gradient flow above. It dominates the annual wind speed and direction at many stations in West Antarctica and coastal East Antarctica (Borisenkov and Dolganov, 1982; Figure A31). At Cape Denison the mean annual windspeed exceeds 20 m s^{-1}, which is the strongest on Earth close to sea level (Wendler et al., 1997b). Extremely high wind speeds can persist for weeks or even a month or two, especially in winter. In summer, solar radiation absorption reduces the katabatic effect (van den Broeke and van Lipzig, 2003). Katabatic winds are important because they produce snowdrift and enhance coastal polynyas and sea ice production (Adolphs and Wendler, 1995), thereby affecting the surface mass and energy budgets. Also, katabatic winds promote mesoscale cyclogenesis in confluence areas near the coast (e.g. Heinemann, 1990; Bromwich, 1991; see Figure A27). Streten (1968) found that katabatic winds are best developed in coastal regions with little synoptic cyclone activity, but with generally lower pressure located to the eastward. However, individual synoptic events may enhance the katabatic winds at certain coastal locations. Modeling suggests that synoptic forcing may not be important in determining these winds over interior East Antarctica. There, they can be explained adequately from consideration of the topography (i.e. channeling effect) and the intensity of the wintertime inversion (Connolley, 1996). The katabatic winds are a critical component of the atmosphere's meridional circulation for southern higher latitudes and are linked to the intensity of the circumpolar vortex in the mid- to upper-troposphere. Katabatic winds may even participate in high latitude–tropical interactions on subseasonal time scales (Yasunari and Kodama, 1993).

Winds on the eastern side of the AP and the western Weddell Sea comprise a strong and persistent southwest to southerly flow, or *barrier wind* (see Figure A27). This wind is important for advecting ice equatorward into the westerly wind belt, thereby maintaining lower air temperatures in the southern South Atlantic than at comparable latitudes in the southeast Pacific (Schwerdtfeger, 1975, 1979). The barrier wind results from very cold and stable air that moves westward over the Weddell Sea, is dammed up against the eastern side of the AP, and sets up a thermal gradient similar to that forcing the katabatic wind. This explanation does not require the presence of a semipermanent low pressure in the Weddell, although such a feature often exists and may enhance the barrier wind (Figure A32). Interannual fluctuations in the intensity of the Weddell Sea low, some of which are ENSO-related (Yuan and Martinson, 2001), are strongly evident in the sea ice conditions of the embayment (Turner et al., 2002a).

Large-scale atmospheric circulation

Mean surface pressure and 500 hPa height fields

The essential features of the atmospheric circulation around the Antarctic have been known since at least the International Geophysical Year (IGY) of 1957–1958 (e.g. Lamb, 1959; van Loon et al., 1972). Mean monthly height, temperature, and wind

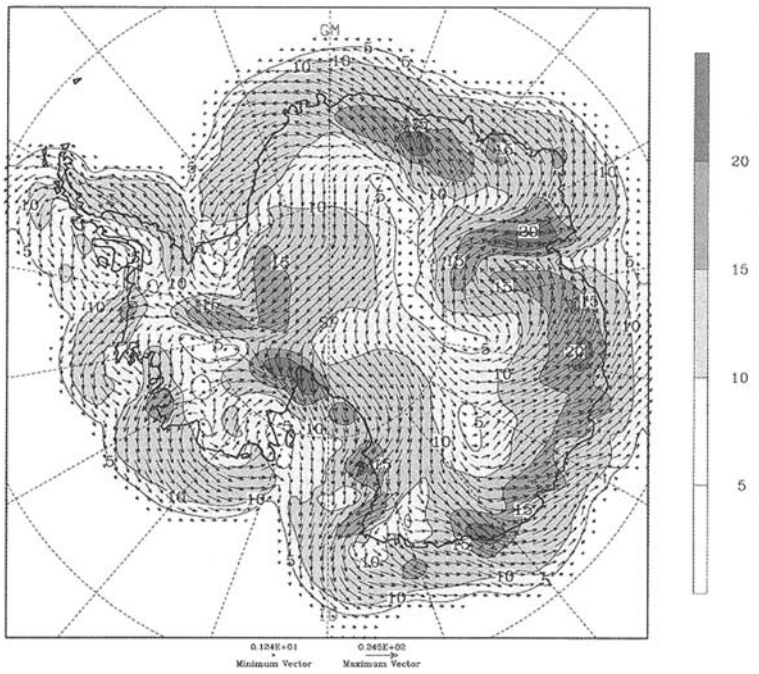

Figure A31 Antarctic near-surface winds for winter; units of $m\,s^{-1}$. (From Guo et al., 2004.)

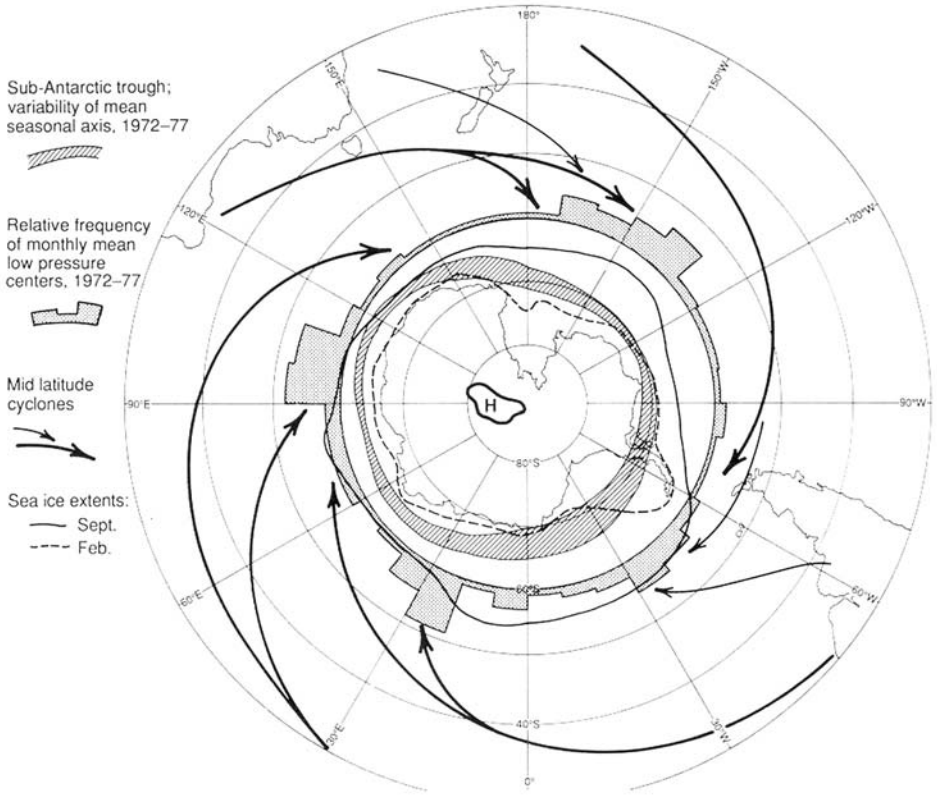

Figure A32 Schematic summarizing dominant features of the synoptic climatology of southern higher latitudes (side legend), compiled from multiple sources (map has similar orientation to that in Figure A27). (From Carleton, 1992.)

fields at different tropospheric levels are available in atlas form (see van Loon et al., 1972), and have been summarized by Schwerdtfeger (1984). Synoptic and dynamic climatologies of the higher latitude circulation derived from the ABM, ECMWF, and other datasets, largely confirm the IGY studies, although greater detail is now known for previously data-void ocean areas (the South Pacific). In addition, much more is known of the circulation variability on interannual and decadal time scales.

The dominant features of the SLP field of southern high latitudes are a thermal anticyclone over the continent (Figures A32 and A33), although this feature is somewhat artificial owing to the method of reducing pressures to sea level. An almost continuous belt of low pressure (the ACT) around the continent and pack ice zone has well-defined centers located near the major Antarctic embayments, and also off Wilkes Land in East Antarctica (Figure A33a,b). The Amundsen– Bellingshausen mean low (ASL) comprises a "pole of maximum variability" in the SLP field (Connolley, 1997). Modeling experiments suggest that the strong interannual variability of the ASL is explained by the displacement of Antarctica's highest elevation areas toward the Indian Ocean (Lachlan-Cope et al., 2001).

The mean lows of the ACT are the summation of individual synoptic cyclones moving in from middle latitudes (Figure A32), and represent areas of stagnation and cyclolysis (Carleton, 1979; Simmonds et al., 2003). However, recent satellite-based studies show that these "cyclone graveyards" are often active sites for mesoscale cyclones forming in cold-air outbreaks just to the westward (e.g. Carleton and Song, 1997). The SLP has lowered over Antarctica since the mid-1970s to late 1970s as the surface and troposphere has cooled. This trend comprises part of the AAO teleconnection pattern.

Although the ACT undergoes little variation in intensity between summer and winter (Figure A33a,b), its latitudinal position changes markedly in connection with the SAO: more equatorward in the solsticial (January, July) months, and closer to Antarctica in the equinoctial (March, September) months. Also, the broad zonality of the Antarctic mean circulation undergoes quite marked meridionality on individual (daily) analyses, especially in the South Pacific. High-pressure ridges frequently interrupt the ACT (see Taljaard, in van Loon et al., 1972). Favored longitudes for ridges are in East Antarctica between 0–15°E, 50–60°E, and 140–150°E. The last location particularly is important in blocking events, which typically are more prevalent during ENSO warm phases (i.e. El Niño) (Marques and Rao, 2000).

In the free atmosphere the Antarctic is dominated by a circumpolar westerly vortex that expands equatorward in winter. Lowest heights (and layer thicknesses, or mean temperatures) occur over the ice sheet, and there is evidence that the intensity of this feature is coupled to the katabatic winds. On average the whole vortex is displaced slightly toward the Indian Ocean sector, or wave number 1 pattern. However, a three-wave pattern of tropospheric troughs and ridges also often occurs (Figure A32), especially during blocking events, with a trough over each of the three major ocean basins (e.g. Kiladis and Mo, 1998). In contrast to their counterparts in the northern hemisphere, the tropospheric waves have low amplitude and their positions do not change much from season to season. Interannual variations of wave number 1 occur preferentially toward either the Australian region or the Falkland Islands, with accompanying large variations in sea-ice conditions in the Scotia Sea (Carleton, 1989). This mode of variability is described by a Trans-Polar Index (TPI), which is based on the SLP anomalies at Hobart and Stanley (Pittock, 1984). However, the negative relationship of SLP between these two places is not stable in the long term (Carleton, 1989). Temporal changes in the tropospheric waves are confirmed from NCEP-NCAR reanalyses (Raphael, 2003b), showing that the largest changes have occurred since about 1975 in the southern late fall through early spring, and from the Indian Ocean eastward to the Weddell Sea.

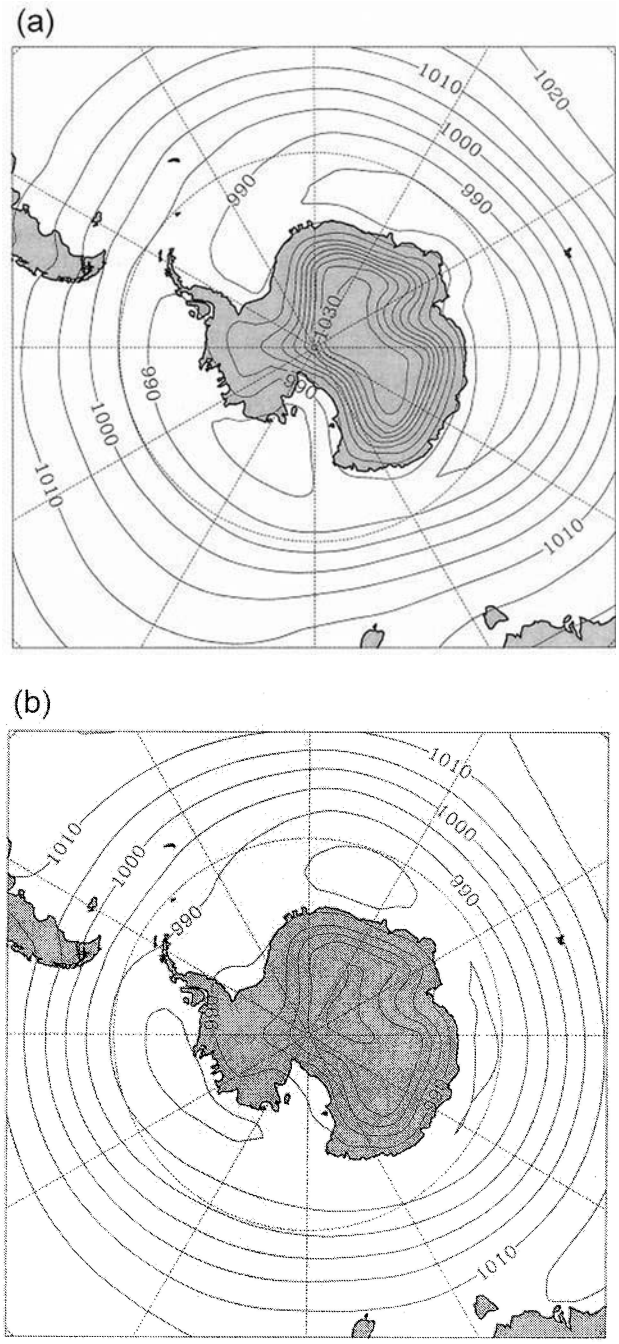

Figure A33 Mean sea level pressure (SLP, contour interval of 5 hPa) derived from NCEP-NCAR reanalyses for **(a)** winter, June through August, of 1979–1999; and **(b)** summer, December through February, of 1980–2000. (From Simmonds et al., 2003.)

Zonal circulation

In accordance with the limited summer-winter variation in the wave pattern (see "Mean surface pressure and 500 hPa height fields", above), there is little seasonal change in the intensity of the zonal westerlies at 500 hPa in middle and high latitudes (Trenberth, 1979). However, there is marked interannual variability, especially in the Pacific sector, where it is dominated by the ENSO – westerly zonal winds in adjacent broad latitude zones vary out-of-phase, or so-called "split jet" flow (Bals-Elsholz et al., 2001). During ENSO warm events the STJ (PFJ) tends to be stronger (weaker) (Figure A34); but in cold, or La Niña events, the STJ (PFJ) is weaker (stronger). These variations modify the momentum and heat transports, as well as storm tracks, over southern middle and higher latitudes. However, it is important to note that there is considerable variability of the above-noted patterns within a given phase of ENSO, especially the El Niño events.

Synoptic indexes long have been used to characterize the zonal atmospheric circulation in the southern extratropics (e.g. the TPI). These are constructed using SLP observations for station pairs across widely separated latitudes (zonal index) or longitudes (meridional index). Indexes of this type capture the SAO in near-surface SLP, and confirm the recent change in the AAO to a more positive (i.e. increased zonality) mode. The increased strength of the southern westerlies that occurs between fall and spring occurs concurrently with the expansion of the sea ice (Ackley, 1981); also, greater zonal wind variability tends to accompany increased variability of the ice. Similarly, between-year regional variations of the ice near maximum extent accompany changes in the zonal index which, in turn, are related to patterns of higher latitude cyclonic activity and the teleconnection patterns of AAO and ENSO (Carleton, 1989; Renwick, 2002).

Synoptic processes

Air masses and air streams

The Antarctic ice sheet is the source region for extremely cold, dry and stable Antarctic continental (cA) air year round (Wendland and McDonald, 1986). It is recognized as inversion air only over the continent and ice shelves because it transforms

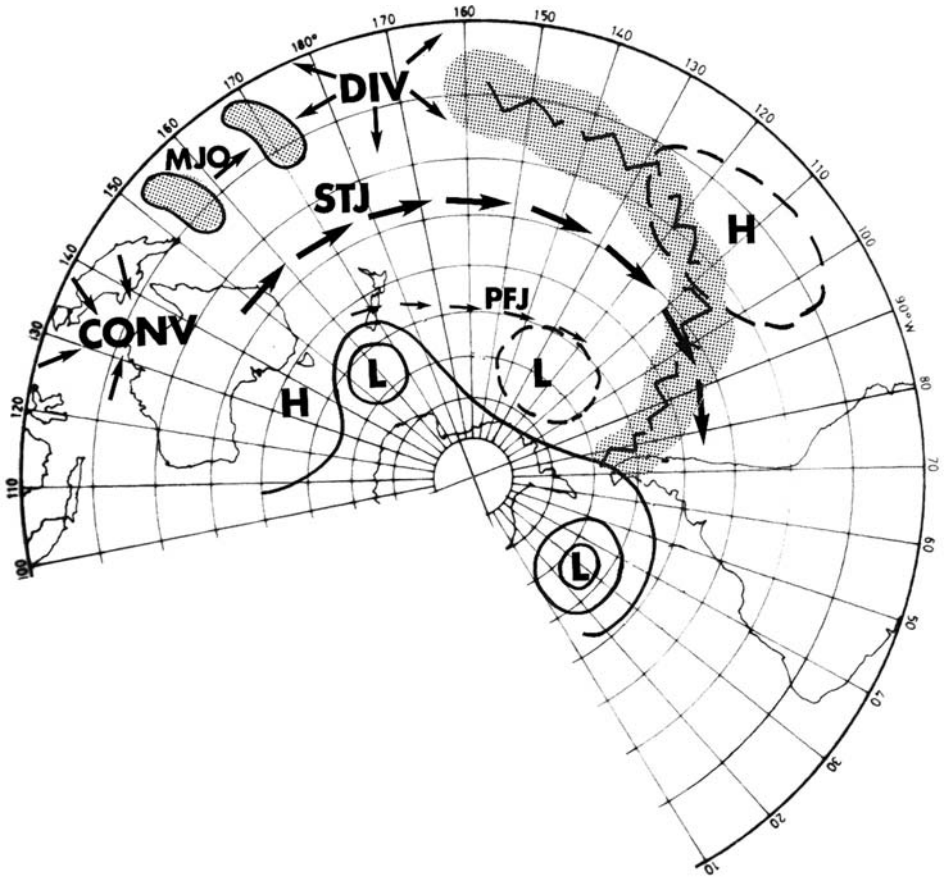

Figure A34 Schematic showing the dominant changes in mid- to upper-tropospheric circulation over the Pacific and southwest Atlantic sectors that accompany a warm (El Niño) event. Features over lower latitudes (MJO: Madden–Julian Oscillation, SPCB: South Pacific Cloud Band) mostly are representative of the summer season. Those over middle and higher latitudes (STJ, PFJ, pressure/height anomalies) apply to the winter season 4–8 months earlier. The solid (dashed) lines indicate that the represented feature is stronger (weaker) during El Niño than in La Niña, for the respective season. (From Carleton, 2003a.)

Table A19 Mean temperature T (°C), mixing ratio q (gm kg^{-1}), and pseudo wet-bulb potential temperature θ_{sw} (°C) of higher latitude air masses in summer (*s*, December-March) and winter (*w*, June-September) at selected stations

			Pressure Level (mb)											
			1000			850			700			500		
Station	Location	Season	*T*	*q*	*θsw*	*T*	*q*	*θsw*	*T*	*q*	*θsw*	*T*	*q*	*θsw*
Maritime Polar Air														
Macquarie I.	55°S, 159°E	*s*	5.7	4.5	4.1	−4.3	2.7	2.8	−12.5	1.3	4.8	−28.4	0.3	8.2
		w	3.7	4.1	1.8	−5.5	2.3	2.0	−14.4	1.0	3.4	−32.7	0.3	5.5
Little America	78°S, 161°W	*s*	—	—	—	−8.3	2.0	−0.1	−15.2	1.5	3.6	−29.9	0.5	7.7
		w	—	—	—	−15.7	1.2	−6.4	−21.1	0.9	0.9	−37.2	0.3	2.9
Maritime Antarctic Air														
Marion I.	47°S, 37°E	*w*	0.3	2.9	−1.2	−9.6	1.6	−1.5	−19.4	0.8	−0.1	−34.3	0.2	4.3
Mirnyi	67°S, 93°E	*w*	—	—	—	−20.3	0.8	−10.6	−22.7	0.7	−2.2	−36.4	0.3	3.5
Little America	78°S, 161°W	*w*	—	—	—	−21.4	0.6	−11.7	−26.8	0.5	−5.5	−41.3	0.2	0.0
Continental Antarctic Air														
Mirnyi	67°S, 93°E	*s*	—	—	—	−12.3	1.2	−4.0	−19.8	0.8	−0.1	−32.1	0.3	6.0
		w	—	—	—	−26.8	0.4	−16.7	−28.2	0.3	−7.0	−40.3	0.1	0.7
Little America	78°S, 161°W	*s*	—	—	—	−12.7	1.1	−4.3	−21.0	0.6	−1.6	−35.1	0.2	4.2
		w	—	—	—	−28.9	0.3	−19.0	−31.9	0.2	−10.0	−44.0	0.1	−2.0

Source: After Taljaard, in van Loon et al. (1972).

strongly during equatorward excursions (Andreas and Makshtas, 1985). Taljaard (in van Loon et al., 1972) identified a transitional airmass (Antarctic maritime, mA) over the pack ice which is present only during winter. It is slightly warmer and less stable than cA (Table A19), but at times may be indistinguishable from that airmass.

Polar maritime (mP) air – sometimes also known as Southern maritime (mS) – dominates the middle and higher-latitude oceans that are ice free. Developed partly over the marked SST gradients of the OPF, mP air exhibits south–north variations in temperature and moisture (Table A19), being strongly destabilized on moving equatorward. Thus, the OPF is the site for many higher-latitude polar mesocyclone ("polar low") systems observed in satellite imagery and a high frequency of lower-level ("boundary-layer") fronts (Carleton, 1995). Modification of mP air also occurs when it returns poleward, typically in advance of frontal cyclones. In this case the air stabilizes and may penetrate far into the interior of Antarctica via the Pacific sector of West Antarctica.

Climatic fronts

The climatic frontal zones (and, hence, major cyclone tracks) of the southern hemisphere (see Figure A32) show a close association with the OPF at middle and high latitudes (Baker, 1979). These polar fronts are manifest as tropospheric thickness gradient maxima (TGM) in association with middle- and high-latitude jet streams (Taljaard, in van Loon et al., 1972). In summer there is some correspondence between the 1000–500 hPa TGM and the summer pack ice margin, implying frontal activity. In winter the higher-latitude frontal frequency maxima occur equatorward of the sea ice margin in the South Pacific, but there are no corresponding bands of TGM at this latitude owing to higher rates of alternation of high- and low-pressure systems (Taljaard, in van Loon et al., 1972). Instead, a well-defined TGM in the 1000–500 hPa layer lies poleward of the ice border along 65–70°S. This has been considered evidence of a secondary Antarctic (as opposed to Polar) Front (see Figure A27). In East Antarctica, TGM in the 500–300 hPa layer may correspond to an Antarctic Jet related to the topography of the ice sheet, as identified during the IGY and subsequently modeled (Mechoso, 1980). Interestingly, there has been little research on the climatology of atmospheric fronts over southern high latitudes in recent years. However, useful insights can be gleaned from satellite passive microwave retrievals of cloud water, column-integrated water vapor, and precipitation over ice-free ocean, as well as the summary maps of extratropical cyclone tracks derived using automatic tracking of systems in digital analyses.

Synoptically, fronts penetrating Antarctica often lose their identity on ascending the ice sheet, although they may temporarily disrupt the strong surface inversion. Warm fronts advancing southward ahead of mP or mA air provide overrunning precipitation, and frequently are involved in warming episodes associated with the coreless winter.

Synoptic cyclone activity

Automated cyclone-tracking routines applied to digital SLP data (Simmonds and Keay, 2000a,b) largely confirm the mean patterns of extratropical cyclones determined in the earlier satellite-based (cloud vortex) and IGY climatologies for the Antarctic and sub-Antarctic (Carleton, 1979; Figure A32). However, they add information on the variability (frequency, spatial locations) of these systems and also their characteristic intensities. Over the Southern Ocean, including the SSIZ, the circulation is dominantly cyclonic all year (see "Large-scale atmospheric circulation; Mean surface pressure and 500 hPa height fields", above), the mean pattern involving cyclogenesis

over middle latitudes of the western South Atlantic, Indian Ocean, and mid-Pacific (Carleton, 1979). Synoptic cyclones bring clouds, precipitation and strong winds to coastal Antarctica. The maturity and dissipation (cyclolysis) of these systems occur at successively higher latitudes along well-defined climatic tracks that merge in the ACT. These "storm tracks" are evident as cloud bands in satellite VIS/IR imagery. They are also retrievable from digital daily analyses as zones of high variance of the v-wind (south–north) component and geopotential height, but low variance in the u-wind (west–east) component (Trenberth, 1987). However, there are some differences in the locations of storm tracks derived in this manner and those obtained from tracking cyclone systems (Jones and Simmonds, 1993). Relatively few lows invade interior East Antarctica, whereas many enter West Antarctica from the South Pacific. The latter region particularly shows an interannual variation in cyclone frequencies related to ENSO (Carleton and Song, 2000). Moreover, a trend to decreased (increased) cyclone frequencies over the sub-Antarctic (Antarctic) seas for the period 1960–1999 is consistent with numerical modeling studies employing anthropogenic forcings (Fyfe, 2003). These imply a poleward migration of the zone of maximum baroclinity under global warming. However, this change may depend, at least partly, on the intensity class of cyclone studied (Pezza and Ambrizzi, 2003).

Similar to earlier studies for the northern hemisphere, explosively deepening cyclones ("bombs") have been identified and studied for the southern extratropics. Those occurring closer to Antarctica have much in common with some "polar lows", in terms of their large-scale synoptic environments (cf. Carleton and Song, 1997, 2000; Simmonds et al., 2003).

The time-averaged centers of cyclolysis within the ACT are located just eastward of the longitudes of maximum variation of sea-ice extent; Carleton and Fitch, 1993; Yuan et al., 1999; cf. Figures A27 and A34). Therefore, the longitudinal frequency of depression centers influences ice distribution and advance/retreat patterns via temperature and dynamical (wind-induced) advection (Cavalieri and Parkinson, 1981). On average there is no clear connection between Antarctic sea ice extent and cyclone tracks, although closer associations can be found for certain time periods and regions (Yuan et al., 1999).

Mesoscale cyclone and "polar low" activity

High-resolution meteorological satellite imagery has shown that mesoscale cyclones, or polar-air mesocyclones (approximate length scales 100–800 km), occur frequently in Antarctic and sub-Antarctic latitudes (Carleton, 1992, 2003b). The improved detection of these systems likely is involved in a statistically significant recent increase in extratropical cyclone frequencies over the southern hemisphere that is not matched by significant changes in SLP (Sinclair et al., 1997). Mesocyclones comprise two main cloud-vortex types: inverted comma-shaped "polar lows", dominated by positive vorticity advection associated with short waves and jet stream maxima; and spiral-shaped (multi-banded) systems generated mostly by strong sea–air interactions of heat and moisture (Carleton, 1995, 1996). One zone of mesocyclone high incidence is located near the winter/spring sea-ice margin, especially in the South Pacific sector (see Figure A27). There, streams of cA or mA air are strongly destabilized in the vicinity of the ice edge and OPF. These storms often track east or northeast through Drake Passage to decay in the Weddell Sea area (Carleton and Song, 1997). The other major zone of meso-cyclogenesis is close to the Antarctic coastline and over the ice shelves; near the confluence areas for the katabatic winds (see Figure A27). There, "vortex stretching" as air descends the steep slope of the ice sheet, enhances cyclonic vorticity. Also, some mesocyclones develop in association with coastal polynyas because of the oceanic large heat losses to the atmosphere. These near-coastal mesocyclones may lack a cloud signature, being detectable only in the AWS data, or be composed mostly of low-level clouds.

The zonally averaged meso-cyclogenesis seems to be greatest in March and September, associated with the SAO (Carleton and Song, 1997). A number of regional-scale "synoptic climatologies" of mesocyclones in the Antarctic have been developed for time periods of varying length; for the Ross Sea, Marie Byrd Land and the Siple Coast, the Bellingshausen and Amundsen seas, and the Weddell Sea (refer to section 2.2.3 in Carleton, 2003b; also Carleton and Carpenter, 1990; Carrasco et al., 2003). In the Bellingshausen–Amundsen seas, strong differences in the ENSO-related SLP and SST anomalies (SSTA) for the southern winters 1988 and 1989 were reflected in major changes in mesocyclone activity (Carleton and Song, 2000). Mesocyclones were more (less) frequent in this sector in 1989 (1988), associated with decreasing (static) SSTA during the respective May to September periods.

Circulation variations and climatic teleconnections

Climate fluctuations in the Antarctic and sub-Antarctic occur interannually (i.e. climate variations), decadally (climate trends), and multidecadally (climate changes). Interannual variations primarily involve teleconnections to the tropical Pacific ENSO, which is, globally, the dominant coupled ocean–atmosphere interaction mode. On decadal time scales, Antarctic-region circulation–climate variations are most closely connected with an Antarctic Circumpolar Wave (ACW) of extratropical coupled anomalies of SST, upper-ocean salinity, SLP, meridional winds, and sea ice. At times the ACW may be linked to, and modulated by, the ENSO. Recent climate changes in the Antarctic, particularly as revealed in the retreat and collapse of ice shelves, and the ongoing warming of the western AP, may be evidence of "global warming". However, a more immediate explanation for these climate changes derives from long-term shifts in the atmospheric circulation; primarily, the zonally varying mode or Antarctic Oscillation (AAO).

The El Niño Southern Oscillation (ENSO) in Antarctica

The climate teleconnections to the ENSO phenomenon also are evident in Antarctica, especially in the Pacific sector (Kwok and Comiso, 2002). Interestingly, the pressure changes that occur over southern higher latitudes in the lead-up to an El Niño may be at least as large as those in the tropics, and often precede the changes there. (In an El Niño, tropical convection shifts eastward from the "maritime continent" to the central tropical Pacific, in association with the area of highest SST.) The associated weakening of the South Pacific subtropical high, a key "center of action" in ENSO, permits the semi-permanent South Pacific Convergence Zone (SPCZ) to move eastward (Figure A34). The SPCZ is a major trough ahead of which energy and moisture are advected rapidly southeastwards into extratropical latitudes. Consequently, its forward side is evident in satellite imagery as a quasi-meridional band of deep clouds that often energizes cyclonic circulations transiting the Pacific

sector of the Southern Ocean. During El Niño the strengthened latitudinal pressure and temperature gradient resulting from the higher SST in the tropical central Pacific, helps intensify the STJ in that sector. At the same time the PFJ tends to weaken. These synoptic interactions are evident on monthly time scales as a standing wave train pattern of alternating anomalies linking the South Pacific and South Atlantic sectors, or so-called Pacific–South America (PSA) pattern (e.g. Mo, 2000). The PSA is reminiscent of the North Pacific PNA pattern, although the pressure/height anomalies generally are of lower magnitude. The PSA pattern during composite El Niño events is shown in Figure A34. Note particularly the out-of-phase relationship of the pressure anomalies between the Bellingshausen–Amundsen sector (Weddell Sea), where SLP anomalies are positive (negative). Similarly, this relationship is evident as out-of-phase anomalies of temperature and sea-ice extent. Thus, El Niño events tend to produce colder conditions, more frequent southerly winds and greater sea-ice extent east of the AP.

The out-of-phase temperature and related pressure anomaly pattern between the seas west and east of the AP comprise an Antarctic Dipole Index (ADP), which correlates well with tropical Pacific SST and surface air temperature, as well as the Antarctic sea ice edge (Yuan and Martinson, 2001). Thus, the ADP appears to link interannual climate variability in the Antarctic seas with the ENSO pattern. The signal is particularly strong in La Niña events, for which it may have some predictive value.

Over most of Antarctica, El Niño events tend to be accompanied by colder conditions than normal and negative anomalies of surface pressure (Smith and Stearns, 1993). The cooling of the troposphere helps intensify the katabatic winds, leading to stronger wind speeds near the coast; at least, as occurred during the major El Niño of 1982–1983. Accordingly, sea ice may be more extensive in those regions while it is reduced in others, such as the Ross Sea.

During La Niña, or ENSO "cold events", the regional pattern of coupled anomalies in pressure, meridional winds, temperature and sea ice over the Southern Ocean are more or less opposite those for El Niño (Sinclair et al., 1997). In the Pacific sector, La Niñas typically are expressed as a strengthened Amundsen Sea low and associated stronger PFJ (a weaker STJ), and a weaker Weddell Sea low (Yuan et al., 2001). Accordingly, the temperature anomalies along the western AP are mostly negative in La Niña, with greater sea-ice extent, in contrast to the eastern side of the peninsula.

As noted for climate variations in other parts of the world, the ENSO teleconnection is not stable through time. In the Pacific sector of West Antarctica a change in the relationship between ENSO and the poleward flux of moisture evidently occurred around 1991; from strongly positive before that time to significantly negative afterward. This change impacted regional precipitation amounts.

The Antarctic Circumpolar Wave (ACW)

Unlike the ENSO climate signal in Antarctica, the subdecadal ACW appears primarily to be of southern extratropical origin, although it likely interacts with the ENSO as a "slow teleconnection" (Peterson and White, 1998). In the atmosphere the ACW is a propagating wave number 2 pattern that makes a complete circuit about Antarctica in about 8 years (4 years per wave). It differs from the ADP, which is a quasistationary wave, although the two may interact in the Amundesen–Weddell Sea sectors (Yuan and Martinson, 2001). Because the western (eastern) sides of a trough are characterized by opposite anomalies of meridional wind and temperature, the patterns of upwelling and downwelling in the ocean – important for sea temperature and salinity differences – and of sea-ice extent, also are opposite across the wave (Motoi et al., 1998). East of a trough and west of a surface high pressure, the northerly winds advect mild air southward, leading to downwelling and decreased near-surface salinity, and a general retreat of the sea-ice extent. Conversely, west of a trough and east of a surface high pressure, the southerly winds advect cold air equatorward, producing upwelling and increased salinity, and advancing sea ice. Thus, the ACW in the upper ocean is evident as a slowly migrating (to the eastward) suite of anomalies that maintain their identity across seasons and through the different regions of the Southern Ocean. Interestingly, a number of modeling studies have successfully simulated an ACW-like phenomenon, yet its period and even wave number can be different from those evident in the data (e.g. Motoi et al., 1998). Similarly, the analysis of datasets for the periods before and after that analysed by Peterson and White (1998) suggests that the ACW is not always a prominent teleconnection (Kidson, 1999). This lack of temporal stability is reminiscent of the Antarctic teleconnection to ENSO.

The Antarctic Oscillation (AAO) and recent climate changes

The AAO, also known as the zonally varying mode, southern annular mode, and high-latitude mode, comprises the first EOF (empirical orthogonal function in a principal components analysis) of SLP and tropospheric height over southern middle and higher latitudes (Rogers and van Loon, 1982; Kidson, 1999). An intensification of the mean pressure centers respectively over middle latitudes and Antarctica results in stronger geostrophic westerly winds in the sub-Antarctic and PFJ, or the positive phase of AAO. Conversely, a weakening of the pressure meridional difference reduces the westerlies and PFJ, or negative phase of AAO. After the 1970s, the trend of the AAO has been one of increasing "positive polarity", partly linked to rising SST in the tropical Pacific and more frequent El Niño events. The stronger westerlies bring in relatively mild and moist air to the western side of the AP, providing at least a partial explanation for the observed winter warming and reduced sea ice there. During the same period the intensification of the polar vortex over the continent accompanied downward trends of temperature there, and reduced surface melt in the summer (Torinesi et al., 2003). Stronger westerlies in the AAO positive mode tend to be associated with a zonally averaged greater extent of the sea ice (Hall and Visbeck, 2002).

Although it is most marked in the troposphere, the AAO has links with the stratosphere, and may modulate the shape and intensity of the annually occurring Antarctic ozone hole (Thompson et al., 2000). In general, greater cooling over Antarctica accompanying positive AAO, better isolates stratospheric air from that in middle latitudes, permitting the formation of more polar stratospheric clouds upon which chlorine compounds accumulate, thereby accelerating the breakdown of ozone during austral springtime (Sexton, 2001). Thus, recent Antarctic-region climate changes involving human activities may be linked to changes in frequency of "natural" teleconnection patterns.

Andrew M. Carleton

Bibliography

Ackley, S.F., 1981. A review of sea-ice weather relationships in the southern hemisphere. In Allison, I., ed., *Sea Level, Ice, and Climatic Change*. International Association for Hydrological Sciences Publication 131. Canberra, Australia, pp. 127–159.

Adolphs, U., and Wendler, G., 1995. A pilot study on the interactions between katabatic winds and polynyas at the Adelie Coast, eastern Antarctica. *Antarctic Science*, **7**(3): 307–314.

Anderssen, E.C., 1965. A study of atmospheric long waves in the Southern Hemisphere, *NOTOS*, **14**: 57–65.

Andreas, E.L., and Makshtas, A.P., 1985. Energy exchange over Antarctic sea ice in the spring. *Journal of Geophysical Research*, **90**: 7199–7212.

Baker, Jr., D.J., 1979. Ocean-atmosphere interactions in high southern latitudes. *Dynamics of Atmospheres and Oceans*, **3**: 213–229.

Bals-Elsholz, T.M., Atallah, E.H., Bosart, L.F., Wasula, T.A., Cempa, M.J., and Lupo, A.R., 2001. The wintertime Southern Hemisphere split jet: structure, variability, and evolution. *Journal of Climate*, **14**(21): 4191–4215.

Bintanja, R., 2000. Surface heat budget of Antarctic snow and blue ice: interpretation of spatial and temporal variability. *Journal of Geophysical Research*, **105**(D19): 24387–24407.

Borisenkov, E.P., and Dolganov, L.V., 1982. Some results of climatic generalization of meteorological observations in the Antarctic. *Journal of Geophysical Research*, **87**(C12): 9653–9666.

Bromwich, D.H., 1991. Mesoscale cyclogenesis over the south-western Ross Sea linked to strong katabatic winds. *Monthly Weather Review*, **119**: 1736–1752.

Bromwich, D.H., Carrasco, J.F., Liu, Z., and Tzeng, R-Y., 1993. Hemispheric atmospheric variations and oceanographic impacts associated with katabatic surges across the Ross Ice Shelf, Antarctica. *Journal of Geophysical Research*, **98**: 13045–13062.

Bromwich, D.H., Monaghan, A.J., and Guo, Z., 2004a. Modeling the ENSO modulation of Antarctic climate in the late 1990s with the Polar MM5. *Journal of Climate*, **17**(1): 109–132.

Bromwich, D.H., Guo, Z., Bai, L., and Chen, Q-S., 2004b. Modeled Antarctic precipitation. Part I: Spatial and temporal variability. *Journal of Climate*, **17**(3): 427–447.

Bromwich, D.H., Rogers, A.N., Kållberg, P., Cullather, R.I., White, J.W.C., and Kreutz, K.J., 2000. ECMWF analyses and reanalyses depiction of ENSO signal in Antarctic precipitation. *Journal of Climate*, **13**: 1406–1420.

Carleton, A.M., 1979. A synoptic climatology of satellite-observed extratropical cyclone activity for the Southern Hemisphere winter. *Archiv für Meteorologie, Geophysik, und Bioklimatologie*, **B27**: 265–279.

Carleton, A.M., 1988: Sea-ice atmosphere signal of the Southern Oscillation in the Weddell Sea, Antarctica. *Journal of Climate*, **1**: 379–388.

Carleton, A.M., 1989. Antarctic sea-ice relationships with indices of the atmospheric circulation of the Southern Hemisphere. *Climate Dynamics*, **3**: 207–220.

Carleton, A.M., 1992. Synoptic interactions between Antarctica and lower latitudes. *Australian Meteorology Magazine*, **40**: 129–147.

Carleton, A.M., 1995. On the interpretation and classification of mesoscale cyclones from satellite infrared imagery. *International Journal of Remote Sensing*, **16**: 2457–2485.

Carleton, A.M., 1996. Satellite climatological aspects of cold air mesocyclones in the Arctic and Antarctic. *Global Atmospheric and Ocean System*, **5**: 1–42.

Carleton, A.M., 2003a. Atmospheric teleconnections involving the Southern Ocean. *Journal of Geophysical Research*, **107**, doi: 10.1029/2000JC000329.

Carleton, A.M., 2003b. The Antarctic, In: Rasmussen, E.A., and Turner, J., eds., *Polar Lows, Mesoscale Weather Systems in the Polar Regions*. Cambridge: Cambridge University Press, pp. 108–149.

Carleton, A.M., and Carpenter, D.A., 1990. Satellite climatology of "polar lows" and broadscale climatic associations for the Southern Hemisphere. *International Journal of Climatology*, **10**: 219–246.

Carleton, A.M., and Fitch, M., 1993. Synoptic aspects of Antarctic mesocyclones. *Journal of Geophysical Research*, **98**: 12997–13018.

Carleton, A.M., and Song, Y., 1997. Synoptic climatology and intrahemispheric associations of cold air mesocyclones in the Australasian sector. *Journal of Geophysical Research*, **102**(D12): 13873–13887.

Carleton, A.M., and Song, Y., 2000. Satellite passive sensing of the marine atmosphere associated with cold-air mesoscale cyclones. *Professional Geographer*, **52**: 289–306.

Carleton, A.M., John, G., and Welsch, R., 1998. Interannual variations and regionality of Antarctic sea-ice–temperature associations. *Annals of Glaciology*, **27**: 403–408.

Carrasco, J.F., Bromwich, D.H., and Monaghan, A.J., 2003. Distribution and characteristics of mesoscale cyclones in the Antarctic: Ross Sea eastward to the Weddell Sea. *Monthly Weather Reviews*, **131**(2): 289–301.

Carroll, J.J., 1982. Long-term means and short-term variability of the surface energy balance components at the South Pole. *Journal of Geophysical Research*, **87**(C6): 4277–4286.

Cavalieri, D.J., and Parkinson, C.L., 1981. Large-scale variations in observed Antarctic sea ice extent and associated atmospheric circulation. *Monthly Weather Review*, **109**: 2323–2336.

Connolley, W.M., 1996. The Antarctic temperature inversion. *International Journal of Climatology*, **16**: 1333–1342.

Connolley, W.M., 1997. Variability in annual mean circulation in southern high latitudes. *Climate Dynamics*, **13**: 745–756.

Doran, P.T., Priscu, J.C., and Lyons, W.B. et al., 2002. Antarctic climate cooling and terrestrial ecosystem response. *Nature*, **415**: 517–520.

Enomoto, H., 1991. Fluctuations of snow accumulation in the Antarctic and sea level pressure in the Southern Hemisphere in the last 100 years. *Climatic Change*, **18**: 67–87.

Enomoto, H., and Ohmura, A. 1990. The influences of atmospheric halfyearly cycle on the sea ice extent in the Antarctic. *Journal of Geophysical Research*, **95**: 9497–9511.

Fyfe, J.C., 2003. Extratropical Southern Hemisphere cyclones: harbingers of climate change. *Journal of Climate*, **16**(17): 2802–2805.

Gille, S.T., 2002. Warming of the Southern Ocean since the 1950s. *Science*, **295**(5558): 1275–1277.

Giovinetto, M.B., Waters, N.M., and Bentley, C.R., 1990. Dependence of Antarctic surface mass balance on temperature, elevation, and distance to open ocean. *Journal of Geophysical Research*, **95**: 3517–3531.

Guo, Z., Bromwich, D.H., and Comiso, J.J., 2003. Evaluation of Polar MM5 simulations of Antarctic atmospheric circulation. *Monthly Weather Review*, **131**(2): 384–411.

Guo, Z., Bromwich, D.H., and Hines, K.M., 2004. Modeled Antarctic precipitation. Part II: ENSO modulation over West Antarctica. *Journal of Climate*, **17**(3): 448–465.

Hall, A., and Visbeck, M., 2002. Synchronous variability in the Southern Hemisphere atmosphere, sea ice, and ocean resulting from the annular mode. *Journal of Climate*, **15**(21): 3043–3057.

Harangozo, S.A., Colwell, S.R., and King, J.C., 1997. An analysis of a 34-year air temperature record from Fossil Bluff (71°S, 68°W), Antarctica. *Antarctic Science*, **9**(3): 355–363.

Hatzianastassiou, N., and Vardavas, I., 2001. Shortwave radiation budget of the Southern Hemisphere using ISCCP-C2 and NCEP-NCAR climatological data. *Journal of Climate*, **14**(22): 4319–4329.

Heinemann, G., 1990. Mesoscale vortices in the Weddell Sea region (Antarctica). *Monthly Weather Review*, **118**: 779–793.

Hines, K.M., and Bromwich, D.H., 2002. A pole to pole west Pacific atmospheric teleconnection during August. *Journal of Geophysical Research*, **107**(D18): 4359, doi: 10.1029/2001JD001335, 2002.

Hurrell, J.W., and van Loon, H., 1994. A modulation of the atmospheric annual cycle in the Southern Hemisphere. *Tellus Series A*, **46**: 325–338.

Jacka, T.H., and Budd, W.F., 1998. Detection of temperature and sea-ice extent changes in the Antarctic and Southern Ocean, 1949–96. *Annals of Glaciology*, **27**: 553–559.

Jacobs, G.A., and Mitchell, J.L., 1996. Ocean circulation variations associated with the Antarctic Circumpolar Wave. *Geophysics Research Letters*, **23**: 2947–2950.

Jacobs, S.S., Giulivi, C.F., and Mele, P.A., 2002. Freshening of the Ross Sea during the late 20th century. *Science*, **297**(5580): 386–389.

Jones, A.E., Bowden, T., and Turner, J., 1998. Predicting total ozone based on GTS data: applications for South American high latitude populations. *Journal of Applied Meteorology*, **37**: 477–485.

Jones, D.A., and Simmonds, I., 1993. Time and space spectral analyses of Southern Hemisphere sea level pressure variability. *Monthly Weather Reviews* **121**: 661–672.

Kidson, J.W., 1999. Principal modes of Southern Hemisphere low-frequency variability obtained from NCEP-NCAR reanalyses. *Journal of Climate*, **12**: 2808–2830.

Kiladis, G.N., and Mo, K.C., 1998. Interannual and intraseasonal variability in the Southern Hemisphere. In Karoly, D.J. and Vincent, D.G., eds., *Meteorology of the Southern Hemisphere*. MA: American Meteorlogical Society, pp. 307–336.

Kwok, R., and Comiso, J.C., 2002. Southern Ocean climate and sea ice anomalies associated with the Southern Oscillation. *Journal of Climate*, **15**: 487–501.

Lachlan-Cope, T.A., Connolley, W.M., and Turner, J., 2001. The role of non-axisymmetric Antarctic orography in forcing the observed pattern of variability of the Antarctic climate. *Geophysics Research Letters*, **28**(21): 4111–4114.

Lamb, H.H., 1959. The southern westerlies: a preliminary survey; main characteristics and apparent associations. *Quarterly Journal of the Royal Meteorological Society*, **85**(363): 1–23.

Large, W.G., and van Loon, H., 1989. Large-scale low frequency variability of the 1979 FGGE surface buoy drifts and winds over the Southern Hemisphere. *Journal of Physical Oceanography*, **19**: 216–232.

Marques, R.F.C., and Rao, V.B., 2000. Interannual variations of blocking in the Southern Hemisphere and their energetics. *Journal of Geophysical Research*, **105**: 4625–4636.

Mechoso, C., 1980. The atmospheric circulation around Antarctica: linear stability and finite amplitude interactions with migrating cyclones. *Journal of Atmospheric Science*, **37**: 2209–2233.

Mo, K.C., 2000. Relationships between low-frequency variability in the Southern Hemisphere and sea surface temperature anomalies. *Journal of Climate*, **13**: 3599–3610.

Motoi, T., Kitoh, A., and Koide, H., 1998. Antarctic Circumpolar Wave in a coupled ocean-atmosphere model. *Annals of Glaciology*, **27**: 483–487.

Murphy, B.F., 2003. Prediction of severe synoptic events in coastal East Antarctica. *Monthly Weather Review*, **131**(2): 354–370.

Nakamura, N., and Oort, A.H., 1988. Atmospheric heat budgets of the polar regions. *Journal of Geophysical Research*, **93**: 9510–9524.

Parish, T.R., and Bromwich, D.H., 1991. Continental-scale simulation of the Antarctic katabatic wind regime. *Journal of Climate*, **4**(2): 135–146.

Parkinson, C.L., 1992. Interannual variability of monthly southern ocean sea ice distributions. *Journal of Geophysical Research*, **97**(C4): 5349–5363.

Peterson, R.G., and White, W.B., 1998. Slow oceanic teleconnections linking the Antarctic Circumpolar Wave with the tropical El Niño Southern Oscillation. *Journal of Geophysical Research* **103**: 24573–24583.

Pezza, A.B., and Ambrizzi, T., 2003. Variability of Southern Hemisphere cyclone and anticyclone behavior: further analysis. *Journal of Climate*, **16**(7): 1075–1083.

Phillpot, H.R., 1991. The derivation of 500 hPa height from automatic weather station surface observations in the Antarctic continental interior. *Australian Meteorology Magazine*, **39**: 79–86.

Pittock, A.B., 1984. On the reality, stability, and usefulness of southern hemisphere teleconnections. *Australian Meteorology Magazine*, **32**: 75–82.

Raphael, M., 2003a. Impact of observed sea-ice concentration on the Southern Hemisphere extratropical atmospheric circulation in summer. *Journal of Geophysical Research* 108(D22), 4687. doi: 10.1029/2002JD003308, 2003.

Raphael, M., 2003b. Recent, large-scale changes in the extratropical Southern Hemisphere atmospheric circulation. *Journal of Climate*, **16**(17): 2915–2924.

Reijmer, C.H., and Oerlemans, J., 2002. Temporal and spatial variability of the surface energy balance in Dronning Maud Land, East Antarctica. *Journal of Geophysical Research* 107(D24), 4759, doi: 10.1029/2000JD000110, 2002.

Renwick, J.A., 2002. Southern Hemisphere circulation and relations with sea ice and sea surface temperature. *Journal of Climate*, **15**(21): 3058–3068.

Reusch, D.B., and Alley, R.B., 2002. Automatic weather stations and artificial neural networks: improving the instrumental record in West Antarctica. *Monthly Weather Review*, **130**(12): 3037–3053.

Rogers, J.C., 1983. Spatial variability of Antarctic temperature anomalies and their association with the Southern Hemisphere atmospheric circulation. *Association of American Geographers Annals*, **73**(4): 502–518.

Rogers, J.C., and van Loon, H., 1982. Spatial variability of sea level pressure and 500 mb height anomalies over the Southern Hemisphere. *Monthly Weather Review*, **110**(10): 1375–1392.

Schneider, D.P., and Steig, E.J., 2002. Spatial and temporal variability of Antarctic ice sheet microwave brightness temperatures. *Geophysical Research Letters*, **29**(20): 1964, doi: 10.1029/2002GL015490, 2002.

Schwerdtfeger, W., 1975. The effect of the Antarctic Peninsula on the temperature regime of the Weddell Sea. *Monthly Weather Review*, **103**(1): 45–51.

Schwerdtfeger, W., 1979. Meteorological aspects of the drift of ice from the Weddell Sea toward the mid-latitude westerlies. *Journal of Geophysical Research*, **84**: 6321–6328.

Schwerdtfeger, W., 1984. *Weather and Climate of the Antarctic. Developments in Atmospheric Science*, vol. 15. Amsterdam: Elsevier.

Sexton, D.M.H., 2001. The effect of stratospheric ozone depletion on the phase of the Antarctic Oscillation. *Geophysical Research Letters*, **28**: 3697–3700.

Simmonds, I., and Jones, D.A., 1998. The mean structure and temporal variability of the semiannual oscillation in the southern extratropics. *International Journal of Climatology*, **18**: 473–504.

Simmonds, I., and Keay, K. 2000a. Mean Southern Hemisphere extratropical cyclone behavior in the 40-year NCEP-NCAR Reanalysis. *Journal of Climate*, **13**: 873–885.

Simmonds, I., and Keay, K., 2000b. Variability of Southern Hemisphere extratropical cyclone behavior, 1958–97. *Journal of Climate*, **13**: 550–561.

Simmonds, I., Keay, K., and Lim, E-P., 2003. Synoptic activity in the seas around Antarctica. *Monthly Weather Review*, **131**(2): 272–288.

Sinclair, M.R., Renwick, J.A., and Kidson, J.W., 1997. Low-frequency variability of Southern Hemisphere sea level pressure and weather system activity. *Monthly Weather Review*, **125**: 2531–2543.

Smith, S.R., and Stearns, C.R., 1993. Antarctic pressure and temperature anomalies surrounding the minimum in the Southern Oscillation Index. *Journal of Geophysical Research*, **98**: 13071–13083.

Streten, N.A., 1968. Some features of mean annual windspeed data for coastal East Antarctica. *Polar Record*, **14**(90): 315–322.

Streten, N.A., 1977. Seasonal climatic variability over the southern oceans. *Archiv für Meteorologie, Geophysik und Bioklimatologie*, **B25**: 1–19.

Streten, N.A., 1980a. Antarctic meteorology: the Australian contribution past, present and future. *Australian Meteorology Magazine*, **28**: 105–140.

Streten, N.A., 1980b. Some synoptic indices of the Southern Hemisphere mean sea level circulation 1972–77. *Monthly Weather Reviews* **108**(1): 18–36.

Streten, N.A., and Pike, D.J., 1980. Characteristics of the broadscale Antarctic sea ice extent and the associated atmospheric circulation 1972–1977. *Archiv für Meteorologie, Geophysik und Bioklimatologie*, **A20**: 279–299.

Streten, N.A., and Zillman, J.W., 1984. Climates of the South Pacific. In van Loon, H., ed., *Climates of the Oceans*. *World Survey of Climatology*, vol. 15. Amsterdam: Elsevier.

Thompson, D.W.J., and Solomon, S., 2002. Interpretation of recent Southern Hemisphere climate change. *Science*, **296**(5569): 895–899.

Thompson, D.W.J., Wallace, J.M., and Hegerl, G.C., 2000. Annular modes in the extratropical circulation, Part 2: Trends. *Journal of Climate*, **13**: 1018–1036.

Torinesi, O., Fily, M., and Genthon, C., 2003. Variability and trends of the summer melt period of Antarctic ice margines since 1980 from microwave sensors. *Journal of Climate*, **16**(7): 1047–1060.

Trenberth, K.E., 1979. Interannual variability of the 500 mb zonal mean flow in the Southern Hemisphere. *Monthly Weather Review*, **107**(11): 1515–1524.

Trenberth, K.E., 1987. The role of eddies in maintaining the westerlies in the Southern Hemisphere winter. *Journal of Atmospheric Science*, **44**: 1498–1508.

Turner, J., Leonard, S., Marshall, G.J., et al., 1999. An assessment of operational Antarctic analyses based on data from the FROST project. *Weather Forecast*, **14**: 817–834.

Turner, J., Harangozo, S.A., Marshall, G.J., King, J.C., and Colwell, S.R., 2002a. Anomalous atmospheric circulation over the Weddell Sea, Antarctica during the austral summer of 2001/02 resulting in extreme sea ice conditions. *Geophysical Research Letters*, **29**(24): 2160, doi: 10.1029/2002GL015565, 2002.

Turner, J., King, J.C., Lachlan-Cope, T.A., and Jones, P.D., 2002b. Communications arising, Recent temperature trends in the Antarctic. *Nature*, **418**: 291–292.

Turner, J., Lachlan-Cope, T.A., Marshall, G.J., Morris, E.M., Mulvaney, R., and Winter, B., 2002c. Spatial variability of Antarctic Peninsula net surface mass balance. *Journal of Geophysical Research*, **107**(D13): doi: 10.1029/2001JD000755, 2002.

Van Loon, H., 1979. The association between latitudinal temperature gradient and eddy transport. Part 1: Transport of sensible heat in winter. *Monthly Weather Review*, **107**: 525–534.
Van Loon, H., and Rogers, J.C., 1984. Interannual variations in the half-yearly cycle of pressure gradients and zonal wind at sea level on the Southern Hemisphere. *Tellus*, **36A**: 76–86.
Van Loon, H., Taljaard, J.J., Sasamori, T., et al., 1972. Meteorology of the Southern Hemisphere. In Newton, C.W., ed., *Meteorological Monographs*, **13**(35). Boston, MA: American Meteorological Society.
Van den Broeke, M., 2000a. On the interpretation of Antarctic temperature trends. *Journal of Climate*, **13**: 3885–3889.
Van den Broeke, M., 2000b. The semi-annual oscillation and Antarctic climate. Part 4: A note on sea ice cover in the Amundsen and Bellingshausen seas. *International Journal of Climatology*, **20**: 455–462.
Van den Broeke, M.R., and van Lipzig, N.P.M., 2003. Factors controlling the near-surface wind field in Antarctica. *Monthly Weather Review*, **131**(4): 733–743.
Vaughan, D.G., and Doake, C.S., 1996. Recent atmospheric warming and retreat of ice shelves on the Antarctic Peninsula. *Nature*, **379**: 328–331.
Vaughan, D.G., Bamber, J.L., Giovinetto, M., Russell, J., and Cooper, A.P.R., 1999. Reassessment of net surface mass balance in Antarctica. *Journal of Climate*, **12**(4): 933–946.
Vaughan, D.G., Marshall, G.J., Connolley, W.M., et al., 2003. Recent rapid regional climate warming on the Antarctic Peninsula. *Climatic Change*, **60**: 243–274.
Watkins, A.B., and Simmonds, I., 1999. A late spring surge in the open water of the Antarctic sea ice pack. *Geophysical Research Letters*, **26**: 1481–1484.
Weller, G., 1982. Polar problems in climate research: some comparisons between the Arctic and Antarctic. *Australian Meteorology Magazine*, **30**: 163–168.
Wendland, W.M., and McDonald, N.S., 1986. Southern Hemisphere airstream climatology. *Monthly Weather Review*, **114**(1): 88–94.
Wendler, G., and Worby, A., 2001. The surface energy budget in the Antarctic summer sea-ice pack. *Annals of Glaciology*, **33**: 275–279.
Wendler, G., Adolphs, U., Hauser, A., and Moore, B., 1997a. On the surface energy budget of sea ice. *Journal of Glaciology*, **43**(143): 122–130.
Wendler, G., Stearns, C., Weidner, G., Dargaud, G., and Parish, T., 1997b. On the extraordinary katabatic winds of Adélie Land. *Journal of Geophysical Research*, **102**(D4): 4463–4474.
Worby, A.P., and Allison, I., 1991. Ocean–atmosphere energy exchange over thin variable concentration Antarctic pack ice. *Annals of Glaciology*, **15**: 184–190.
World Meteorological Organization, 1967. *Polar Meteorology*, Technical Note No. 87. Geneva: World Meteorological Organization.
Wu, X., Budd, W.F., and Jacka, T.H., 1999. Simulations of Southern Hemisphere warming and Antarctic sea-ice changes using global climate models. *Annals of Glaciology*, **29**: 61–65.
Wu, X., Budd, W.F., Worby, A.P., and Allison, I., 2001. Sensitivity of the Antarctic sea-ice distribution to oceanic heat flux in a coupled atmosphere–sea ice model. *Annals of Glaciology*, **33**: 577–584.
Yasunari, T., and Kodama, S., 1993. Intraseasonal variability of katabatic wind over East Antarctica and planetary flow regime in the Southern Hemisphere. *Journal of Geophysical Research*, **98**: 13063–13070.
Yuan, X., and Martinson, D.G., 2001. The Antarctic Dipole and its predictability. *Geophysical Research Letters*, **28**(18): 3609–3612.
Yuan, X., Martinson, D.G., and Liu, W.T., 1999. Effect of air-sea-ice interaction on winter 1996 Southern Ocean subpolar storm distribution. *Journal of Geophysical Research*, **104**(D2): 1991–2007.

Cross-references

Albedo and Reflectivity
Arctic Climates
Atmosphere Circulation, Global
Energy Budget Climatology
Ocean Circulation
Oscillations
Sea Ice and Climate

APPLIED CLIMATOLOGY

Applied climatology has been the foundation upon which the world's weather-sensitive activities and infrastructure have been developed. Applications of climate data and information have likely contributed more to the development of most nations than any other function of the atmospheric sciences. Today weather forecasts are very useful and important but these only became available in the twentieth century, more than 150 years after applied climatology had been in service to the nation.

What is applied climatology? The answer may seem obvious, but the definition of applied climatology is elusive for several reasons. Activities falling under the umbrella of applied climatology are spread among many disciplines. The activities also have interfaces with many parts of the atmospheric sciences, forming a myriad number of interactions. The field is truly interdisciplinary, embracing climatologists and those of other disciplines including hydrology, agriculture, engineering, and business. This breadth of the field and its evolution over time make the history of applied climatology interesting.

Over 50 years ago, leaders in the field defined applied climatology as the scientific analysis of climate data in light of a useful application for an operational purpose (Landsberg and Jacobs, 1951). A recently published glossary of meteorological terms indicates that applied climatology includes agricultural climatology, aviation climatology, bioclimatology, industrial climatology, and others (AMS, 2000).

My interpretation is that applied climatology describes, defines, interprets, and explains the relationships between climate conditions and countless weather-sensitive activities. For example, if viewed in a business sense, applied climatology would embrace interactions with marketing, sales, customer services, research support, and the delivery arm for climatological data and information. The diversity of the field is one of its hallmarks.

Applied climatology does not include fundamental, basic studies of the climate system, but it does embrace causation as a functional part of explaining climatic relationships to other phenomena. For example, a climatological study of rainfall effects on streamflow may include an explanation of the atmospheric factors influencing the rainfall variability between days, months, or years.

The field of applied climatology has evolved over the past 60 years, into interactive groups embracing three functional areas. First is the inner core of applied climatology – focusing on instruments and data. Functions include data collection, transmission, quality assessment, archival, its representativeness in space and time, and access to it.

Functions found in the second group relate to the interpretation and generation of climate information generally based on interactions with users. Activities include statistical and physical analyses, performance of special interpretive studies, and generation of information (published or computer-based). Within the atmospheric sciences, applied climatology extends well into the areas of dynamic climatology, instrumentation, and climate data. Applied climatological research develops the informational products for the users, studies the climate–sector relationships, develops statistical techniques to express climate information effectively, contributes to weather data collection efforts, and develops databases to fulfill its mission. Today

these functions are handled by state climatologists, university-based scientists, and staffs at regional climate centers, the National Climatic Data Center, the Climate Prediction Center, and the private sector that addresses climate services.

The third group consists of users of applied climatology products, and is easily the largest group. Users include scientists in many disciplines and decision makers in business and government. Effective relationships between applied climatologists and users require a two-way interaction to share needs and information. Applications of climate information fall into four classes: (1) design of structures and planning activities, (2) assessments of current and past conditions including evaluation of extreme events, (3) study of the relationships between weather–climate conditions and those in other parts of the physical and socioeconomic worlds, and (4) operation of weather-sensitive systems that employ climatic information in making decisions.

History

Applied climatology, as one sector of today's world of atmospheric sciences, was the first atmospheric sciences activity to serve humankind, and applied climatology remains a most successful contributor to the nation's well-being.

Persons such as Thomas Jefferson were among the nation's early users of climate information. Jefferson planned farming operations around local climate conditions and applied climate information in the equipment he designed and used and in building construction (Martin, 1952). Crop selection, construction styles, and building placement in the eighteenth century reflected awareness of climate conditions and their effects.

The beginning of weather observations, both privately and at military forts, helped further applications of climate data. The expansion and organization of the nation's weather data collection system, and science in general, occurred during the nineteenth century.

Early leaders in the emerging field of meteorology, such as James Espy and Elias Loomis, recognized regional differences in the nation's climate and identified how these differences created profoundly different effects on human endeavors (Fleming, 1990). A key scientist of the century, Joseph Henry, made invaluable studies in applied climatology, and in the 1850s analyzed the impacts of climate on US agriculture of the time. Koeppen (1885) and other scientists began associating climate conditions with various land uses and plant environments as a means to define climate regions in each continent.

Further growth in the understanding of climate interactions with various physical systems, such as water resources, had to await the systematic collection of data on climate as well as weather-sensitive conditions. As the nation entered the twentieth century data collection had been in progress sufficiently long to allow new, more definitive studies of how climate impacted activities. For example, Thiessen was a civil engineer who in 1912 defined how climate conditions were to be used in engineering designs. Famed hydrologist Robert Horton made basic discoveries regarding the components of the hydrologic cycle, and unraveled the complexities of climate–hydrology conditions of the Great Lakes in the 1920s (Horton, 1927). Early key studies of effects of climate on human health and behavior included those of C.F. Brooks (1925).

A national priority of the nineteenth century was to enhance agricultural production, and this led to the establishment of the US Weather Bureau in 1888, as part of the Department of Agriculture (Whitnah, 1961). Establishment of experimental farms around the nation ultimately produced the data needed to make definitive studies of how various components of the climate affected each crop, as well as livestock. Wallace (1920) made strides by developing the first climate–crop yield models. Thornthwaite (1937) pioneered modeling of the hydrologic system so as to derive measures of evapotranspiration and soil moisture and their effects on both plants and crops.

By 1940 many of the fundamental relationships between climate conditions and other physical systems had been sufficiently delineated to allow highly effective designs of structures, selections of regionally appropriate crop varieties, and wise management of water resource systems in the varying climatic zones of the nation (Landsberg, 1946). The pressures of World War II for climate data and expertise brought forth a new dimension to applied climatology (Jacobs, 1947). For example, studies focused on severe weather conditions such as tornadoes and hail, and their effects on crops, property, and human life (Flora, 1953). A flood of publications within the realm of applied climatology appeared during the 1940s and 1950s (Landsberg and Jacobs, 1951). This explosion of research and information generation was also tied to the creation of computers during World War II and use of punch cards as a means of digitizing historical weather data. By 1948 a national center housing all historical climate data had been established. The National Climatic Data Center (NCDC) staff began generating a myriad of publications giving potential users access to information never before widely available (Changnon, 1995).

Ever-improving computers and digitized data allowed major achievements in modeling of climate effects such as hydrologic models that related various climatic variables to streamflow behavior (Linsley et al., 1958). Heavy rainfall design information, critical to planning and designs to manage flooding, was generated (Hershfield, 1961; Huff, 1986). A highly useful national drought index was devised (Palmer, 1965), and sophisticated climate–crop yield models appeared, allowing accurate predictions of yield outcomes well before harvest (Thompson, 1964). Other studies addressed another important sector of applied climatology – the economic and environmental impacts of all forms of climate (Maunder, 1970; McQuigg, 1974). Major advances in statistical techniques for applied climate analysis occurred (Conrad and Pollack, 1944; Court, 1949). An area of applied climatology that has evolved over the past 100 years concerns urban climates and other human-induced changes to the landscape leading to altered local and regional climates (Landsberg, 1956; Changnon, 1973; Oke, 1973). The impacts of these changes on the physical world and socioeconomic sectors have also been assessed (Changnon, 1984; Hare, 1985) with climate guidance to urban planners (Changnon, 1979). Finally, textbooks that addressed applied climatology appeared (Oliver, 1973, 1981; Thompson and Perry, 1997), serving to enhance training and attention to the field.

By 1970 applied climatology had moved to a new level of recognition and ever-higher value to the user community. Atmospheric scientists within the field turned their attention to improvements to: weather-sensing instruments, data quality and its archival, access of data and climate information, and generation of user-friendly climate products.

The golden age

The era since about 1970 has seen a series of scientific and technological changes that have vastly enhanced the field of

applied climatology. Coupled with these advances have been national and global economic conditions that acted to increase the demand for climate products. The golden age of applied climatology had begun.

The agricultural economy became global, and with this expansion came huge economic pressures. American firms searched for every activity that would give them an advantage. One of these was use of climate predictions. Firms that had previously ignored use of uncertain climate outlooks now shifted and became users. Other business sectors also became global, and the net effect was more use of climate data and information.

Another factor enhancing wide interest and use of climate information comprised major global climate anomalies of the 1970s and early 1980s and their severe impacts (Kates, 1980; Panel, 1981). This included the devastating Sahel drought, the record cold winters of 1976–1980 in the US, and the droughts of 1980, 1983, and 1988. Climate, and the problems it created, including escalation of federal relief payment for weather–climate disasters, attracted the attention of the federal government, and Congress passed the National Climate Program Act in 1978. This program fostered new climate institutions, enhanced applied research, and funded new data collection–transmission systems. However, at the federal level the program became overshadowed in the late 1980s by the rapidly expanding national climate change endeavors. Concerns over a climate change related to global warming became the new thrust enveloping most of the atmospheric sciences. An era of numerous weather extremes and large global losses during the 1990s has led applied climatologists to pursue climatological assessments (Changnon, 1999a,b). Some have assessed whether these increasing losses were due to the start of a climate change due to global warming, to increasing societal vulnerability to climate (Changnon et al., 2000), and/or to inadequate government policies (Changnon and Easterling, 2000). Recent major urban droughts in the US initiated new societal problems, indicating that the future of water supplies for major urban areas looks questionable (Changnon, 2000).

Development during the 1960s and 1970s of reasonably inexpensive computer systems capable of handling large volumes of climate data was another key factor in the recent growth of applied climatology. The systems allowed continual updates of information, and the development and delivery of near real-time climate information, coupled with wide use of PCs. Everyone could access a wealth of climate information quickly and at low cost (Kunkel et al., 1990). This enhanced use of climate information has helped create greater awareness of the value of applied climatology.

The above-mentioned fast access was facilitated by another critical step forward – the development of inexpensive means to quickly collect data, and to transmit climate data and information. This included satellites and the Internet. These allowed real-time transmittal of data and quick access to it, a huge step forward (Changnon and Kunkel, 1999). Closely coupled with this advance were the establishment of new climate service/research centers, which had been fostered by the National Climate Program (Changnon et al., 1990), as well as the growth of private sector providers of climate information (Vogelstein, 1998). The development of these new institutions with expertise and systems to serve the needs of users of climate data and information led to other advances in applied climatology.

Interdisciplinary research of climatologists and other physical and social scientists increased, and this led to a new level of sophisticated climate-effect models (crops, water, transportation, etc.). Further, these models, when fed with real-time data, allowed their use in operational settings. Thus, near real-time estimates of current and projected climate effects were generated for decision makers. These activities moved forward in the right arenas based on assessments of user needs that began during the 1970s, a form of market analysis for climate products (Changnon et al., 1988; Changnon, 1992).

Since the 1970s the nation and world have seen an increase in society's sensitivity to climate conditions and especially extremes. Population growth, coupled with demographic changes and wealth, have created greater vulnerability and hence higher costs from climate anomalies. These impacts in the US have further promoted the growth in the use of climate data and information to more effectively react, manage, and compete (Stern and Easterling, 1999). Climate information has taken on greater value. One reflection of this in the business world has been the development and use of "weather derivatives" during the 1990s, a means of insuring against climatological risk (Zeng, 2000). One company offers coverage for a fixed price against a climate outcome, say a cold winter, that a utility fears economically. If the cold winter occurs, the coverage firm pays the other for its losses, but if the cold winter does not occur, the coverage firm retains the original payment. Such risks are assessed using climate data.

One of the applied climate products long sought by weather-sensitive entities has been accurate long-term climate predictions. The past 15 years have seen major advances in climate prediction quality, related to a greater understanding of the climate system such as the effects of El Niño on the nation's climate (Kousky and Bell, 2000). Government predictions have improved, both in accuracy and formats needed by users (Changnon et al., 1995). Private firms now work more closely with firms to interpret predictions to meet specific corporate needs.

As stated, applied climatology has moved into its golden age in service to society. In a recent book Thompson and Perry (1997) provide a broad, all-encompassing view of the world of applied climatology. They and 27 other applied climatologists prepared chapters on wide-ranging topics such as climate effects on tourism, glaciers, fisheries, and air pollution. Hobbs (1997), in a sweeping assessment of applied climatology, points to the growing awareness of applied climatology and increasing use of climate information.

However, not all things are occurring at an optimum level. Some problems still face the field. Ironically, teaching of applied climatology is too limited and often not done at many colleges and universities. To be effective, quality instruction in applied climatology requires interdisciplinary training and experience (Changnon, 1995).

A second concern relates to the adequacy of weather instrumentation and data collection. Since the structure of weather data collection endeavors in the US is still dominated by the needs of forecasters, there are continuing problems with sustaining adequate spatial sampling of climate conditions and with the use of instruments that allow continuity with historical data (NRC, 1998). For example, the automated surface observation system installed during the 1990s for measuring many weather conditions at nation's first-order weather stations has led to alterations in the quality of certain data.

As noted above, the use of climate data and information has grown rapidly in the past 30 years, but sampling reveals many potential users are still not served and often unaware of

applications (Changnon and Changnon, 2003). An outreach effort by government agencies involved in climate services and by private sector partners is needed to educate and demonstrate how to use climate information and the potential values apt to be realized from usage to manage climate risks.

There is no systematic collection of data on the impacts of climate extremes, and a national effort to begin such data collection is needed (NRC, 1999). Uncertainty over impacts under a changing future climate due to global warming is a current dilemma and one that will continue. Hare (1985) first noted the need to consider impacts of future climate change. Some have predicted future climate conditions exceed extremes sampled in the past 100 years, making use of existing climate-impact regression models as predictors of future impacts invalid. The implications of future climate changes remain a major challenge for applied climatologists. This is reflected in a recent book about applied climatology which includes four chapters addressing potential impacts of future climate change (Thompson and Perry, 1997).

Resolution of these four issues – better training, stabilization of weather measurements, better information on climate impacts, and effects of global warming induced climate change – needs to be accomplished to realize the full potential of applied climatology. Regardless, applied climatology is the oldest atmospheric sciences activity in service to society, and its most successful.

Stanley A. Changnon

Bibliography

American Meteorological Society, 2000. *Glossary of Meteorology*. Boston, MA.

Brooks, C.F., 1925. The cooling of man under various weather conditions. *Monthly Weather Review*, **53**: 28–33.

Changnon, D., 1998. Design and test of a "hands-on" applied climate course in an undergraduate meteorology program. *Bulletin of the American Meteorological Society*, **79**: 79–84.

Changnon, S.A., 1973. Atmospheric alterations from man-made biospheric changes. In *Weather Modification: social concerns and public policies.* Western Geographical Series, pp. 134–184.

Changnon, S.A., 1979. What to do about urban-generated weather and climate changes. *Journal of the American Planning Association*, **45**: 36–48.

Changnon, S.A., 1984. Purposeful and accidental weather modification: our current understanding. *Physical Geography*, **4**: 126–139.

Changnon, S.A., 1992. Contents of climate predictions desired by agricultural decision makers. *Journal of Applied Meteorology*, **31**: 1488–1491.

Changnon, S.A., 1995. Applied climatology: a glorious past, and uncertain future. *Historical Essays in Meteorology, American Meteorological Society*, **11**: 379–393.

Changnon, S.A., 1999a. Factors affecting temporal fluctuations in damaging storm activity in the U.S. based on insurance loss data. *Meteorological Applications*, **6**: 1–11.

Changnon, S.A., 1999b. Record high losses for weather hazards during the 1990s: how excessive and why? *Natural Hazards*, **18**: 287–300.

Changnon, S.A., 2000. Reactions and responses to recent urban droughts. *Physical Geography*, **21**: 1–20.

Changnon, D., and Changnon, S., 2003. Assessment of issues related to usage of climate predictions in the U.S. agribusiness sector and utility industry. *Proceedings, Workshop on Climate Predictions. American Meteorological Society*, Washington, DC.

Changnon, S.A., and Easterling, D.R., 2000. U.S. policies pertaining to weather and climate extremes. *Science*, **289**: 2053–2055.

Changnon, S.A., and Kunkel, K.E., 1999. Rapidly expanding uses of climate data and information in agriculture and water resources. *Bulletin of the American Meteorological Society*, **80**: 821–830.

Changnon, S.A., Sonka, S., and Hofing, S., 1988. Assessing climate information use in agribusiness. Part 1: Actual and potential use and impediments to use. *Journal of Climate*, **1**: 757–765.

Changnon, S.A., Lamb, P., and Hubbard, K., 1990. Regional climate centers: new institutions for climate services and climate impact records. *Bulletin of the American Meteorological Society*, **71**: 527–537.

Changnon, S.A., Changnon, J., and Changnon, D., 1995. Assessment of uses of climate forecasts in the utility industry in the central U.S. *Bulletin of the American Meteorological Society*, **76**: 711–720.

Changnon, S.A., Pielke, R.A., Changnon, D., Sylves, R., and Pulwarty, R., 2000. Human factors explain the increased losses from weather and climate extremes. *Bulletin of the American Meteorological Society*, **81**: 437–442.

Conrad, V., and Pollack, L., 1944. *Methods in Climatology.* Boston, MA: Harvard University Press.

Court, A., 1949. Separating frequency distributions into normal components. *Science*, **110**: 500–510.

Fleming, J.R., 1990. *Meteorology in America, 1800–1870*. Baltimore, MD: Johns Hopkins University Press.

Flora, S.D., 1953. *Tornadoes of the U.S.* Norman, OK: University of Oklahoma Press.

Hare, K.F., 1985. Future environments – can they be predicted? *Transactions, Institute of British Geographers*, **10**: 131–137.

Hershfield, D.M., 1961. *Rainfall Frequency Atlas of the U.S. Weather Bureau.* Washington, DC.

Hobbs, J.E., 1997. Introduction: the emergence of applied climatology and climate impact assessment. In *Applied Climatology Principles and Practice*. New York: Routledge, pp. 1–12.

Horton, R.E., 1927. *On the Hydrology of the Great Lakes.* Sanitary District of Chicago, Chicago, IL: Engineering Board of Review.

Huff, F.A., 1986. Urban hydrometeorology review. *Bulletin of the American Meteorological Society*, **67**: 703–711.

Jacobs, W.C., 1947. Wartime development in applied climatology. *Meteorology Monographs*, **1**(1): 1–52.

Kates, R.W., 1980. Climate and society: lessons from recent events. *Weather*, **35**: 17–25.

Koeppen, W., 1885. Zur Charaskteristik der regen in NW Europa and Nordaamerika. *Meteorologie Zhurnal*, **10**: 24.

Kousky, V.E., and Bell, G.D., 2000. Causes, predictions, and outcomes of El Nino 1997–1998. In *El Nino 1997–1998, the Climate Event of the Century.* New York: Oxford University Press, pp. 28–48.

Kunkel, K.E., Changnon, S.A., Lonnquist, C., and Angel, J.R., 1990. A real-time climate information system for the Midwestern U.S. *Bulletin of the American Meteorological Society*, **71**: 601–609.

Landsberg, H., 1946. Climate as a natural resource. *Scientific Monthly*, **63**: 293–298.

Landsberg, H., 1956. The climate of towns. In ed., *Man's Role in Changing the Face of the Earth*, Chicago, IL: University of Chicago Press.

Landsberg, H., and Jacobs, W.C., 1951. Applied climatology. In Malone, T.F., ed., *Compendium of Meteorology*. Boston, MA: American Meteorological Society, pp. 976–992.

Linsley, R.K., Kohler, M., and Paulhus, J., 1958. *Hydrology for Engineers.* New York: McGraw-Hill.

Martin, E.T., 1952. *Thomas Jefferson: Scientist.* New York: H. Schuman.

Maunder, W.J., 1970. *The Value of the Weather*. London: Methuen.

McQuigg, J.D., 1974. The use of meteorological information in economic development. Applications of meteorology to economic and social development. *World Meteorological Organization Technical Note*, **132**: 7–59.

National Research Council, 1998. *Future of the National Weather Service Cooperative Network*. Washington, DC: National Academy Press.

National Research Council, 1999. *The Costs of Natural Disasters: A Framework for Assessment*. Washington, DC: National Academy Press.

Oke, T.R., 1973. City size and the urban heat island. *Atmospheric Environment*, **7**: 769–779.

Oliver, J.E., 1973. *Climate and Man's Environment: An Introduction to Applied Climatology*. New York: Wiley.

Oliver, J. E., 1981. *Climatology: Selected Applications*. New York: Wiley.

Palmer, W.C., 1965. Meteorological drought. *U.S. Weather Bureau Research Paper* 45. Washington, DC.

Panel on the Effective Use of Climate Information in Decision Making, 1981. *Managing Climatic Resources and Risks*. Washington, DC: National Academy Press.

Stern, P., and Easterling, W., 1999. *Making Climate Forecasts Matter*. Washington, DC: National Academy Press.

Thompson, L.M., 1964. Our recent high yields – how much is due to weather? "Research in Water". *Soil Society of America*, **6**: 74–84.
Thompson, R.D., and Perry, A., 1997. *Applied Climatology Principles and Practice*. New York: Routledge.
Thornthwaite, C.W., 1937. The hydrologic cycle re-examined. *Soil Conservation*, **3**: 85–91.
Vogelstein, F., 1998. Corporate America loves the weather. *U.S. News & World Report*, 13 April, pp. 48–50.
Wallace, H.A., 1920. Mathematical inquiry into the effect of weather on corn yields in the eight corn belt states. *Monthly Weather Review*, **48**: 439–446.
Whitnah, D., 1961. *A History of the U.S. Weather Bureau.* Urbana, IL: University of Illinois Press.
Zeng, L., 2000. Weather derivatives and weather insurance: concept, application, and analysis. *Bulletin of the American Meteorological Society*, **81**: 2075–2082.

Cross-references

Art and Climate
Bioclimatology
Climate Hazards
Commerce and Climate
Crime and Climate
Hydroclimatology
Tourism and Climate

ARCHEOCLIMATOLOGY

The term archeoclimatology was coined by Reid A. and Robert U. Bryson, about 1990, to designate a particular approach to the estimation of past climates on the time and spatial scales appropriate for the use of archeologists (Bryson and Bryson, 1994). Because cultures change on less than the millennial scale, and because people live in relatively restricted areas, whatever data or model is used must be nearly site-specific and of high time-resolution. Ideally the method should be rather economical, since archaeology tends to be funded at a low level.

This subspecialty of paleoclimatology is largely concerned with bringing together various sources of estimation of past climates, models and proxy estimates from field studies, to provide the most consistent estimates of the past climatic environment at particular places and times. The study of proxy records has been well advanced by various other Earth and biological sciences, so archeoclimatology thus far has been concerned with climatic models designed with this particular end in sight rather than on studies of the atmosphere itself.

The definition of climate

The way a segment of the world is studied depends on how the topic is defined relative to the expertise of the scientist and the historical precedents of the scientist's discipline as much as on rational analysis. This may lead to definitions and biases that affect the study of the topic.

The usual definition of climate according to meteorologists is approximately that given in the *Glossary of Meteorology* (Huschke, 1959). Here climate is defined by reference to C.S. Durst, a meteorologist, as "The synthesis of the weather". Huschke then goes on: "More rigorously, the climate of a specified area is represented by the statistical collective of its weather conditions during a specified interval of time (usually several decades)."

Geographers tend to use a similar definition, witness Trewartha's "Climate . . . refers to a more enduring regime of the atmosphere; it is an abstract concept. It represents a composite of the day-to-day weather conditions, and of the atmospheric elements, within a specified area over a long period of time" (Trewartha and Horn, 1980). (How one can use facts, figures and equations to study an "abstract concept" is more than a little puzzling.) Lamb uses a similar definition of climate: "Climate is the sum total of the weather experienced at a place in the course of the year and over the years" (Lamb, 1972).

Viewing climate as essentially a summation of the weather has profound implications for the development of a body of climatological theory. Indeed, the preceding sentence might evoke disagreement from many atmospheric scientists for the common definition of climate indicates that there is no distinct body of theory separate from that of the weather, except perhaps statistical theory. With this viewpoint one might disagree, based on a quite different view of the relation of climate and weather.

The relation of climate and weather

An experienced meteorologist can identify the atmospheric circulation pattern on a weather map immediately as to whether it represents a summer pattern or a winter pattern. Usually the identification of the season can be even closer. The reason the array of weather patterns characteristic of a season differs from the array of another season is that the climate differs from season to season. This statement, of course, does not make sense if the climate is the summation of the weather. It does make sense if the thermodynamic status of the Earth–atmosphere–hydrosphere–cryosphere system *determines* the array of possible (and necessary) weather patterns. This status, which changes with time and season, *along with* the associated weather patterns, constitutes the climate.

The basis of the present discussion, and the research of which it is an elaboration, is that the climate is a consequence of external controls on the atmosphere–hydrosphere–cryosphere system. These "boundary conditions" force the state of the climate system, which in turn produces and requires sets of weather complexes, which differ as the climate differs from one time to another. For example, the climatic state thought of as summer has a different array of associated weather patterns than does the climatic state called winter (Bryson, 1997).

Modeling the climate on this basis utilizes what is here called a macrophysical approach. Relationships of large-scale nature are used, such as the Rossby long-wave equations, the thermal wind relationship, or the Z-criterion derived from the work of Smagorinsky (1963). The model on which archeoclimatology is based required first a model of global glacial volume, from which the glaciated area could be calculated and the ice albedo effect estimated (Bryson and Goodman, 1986). A hemispheric temperature model was then possible using the so-called Milankovitch-type variations in solar irradiance as modulated by volcanic aerosols (Bryson, 1988). This section of the overall model is essentially a "heat budget model" but with improved treatment of the volcanic modulation.

Going from hemispheric or global models to regional models requires that some broad-scale relationships be used. For example, one knows that the westerlies must become stronger with height up to about 10 km because the Earth is colder at the poles than at the equator, and the rate of increase is proportional

to the magnitude of the south–north temperature gradient. Since equatorial temperatures change relatively little even from glacial to non-glacial times, the average hemispheric temperature and the temperature gradient must both depend primarily on high-latitude temperatures.

Assuming that the zonal component of the wind at 500 mb is proportional to the meridional temperature gradient, this concept was applied to North Africa, using the "Z-criterion" to calculate the latitude of the subtropical anticyclone and the latitude of the jet axis at 500 mb (Bryson, 1992). Empirical values of the appropriate gradients were derived from the inter-monthly variation, including the relation between the latitude of the anticyclone and the latitude of the intertropical convergence (ITC). Ilesanmi's model (1971) relating position of the ITC to rainfall south of it could then be used to estimate the rainfall in the Sahel at two- or five-century intervals for the late Pleistocene and Holocene. The match with palaeolimnological and archaeological field data was excellent. Ilesanmi's model is an example of the kind of synoptic climatology that constitutes the final calculation of the local climatic effect from the large-scale features of the atmospheric circulation.

The hierarchical steps and the fundamental assumptions

Step 1: Model glacier volume and area

Examination of the geological evidence tells us that the volume of glacier changes very slightly in the southern hemisphere from glacial to interglacial, and that most of the Pleistocene northern hemisphere glacier was in North America, with a large part of the rest being in northwestern Europe.

Synoptic climatology tells us that the snowiest winters in the major North American glacier accumulation areas are mild winters. Logic and experience tell us that snow melts slower in a cool, cloudy wastage season.

Assumption 1
Assume that the seasonal temperature of the hemisphere is related to the amount of radiation received and absorbed near the surface by the hemisphere in that season. (And secondarily, that the winter temperatures in the ice accumulation area of North America are essentially always well below freezing, even as now.)

It follows that accumulation rate minus wastage rate will be inversely related to the radiation seasonality of the hemisphere.

It also follows that the difference of these two rates is also a rate, so that this net accumulation rate must be integrated to simulate the total glacier volume at any particular time (arbitrary units).

The northern hemisphere irradiance seasonality may be computed using the "Milankovitch" periodicities in the usual Fourier series form, which may be readily integrated. This series contains no high-frequency terms (Bryson and Goodman, 1986).

Assumption 2
Assume that volcanic aerosol is the major source of modulation of the incoming radiation in ancient times.

Volcanic eruption chronologies may be extended back to about 30 000 years, however, using radiocarbon-dated eruptions. Using historically observed eruptions, Goodman was able to show that most of the variance of the observed aerosol loading can be explained by the volcanic record (Goodman, 1984).

Using the radiocarbon-dated volcanic eruption chronology it is possible to construct a proxy record of volcanic aerosol that extends back at least 30 000 years. This may be used to modulate the radiation for the integrated Milankovitch-based glacier volume modeling, and thus introduce higher-frequency terms into the glacier model.

The result of this modulation and the introduction of higher-frequency terms is a simulation in arbitrary units of glacial volume that follows the known geological record quite well, including such short-term features as the "Younger Dryas", and Neo-Glaciation. The arbitrary units may be readily calibrated into standard volume units by scaling (Bryson, 1988).

Step 2: Model hemispheric seasonal temperatures

Assumption 1
Assume that the largest source of variation in hemispheric albedo is due to variation in ice and snow cover.

Estimates of glacial volume from step 1 may be converted to glaciated area using the relationship developed by Moran and Bryson for typical glacial profiles (Moran and Bryson, 1969).

Measurements of typical albedos clearly indicate the dominance of ice as the source of variation in time for the total range of albedo for the other surfaces is less than even the range within various forms of ice cover (Kung et al., 1964).

Assumption 2
Assume equivalent opaque cloud cover. With the definition of equivalent opaque cloud cover developed by Dittberner and Bryson, the cloud amount drops out of the heat budget equations *but only for climatic scales* (Bryson and Dittberner, 1976).

Assumption 3
Assume that, throughout most of geological history, carbon dioxide and water vapor content of the atmosphere have been dependent variables, dependent on the temperature, and as a first approximation linearly so (Bryson, 1988).

Step 3: Model monthly hemispheric temperature, evaporation, and net radiation

Using the Lettau climatonomic method of obtaining a mutually consistent set of monthly surface heat budget components monthly temperatures may be obtained (Lettau and Lettau, 1975; Lettau, 1977, 1984).

Step 4: Calculate the position of the "centers of action" (large-scale features such as the subtropical anticyclones and the jet stream)

Assumption 1
Assume that the latitude of dynamic instability of the westerlies as calculated by Smagorinsky is a valid estimate of the latitude of the subtropical anticyclones. That this is valid was first suggested by Flohn, who used the term "Z-criterion". Tests with modern data give abundant evidence that the assumption is valid even regionally, and gives very close estimates (Flohn, 1965; Smagorinsky, 1963).

The Z-criterion calculation requires only the large-scale meridional and vertical temperature gradients.

Assumption 2
Assume that, since equatorial temperatures hardly vary during the course of the year and in time, that the meridional temperature gradient is a function of the mean hemispheric temperature and that the vertical temperature gradient is a function of season. These relationships may be determined empirically using modern data.

Assumption 3
Assume that the latitude of the jet stream is closely related to the outer edge of the westerlies as calculated with the Z-criterion (Bryson, 1992).

It has been shown that the latitude of the intertropical convergence is closely related to the latitude of the related subtropical high(s) (Bryson, 1973).

At this point one may have calculated the monthly latitude of the subtropical anticyclones, latitude of the jet stream and position of the intertropical convergence for each sector of the hemisphere for as far into the past as the volcanic aerosol record and Milankovitch calculations allow, and at intervals of centuries dictated by the quality of the volcanic record.

Step 5: Calculate local climate history from output of the above steps

At this stage, knowing the mean locations of the major anticyclones, mean latitude of the jet stream, and mean latitude of the intertropical convergence, sector by sector and month by month, one may use the well-established techniques of synoptic climatology to calculate the mean monthly local values of temperature, precipitation, rainfall frequency, potential evapotranspiration, etc. at one's station of interest.

For example, one might want to calculate the past precipitation amount for a location in the midwestern United States, such as Madison, Wisconsin. It is well known that tropical air from the North Atlantic cyclone brings warm-season rain when it is far north, but this is not a linear relationship. It is also known that the cyclonic storms associated with the storm track represented by the jet stream position bring the maximum rains of spring and early fall, and lesser amounts in winter. Other times, especially in winter, air from the Pacific anticyclone streams across the country, usually suppressing the rains in Madison. The problem then is to say how the mean monthly precipitation at Madison responds to the position of these circulation features. The synoptic climatology approach to this problem is empirical. By examination of the relationship of the precipitation at Madison to these circulation elements within the instrumental period, one can establish a quantitative relationship, which is

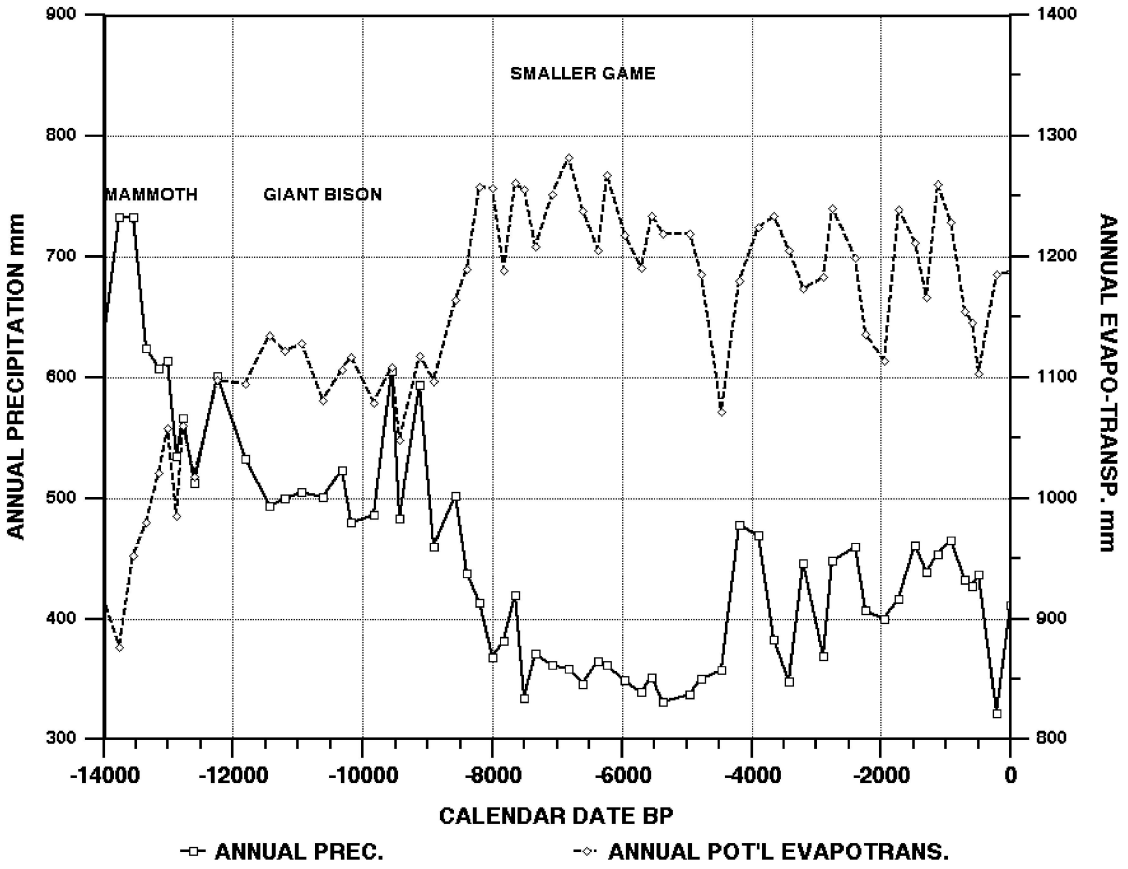

Figure A35 Modeled water supply history for Portales, New Mexico.

assumed to apply as far back as the general geographic pattern of waters and topography is relatively constant.

One virtue of the synoptic climatology approach is that the local and regional topography, etc. is implicitly included in the precipitation, temperature, etc. values that have been observed. For example, the data from Milwaukee, 75 miles east of Madison, differ from the data for Madison, in part because Miewaukee is on the shore of a great lake, and thus the relationship of the precipitation there to the large-scale circulation features would contain, implicitly, the effect of its location.

We can then say that the archeoclimatic model for North American precipitation at a particular place consists of the latitudes of the oceanic anticyclones, the jet stream and the intertropical convergence as inputs, and the calibrated response of the local mean values of the precipitation at that place as the output. Since the circulation features have been calculated far into the past, we can assume that the calibration was the same then, and calculate the local past climate. As a first approximation non-linear regression is used for calibration. Lacking a long series of observed values of all the needed data, the annual march of monthly positions of the circulation elements and of the precipitation are used, and in over 2000 trial cases seems to be an adequate first approximation.

The position of the intertropical convergence is used, even for northern locations, because it is related to the insertion of very moist air into the westerlies, sometimes in tropical cyclones, and hence is related to the precipitation even at higher latitudes.

On the other hand, the positions of the polar anticyclones are omitted because they are more dependent on topography and errors of pressure reduction to sea level than they are to dynamics of the atmosphere, and the latitude of the jet stream gives the outer limit of polar air.

Example 1: North America

Eastern New Mexico has been of particular interest to archeologists because it is a well-known locale for early big-game hunters in North America. These included hunters of mammoth and giant bison, the Clovis and Folsom cultures. Clovis, New Mexico, is the type locality for the distinctive projectile point of the Clovis people, a form found over a vast area of North America. The archeoclimatic model of the past climate of nearby Portales, NM yielded the next two graphs (Figures A35 and A36) of the precipitation, potential evapotranspiration and temperature history of the locale.

The graph of precipitation shows the high precipitation and lower evapotranspiration of latest Pleistocene time necessary to produce the rather lush vegetation required to support mammoths. This situation changes rapidly after the "Younger Dryas" peak precipitation to a quite different situation by 10 500 years before the present, and the typical big game changed to bison. With the advent of the Middle Holocene, after 8000 radiocarbon years ago, the environment only supports smaller game, and indigenous cultures no longer hunt big game. This pattern seems to agree with the field evidence.

Example 2: The Mediterranean

In 1965 Rhys Carpenter, a distinguished scholar of ancient Greece, proposed that the famous and very important Kingdom based at Mycenae, in the Peloponnesus, had

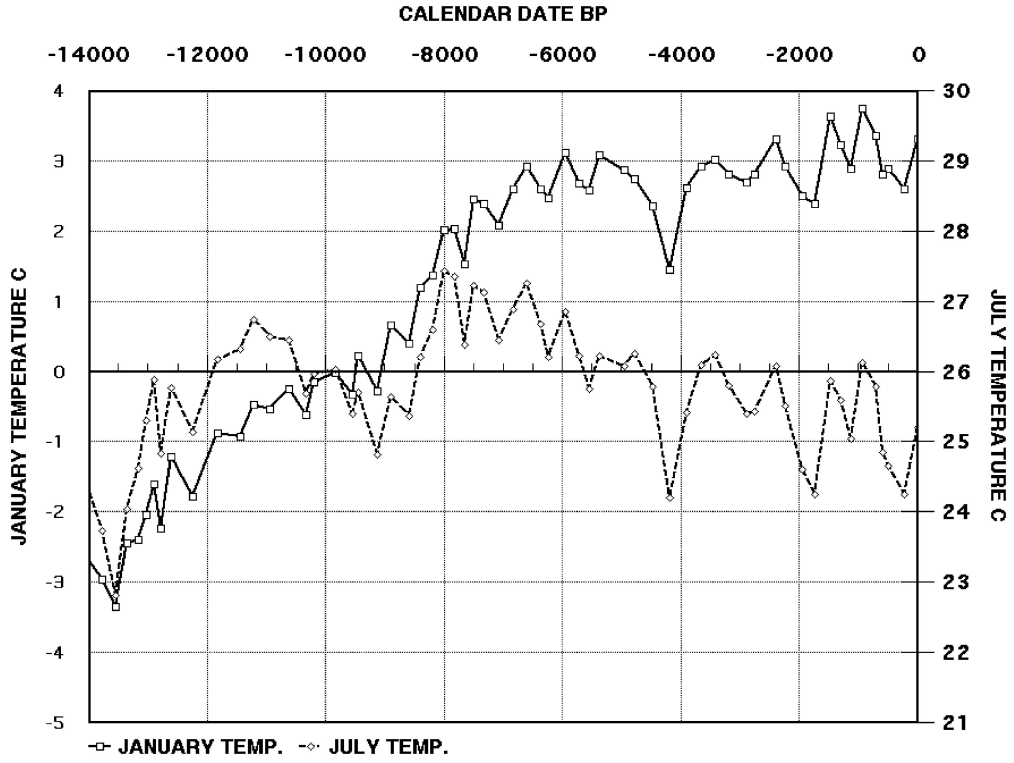

Figure A36 Modeled temperature history for Portales, New Mexico.

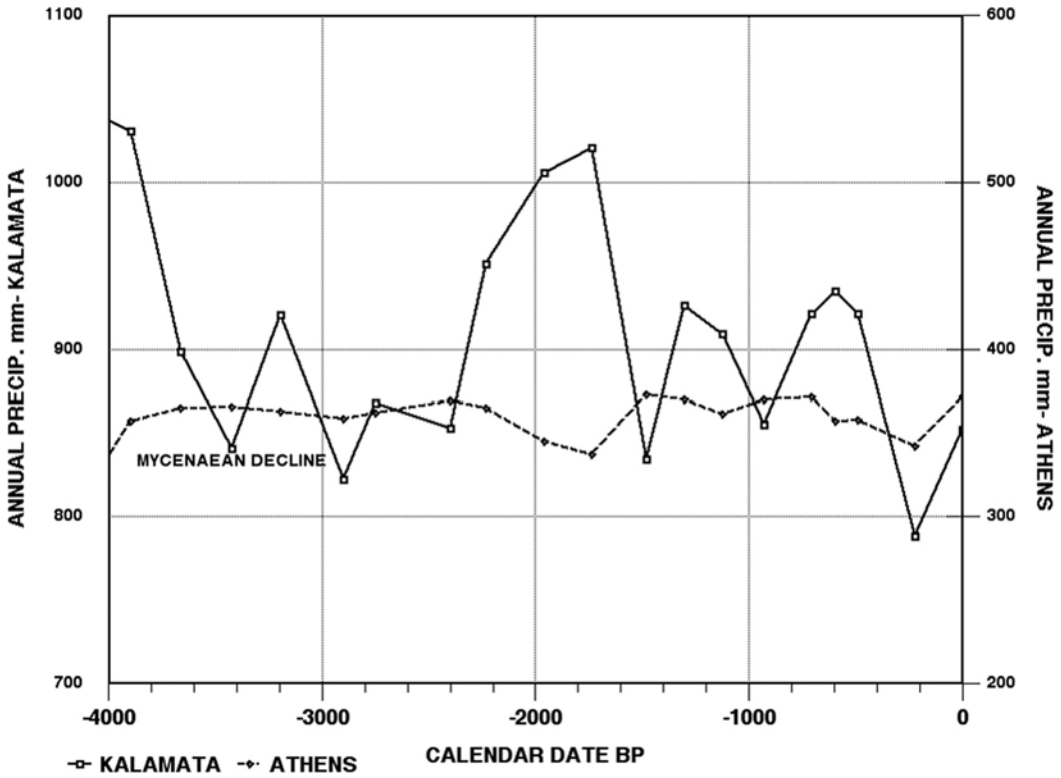

Figure A37 Modeled precipitation history for Peloponnesus (Kalamata) and Attica (Athens).

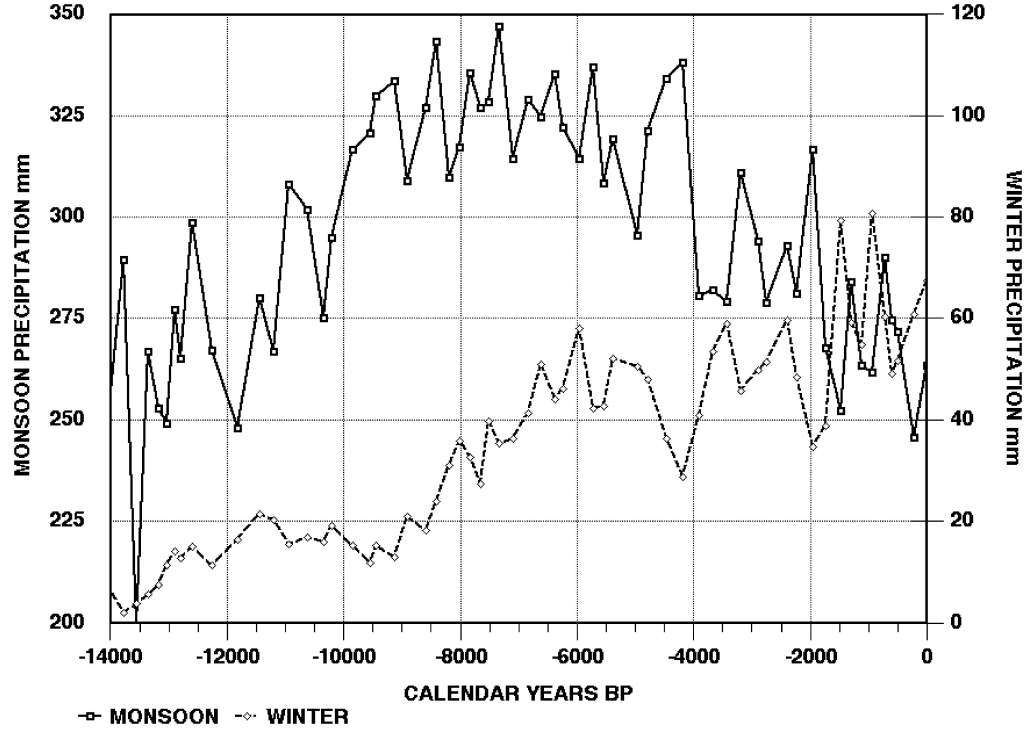

Figure A38 Modeled precipitation history for Harappa.

declined and had been abandoned due to a prolonged drought (1966). He proposed that the drought had been localized to regions by the terrain so that, while it affected the Peloponnesus, it did not affect the Attic Plain (Athens area). Using the archeoclimatic model we may compare the modeled history of these two neighboring areas to see whether such a pattern can be detected. Figure A37 shows the modeled history of precipitation for these two places.

This figure also shows the modeled precipitation for Kalamata in the southern Peloponnesus and for Athens on the Attic plain. Mycenae itself was nearer to Athens than Kalamata.

Some studies showed that Carpenter's drought hypothesis represented a possible, and even probable, pattern (Bryson et al., 1974). Archeoclimatic modeling also supports the hypothesis, and suggests that when the Peloponnesus became dry *ca* 1200 BCE, the Attic Plain did indeed not have a corresponding drought, even though the actual precipitation was usually less.

Example 3: Asia

In northwestern India and Pakistan, in an area now desert or semiarid, the extensive agriculture-based Indus culture existed between about 5500 and 3500 radiocarbon years ago. Studies of pollen in the northwestern Indian desert suggested that the termination of this culture was associated with a decrease in rainfall (Singh et al., 1974; Bryson and Swain, 1981). Figure A38, which shows the rainfall near Harappa, a major city of the Indus culture in the Indus valley, also suggests that there was a rapid change toward lower rainfall about 3500 years ago.

Reid Bryson

Bibliography

Bryson, R.A., 1973. Drought in Sahelia, who or what is to blame? *Ecologist,* **3**(10): 366–371.

Bryson, R.A., and Dittberner, G.J., 1976. A non-equilibrium model of hemispheric mean surface temperatures. *Journal of Atmospheric Sciences*, **33**: 2094–2106.

Bryson, R.A., 1988. Late Quaternary volcanic modulation of Milankovitch climate forcing. *Theoretical and Applied Climatology,* **39**: 115–125.

Bryson, R.A., 1992. A macrophysical model of the Holocene intertropical convergence and jetstream positions and rainfall for the Saharan region. *Meteorology and Atmospheric Physics,* **47**: 247–258.

Bryson, R.A., 1997. The paradigm of climatology: an essay. *Bulletin of the American Meteorological Society,* **78**(3): 449–455.

Bryson, R.U., and Bryson, R.A., 1994. A comparison of cultural evidence and simulated Holocene climates of the Pacific Northwest. Abstracts of the 59th Annual Meeting, Society for American Archaeology, Anaheim, CA, 20–24 April, p. 29.

Bryson, R.A., and Goodman, B.M., 1986. Milankovitch and global ice volume simulation. *Theoretical and Applied Climatology,* **37**: 22–28.

Bryson, R.A., and Swain, A.M., 1981. Holocene variations of monsoon rainfall in Rajasthan. *Quaternary Research,* **16**(2): 135–145.

Bryson, R.A., Lamb, H.H., and Donley, D.L., 1974. Drought and the decline of Mycenae. *Antiquity*, **XLVIII**, 46-50; also IES Report no. 20.

Carpenter, R., 1966. *Discontinuity in Greek Civilization*. Cambridge: Cambridge University Press.

Flohn, H., 1965. Probleme der theoretischen Klimatologie. *Naturwissenschaftliche Rundschau,* **10**: 385–392.

Goodman, B.M., 1984. The climatic impact of volcanic activity. Ph.D. thesis, Department of Meteorology, University of Wisconsin–Madison.

Huschke, R.E., ed., 1959. *Glossary of Meteorology*. Boston: American Meteorological Society.

Ilesanmi, Oluwafemi O., 1971. An empirical formulation of an ITD rainfall model for the tropics – a case study of Nigeria. *Journal of Applied Meteorology,* **10**: 882–891.

Kung, E.C., Bryson, R.A., and Lenschow, D.H., 1964. Study of a continental surface albedo on the basis of flight measurements and structure of the Earth's surface cover over North America. *Monthly Weather Review,* **92**(12): 543–564.

Lamb, H.H., 1972. *Climate: Past, Present, and Future,* Vol. 1: *Fundamentals and Climate Now*. London: Methuen.

Lettau, H.H., and Lettau, K., 1975. Regional climatonomy of tundra and boreal forests in Canada. In Wellers, G., and Bowling, S., eds., *Climate of the Arctic*. Fairbanks: University of Alaska, pp. 209–221.

Lettau, H.H., 1977. Climatonomic modeling of temperature response to dust contamination of Antarctic snow surfaces. *Boundary-Layer Meteorology,* **12**: 213–229.

Lettau, H.H., 1984. The Sauberer–Mahringer soilheat diffusion experiment: a re-analysis using force-response modeling equations. International Symposium in Memory of Dr Franz Sauberer, Universitat für Bodenkultur, Wien, pp. 21–28.

Moran, J.M., and Bryson, R.A., 1969. The contribution of Laurentide ice wastage to the eustatic rise of sea-level: 10 000 to 6000 Years BP. *Arctic and Alpine Research,* **1**(2): 97–104.

Singh, G., Joshi, R.A., Chopra, S.K., and Singh, A.B., 1974. Late Quaternary history of vegetation and climate of the Rajasthan Desert, India. *Philosophical Transactions of the Royal Society of London B,* **267**: 467–501.

Smagorinsky, J., 1963. General circulation experiments with the primitive equations, I: The basic experiment. *Monthly Weather Review,* **91**: 99–164.

Trewartha, G.T., and Horn, L.H., 1980. *An Introduction to Climate,* 5th edn. New York: McGraw-Hill.

Cross-references

Climate Change and Ancient Civilizations
Cultural Climatology

ARCHITECTURE AND CLIMATE

There are dramatic new building forms emerging around the world that have been generated by a growing understanding of climate and its importance to sustainability. From England to the US, from Malaysia to Malta, emerging architecture demonstrates the power of sun, wind, light, moisture and diurnal swing to generate innovative building forms, material detailing and systems integration for sustainability.

In an era of rediscovery, a growing number of architects and engineers begin their design efforts with regional climate graphics, study indigenous responses to climate, use climate-driven computer simulation tools for design development and specifications, and celebrate climatic variability through unique architectural results. These professionals will increasingly need accessible and consistent climate data worldwide, field testing of regional performance of climate-responsive buildings, regional design guidelines, and design simulation and modeling tools. The opportunities for improving environmental quality and reducing environmental costs could transform land-use and community development, building design and renovation, as well as speed the introduction of new materials and technologies – celebrating regional climates and sustainability in the pursuit of environmental security.

Climate change and architecture

In the face of climate change, surprisingly few global leaders have identified buildings and land-use as critical factors. Yet increasing levels of floods, hurricanes, quakes, and natural disasters are most clearly manifested in loss of property. Similarly, pollution, inversions, and warming are driven by combined forces of climate and building decision making. Even growing concerns about chemical and biological attack, and strategies for energy security, will only be addressed by a better understanding of climate and the built environment. International emphasis on avoiding environmental failure and improving environmental security must be fully tied to a rich understanding of regional climates, to ensure individual comfort and health, organizational effectiveness, and environmental sustainability.

Interface between climate and building performance

Total building performance

Today's design challenge is to "balance the high tech and the natural tech" to simultaneously ensure all building performance mandates – thermal comfort, acoustic comfort, visual comfort, air quality, spatial quality, and building integrity – for individual, organizational and environmental effectiveness.

To comprehend the breadth of this challenge it is important to begin with a complete definition of the building performance to be met assiduously by building policy makers, programmers, architects, engineers, contractors, owners, and managers.

First, there has been a fundamental mandate over the centuries for building-enclosure integrity, that is, protection from environmental degradation through moisture, temperature, air movement, radiation, chemical and biological attack, and environmental disasters (such as fires, floods, and earthquakes). Established by concerns for health, safety, welfare, resource management (energy, money), and image, the requirements for building integrity can be stated as limits of acceptable degradation and debilitation.

Second, there are a series of mandates relating to interior occupancy requirements (human, animal, plant, artifact, machine) and the elemental parameters of comfort, that is, thermal comfort, acoustic comfort, visual comfort, air quality, and functional comfort. Table A20 lists performance mandates of primary concern to the building industry, with admittedly lopsided emphasis given to building integrity (protection from degradation, debilitation, and devastation) reflecting the industry's focus on building failures in this area.

Table A20 Building performance mandates

- Building integrity
  - Moisture (rain, snow, ice, vapor)
    - penetration
    - migration
    - condensation
  - Temperature
    - insulation effectiveness
    - thermal bridging
    - freeze–thaw cycle
    - differential thermal expansion and contraction
  - Air movement
    - air exfiltrtion
    - air infiltration
  - Radiation and light
    - environmental radiation
    - solar radiation (e.g., ultraviolet)
    - visible light spectrum
  - Chemical attack
  - Biological attack
  - Fire safety
  - Disaster (earthquake, flood, hurricane, etc.)
- Thermal comfort
  - Air temperature
  - Radiant temperature
  - Humidity
  - Air speed
  - Occupancy factors and controls
- Acoustic comfort
  - Noise level and frequency
  - Reverberation
  - Speech privacy, articulation index
  - Vibration
  - Occupancy factors and controls
- Visual comfort
  - Ambient and task levels (artificial and daylight)
  - Contrast, brightness ratios (flare)
  - Color rendition
  - Occupany factor and controls
- Air quality
  - Ventilation rate: fresh air supply, circulation
  - Mass pollution (gases, vapors, microorganisms, fumes, smokes, dust)
  - Energy pollution (ionizing radiation, microwaves, radio waves, light waves, infrared)
  - Occupancy factors and controls
- Spatial comfort
  - Workstation layout (space, furniture surface, storage, seating, ergonomics)
  - Workgroup layout: adjacencies, compartmentalization, usable space; circulation/accessibility/way-finding/signage, indoor–outdoor relationships)
  - Conveniences, functional servicing (sanitary, electrical, security, telecommunication, circulation/transportation services)
  - Amenities
  - Occupancy factors and controls

Limits of acceptability

Each building performance mandate has a "comfort zone" that establishes the limits of acceptability for the type of occupancy concerned. These limits, often translated into standards and codes, budgets and guidelines, are established by the physiological, psychological, sociological, and economic requirements of a nation and its citizenry. The limits must be established in each country for the range of building functions and the range of occupancy types (human, artifact, plant, animal).

In regard to human occupancy, physiological requirements aim to ensure the health and safety of the building occupants, sheltering basic bodily functions from wear or destruction over time, against such conditions as fire, building collapse, poisonous fumes, high and low temperatures, and poor light. Psychological requirements aim to support individual mental health through appropriate provisions for privacy, interaction, access to the natural environment, clarity, status, change, and so forth. Sociological requirements (also referred to as sociocultural requirements) aim to support the effectiveness of the organization and the well-being of the community, relating the needs of the individual to those of the collective, including rising expectations for environmental quality. Finally, economic requirements

aim to allocate resources – energy, water, land, air, materials – in the most efficient manner in the overall goal to serve user needs.

Although the distinction between climate and weather data is of major significance in the study of meteorology, the needs of the building industry span the range of *descriptive* climate data and *predictive* forecasted data without lucid differentiation. Consequently, both climate and weather data will be discussed under the broader term *climate*, with descriptive data referring to the long-term climate conditions and predictive or forecasted data referring to weather conditions.

Climate and thermal comfort

The climate database requirements for ensuring thermal comfort in buildings continues to be of great importance. Descriptive summaries of average temperatures are needed to estimate annual heat loss and heat gain, in order to establish building energy budgets. Record and extreme temperature conditions must be known to predict peak heat losses and gains, and to determine the size of mechanical conditioning equipment required in a given building. Forecasts of daily temperature and temperature swings must be given for setting mechanical system operating schedules and relieving day–night and seasonal conditioning imbalances. In addition, records of coincident wet-bulb temperatures or humidity conditions must be incorporated into air-conditioning system design, while predictive data will determine the level of humidification or desiccation needed. Annual, monthly, and typical-day solar data aids in estimating both solar heating contribution in winter and solar overheating potential in summer, with design responses to lower annual operating budgets and to allow the use of smaller mechanical conditioning equipment. Predictive solar data allow building operators to anticipate building thermal imbalances and to maximize the use of free heat. Finally, descriptive summaries of wind direction and speed, particularly coincident with temperature and humidity conditions, enable designers to prevent serious winter infiltration through vulnerable building components and to maximize the potential for natural ventilation.

The widespread shift to deeper section buildings that began in the mid-1970s, with less perimeter and more core, a move intended to reduce "climate-driven" conditioning loads, has instead dramatically compromised natural conditioning of buildings. Today, many commercial buildings have become so massive in plan and/or maintain such significant internal loads (from lights, equipment, and people) that energy costs include both high cooling loads in the core, as well as climate-related cooling and heating loads at the perimeter. The EU-funded PROBE studies identified 40–60% higher conditioning loads in newer commercial buildings than traditional, thinner buildings with identical functions (Bordass and Leaman, 2001).

Even in buildings that cannot take advantage of passive conditioning (daylighting, natural ventilation, solar heating, time lag cooling, etc.) attention to climate conditions is still critical for building energy conservation (Figure A39). Heating and cooling equipment size and consequent capital costs are set by peak heat loss and gain conditions, both of which are established at the perimeter. Annual heating and cooling costs (and associated personnel costs) are often significantly escalated by heating and cooling system "battles," resulting from the attempt to respond to daily shifts in temperature, sunshine, and wind infiltration in perimeter spaces. Energy reliability and utility rates are often set by peak demand, a condition that results from core internal loads being aggravated by poor climatic design at the perimeter (solar overheated roofs and facades in summer, cold air infiltration in winter). Finally, significant energy savings can be generated by conditioning buildings with fresh outside air through the use of the economizer cycle (passive conditioning with some energy cost). In the future we will need to shift away from massive, core-dominated buildings in order to provide thermal comfort through strategic combinations of passive conditioning and energy conservation, set climate by climate, as well as to reinstate the physiological and psychological "healthiness" of access to the natural environment.

Climate and lighting comfort

A significant descriptive and predictive database on sky cover conditions, daylight hours, and the quantity of direct, diffuse, and reflected radiation is needed for effective lighting and daylighting design. Artificial lighting effectiveness depends on absence of glare (caused most frequently by direct and diffuse sunshine), presence of adequate contrast to prevent eyestrain, and a controlled mix of wavelengths to provide effective color rendition. On the other hand, individual productivity, energy conservation, and a measurable amount of visual delight is achieved with effective daylighting. In the US more than 10% of all national energy use is for electric lighting in buildings, and most of that during the daytime (DOE/EIA 2002). A predominant number of new sustainable buildings, such as those achieving LEEDJ certification (US Green Building Council), clearly demonstrate that daylight can cost-effectively provide both ambient lighting for general way-finding and task lighting for the range of visual tasks in buildings. The use of daylight can offer major energy savings as well as improved health, productivity, and morale. Daylight, and all the climatic variables associated with daylight, also have the unique ability to provide "kinetic feedback" that gives the user a critical sense of time, place, and dynamic excitement (contributing to the emerging field of biophilia).

Climate and air quality

Wind speed and direction, relative humidity, and atmospheric composition are instrumental in maintaining or improving air quality within and around buildings. Interior pollution migration in large buildings is determined by variation in building pressurization and temperatures, which, in turn, depend on wind direction, wind speed, temperature differentials and possible solar-induced air flows. Controlling indoor pollution migration will also be critical to reducing chemical and biological risk. Anticipating pollution migration from neighboring sites also depends on the climate database, while avoiding pollution buildup in cities, commonly caused by temperature inversions, depends on access to a combination of wind, temperature, and atmospheric composition data sets. Moisture conditions also play a major role in building air quality. Requirements for humidification and dehumidification, linked to absolute and relative humidity conditions, remain one of the major conditioning challenges in building construction and operation. Water management, from driving rain and melting snow, and moisture management from infiltration and condensation on cold surfaces, is critical to avoiding long-term air quality risks from mold and mildew – demanding knowledge of climate data, weather events, and the interpretive power of building physics.

Figure A39 Atop a 100-year-old building, the dynamic enclosure of the Intelligent Workplace ™ at Carnegie Mellon University uses sunlight and natural ventilation to achieve an 80% reduction in heating, cooling and lighting loads of typical office buildings.

Climate and spatial comfort

One of the central activities of urban planners and building designers – the layout of spaces and functions for accessibility, way-finding, and effective use – also depends on climate data if the best use of the building site is to be ensured. Entering and exiting a building comfortably and safely depends on the designer's and operator's comprehension of local wind conditions, combined with occurrences of snow, rain, and ice. Servicing the building with water, electricity, and other transported goods also depends on reliable data of the averages and extremes of temperature, snow, ice, rain, and wind.

Moreover, planning for effective use of outdoor spaces and indoor–outdoor movement during comfortable periods, requires a full understanding of coincident climate conditions. In the design of outdoor spaces at least three microclimates can be created by the building itself: outdoor comfort without sun or wind; outdoor comfort with sun but without wind (extending the comfortable period into early spring and late fall); and outdoor comfort with wind but without sun (extending the comfortable period into the heat of the summer). In the past 10 years, architects and engineers have pursued a new generation of atrium spaces with passively moderated climates to support significant programmatic needs. Double envelopes have been developed for a number of landmark buildings in Europe, with modulated climate zones in the 1–5 meters between the inside and outside glazing. In one of the most dramatic projects the building's programmed spaces are laid out in a village configuration within a highly dynamic, climate-responsive glazed superstructure that moderates the northern German climate to be more like Tuscany (Figure A40). With knowledge of regional and local climate data, building designers can extend the use of outdoor spaces, enrich indoor–outdoor movement, create modified climates in buffer and atria spaces, and provide building occupants with the delight of daily, seasonal, and annual climate variability and manageability.

Climate and building integrity

The final and perhaps most touted area of overlap between climate and architecture is the contribution of climatic forces to building degradation, debilitation, and destruction.

Figure A40 The glazed superstructure over the office space of Moncenis in Essen moderates the northern German climate to be more like Tuscany.

Humidity and precipitation contribute most heavily to these three failures in building integrity. Streaking, corrosion, efflorescence, and decay start as unsightly signs of age. With time this degradation leads to more serious debilitation, the inability to keep out the rain or to provide thermal comfort. However, at the point when the humidity, rain, snow, or ice begins to endanger structural integrity (through excessive loading, for example), the partial or complete reconstruction of the building may be inevitable. Wind and sun conditions also contribute to the loss of building integrity. Information about wind speed and direction and commensurate atmospheric conditions is needed to prevent corrosion (from sand and wind, for example), lifting, shear failure, cracking, and the popping in or out of claddings due to pressure differentials. Data on seasonal and daily solar intensity and position warn against potential fading, cracking, breaking due to expansion, or corroding due to dryness.

Each of these climatic stresses – precipitation, wind and sun – is aggravated by extreme temperatures or major temperature swings in a short period of time. The movement of the sun on extremely cold days and the action of changing solar gain values cause the greatest stress in materials and component assemblies. The combination of snow and freezing rain can cause the extreme structural loading that leads to failure. Consequently, descriptive and predictive database requirements for the prevention of building degradation, debilitation, and destruction are unique. In addition to predictive data as to climatic disasters (hurricanes, floods, tornadoes, and earthquakes), descriptive data on recent and repeated coincident climate conditions (average and extreme) are also needed. Finally, builders must track daily forecasts to ensure that potential material and component failures, leading to degradation, debilitation, or destruction, are not sealed into the building during the construction phase.

Rationale for action

These six performance mandates for buildings – thermal, acoustic, visual, air quality, spatial and building integrity – outline the breadth of the interchange needed between builders and climatologists. However, the rationale for action depends on the physiological, psychological, sociological, and economic limits society is willing to establish for *each* of the performance mandates. For a majority of developed nations these limits translate into five reasons for action.

Increasing environmental contact

Increasing environmental contact for passive conditioning was traditionally a prominent design criterion, but this climate-responsive design expertise was lost with the advent of air conditioning and the ability to mechanically condition year-round. With year-round conditioning, previously uninhabitable regions could be rapidly developed – especially desert and tropical regions. Designers could ensure comfort in any climate, with any building materials, packaged into any building image. However, the psychological unacceptability of this homogeneous and sealed-in approach to architecture has grown, despite its inherent development benefits. Indeed, pedestrianization (making outdoor spaces and facades more suitable for pedestrians), daylighting, natural ventilation, and outdoor space utilization have become novel foci for emerging design theory. It is on this basis that the newest rationale for climate data in building design is introduced – the desire to increase environmental contact.

Increasing environmental comfort

Even though the architectural and engineering community tout human comfort, the use of regional and local climate data to design for increasing environmental comfort within and around buildings has not been a primary step. The majority of urban planners, building designers, contractors, and managers rely heavily on deep, sealed buildings with mechanical conditioning to artificially provide thermal comfort, lighting comfort, and air quality. Indeed, little has been done to mitigate the liabilities of climate (cold wind infiltration and cold mean radiant temperatures in winter, glare and solar overheating in summer) or to use the assets of climate (solar gain and daylighting in winter, natural ventilation in summer) to provide a balanced environment *as a basis* for mechanical system design and operation. Yet thermal, visual and indoor air quality concerns have actually grown during this time due to an over-reliance on advanced technologies in sealed buildings that are oblivious to climate and energy consumption. Moreover, building energy consumption has also grown, for simultaneous heating and cooling, increased fan and pump energy, electric lighting during the daytime, and for ensuring adequate ventilation to purge indoor pollutants. The economic motivation for *energy conservation* is what puts emphasis on this second rationale for introducing climate data – to naturally increase environmental comfort within and around buildings.

Reducing environmental failure

The third rationale for action, reducing environmental failure, is well established in the building industry. Whether triggered by the desire to keep up appearances (psychological limits of acceptability) or by the need to prevent failure and consequent risk to life (physiological limits of acceptability), data on extreme climate conditions have become a part of most building design codes. Today, design for the safety and security of building occupants, in the face of earthquakes, hurricanes, tornadoes, and heavy snow loads, ensures that extreme climate conditions are well documented in the codes. It is the joint responsibility of the architectural, engineering and construction community and the climatologist to establish whether these data are of the appropriate amount and in the appropriate form to adequately ensure both the psychological and physiological limits of acceptable environmental stress on building integrity.

Reducing environmental costs

Reducing environmental costs is a fourth argument for including climate data in the building decision-making process. This rationale for action promotes the value of all resources: money, labor, materials, air, water, and energy in the face of carelessness and abuse. The introduction of climatic facts and thresholds into analyses of the renewability of air, water, soil, energy, and capital-intensive building materials has the potential to significantly reduce the environmental costs (from leaky roofs to pollution build-up) imposed by building development (see Table A21). Growing concerns about climate change, pollution build-up, water shortages and depleting resources should significantly

Table A21 Environmental costs of poor planning and design decision making

Construction category	Annual volume[a]		Potentially weather sensitive: Perishable material[a]		On-site wages[a]		Equipment[a]		Overhead and profit[a]		Total sensitive percent of annual volume	
	1964	1979	1964	1979	1964	1979	1964	1979	1964	1979	1964	1979
Residential	17.2	87.6	0.960	5.76	1.624	7.88	0.073	0.37	2.141	10.51	27.9	27.4
General building	29.7	86.9	1.928	5.21	4.029	12.17	0.222	0.87	2.670	7.82	30.0	30.0
Highways	6.6	9.5	1.666	2.38	1.633	2.38	0.773	1.14	0.727	1.05	72.7	73.0
Heavy and special	12.5	17.6	1.875	2.64	3.125	4.40	2.500	3.52	2.500	3.52	80.0	80.0
Repair and maintain	22.0	50.4	2.674	6.05	3.996	9.07	1.386	3.02	3.143	7.06	50.9	50.0
Totals	88.0	252.0	9.1	21.54	14.4	35.90	5.0	8.92	11.2	29.96	45.1	38.2

Sources: Original 1964 data and calculations after Russo (1966); 1979 construction volume from Bureau of Census and Bureau Business Development, US Department of Commerce; otherwise 1979 data calculated on same ratio as 1964 data.

[a] Billions of dollars.

boost the demand by the design community for climate data. It is important for the meteorological community to anticipate these demands and create interpretive databases on the vulnerability of regions and local ecosystems in relation to air, water, soil, natural energies, and material resources.

Increasing environmental security

In a parallel effort, it is important for the meteorological community to create interpretive databases on the opportunities of regions and local ecosystems to replenish air, water, soil, natural energies, and material resources. With growing international attention on energy and water security, the meteorological community has a major opportunity to emphasize the importance of sun, wind, hygrothermal and other data in the design and retrofit of buildings and communities. The best protection from chemical and biological attack within a building's mechanical system may be replacing central systems with natural conditioning. The best protection from brownouts and blackouts may be the effective use of solar electric, thermal and daylighting energies. The importance of climate data to environmental security – both reducing vulnerability and providing sustainable resources – cannot be overstated.

Climatic data and building decision making

Given these five rationales for action – to increase environmental contact, comfort, and security while decreasing environmental failure and costs – climate data form an essential resource for the building industry. By focusing on the steps in the building decision-making process, these data can be introduced in a form conducive to action. Table A22 outlines the decisions made in the early stages of planning and design and the eventual operational decisions that must be made in building construction and management.

Table A22 Building decision making

Land-use/town planning
Geological change (soils, vegetation, topography)
Density
Spacing
Collective massing
Height
Functional mix
Building design
Massing and orientation
Organization of spaces
Enclosure design
Opening design
Systems integration
Building construction
Worker comfort and stress
Worker safety and health
Material stress
Operational planning
Building management, maintenance, operation, and use
Occupant comfort and stress
Occupant safety and health
Building image over time
Facility management costs over time
Energy and environmental costs over time

Climate and land-use/town planning

Land-use development involves decisions concerning building density, spacing, height, collective massing, and functional mix. Land-use decision-making has a direct impact on air quality, pollution, thermal build-up, runoff and flooding potential, and water quality and availability, as well as changes in wind and sunlight conditions. Consequently, an understanding of a region's climatic profile and thresholds for concern are critical to the effective planning and design of building communities.

If regional and local wind conditions are to provide natural ventilation for thermal comfort, reduce pollution build-up, and improve use of outdoor spaces, then prevailing wind speeds and directions, as well as microclimate variations, must be known. Average and extreme wind conditions must also be addressed if liabilities are to be mitigated, including thermal discomfort through infiltration, acoustic discomfort through noise transportation, poor air quality through pollution transportation, and building degradation and destructive failure. Early design decisions regarding building density, massing, and functional mix dictate the availability or mitigation or regional wind conditions at the building microclimate level. According to Landsberg (1976):

> The major effect of urban areas on the wind circulation is a result of the increased roughness introduced by the building complexes. These induce many smaller and larger eddies which swirl around in the city. The arrangement of streets and avenues will cause channeling of the wind. The results may then be that strong currents flow through one set of streets, while relative calm prevails in the streets at right angles. The eddy currents that are caused by the buildings, especially the tall ones, can lead to very high wind gusts at street level. They can be so strong that it becomes difficult to walk on pavements and to open doors unless special protective overhangs are included in the design.

Sun conditions are equally affected by land-use decisions. If the benefits of solar heating, daylighting, and outdoor space utilization are to be realized, regional sunlight conditions and microclimate modifications must be optimized through careful control of density, height, and collective massing (Knowles, 1994). If the liabilities of solar overheating, thermal inversions causing poor air quality, and ultraviolet building degradation are to be reduced, regional sun position, intensity, variability, and potential microclimate shifts must be fully incorporated into site planning decisions.

Without a regional comprehension of overheated, underheated, and comfortable climate conditions, land-use decisions as to density, massing, and functional mix can aggravate a region's disadvantages, while losing the opportunity to make use of its climatic advantages. Still today, urban planning takes little advantage of the comfortable season for natural thermal conditioning or outdoor space utilization. In fact, town planning often shortens the natural season by poor manipulation of natural wind and sun conditions. Landsberg (1976) states that "on a local scale, the formation of an area of higher temperatures compared with rural environs is generally the first obvious manifestation of settlements, and can be directly related to the building density." Heat islands, which result from the complex actions of urban pollution, solar and heat build-up, and poor air flow, can be anticipated with climate information. In addition to increased thermal discomfort and reduced access to outdoor spaces, our poor understanding of regional temperature conditions and corresponding wind,

sun, and humidity conditions leads to unsightly building degradation, unacceptable debilitation (inability to provide shelter), and, eventually, unsafe destruction.

Finally, regional humidity and precipitation data are needed in the effective planning of urban density, spacing, building height, and collective massing. To the designer's advantage, low humidity allows for effective evaporative cooling to provide thermal comfort and reduced conditioning costs. Design for the utilization of precipitation can provide for our water needs and improve air quality as well as reduce degradation of buildings due to pollution. However, comprehension of the serious liability presented by regional humidity and precipitation is also critical. Extreme humidity can be the major cost in conditioning for thermal comfort and air quality, as well as growing concerns about the health consequences of mold and mildew. While average precipitation contributes to building degradation and debilitation over time, extremes in precipitation, aggravated by extreme wind conditions, constitute the greatest cause for building and infrastructure debilitation and destructive failure.

Climate and building design

Although many design decisions regarding massing and orientation, organization of spaces, enclosure design, opening design, and systems integration are made without the benefit of regional and microclimate data, the importance of climatic conditions to thermal and lighting comfort, air quality, and building integrity (versus degradation and destruction) cannot be understated. Table A23 clarifies the advantages and disadvantages of various climatic forces on building performance as well as the building design decisions that are consequently affected.

Records of average wind speeds and directions are necessary if natural ventilation is to be provided, dictating appropriate building orientation, spatial organization, opening design, and systems integration. The liability of wind to thermal comfort, air quality, and building integrity must also be considered, demanding that building massing, organization, enclosure detailing, and opening design minimize the unacceptable wind forces around and through the building. Today, the most advanced architectural/engineering teams use computational fluid dynamic tools (CFD) to create innovative naturally ventilated buildings and even power-generating wind turbine designs integral with the building design (Hamzah et al., 2001).

The natural conditioning benefits of sunshine for solar heating, daylighting, and outdoor space utilization require a working knowledge of seasonal and daily sun position and intensity, along with their implications for building massing and orientation,

Table A23 Climate and building design decision making

	Massing and orientation	Spatial organization	Enclosure design	Opening design	Systems integration
Wind asset					
Thermal: natural ventilation	X	X		X	X
Air quality: pollution mitigation	X	X		X	X
Wind liability					
Thermal: infiltration	X	X	X	X	
Air quality: pollution migrations	X	X		X	
Building integrity: degradation/destruction	X	X	X	X	
Solar asset					
Thermal: solar heating	X	X		X	X
Lighting: daylighting	X	X		X	X
Spatial: outdoor utilization	X	X		X	
Solar liability					
Thermal: solar overheating	X	X	X	X	X
Lighting: glare	X	X		X	X
Building integrity: degradation	X		X	X	
Temperature asset					
Thermal: net comfort, time-lag cooling	X	X		X	X
Spatial: indoor–outdoor utilization	X	X		X	X
Temperature liability					
Thermal: heat loss/heat gain	X	X	X	X	
Building integrity: degradation/ debilitation/destruction	X		X	X	
Humidity/precipitation asset					
Thermal: evaporative cooling		X		X	X
Air quality: humidification, cleansing				X	X
Humidity/precipitation liability					
Thermal: dehydration, excess relative humidity				X	X
Spatial: building access, outdoot utilization	X	X		X	X
Building integrity: degradation, debilitation, destruction	X		X	X	

organization of spaces, opening design, and system integration. Average and extreme solar and sky conditions must also be considered by designers if solar overheating in summer, glare causing lighting discomfort, and building degradation are to be reduced. Today, the most advanced architectural/engineering teams use daylighting and solar thermal simulation tools to maximize passive solar heating, daylighting and power generation utilizing buildings rooftops and facades.

When temperature conditions offer significant periods of natural comfort, with or without the assistance of sunshine for warmth or wind for cooling, the massing of a building and its potential for indoor-to-outdoor movement through the appropriate organization of spaces and displacement of openings should be significantly affected. Often, however, the design of the building's mechanical system is not integrated effectively with climatic data, thereby eliminating the advantage of this natural conditioning potential. Today, the most advanced architectural/engineering teams use hour-by-hour simulation tools to design thermal mass and thermal distribution strategies – such as core-to-perimeter, E-S-W-N, and day to night load balancing systems to take advantage of diurnal energies in specific climates.

Knowledge of regional humidity conditions allows the designer to take advantage of evaporative cooling for thermal comfort and air quality, reducing the conditioning liability of excessively dry climates through careful opening design and systems integration. In humid climates the minimization of moisture build-up and the effective use of ventilation and solar "drying" or desiccant systems places equal demands on enclosure design and systems integration. Spatial comfort, including the ability to enter or exit a building and the usableness of outdoor spaces, is assured through an understanding of average and extreme rain, snow, and ice conditions, along with coincident wind and temperature data. Full knowledge of these coincident climatic liabilities is also necessary to prevent all three threats to building integrity: degradation; debilitation to such a degree that the building no longer provides comfort or shelter; and destructive failure. Tveit (1970) presents an illustrative discussion:

> Water may be brought into porous materials as liquid or as vapour. The driving force may originate from differences in hydrostatic pressure, osmotic pressure, vapour pressure, as well as from free surface energy. Considering rain penetration into building structures, this would be caused by (1) capillary action due to free surface energy; (2) kinetic energy of rain drops or water streams; (3) hydrostatic pressure due to gravity or to wind pressure on water films or menisci; or (4) air flow through the structures. The ability of a building structure to dry out and keep dry generally depends on the successful design in every detail of the building and its various structural components and draining systems above or under the ground as well as on certain physical properties of the applied materials and workmanship, all in relation to the ambient climate. Some of these principles are related to the design and construction of certain building components and are in exposed areas frequently reflected in a characteristic of local design and building practice.

Consequently, increased understanding of regional and local climatic assets, their combinations, and manageability could change significantly the present-day isolationist or "sealed box" tendencies of building designers. Setting regional priorities among these climatic assets and liabilities to ensure long-term thermal comfort, lighting comfort, air quality, spatial comfort, and building integrity, is the genius of climate-responsive building design. The regionalization of architecture is not a return to the past but a reconfirmation of the natural forces and resulting material availabilities that make survival and comfort in each location unique. The all-glass building in hot and humid Houston, the flat roof in rainy England, the pedestal building in windy Chicago all attempt to deny the very climate in which they sit. Today, armed with a full understanding of a building's climate and consequent microclimate, design priorities can be set that maximize the benefits of the various climate assets for natural conditioning while minimizing the liabilities – a delicate balance that will ensure building quality over time.

Climate and building construction

The building construction industry has several responsibilities that depend greatly on climate data. Worker comfort in relation to precipitation, hot or cold temperatures, biting or dehydrating winds, excessive solar gain, serious humidity and pollution conditions as well as protection against the stresses of heat stroke and frost bite, require that project managers keep a close watch on daily and hourly weather forecasts. The safety of the worker requires knowledge of climate conditions – wind speeds in high-rise construction, snow and ice conditions on various ground surfaces, excessive overheating or freezing of building materials as well as components that must be handled or walked on. The seriousness of these responsibilities, and the corresponding need for predictive weather information, is already an innate part of the standards and liability laws of the construction industry. However, material stress resulting from adverse climatic conditions (average, coincident, and extreme) is less enshrined in the working standards of the construction industry. Not only do extreme temperature, humidity, precipitation, wind, and sun conditions greatly affect the integrity of building materials, components, and assemblies on the job site, but historic average conditions also indicate the feasibility of using particular materials and assemblies in various climates. Without a working knowledge of the impact of average and extreme climate conditions on building integrity, the unsightly degradation of buildings, the debilitation of buildings to an extent where they no longer provide comfort or shelter, and the destructive failure of buildings will be initiated from the laying of the first foundation.

Balancing these climatic variables that dictate worker comfort and safety as well as material stress over time, against other construction variables such as worker availability, material delivery, financing, and occupancy schedules form the basis of operational planning on the construction site. However, because of the lack of descriptive and predictive climate data in a form readily usable by the construction industry, only sketchy climate information is used in construction planning, despite long-term implications of precise climate data for the performance of components and systems.

Climate and building management: maintenance, operation and use

The daily operation and use of a building for occupant comfort require data on present and near-term anticipated climate conditions. To provide thermal and visual comfort for the occupants, as well as the air quality they need, building operators (or automated operating systems) require informaton on outdoor temperature, humidity, and sun conditions. Energy load balancing from north to south, from day to night, and from season to season to reduce peak demands and annual energy costs requires descriptive average and extreme climate data, in addition to 24-hour weather forecasts. Table A24 shows that over 50% of

Table A24 Winnipeg office building: annual load breakdown and climate dependencies

	kWh/sq ft/ year	Operating dollars 1981	Climate impact annuals	Climate negotiable capital costs[a]
Process electricty (kitchen, power, computers)	4.0	22 000	—	No
Electric conditioning				
Lights	5.0	28 000	10 000[b]	Yes
Fans for air quality[c]	2.0	11 000	—	No
Fans for "core"/cooling				
Lights[d]	1.2	6600	2000	Yes
Equipment[e]	1.8	10 000	—	No
Fans for perimeter cooling	1.0			
Air conditioning for perfimeter[f]	2.0	16 000	16 000	Yes
Nature gas conditioning				
Heating	13.0	72 000	72 000	Yes
How water	2.5	14 000	—	No
Total	32.5	180 200	100 600[g]	

[a] Initial capital costs of equipment could be reduced if climate-responsive design.
[b] Only perimeter lighting can be reduced through daylight management.
[c] Majority of ventilation for air quality is provided through cooling and heating fanpower.
[d] 60% of total wattage is translated into cooling demand.
[e] 100% of total wattage is translated into cooling demand.
[f] Due to cold climate, the majority of air conditioning is provided through fan economizer (free cooling) cycles.
[g] Consequently 55% of total energy demand in this building is dependent on appropriate climate-responsive building design.
Source: Statistics from Public Works of Canada.

the annual operating costs in a 300 000 square-foot office building in Winnipeg, Canada, depend on outdoor climate. These operating costs, and the occupant comfort that is associated with them, generate the demand for on-site weather monitoring equipment today. The innovative use of such equipment can yield tremendous improvement in the understanding of occupancy comfort and stress that is directly affected by climate and related building decision making.

Occupant safety, given adverse weather conditions and long-term building degradation due to these conditions, also constitutes a major demand for climate information. Wind, rain, snow, and ice can make certain parking areas, pedestrain areas, and entries unsafe. Material expansion and contraction, caused by swinging temperatures, fluctuating humidities, and sunshine, can make various building components unsafe to walk on or under. Material corrosion and degradation due to moisture migration and rain penetration can lead to building failures that are dangerous to occupants and passers-by. Disasters such as hurricanes, floods, tornadoes, or snowfalls followed by freezing rain can cause total building collapse, a phenomenon that should be anticipated in building design and upheld through building maintenance. Consequently, 24-hour and weekly forecasts are needed by building managers to anticipate building stress and occupant safety risks. Long-term historic data are needed to establish annual maintenance budgets for each building, while short-term historic data will compel building managers to undertake preventive maintenance programs for building materials and assemblies that have been under unexpected, but recorded, stress.

The image of the building – of interest to the occupants, the owner, and the community at large – is also a major factor in building maintenance programs. Before the building is occupied, the climatic liabilities of the region and site can be mitigated with careful planning, design, detailing, and construction. However, after the building is occupied, the stresses placed on the building fabric and site by climate will require continuous cycles of maintenance. Preventive maintenance, like preventive medicine, can slow the degradation of buildings and potentially prevent debilitation to the point where the building no longer provides comfort or shelter. For example, anticipating excessive rainfall, gutters can be cleared out and drainage channels opened, preventing the major roof leak that eventually demands millions of dollars of repair. In many countries, records of major snowfalls become mandates for maintenance crews to clear roofs, preventing excessive structural loading and eventual failure. Material and product manufacturers often establish preventive maintenance programs, given a range of average climate conditions. Table A25 lists the weather mechanisms that contribute to stone decay; factors that can be translated directly into building maintenance programs (Tombach, 1982). Eventually, these maintenance schedules, as well as the reactive maintenance required in the aftermath of major climatic events, will be computerized along with the descriptive, predictive, and historic climate data that necessitate the activities, providing each building owner with a specific climate-responsive maintenance program.

Methods of intervention

There is little question that the availability of climatic data is far greater than their use. Indeed, the willingness of climatologists to be of service to the building community is far greater than the demand for their services. Several theories have been advanced as to why this is so. John Page (1970) writes:

> "When an applied science is not applied in practice, it is always valuable to inquire why this situation should persist in spite of a host of apparently good scientific reasons why the situation should be otherwise. The aviation services use the

Table A25 Classification of mechanisms contributing to stone decay

Mechanism	Rainfall	Fog	Humidity	Temperature	Solar insolation	Wind	Gaseous pollutants	Aerosol
External abrasion								
Erosion by wind-borne particles						•		•
Erosion by rainfall	•							
Erosion by surface ice	•	•		•				
Volume change of stone								
Differential expansion of mineral grains				•			○	
Differential bulk expansion due to uneven heating				•	•			
Differential bulk expansion due to uneven moisture content	•	•	•	•	•	○	○	○
Differential expansion of differing material at joints				•				
Volume change of material in capillaries and interstices								
Freezing of water	•	•		•				
Expansion of water when heated by sun	•	•		•	•			
Trapping of water under pressure when surface freezes	•	•		•				
Swelling of water-imbibing minerals by osmotic pressure	•	•	•				○	○
Hydration of efflorescences, internal impurities, and stone constituents	•		•				○	○
Crystallization of salts			•	•	•	•	○	○
Oxidation of materials into more voluminous forms	•	•					○	
Dissolution of stone or change of chemical form								
Dissolution in rainwater	•			•		•	•	
Dissolution by acids formed on stone by atmospheric gases or particles and water	•	•	•	•			•	•
Reaction of stone with SO_2 to form water-soluble material	•	•		•			•	
Reaction of stone with acidic clay aerosol particles	•	•		•				•
Biological activity								
Chemical attack by chelating, nitrifying, sulfur-reducing, or sulfur-oxidizing bacteria			•	•			•	
Erosion by symbiotic assemblages and higher plants that penetrate stone or produce damaging excretions	○	○	•	•				

Source: From Tombach (1982).
Note: Solid circles denote principal atmospheric factors; open circles denotes secondary factors.

meteorological networks without persuasion, why not the architects, town planners, and civil engineers? There would seem to be three fundamental reasons for rejecting scientific information in any practical field of human activity: (1) the information provided is considered irrelevant by the potential user; (2) the information provided in the form presented is considered inapplicable by the potential user; and (3) the information provided is considered incomprehensible by the potential user. The first question implies a lack of understanding of the problem by the scientific worker, the third question a lack of understanding by the designer of the problem, and the second question shows a lack of communication between the two.

John Eberhard of the National Academy of Sciences (1986) adds:

> The resistance to change is a natural, and probably necessary, instinct in all people and consequently in human institutions. The organizations and institutions associated with the building industries of the United States are no exception – in fact they appear more resistant to change than many other sectors of the economy. One major indicator, and also contributor, to this lack of innovation is the relatively low volume of research and development. While industries such as electronics and aircraft are spending more than 20 percent of their revenue on R&D, all indications are that the industries of building spend less than one percent on Research and Development – in fact if quality control and product testing to meet government regulations is subtracted from the so-called R&D budgets of building industry organizations, the budget left to devote to new ideas and new knowledge is probably very small indeed.

These weaknesses in information transfer and in applied research are compounded by the unfamiliarity of the climatologist with the exact nature of individual building decisions and the uncertainty of the planner, designer, engineer, contractor, and building manager as to what climatology has to offer. Despite this overall lack of familiarity there are several concrete steps that can be taken to improve the contribution of climate data in the building decision-making process: accessible climate databases; climate data information packaging; algorithm development and information processing; model testing; field case studies and documentation; and advanced computer simulation tools.

Important climatic variables

For effective decision making in the early stages of land-use planning and building design and in the later stages of construction and building management, the building community needs a considerable quantity of average and extreme temperature, humidity, atmospheric content, wind, sun, and precipitation data. In the majority of industrialized nations this database exists to

such an extent that data collection needs are insignificant in comparison to the needs for applied data packaging and processing in relation to the building sciences. The efforts of the European Community to consolidate solar and other climate databases for EC members in the publicly accessible web site – SoDa (2002) – will greatly enhance decision making in those climates.

However, there is a major gap in two areas of data collection and presentation: the availability of information on complex, coincident climate conditions often critical to building performance; and the development of micrometeorology. Lacy (1972) writes:

> Although in many multi-variate problems, an analysis of the simultaneous occurrence of various elements is usually required, there are others in which the sequence in which events occur is important. Ultra-violet radiation will only react with a material if the material has already been wetted by dew or rain. Frost will only damage porous materials if they have been wetted by rain a sufficiently short time before the frost occurs, so that there has been insufficient time for water loss by evaporation. Condensation of water on structures can be caused if a prolonged cold spell is followed rapidly by a mild one, so that the atmospheric dew-point rises more rapidly than the temperature of surfaces which have been chilled during the cold spell. In such cases the conventional statistical analyses of weather elements may be useless, and it is necessary to study the actual weather situations which cause such problems, and estimate their frequency of recurrence.

Only coincident climate data can ascertain the availability of wind when the temperatures are warm enough to merit natural ventilation, or the direction and speed of wind when it is raining to ensure appropriate enclosure detailing and opening design.

Equally important is the development of microclimate databases or scientific methods for the prediction of microclimates on specific building sites. Building design decision making will rely on whatever sketchy microclimatic databases exist, until the predictive science of micrometeorology is developed. Finally, the industrialized nations should be committed to establishing climate databases for the developing world as well, if climate responsive community and building design, construction and operation is to be achieved world-wide for environmental safety, comfort and security.

Information packaging and climate graphics

Graphic interpretations of climate data are critical for professionals to understand the variations and coincident conditions that should significantly impact building and community design. From the early work of the H.E. Landsberg for the AIA (1950), the Olgyay brothers (1963), Loftness (1982), Brown and Dekary (2001), and a host of recent leading international designers (e.g. Short, Foster, Yeang) a commitment to graphically communicating climatic forces is key to climate-responsive design.

Based on the assumption that the greatest amount of information is learned in the doing, a how-to publication, *Climate/Energy Graphics*, was written by Loftness (1982) for the World Meteorological Organization. Loftness outlines 15 graphic exercises that can be completed by meteorologists, technicians, engineers, or architects using data from local weather stations. As shown in Figures A41 and A42, available climate data should be used to generate climate graphics and result in a summary translation with written design guidelines to ensure the climate-responsive design of building massing and orientation, spatial organization, enclosure and opening design, and systems integration (Figure A43).

Algorithms and climate information processing

To get beyond the elementary knowledge concerning regional and local climates that can be achieved through climate graphics, it is necessary to develop an understanding of the fundamental algorithms that relate climate to building success and failure. Boer (1970), in an article outlining a training and education syllabus, stipulates:

> Knowledge of the interaction between meteorological parameters and/or processes and building activities, of single structures and built-up areas, is an essential prerequisite for a functioning information system of building meteorology.

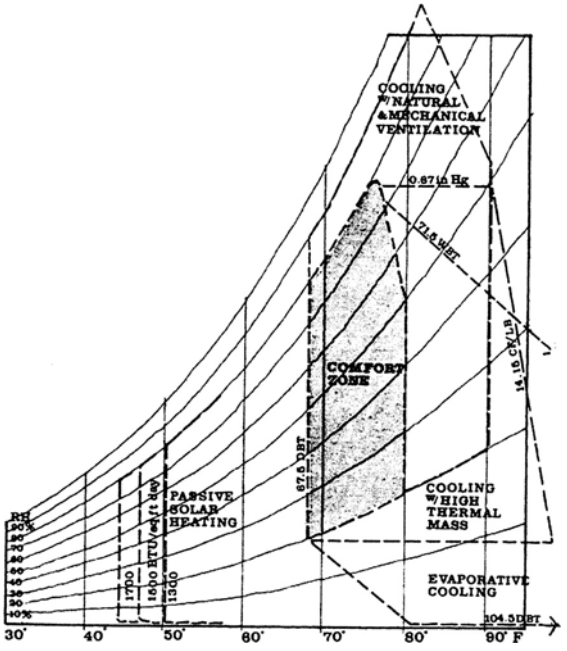

Figure A41 Evaluating passive conditioning potential (from Loftness, 1982).

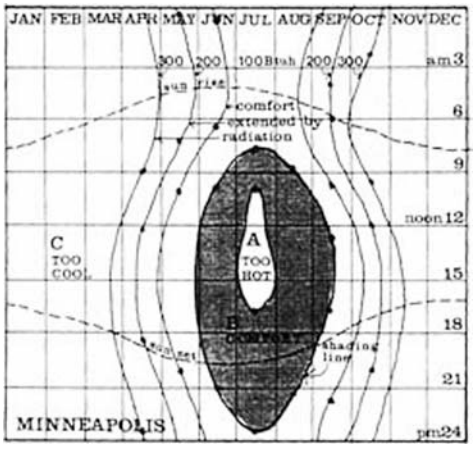

Figure A42 Climate design priorities for Minneapolis, Minnesota (from Loftness, 1982, based on Olgyay, 1963).

		RANK	A Bldg. & Landcaping	B Building Grouping	C Bldg. Shape & Configuration	D Bldg. Orientation	E Building Organization	F Envelope/ Enclosure Design	G Envelope/ Opening Design	H Systems Integration
HEATING										
Limit LIABILITY	Isolation from cold /hot temps	1	Group buildings, berm or site underground		Compact building form		Organize bldg. Into zones	High r-Value materials	Size & Type Windows Movable ins.	
	Isolation from cold winds	5	Protect bldg. By vegetation, grouping…		Form & orient bldgs to provide winter wind protection		Protect entries	Tight const. to limit infiltration	Place & detail windows vs. infiltration	
Use ASSET	Opening to solar heating	3	Site, landscape & group bldgs. For winter sun access			Orient bldg. To winter sun	Provide adequate collection & storage areas		Size opening & type glass	Radiant & convective DistRibuti on systems
COOLING										
Limit LIABILITY	Isolation from hot sun	3	Protect bldg. By vegetation Or berming	Self-shading forms and min. east & West exposures				Effective shading devices For walls & Windows exposed to summer sun		
	Isolation from high humidity	6								Prevent excess humidity creation
Use ASSET	Responding to diurnal temps.									
	Opening to cooling winds	2	Site & place bldgs. For natural ventilation			Orient bldg. For natural ventilation	Open spaces to each other		Size & orient opening for nat, ventil .	Induce & assist ventil.
	Opening to evap-cooling									
	Opening to radiant cooling									
COMFORTABLE										
Use ASSET	Opening to Comfort	4	Provide open spaces for winter, spring & Autumn uses					Provide connections w/ outside for winter, spring & autumn uses		

Figure A43 Developing design strategies from climate priorities (Charleston, from Loftness 1982).

The algorithms that explain the interaction between meteorological parameters and design decision making can be as simple as the snow loading that leads to failure of various structural systems and as complex as the relationship of town planning decisions to the alteration of regional wind patterns. While computational tools such as DOE 2.2 support the integration of on-line climate databases into energy-effective design decision making, there are numerous performance simulation challenges that remain, including the potential impact of time-lag, of radiant cooling, and the hygrothermal performance of materials and assemblies. In his book *Climate Considerations in Building and Urban Design* (1998), Baruch Givoni documents the importance of algorithms to describe the effect of mass in buildings with continuous ventilation, nocturnal ventilation, and night-time radiant exchange (Figure A44). In practice, Dr. Givoni continues to explore innovative cooling strategies using combined forces of wind, thermal stratification, and evaporative cooling, to create, for example, the dramatic Ashower cooling towers that captured the imagination of all who attended the 1992 World Expo in Seville, Spain (see Figure A45).

Laboratory and field case studies and documentation

Field studies of innovative indigenous and advanced buildings in a range of climates could aid in the development of performance algorithms linking climate and architecture, to enable designers to understand the regional appropriateness of climate-responsive design innovations. A range of diagnostic tools, equipment, and procedures should be further developed to determine the overall performance of building materials, assemblies and integrated systems in the full range of climates. According to Markus and Morris (1980):

> Historical studies of vernacular buildings are helping in the development of a new kind of planning and architectural theory – concerned not with monumental planning and design, but with the pattern of cities, settlements, and buildings as expressive of the structural relationship between technological, social, symbolic and natural forces – that is, a cultural theory of form. This theory attempts to unravel the meaning of patterns found in primitive and vernacular creations of the past and, by studying the processes and forms of still active authentic societies, to draw conclusions for design today.

Until now, field instrumentation has generally focused on the evaluation of building degradation, debilitation, and destruction. Indeed, there are no comprehensive approaches to evaluating the performance of materials, buildings or land-use alternatives in a range of climates for universities or professionals to decisively study indigenous and innovative climate-responsive architecture.

On the other hand, climate testing of scale models set in average and extreme wind or sun conditions has been pursued by a small number of designers for major projects or climatically challenging projects. Model wind testing is used on some large projects to visualize pedestrian safety and comfort, the integrity of cladding and structure against degradation or destruction, the viability of natural ventilation, and the predictability of pollution migration. Model sun/daylight testing is used to illuminate the solar availability in public spaces, the effectiveness of shading devices, the potential of solar heating, and daylight penetration. However, scale model testing could go much further. Model wind/snow testing could clarify the build-up of snow on roads, airports, building entries, roofs, and in recreational areas such as ski resorts. Model rain testing could be undertaken to demonstrate watersheds, storm runoff and site drainage effectiveness and the consequent impact on communities and regions.

Both laboratory and field studies of climate-responsive building materials, assemblies and integrated systems are critically needed for designers to regionally increase environmental contact, comfort, and security while decreasing environmental failure and costs. There should be a concerted effort to completely document field studies of both indigenous climate-responsive buildings and communities and recent innovations in a range of climates to inform the entire building community, from building owners to material suppliers, of the significance of climate in building decision making.

Advanced computer simulation tools

The computer plays a more active role in land-use planning and building design, construction, and management today, with climate data integral to performance simulation. However, more laboratory and field case studies linking the performance of materials, assemblies and integrated systems to regional climate conditions will help to mainstream the use of simulation tools in design and construction. When an adequate number of building climatological algorithms and descriptive case studies can be simplified into computer-simulation packages, the demand for climate data in building decision making will be clearly established. The environmental costs of inappropriate land-use and building and their corresponding change in soil, vegetation, and topography should be too graphic to ignore. The loss of environmental comfort through poor building orientation, organization, and opening design should be quickly simulated and alternatives chosen. The environmental stress placed on building materials in the face of anticipated and recorded climate conditions should be avoided through computerized construction management programs. Material manufacturers should be able to establish regional performance priorities and preventive maintenance schedules suited to the unique history of climate conditions surrounding the project. The acceptable averages and threshold of coincident climate conditions should be automatically processed through the algorithms of physiological, psychological, and economic comfort to continuously guide decision making in building design, construction, and use.

Although no attempt is made to establish which of these methods of intervention will generate the greatest impact – data packaging, data processing through algorithms, field studies, model testing, or computer simulation – each of them will reap results. Each method of intervention "describes historical and more recent notions of buildings as shelters; i.e., structures which intervene by acting as barriers and as responsive filters between the natural and urban environment, and the range of environments required for human activity" (Markus and Morris, 1980).

Vivian Loftness

Bibliography

AIA/House Beautiful, 1949–1952. *Regional Climate Analysis and Design Data: The House Beautiful Climate Control Project*. Ann Arbor, Mich.: Xerox University Microfilms.

Boer, W., 1970. Problems of distribution and effective exploitation of meteorological information for architecture and building Industry. In *Building Climatology, Technical Note 109*. Geneva: World Meteorological Organization, pp. 191–197.

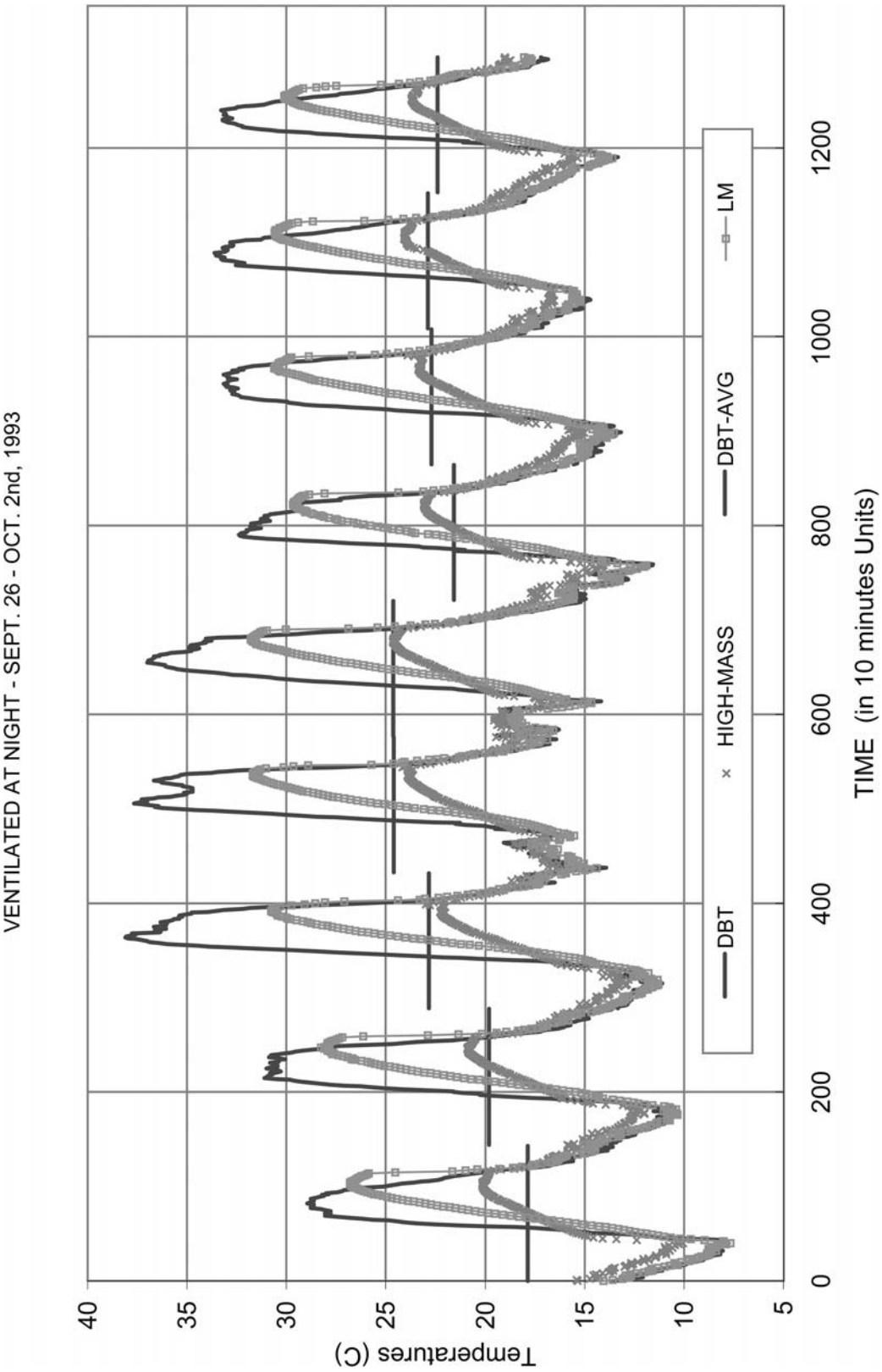

Figure A44 Dr. Baruch Givoni documents the importance of developing algorithms from field measurements to describe the effects of mass in buildings, in this case with night ventilation.

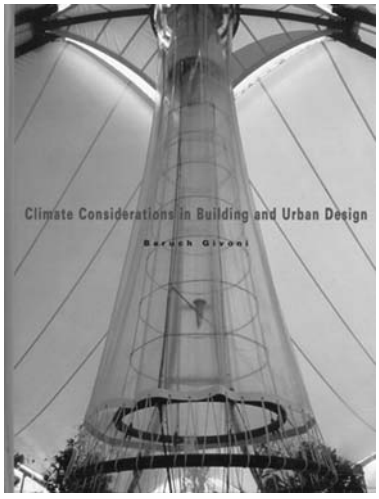

Figure A45 An evaporative cooling tower passively cooled an outdoor rest area at the 1992 EXPO in Seville, Spain with dramatic form.

Bordass, W., and Leaman, A. PROBE – Post occupancy Review of Buildings and their Engineering <http://www.usablebuildings.co.uk/probe/ProbeIndex.html> ESD Limited, Overmoor, Neston, Corsham, Wiltshire, SN13 9TZ, United Kingdom, 2004.

Briggs, R., Lucas, R., and Todd Taylor, Z., 2002. *Climate Classification for Building Energy Codes and Standards*. Technical paper Pacific Northwest National Laboratory.

Brown, G.Z. and Dekay, M., 2001. *Sun, Wind and Light: Architectural Design Strategies*. NewYork: John Wiley and Sons.

DOE2.2 (2002). PowerDOE, eQuest, www.DOE.com

Energy Information Agency, Building Energy Use Data, http://www.eia.doe.gov/

Givoni, B., 1998. *Climate Considerations in Building and Urban Design*. New York: Van Nostrand Reinhold.

Hamzah, T.R., Yeang, K., and Richards, I., 2001. *Ecology of the Sky*. Australia: Images Publishing.

Knowles, R., 1994. *Energy and Form: An Ecological Approach to Urban Growth*. Boston, MA: MIT Press.

Lacy, R.E., 1972. *Survey of Meteorological Information for Architecture and Building*. CIB Working Commission W4A.

Landsberg, H.E., 1976. Weather, climate and human settlements. Special Environmental Report 7. Geneva: World Meteorological Organization.

Leadership in Energy and Environmental Design of the US Green Building Council, http://www.usgbc.org/

Loftness, V., 1982. *Climate/Energy Graphics*: *Climate Data Applications in Architecture*. World Climate Program Publication WCP-30. Geneva: World Meteorological Organization.

Lloyd Jones, D. 1998, *Architecture and the Environment: Bioclimatic Building Design*. London: Laurence King.

Markus, T.A., and Morris, E.N., 1980. *Buildings, Climate and Energy*. London: Pitman.

National Academy of Sciences, Board on Applied Climatology, 1986. *Climate Data Management*. Final Report. Washington, DC: US National Research Council.

National Academy of Sciences, Building Research Advisory Board, 1950. *Weather and the Building Industry*. Conference Report 1. Washington, DC: US National Research Council.

Olgyay, V. 1963. *Design With Climate*. Princeton: Princeton University Press.

Page, J.K., 1970. The fundamental problems of building climatology considered from the point of view of decision making by the architect and urban designer. In *Building Climatology*. Technical Note 109. Geneva: World Meteorological Organization, pp. 9–21.

Page, J.K., 1976. *Application of Building Climatology to the Problems of Housing and Building for Human Settlements*. Technical Note 150. Geneva: World Meteorological Organization.

Page, J.K., 1992. Basic Climate Data in Energy in Architecture. In Goulding, J.R., Owen Lewis, J., and Steemers, T.C., eds., *The European Passive Solar Handbook*. EUR 13446. Brussels: Batsford, for the Commission of the European Communities, Chapter 2 and appendices.

Prior, M.J., and King, E.G., 1981. Weather forecasting for construction sites, *Meteorological Magazine,* **110**: 260–266.

SoDa, 2002. Solar Radiation Databases, http://soda.jrc.it for the Commission of the European Communities, Brussels.

Tombach, I., 1982. Measurement of local climatological and air pollution factors affecting stone decay. In *Conservation of Historic Stone Buildings and Monuments.* Washington, DC: National Academy of Sciences, pp. 197–210.

Tveit, A., 1970. Moisture absorption, penetration and transfer in building structures. In *Building Climatology,* Technical Note 109. Geneva: World Meteorological Organization, pp. 151–158.

Cross-references

Human Health and Climate
Urban Climatology

ARCTIC CLIMATES

The Arctic is the northern hemisphere heat sink that establishes latitudinal pressure gradients which drive the general circulation of the atmosphere. The Arctic typically conjures up mental images of a region dominated by extreme cold, snow cover and floating sea ice; but Arctic climates are quite diverse, both by season and region. This diversity reflects the pronounced seasonal cycle in solar radiation receipts, regional aspects of the atmospheric circulation and the contrasting thermal properties of different surface types. The most formal definition of the Arctic is the region north of the Arctic circle, approximately 66.5°N. At this latitude the sun does not rise above the horizon at the winter solstice and does not fall below the horizon at the summer solstice. However, climate conditions of Arctic "flavor" can be found south of the Arctic Circle, while surprisingly mild winter temperatures extend well north in the Atlantic sector. Other definitions of the Arctic include the region north of the 0°C mean annual isotherm, and the region north of the tree line.

Key physical features

The geography of the Arctic is in striking contrast to its southern counterpart. The Antarctic is characterized by a continental ice sheet surrounded by ocean. By comparison, most of the area north of latitude 70°N is occupied by the Arctic Ocean, which apart from the sector between about 20°E and 20°W longitude is almost entirely surrounded by land. The most striking feature of the Arctic Ocean is its floating sea ice cover. Total northern hemisphere sea ice extent ranges from about 14.8 million square kilometers in March to roughly half that value in September (Figure A46). Typical ice thicknesses in the Arctic Ocean are 1–5 m. The sea ice cover is not a solid slab, but contains roughly linear openings, known as leads, and more irregular areas of open water, termed polynyas. The ice cover is in near-constant motion due to winds and ocean currents. Snow cover overlies the sea ice and surrounding land for most of the year. Maximum snow depths range widely, especially on local scales, but values of 30–80 cm are typical.

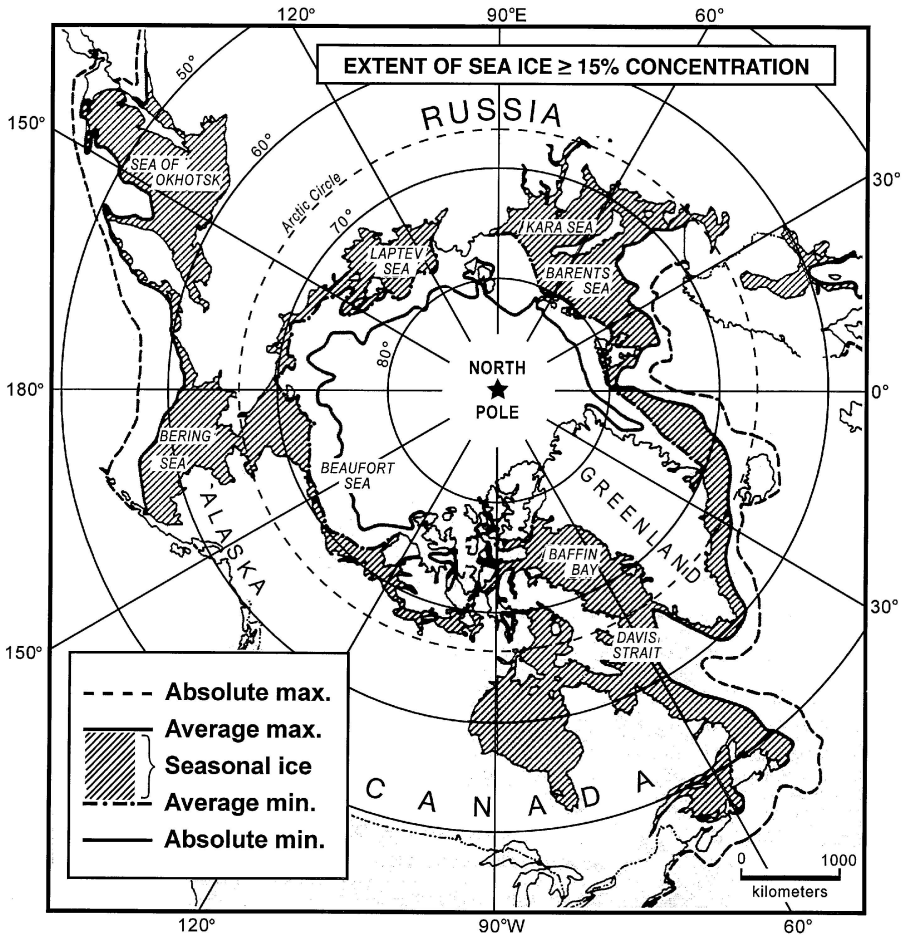

Figure A46 Geography of the Arctic region and limits of sea ice (adapted from Barry, 1983).

Apart from the Greenland ice sheet, which contains about 7.5 m of global sea level equivalent, ice caps and glaciers are primarily limited to the mountainous parts of the Siberian and Canadian Arctic Archipelagos, Svalbard and Iceland. However, most of the Arctic lands are underlain by perennially frozen ground, known as permafrost. The upper part of the ground in permafrost regions, termed the active layer, freezes and thaws seasonally, generally to depths of 100–200 cm. Permafrost acts as an impermeable barrier, which keeps moisture near the surface. Hence, many areas with poor drainage are covered by shallow thaw lakes in summer. In areas with more pronounced drainage, permafrost fosters rapid channeling of snow melt and precipitation into streams and river channels.

Much of the land surface is characterized as tundra. The most extreme and generally northernmost tundra landscape, polar desert, often has less than 5% vegetation cover. In lower latitudes, tundra commonly includes shrub vegetation of birch and willow, together with sedges and grasses. Vegetation covers 80–100% of the surface. At lower latitudes there is a forest–tundra transition, or ecotone, south of which is found the boreal forest.

Atmospheric circulation

The primary feature of the northern high-latitude mid-tropospheric circulation is the polar vortex, which in winter (Figure A47a) has major troughs over eastern North America and eastern Asia, a weaker trough over western Eurasia, and a strong ridge over western North America. The lowest winter pressure heights are located over northern Canada. These features are related to orography, land–ocean distribution and radiative forcing. The mean winter circulation at sea level (Figure A47b) is dominated by three "centers of action": (1) the Icelandic Low off the southeast coast of Greenland; (2) the Aleutian Low in the North Pacific basin; (3) the Siberian High over east-central Eurasia. The Icelandic and Aleutian lows are complex features. In the most fundamental sense they reflect position downstream of the major mid-tropospheric stationary troughs where cyclone activity is favored (they are hence part of the primary North Atlantic and East Asian cyclone tracks, respectively) and thermal effects of the relatively warm underlying ocean. The Icelandic Low is part of a broad area of low pressure extending into the Barents and Kara seas. This manifests open ocean waters and the penetration of cyclones (with associated strong horizontal heat and moisture transports) well into the Arctic Ocean. The Siberian High is a cold, shallow feature, driven largely by radiative cooling to space.

The polar vortex during summer is weaker and more symmetric (Figure A48a). The sea level Icelandic and Aleutian Lows essentially disappear and the Siberian High is replaced by a broad region of low pressure (Figure A48b). Mean low pressure is also found near the pole. Cyclone activity increases over land. Reflecting the mean low pressure, a summer cyclone

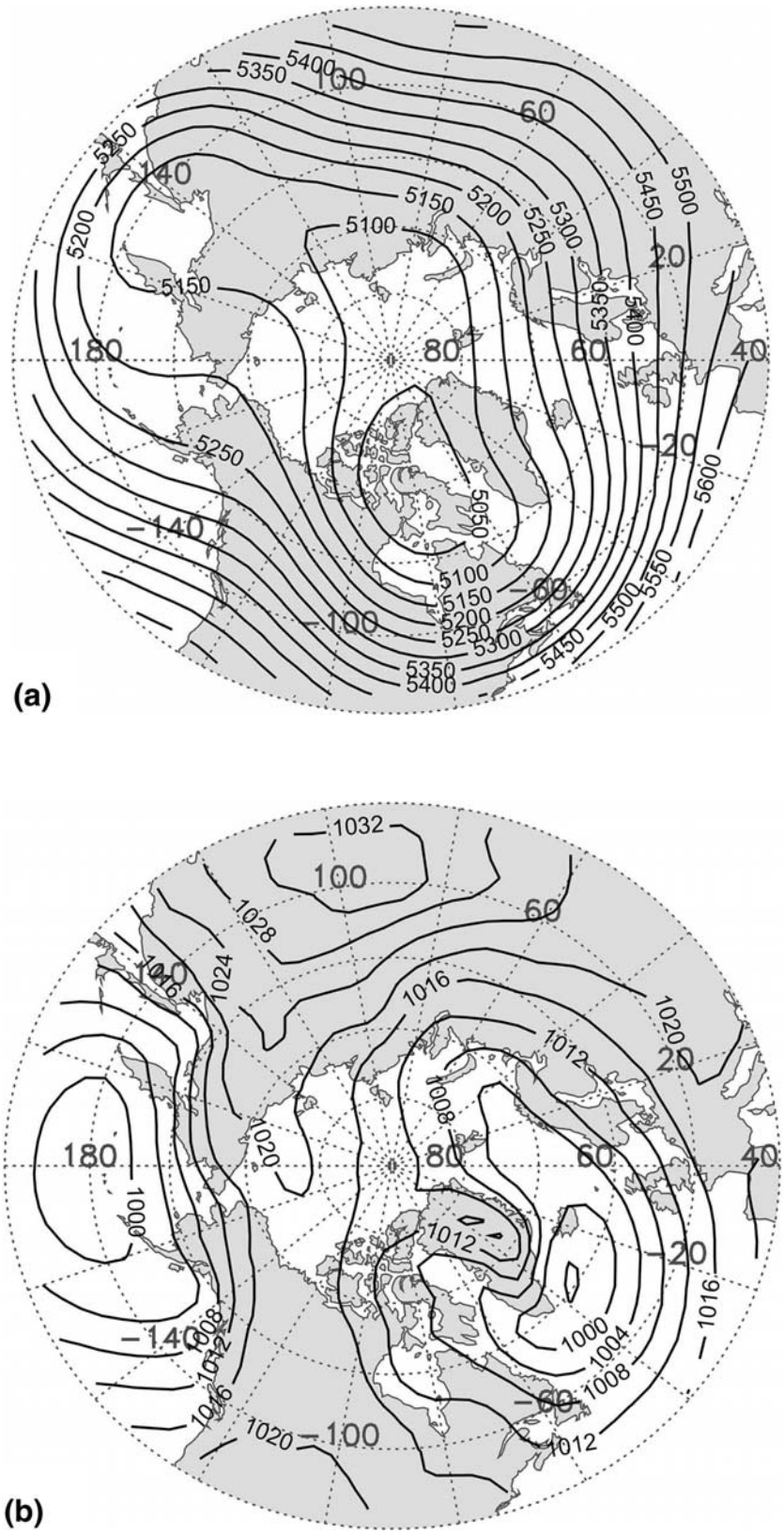

Figure A47 (**a**) Mean 500 hPa height (meters) and (**b**) sea level pressure (hPa) for January, based on National Center for Environmental Prediction/National Center for Atmospheric Research (NCEP/NCAR) reanalysis data for the period 1970–1999.

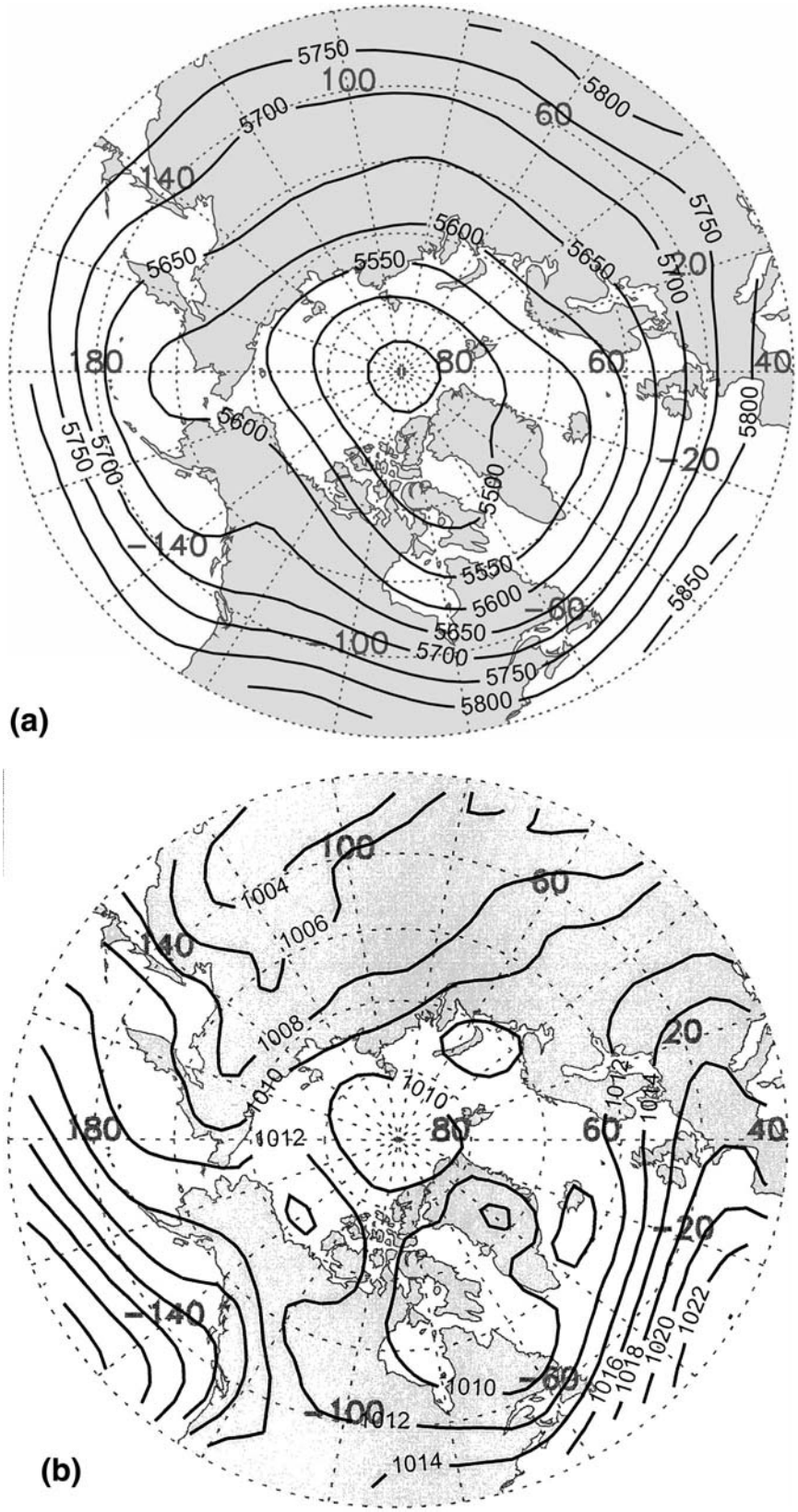

Figure A48 (**a**) Mean 500 hPa height (meters) and (**b**) sea level pressure (hPa) for July, based on NCEP/NCAR reanalysis data for the period 1970–1999. Note the different contour interval for sea level pressure (2 hPa) compared to the corresponding January plot (4 hPa) in Figure A47b.

maximum is also found over the central Arctic Ocean. This is largely due to the migration of cyclones generated over Eurasia and along the weakened North Atlantic track. Serreze (1995) provides further reading.

Surface air temperature

Figure A49 shows patterns of mean surface air temperature (at approximately the 2-m level) for the four mid-season months. January means near the North Pole are −32 to −33°C. The coldest conditions are found in northeastern Siberia in association with the winter Siberian High. Mean values of below −40°C are found in January. Locally, in valleys, temperatures are lower. Verkhoyansk, located along the Yana River valley at 67°N, is notorious for its extreme winter cold. The highest winter temperatures are found in the Atlantic sector. Building from previous discussion, this manifests warm, open water and horizontal transports of sensible and latent heat associated with the North Atlantic cyclone track. Over the ice-covered Arctic Ocean, leads and polynyas permit locally strong vertical heat fluxes from the ocean to the atmosphere. This prevents winter temperatures over the central Arctic Ocean from reaching the extremes observed in Siberia.

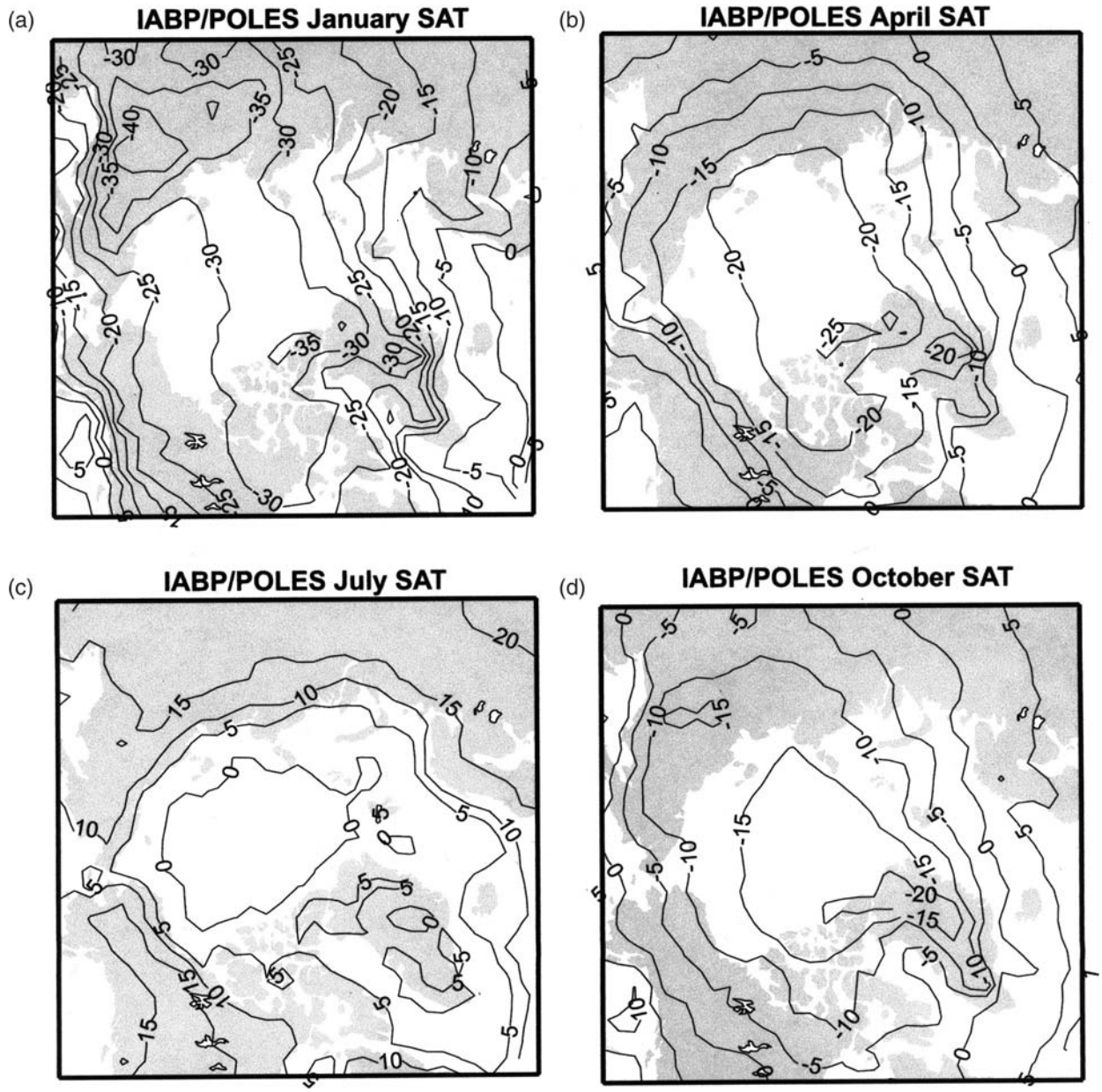

Figure A49 Mean surface air temperature (°C) for: (**a**) January; (**b**) April; (**c**) July; (**d**) October, based on the University of Washington International Arctic Buoy Programme/Polar Exchange at the Sea Surface (IABP/POLES) data set (updated and adapted from Rigor et al., 2000).

By April the Siberian temperature minimum has disappeared. The lowest temperatures are found over the Arctic Ocean and the Canadian Arctic Archipelago. Temperatures rise to the melting point over the coasts by the end of May and over most of the central Arctic Ocean by mid-June. The melt season over the central pack ice is about 60 days long. Summer temperatures over the central Arctic Ocean are constrained to hover near freezing point due to the presence of the melting sea ice cover. Because of strong differential heating between the Arctic Ocean and snow-free land, summer sees a sharp temperature gradient along the Eurasian and Alaskan coasts. Inland Arctic temperatures for July range from 10°C to 15°C. The sharp coastal gradient is not observed along the Canadian Arctic Archipelago due to the many ice-covered channels separating the islands.

A notable aspect of the Arctic environment is the presence of strong low-level temperature inversions (increasing temperature with height) during winter. These surface or near-surface-based features generally extend to about 1200 m during January–March, with a temperature difference from the inversion base to top of typically 11–12°C (Serreze et al., 1992). The inversion layer tends to be maintained by a radiative equilibrium associated with the different longwave emissivities of the surface (nearly a blackbody) and of the temperature maximum layer aloft, with northward heat advection balancing the outward radiation loss to space (Overland and Guest, 1991). Especially strong winter inversions are found inland in northwest Canada and eastern Siberia in inter-montane basins and valleys (e.g. at Verkhoyansk). In summer the Arctic is characterized by weaker, elevated inversions.

Precipitation

Mean annual precipitation totals across the Arctic (Figure A50a) vary by a factor of 20. The lowest annual totals of less than 100 mm are found over the northern Canadian Arctic Archipelago. Over the central Arctic Ocean the mean totals are around 250 mm. The largest annual amounts, locally exceeding 2000 mm, are found over the Atlantic sector. There is a strong seasonality in precipitation, illustrated by the January (Figure A50b) and July (Figure A50c) fields. The high annual totals in the Atlantic sector are largely driven by winter precipitation. This is a response to the strong Icelandic Low and North Atlantic cyclone track in this season. By contrast, most land areas and the central Arctic Ocean exhibit a summer maximum and winter minimum in precipitation. The winter minimum manifests the low moisture-holding capacity of the cold air in these regions and the relative infrequency of cyclone activity. The summer maximum over land areas is strongly associated with surface evaporation and more frequent cyclone activity. Convective precipitation is common over Alaska and Eurasia. The summer maximum for the central Arctic Ocean also manifests the summer cyclone maximum for this region.

Cloud cover

The Arctic is a cloudy place. Winter cloud fractions range from 40% to 70%, greatest over the Atlantic side where cyclone activity is frequent. Total cloud fractions rise to 70–90% in summer. Over the central Arctic Ocean there is a rapid increase between April and May, driven primarily by an increase in

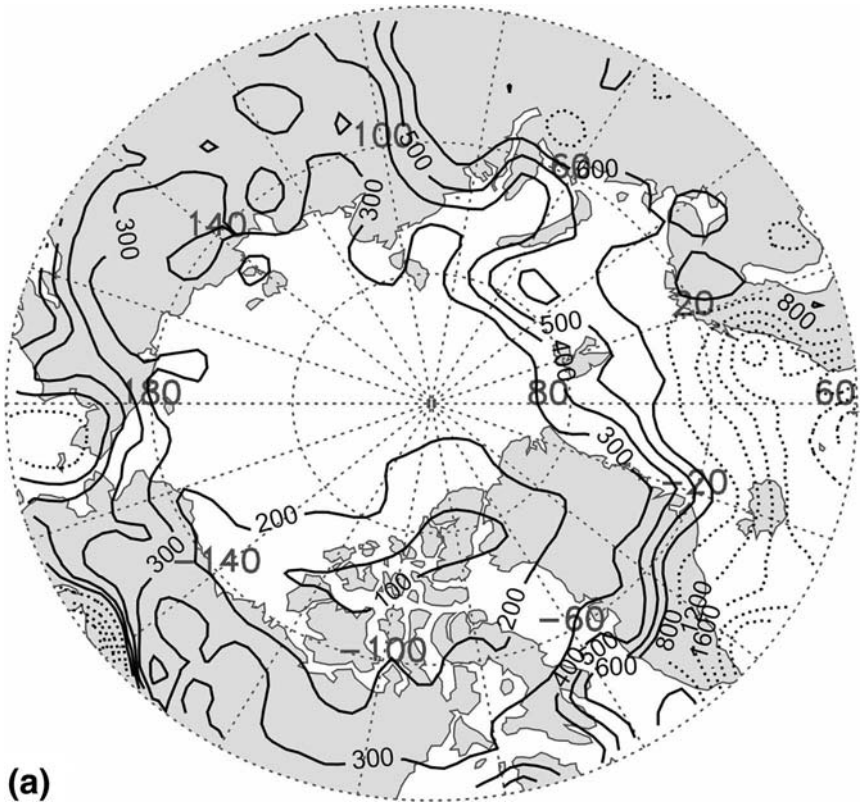

Figure A50 (*Continued*)

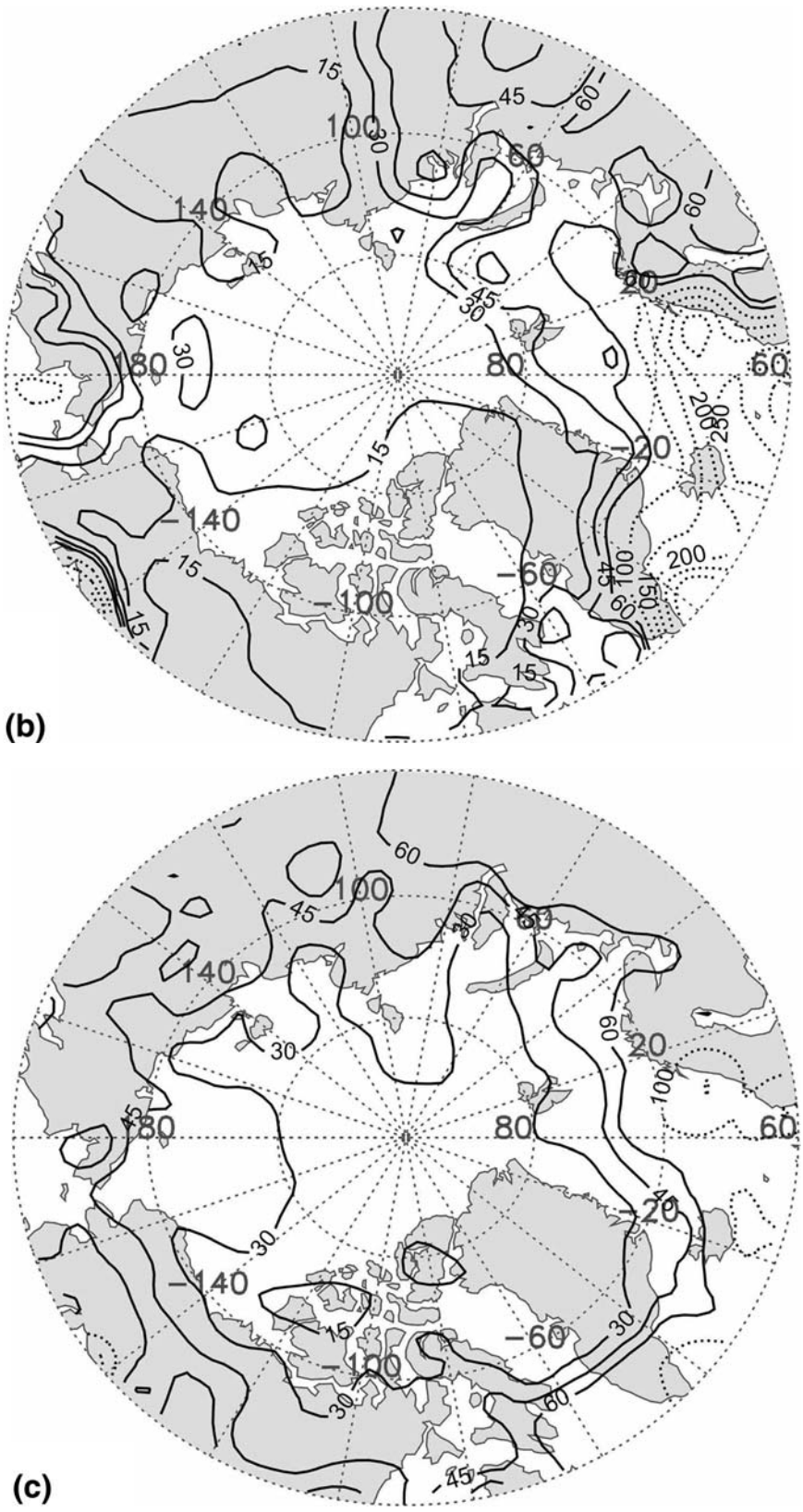

Figure A50 (**a**) Mean annual, (**b**) January and (**c**) July precipitation (millimeters) with estimated adjustments for wind-induced gauge undercatch, changes in instrument types and differences in observing methods. The annual map has isolines at every 100 mm up to 600 mm and at every 400 mm for higher amounts. The maps for January and July have isolines at every 15 mm up to 60 mm and at every 50 mm for higher amounts.

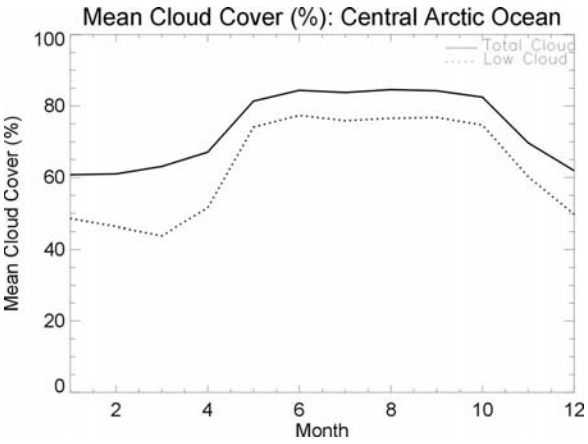

Figure A51 Mean monthly cloud cover (%) for the central Arctic Ocean based on available surface-based observations. Total (low-level) cloud cover is indicated by solid (dotted) line.

low-level stratus. While, traditionally, this summer increase is viewed as an airmass modification process whereby relatively moist air is chilled as it passes over the cold sea ice cover, the formative processes are not completely understood (Beesley and Moritz, 1999). The seasonal cycle of total and low-level cloud cover for the central Arctic Ocean is illustrated in Figure A51. While the dominance of low-level clouds is obvious, one can nevertheless observe many of the basic cloud types observed in middle latitudes. Perhaps surprisingly, convective cloud cover is frequent during winter over the Norwegian Sea – cold outbreaks from the north, when reaching the fairly warm, ice-free waters, result in destabilization of the air. Winter also finds low-level ice crystal clouds and "clear-sky" ice crystal precipitation (often termed "diamond dust") in stable boundary layers, along with ice crystal "plumes" emanating from open leads.

Surface energy budget

The surface net allwave radiation flux (the sum of shortwave and longwave exchanges) in the Arctic is negative for most of the year. Surface-based and satellite-derived sources indicate that, for the central Arctic Ocean, a net radiation deficit prevails from October through March, with winter monthly means of -20 to -35 Watts per square meter. There is a surplus from April through September, largest in July with typical means of $+80$ to $+95$ Watts per square meter. Winter deficits over land areas are broadly similar, but summer surpluses are higher, in the range of $+100$ to $+130$ Watts per square meter in July. That net allwave fluxes are small should come as no surprise. From October through March, solar radiation is either small or absent (6 months of polar darkness at the pole), such that the radiation budget is dominated by the longwave budget, which is almost always negative. Except in summer over land and ice-free waters, the high surface albedo (reflectivity in solar wavelengths) of snow and ice results in most of the incident solar flux being lost to space. The albedo of fresh snow exceeds 0.80 and is above 0.50 even for bare sea ice. Compared to other regions the Greenland ice sheet sees stronger net radiation losses in winter and smaller gains in summer. This is due to the high elevation, promoting stronger longwave losses, and the persistently high surface albedo.

With respect to the non-radiative terms, the fundamental difference between the surface energy budgets of the Arctic Ocean and tundra is the portion of net radiation used to melt snow and ice. Once the snow is melted from the tundra in summer, energy can be used in sensible heating and to evaporate water. By comparison, during summer, most of the available net radiation over sea ice is used for melt. This is consistent with Figure A49, which shows that July surface air temperatures over the central Arctic remain at about the freezing point. A major exception to the generally small turbulent heat exchanges over sea ice can be found in winter over leads and polynyas. Here, the exposure of warm, open water can yield sensible heat fluxes reaching 600 Watts per square meter.

A final point to be made is the strong role on the surface radiation budget played by cloud cover. For most of the year the cloud radiative forcing is positive in the Arctic, meaning that clouds have a warming effect at the surface. During polar darkness this can be fairly simply understood in that cloud cover represents an effective "blanket" that reduces longwave losses to space. When solar radiation is present the problem is more complex. One most consider the reduction in longwave losses in comparison to the reduction in the shortwave gains due to the cloud albedo, along with other factors such as shortwave absorption by clouds, the surface albedo, and multiple reflections between the surface and cloud base. Curry et al. (1996) review the problem.

Climate variability and change

The Arctic exhibits pronounced climate variability on interannual to decadal scales. A major source is the North Atlantic Oscillation (NAO). The NAO describes co-variability in the strengths of the Icelandic Low and Azores High (a semipermanent area of high pressure in the middle latitudes of the North Atlantic). When the Icelandic Low and Azores High are both strong, the NAO is in a positive state. Surface air temperatures are above normal over Eurasian Arctic lands and below normal over northeastern Canada. The North Atlantic cyclone track extends deeper into the Arctic Ocean and precipitation increases in the Atlantic sector of the Arctic. When the Icelandic Low and Azores High are both weak, the NAO is in a negative state, with roughly opposing climate signals. Climate signals associated with the NAO are best expressed in winter and have been recognized for centuries. In recent years many investigators have preferred to view the NAO as a component of a more fundamental northern hemisphere annular mode (NAM), popularly known as the Arctic oscillation, or AO (Thompson and Wallace, 1998).

From about 1970 through the late 1990s, the NAO and AO changed from primarily negative to positive states. Among other changes this has been attended by surface air temperature increases over most of the northern continental landmasses and the central Arctic Ocean (strongest in winter and spring), a downward tendency in summer sea ice extent, and changes in the circulation of the sea ice and ocean.

Global climate models predict that the effects of anthropogenic greenhouse warming will be amplified in the Arctic due to feedbacks in which variations in snow and sea ice extent, the stability of the lower troposphere and thawing of permafrost play key roles. There is some evidence that positive phases of the NAO and AO may be favored by increased greenhouse gas concentrations or stratospheric ozone loss. Interestingly, paleoclimate evidence suggests that Arctic temperatures of the late twentieth century were the highest of the past 400 years (Overpeck et al., 1997).

Mark C. Serreze

Bibliography

Barry, R.G., 1983. Arctic Ocean ice and climate: perspectives on a century of polar research. *Annals, Association of American Geographers*, **73**: 485–501.

Barry, R.G., Serreze, M.C., Maslanik, J.A., and Preller, R.H., 1993. The Arctic sea-ice climate system: observations and modeling. *Reviews of Geophysics*, **31**: 397–422.

Beesley, J.A., and Moritz, R.E., 1999. Toward an explanation of the annual cycle of cloudiness over the Arctic Ocean. *Journal of Climate*, **12**: 395–415.

Curry, J.A., Rossow, W.B., Randall, D., and Schramm, J.L., 1996. Overview of Arctic cloud and radiation characteristics. *Journal of Climate*, **9**: 1731–1764.

Overland, J.E., and Guest, P.S., 1991. The Arctic snow and air temperature budget over sea ice during winter. *Journal of Geophysical Research*, **96**(C3): 4651–4662.

Overpeck, J., Hughen, K., Hardy, D., et al., 1997. Arctic environmental change of the last four centuries. *Science*, **278**: 1251–1256.

Rigor, I.G., Colony, R.L., and Martin, S., 2000. Variations in surface air temperature observations in the Arctic, 1979–1997. *Journal of Climate*, **13**: 896–895.

Serreze, M.C., 1995. Climatological aspects of cyclone development and decay in the Arctic. *Atmosphere-Ocean*, **33**: 1–23.

Serreze, M.C., Kahl, J.D., and Schnell, R.C., 1992. Low-level temperature inversions of the Eurasian Arctic and comparisons with Soviet drifting station data. *Journal of Climate*, **5**: 615–629.

Serreze, M.C., Walsh, J.E., Chapin III, F.S. et al., 2000 Observational evidence of recent change in the northern high latitude environment. *Climatic Change*, **46**: 159–207.

Thompson, D.W.J., and Wallace, J.M., 1998. The Arctic Oscillation signature in the wintertime geopotential height and temperature fields. *Geophysical Research Letters*, **25**: 1297–1300.

Cross-references

Aleutian Low
Antarctic Climates
Asia, Climates of Siberia, Central and East Asia
Cloud Climatology
Energy Budget Climatology
North American High
Ocean Circulation
Siberian High
Snow and Snow Cover

ARID CLIMATES

The Earth's variable climate is a function of an unequal distribution of solar radiation. Average yearly net gains in insulation occur equatorward of 36° latitude, and net losses poleward this latitude. It follows that variations in air temperature and atmospheric pressure occur about the planet, which drive atmospheric circulation and ocean currents. Moisture content in the atmosphere is a function of air temperature and proximity to water sources. Warm tropical air rises, expands, cools adiabatically, condenses, forms clouds, and yields precipitation throughout much of the tropical zone. A rotating Earth causes air masses to migrate poleward where at about 20–40° north and south latitudes the air subsides, compresses, warms adiabatically, increases its moisture-holding tendency, and ultimately results in very warm, dry air at the surface. This middle tropospheric warming inhibits deep convection necessary for heavy rain to form. Arid climatic conditions ensure many of the world's deserts reside within these belts of high pressure that ring the planet. The Arctic and Antarctic contain polar deserts which will not be addressed here.

Aridity

Aridity refers to the dryness of the atmosphere. Aridity is a function of a continuum of environmental factors including temperature, precipitation, evaporation, and low vegetative cover. Aridity indexes are quantitative indicators of the degree of water deficiency at a given location (Stadler, 1987). Perhaps the best-known methods at identifying the arid zones of the world are classified by Köppen (1931), Thornthwaite (1931, 1948), and Meigs (1953), although the term aridity index specifically applies to Thornthwaite's work. A brief summary of these three works follows, but a more comprehensive treatment of aridity indexes may be found under Aridity Indexes (this volume).

Köppen devised a method for the identification of aridity that took into account the season of occurrence of precipitation. Rainfall occurring during a hot summer is less effective than the same amount of precipitation falling in winter. He classified arid environments as BW for arid deserts and BS for semiarid steppe regions. He also created a subcategory to distinguish between hot (h) and cold (k) dry climates. The B classification (dry climates in which potential evapotranspiration exceeds precipitation) is assigned to a region meeting one of the following criteria relating to mean annual precipitation (R in centimeters), and mean annual temperature in °C.

1. At least 70% of R occurs during the warmer 6 months, and $R < 2T + 28$.
2. If at least 70% of R occurs during the cooler 6 months, and $R < 2T$.
3. If neither half of the year includes more than 70% of R and $R < 2T + 14$.

Thornthwaite (1931, 1948) created indices based upon a percentage of water deficiency and water need during a growing season. The *Aridity Index* $AI = 100 \times d/n$, where d is water deficiency or the sum of the absolute values of monthly differences between rainfall and potential evapotranspiration when rainfall is less than potential evapotranspiration, and n is the water needed at a particular site calculated as the sum of the monthly values of potential evapotranspiration for months having a water deficiency. He also created a *Humidity Index* $HI = 100 \times s/m$, where s is excess water representing the sum of the monthly differences between rainfall and potential evapotranspiration for the months when precipitation exceeds evapotranspiration; and m is water needed at a site calculated as the sum of the monthly values for evapotranspiration during months having excess rainfall. The higher the Aridity or Humidity Index, the more arid or wet the region respectively.

Thornthwaite (1948) combined the Aridity Index with a Humidity Index to form a *Moisture Index* ($MI = HI - 0.60 \times AI$). This is a measure of precipitation effectiveness for plant growth that takes into account deficiency and excess water at a particular site. A climate classification was developed from this index where a MI less than 0 is assigned semiarid, and a MI less than -40 is assigned arid. Thornthwaite further considered regions arid when annual precipitation is less than 33% of potential evapotranspiration, and semiarid when annual precipitation is between 33% and 67% of potential evapotranspiration. Despite these indices there is little agreement on the complex number of factors leading to aridity, or how aridity can be compared using these indices.

Meigs (1953, 1960), under the auspices of UNESCO's Advisory Committee on Arid Zone Research, devised a system that delimited the arid zone and identified climatic differences within the zone. He identified arid climates (A) as those in

which there is not enough precipitation for crop production. In addition, he identified an extremely arid zone (E) on the basis of a dry period of 12 months or more in which no precipitation fell (Thornthwaite's moisture index values of less than −40 can be used to make specific determinations of the boundaries of these zones).

Meigs followed Köppen in recognizing the importance of season of precipitation, and Thornthwaite in stressing heat as a factor essential for the growth and ripening of plants. Where water is available for irrigation in arid lands, temperature becomes a more important factor than moisture in the regional climate. Meig's maps of arid climate types include a number of subdivisions where the first digit represents the coldest month and the second digit the warmest month. A value of 03 indicates a winter month with temperatures below 0°C and 3 indicates a summer month with average temperatures of 20–30°C. Meigs distribution of arid climates is shown in the article on Deserts in this volume.

The arid environment

Arid environments occur at the poles, along the equator, on mountains, plateaus, below sea level, along coasts, and within mid-continents. They may be hot or cold climate types. Deserts grade imperceptibly into semiarid deserts forming expansive dry lands about the planet. Deserts are both arid and semiarid lands, and account for over 35% (>61 million km^2) of the Earth's land area (Mares, 1999). They are not capable of supporting a continuous cover of vegetation, and in the dryer portions of the arid zone, vast areas are without vegetation. Shortages of water characterize the arid climate. Water becomes a critical resource for the survival of plants and animals struggling to survive in this harsh environment. Arid zones are broad expanses (fuzzy boundaries) in which xerophytic vegetation composed of shrubs and succulents is widely scattered. It is along the desert margins that humans have tested nature by encroaching on areas that are often considered best left in their natural state.

The effect of the clear skies on temperature is readily apparent in deserts. Temperature ranges of 15°C to 22°C are common and objects in the shade are appreciably cooler than those in the sun. Some of the highest temperatures ever recorded have been measured in the arid lands. The highest temperature (58°C) was recorded at El Azizia about 40 km south of Tripoli (Kendrew, 1961). Temperatures in the tropical deserts are generally lower than this, but are usually above 40°C each day during the summer months. Nighttime temperatures are normally 16°C to 18°C lower. In winter, freezing temperatures at or near the surface are not unusual at night. Arid lands in higher latitudes experience temperature conditions comparable to those of adjacent humid environments. Advection of warm and cold air into these areas is more frequent and radiational cooling and heating of less significance.

Arid environments suffer a negative water balance in that the potential evaporating moisture exceeds the moisture supply provided by rainfall; therefore, potential evapotranspiration (the amount of moisture that would evaporate from soil and vegetation if a continuous supply of water were available) is directly proportional to temperature, wind speed, and relative humidity. Since transpiration is the most profuse of the two, if precipitation evaporates rapidly after falling, a much greater amount of moisture is required in the soil for the growth of plants than if precipitation evaporates slowly.

The results of climatic and human-induced arid conditions may initiate a threshold that spawns a physical transformation called desertification. The United Nations (1980) defines desertification as "a diminution or destruction of the biological potential of the land [which] can ultimately lead to desert-like conditions". In 1977 the United Nations announced that 35 million square kilometers were affected by desertification, and 35% of the Earth's surface at risk of similar changes. Disagreement exists on causes, processes, extent, and which changes are human-induced and what are natural. The question that begs to be answered is will the land that is desertified be reversible, and how much land is clearly at risk of change to deserts?

Identification and location of arid regions

In general terms arid regions (true deserts) typically receive less than 200–250 mm of irregular precipitation annually, with high evaporation rates. Hyperarid deserts receive less than 25 mm of precipitation annually, and have no rainy season and semiarid (steppe) regions receive greater than 250 mm and less than 600 mm of precipitation annually.

Deserts often form due to their proximity to cool, offshore ocean currents. Upwelling of colder water (Humboldt current off eastern South America, Benguela current off the southeast Africa coast) promotes cooler air at the lower contact with the ocean. Subtropical highs centered on the eastern half of oceans create equatorial movement of air along the western continental margins. This brings cooler, denser air to the warmer, subtropics enhancing the sinking motion associated with anticyclones. The relative humidity decreases, sharp temperature inversions develop that inhibit vertical convective activity, thus condensation and precipitation fail do develop. Little moisture is transferred from the colder waters flowing along the continental margins to air reaching land. The already dry, descending air mass becomes even dryer, resulting in some of the most arid deserts in the world (Sechura/Atacama Desert system of Chile and Peru 20–28° south latitude, western Sahara Desert of west Africa 18–30° north latitude, Namib Desert of southwest Africa 18–30° south latitude, and the Sonoran Desert of southern California and northern Mexico 30–33° north latitude (Lydolph, 1973).

Continental deserts form as moist air traveling from the oceans, inland, loses its moisture (Gobi Desert of central Asia and central Australian deserts 40–50° north latitude). Rainshadow deserts form when moisture is removed as air rises, cools, and condenses on the windward side of mountain barriers, descends the leeward side, is compressed, and warmed (Great Basin in the USA). In those areas subject to surges of tropical air where thunderstorms occur, intensities near the centers of the storms are high, but duration is generally short. In those arid lands reached by tropical cyclones, rainfall intensities are great, and the storms can persist for several days, resulting in areas of heavy precipitation. Such storms are of particular significance in North America and Australia. In other arid lands, unusually heavy precipitation is generally associated with isolated thunderstorms that produce flash floods in desert washes and wadis.

In desert areas where virtually no rain occurs, dew and fog drip represent the only forms of atmospheric moisture available. In the coastal deserts of Peru and Chile, moisture obtained from the fog that moves inland across the Coast Ranges sustains a

moderately dense shrub forest. Because of the great amount of radiational cooling in the deserts, the formation of dew is a frequent occurrence. In the days of Roman occupation of North Africa, large rock piles above a cistern were used to collect dew for domestic water supply. Dew is an important contributor to the water budgets of many desert regions.

Perhaps the greatest amount of research into moisture sources in the arid regions has been directed at problems relating to reliability, frequency, duration, and intensity of precipitation. Generalizations about these matters are difficult because of the different kinds of atmospheric conditions that prevail in different parts of the world. For all of the arid lands it is safe to say that precipitation occurs infrequently.

Select references focusing on research organizations (Hunchinson and Varady, 1988; Hopkins and Jones, 1983), and discussions on world regional deserts (Mares, 1999; Ferrari, 1996; Bender, 1982; Petrov, 1976) are noteworthy.

World arid regions

One of the problems in delineating absolute boundaries to arid lands is that even the slightest climatic changes in these fragile environments may result in widespread changes in the natural and in human–environment relationships. Conversely, changes that humans make in the environment also result in changes in climate. General meteorological conditions are discussed for arid and hyperarid desert regions throughout the world. Table A26 lists many of the world's true deserts and hyperarid regions as classified by precipitation. Semiarid (steppe) regions are not included in this list.

African arid regions

The Sahara is a vast desert region that lies within the subtropical high-pressure belt. Across its northern margins, cyclonic storms that penetrate and cross the Mediterranean Sea from west to east drop precipitation, occasionally in the form of snow in the winter season. On the southern margins, precipitation is associated with the northward migration of the intertropical convergence zone. In the desert, dust storms associated with strong winds present problems for both sedentary agriculture and for migratory nomadic groups.

In southwest Africa, the Namib Desert along the coast and the Kalahari Desert inland are associated with the descending air masses and stable atmospheric conditions found at the eastern end of the South Atlantic subtropical high-pressure area. Portions of the Namib are extremely arid and devoid of vegetation. Stability of the air mass in the region is enhanced by cold upwelling water found on the coastal side of the Benguela Current. The outer desert of the Kalahari receives less than 250 mm of precipitation, while further into the interior precipitation amounts greater than 250 mm provide sufficient water to sustain a scrub forest.

Australian arid regions

Over half the continent is a desert with subtropical and tropical grasslands occupying much of the remainder. In the southern hemisphere summer the intertropical front dips southward into the continent, occasionally penetrating far into the desert interior. Runoff from heavy rains floods desert washes and creates vast playa lakes. Tropical cyclones affect the Queensland coast, and in the northwest the dreaded Willy Willies cause extensive destruction to coastal settlements. Winter precipitation is associated with the troughs of low pressure that lie between the migratory anticyclones that encircle the globe north of Antarctica. Cold fronts force moist marine air to rise over the low hills and mountains of the coastal zones. The easterly flow of air on the backsides of the migratory anticyclones is forced to rise along the slopes of the Great Dividing Range to produce precipitation on the eastern coast of New South Wales and Queensland.

Within the Great Australian Desert differences in the appearance of the landscape resulting from variation in environmental factors are reflected in local names for that portion of the desert. The Great Sand, Simpson, Gibson, Great Victoria, and Sturt deserts reflect the variety of landscapes to be observed within the continent.

North American arid regions

The arid zone of North America comes under the influence of the belt of subtropical high pressure. Portions lie behind mountain barriers, and much of it is remote from sources of moisture. The driest portion, the Sonoran Desert, is dominated by the Pacific High for most of the year. In winter, occasional cyclonic storms penetrate the region, bringing small amounts of precipitation, occasionally in the form of snow. However, summer is the season of maximum precipitation. Afternoon thunderstorms associated with surges of tropical air may drop copious amounts of moisture on limited areas, causing temporary flooding. By far the heaviest precipitation and the most serious flooding comes with tropical storms that migrate into the area from the southeast Pacific Ocean in late summer and early fall.

In the Great Basin, maximum amounts of precipitation are associated with the cyclonic storms of winter that cross the area. However, these storms have lost most of their moisture in crossing the Sierra–Cascade barrier, and rainfall is generally light. Snow falling in the surrounding mountains represents a major source of water used in the region. In the summer season, thunderstorms forming in tongues of moist tropical air occasionally produce heavy rain and runoff.

The Chihuahua Desert of the Rio Grande Valley and north central Mexico lie in an area that is protected from air masses from the Pacific and Atlantic oceans by mountain ranges. Aloft, stable descending air limits the formation of convective storms. Heavy rains occur only in summer, when tropical hurricanes and easterly waves from the Caribbean and Gulf of Mexico penetrate the area.

South American arid regions

The Peruvian and Atacama Deserts of the west coast of South America are among the driest areas on earth. On the north, the intertropical convergence zone only occasionally penetrates more than several degrees south of the equator. When it does, a warm ocean current – El Niño – appears offshore and heavy rains cause innumerable problems for the irrigated oases of northwest Peru. On the south, the cyclonic storms of winter rarely bring precipitation much farther north than 32°S. Offshore, the cold Humboldt Current enhances the stability of the air in the South Pacific High, and fog frequently blankets the hills of the coastal zone.

On the eastern flanks of the Andes lie the deserts and grasslands of Argentina, Bolivia, and Paraguay. Storms sweeping out of the Pacific Ocean drop their moisture on the western slopes

Table A26 Desert regions about the world. Some deserts appear in both arid and hyperarid columns because of varied climate

Continent	Arid region	Hyperarid region
Africa	Namib Desert (southwest coast, Namibia/Angola). Libya Desert (Sahara). Sahara Desert (Nubian Desert in Sudan and Ethiopia). Sinai Desert (Egypt).	Libya Desert (Sahara). Namib Desert (southwest coast, Namibia/Angola).
Australia	Great Sandy Desert. Tanami Desert. Gibson Desert. Simpson Desert. Great Victoria Desert. Nullarbor Plain.	
North America (Mexico and USA)	Chihuahuan Desert (USA/Mexico). Great Basin Desert (USA). Sonoran Desert (USA/Mexico). Mojave Desert (USA).	Mojave Desert (USA).
South America	Peruvian/Chilean Desert. Monte Desert (Argentina). Patagonia.	Sechura Desert (Peru). Atacama Desert (Chili). Peruvian/Chilean Desert.
Asia	Sistan depression (Sistan Desert, Afghanistan). Ust-Urt (midwest Asia). Kyzyl-Kum (Uzbekistan). Kara-Kau (Turkmenistan). Bet-Pak-Dala (Kazakhistan). Kara Kum (Irano-Turanian Region). Turanian Plain (Irano-Turanian Region). Dusht-e-Kavir Desert (Iran). Dasht-e-Naumid Desert (Iran). Ala-Shan Desert (China). Gobi Desert (Mongolia/China). Takla Makan Desert (China). Thar (India/Pakistan). Syrian Desert (Syria/Iraq/Jordan). Negev Desert (Israel, western Arabian Desert, Sinai Peninsula). Ordos (China).	Registan (Afghanistan). Dusht-e-Margo (Afghanistan). Dusht-e-Lut Desert (Iran). Tsaidam Desert (China).

of the Andes Mountains. The desiccated air flowing downslope on the eastern side is warmed by compression, and contributes to the aridity of the region by absorbing the available moisture as it crosses the plains.

Two unusual zones of aridity are located along the northern coast of Venezuela and in northeast Brazil. Both of these areas have been the subject of intensive investigations and are considered to be somewhat anomalous. The Brazilian arid zone, in particular, has been of great concern to that nation because of recurrent drought and forced migrations from the region because of the lack of food and water.

Asian arid regions

The Arabian, Iranian, and Thar Deserts fall under the influence of the subtropical high-pressure area of the northern hemisphere, but are also located far from the principal source of moisture in the storms that cross the area. In the winter season, cyclonic storms that originate over the Atlantic Ocean or Mediterranean Sea pass through the area. However, only small amounts of moisture are left by the time the storms reach these interior locations. Additionally, mountains and high pressure tend to block their movements and divert the paths of the storms to the north.

The Turkestan, Takla-Makan, and Gobi Desert regions lie at the interior of the Eurasian continent, remote from sources of oceanic moisture and shielded from tropical air masses by gigantic mountain systems. In winter the Asiatic High blocks the movement of cyclonic storms across the region. In the summer the moist stream of air associated with the summer monsoon is diverted around the southeastern corner of Asia by the mountain masses of Pakistan, India, China, and Malaysia.

Danny M. Vaughn

Bibliography

Bender, G.L., 1982. *Reference Handbook on the Deserts of North America*. Westport, CT: Greenwood Press. Westport, Conn.

Ferrari, M., 1996. *Deserts*. New York: Smithmark.

Hopkins, S.T., and Jones, D.E., 1983. *Research Guide to the Arid Lands of the World*. Phoenix, AZ: Oryx Press.

Hutchinson, B.S., and Varady, R.G., 1988. *Arid lands Research Institutions*. New York: Allerton Press.

Kendrew, W.G., 1961. *Climates of the Continents*. Oxford: Clarendon Press.

Köppen, W., 1931. *Grundriss der Klimakunde*, 2nd edn. Berlin: Walter de Gruyter.

Lydolph, P., 1973. *On the Causes of Aridity Along a Selected Group of Coasts*. In Amiran, D., and Wilson, A., eds., *Coastal Deserts: Their Natural and Human Environments*. Tucon, AZ: 1973.
Mares, M.A. (ed.), 1999. *Encyclopedia of Deserts*. Norman, OK: University of Oklahoma Press.
Meigs, P., 1953. *World Distribution of Arid and Semi-arid Homoclimates*. In *Reviews of Research on Arid Zone Hydrology*. Paris: UNESCO, Arid Zone Research, pp. 203–210.
Meigs, P., 1960. *Distribution of Arid and Semi-arid Homoclimates: Eastern Hemisphere; Western Hemisphere*. United Nations Maps No. 392 and No. 393, Revision 1. Paris: UNESCO.
National Science Board, 1972. *Drought: The Causes and Nature of Draught and Its Prediction*. In *Environmental Science,* Washington, DC.
Petrov, M.P., 1976. *Deserts of the World*. New York: Wiley.
Stadler, S.J., 1987. Aridity Indexes. In Oliver, J.E., and Fairbridge, R.W., eds., *The Encyclopedia of Climatology*. New York: Van Nostrand Reinhold, pp. 102–107.
Schneider, S.H. (ed.), 1996. *Encyclopedia of Climate and Weather*, Vol. 1. New York: Oxford University Press.
Thornthwaite, C.W., 1931. The climates of North America according to a new classification. *Geography Review*, **21**: 633–655.
Thornthwaite, C.W., 1948. An approach toward a rational classification of climate. *Geography Review*, **38**: 55–94.
United Nations, 1980. *Desertification*. Oxford: UN.

Cross-references

Aridity Indexes
Climate Classification
Desertification
Deserts
Rainshadow

ARIDITY INDEXES

Aridity indexes are quantitative indicators of the degree of water deficiency present at a given location. A variety of aridity indexes have been formulated, although the term *Aridity Index* specifically refers to the 1948 work of Thornthwaite. Aridity indexes have been applied at continental and subcontinental levels and are most commonly related to distributions of natural vegetation and crops. Critical values of the indexes have been derived from observed vegetation boundaries. For instance, Köppen's 1918 classification defines the desert/steppe boundary as the 200-mm annual isohyet in regions where there is no seasonality of rainfall and the mean annual temperature is 5–10°C.

Formulation of aridity indexes is not straightforward due to the nature of aridity. First, aridity is a function of the interplay between rainfall, temperature, and evaporation. Use of mean annual rainfall as an index of aridity ignores the importance of temperature and evaporation. Aridity indexes that have gained widespread acceptance directly or indirectly take into account all three factors. Second, the arid regions generally have been recognized as having a paucity of climatological data. Given the temporal variability of precipitation inherent in arid regions, the lack of climatological data has been detrimental in attempts to quantitatively define the boundaries of aridity. Third, aridity indexes must be considered from the standpoint of their eventual use. For example, the 1968 US Army World Desert Classification defines aridity with respect to military operations; application to world vegetation patterns would be inappropriate. A particular aridity index may serve several purposes, but no one index is appropriate for all uses. However, aridity indexes are often mathematically related and to some extent have been used interchangeably on a global scale.

Identification of the arid zones of the Earth has roots that can be traced two millennia. Classical Greek thought identified the latitudinally controlled torrid, temperate, and frigid zones of the world. Implicit in their thought was the concept that the torrid, low-latitude climates were arid. Not until long-term instrumental records and reliable world vegetation maps became available could true aridity indexes be developed. Thus, aridity indexes are a product of the twentieth century. Table A27 outlines the major developments regarding aridity indexes. For additional information, see Dzerdzeevskii (1958), Hare (1977), and International Crops Research Institute for the Semi-Arid Tropics (1980).

In 1900 Köppen originally qualitatively classified as arid those places that had desert vegetation. V.V. Dokutchaev in 1900 and A. Penck in 1910 qualitatively defined arid regions as places where annual evaporation exceeds precipitation. In 1905 both E.N. Transeau and G.N. Vyssotsky quantified this relationship. Yet this approach was not totally satisfactory because of the lack of reliable, worldwide evaporation measurements. Köppen's influential series of climatic classifications used mean annual temperature and precipitation combinations to define arid climates (1918, 1936). In a similar vein W. Lang's 1920 Rain Factor Index was a ratio between mean annual precipitation and mean annual temperature. Lang's index, and a modified version done by E. de Martonne in 1925, were widely used because their data requirements were minimal. However, their approach was limited in that the seasonality of temperature and precipitation were not addressed.

A. Meyer's 1926 Precipitation–Saturation Deficit Ratio was an attempt to obviate the need for dependable evaporation data. Meyer assumed the evaporation rate to be a function of the saturation deficit (saturation vapor pressure minus actual vapor pressure at a particular temperature). The Precipitation–Saturation Deficit Ratio was calculated from long-term temperature, precipitation, and relative humidity data and was found to be more reliable than temperature/precipitation-based indexes. Data availability limited the application of Meyer's ratio in that relative humidity data generally were not as available as were temperature and precipitation records.

Thornthwaite's work had an immense influence on the quantitative calculation of aridity. His Precipitation Effectiveness Index of 1931 is computed as ten times the sum of the monthly precipitation to evaporation ratio at a given location. Of practical importance was his accompanying empirical formula for deriving the Precipitation Effectiveness Index for stations recording only mean monthly temperature and precipitation. In 1948, and in subsequent revisions of his climatic classification, Thornthwaite employed the Aridity Index, which relates annual moisture deficit to annual potential evapotranspiration (see Water Budget Analysis). Weighted by 0.6 and subtracted from Thornthwaite's Humidity Index, the Aridity Index is a component of Thornthwaite's Index of Moisture. On the basis of the Index of Moisture, Thornthwaite categorized the world into nine moisture zones ranging from arid to perhumid. Evapotranspiration prominently figured in Thornthwaite's indexes, yet it was measured at only a handful of sites worldwide. So Thornthwaite devised a formula to estimate evapotranspiration through the use of a station's latitude and temperature.

Table A27 Selected summary of aridity indexes

Year	Author	Remarks	Formula
1900	W. Köppen	*Xerophytic* (arid and seimarid) climates qualitatively defined through presence of vegetative types. No formula used.	
1900	V.V. Dokutchaev	Defined aridity through comparison of annual precipitation with annual evaporation from a water surface. No formula used.	
1905	E.N. Transeau	Used ratio of annual precipitation to evaporation to describe aridity. Along with Vyssotsky, the first quantitative aridity index	$\frac{P}{E}$
1905	G.N. Vyssotsky	Used ratio of annual precipitation to evaporation to describe aridity. Along with Transeau, the first quantitative aridity index.	$\frac{P}{E}$
1910	A. Penck	Defined aridity through comparison of annual precipitation with annual evaporation from a water surface. An attempt to relate climate to landforms. No formula used.	
1911	E.M. Oldekop	Precipitation compared with potential evaporation. E computed by multiplying the saturation deficit of the air by a *coefficient of proportionality*.	$\frac{P}{E}$
1918	W. Köppen	Arbitrary climatic boundaries based on presumed vegetation boundaries. For example, desert and steppe were partitioned by 200 mm annual isohyet in areas where the mean annual temperature was 5–l0°C; they were separated by the 320-mm isohyet where the mean annual temperature was 25°C. No formula used.	
1920	W. Lang	Rain factor. Mean annual precipitation (mm) and mean annual temperature (C) compared.	$\frac{P}{T}$
1922	W. Köppen	Precipitation compared formula at right. Several revisions of Köppen's scheme were formulated by the author himself and by others.	$2(T + 7)$
1926	E. de Martonne	Index of Aridity. A modification of Lang's Rain Factor Index.	$\frac{P}{T + 10}$
1926	A. Meyer	Absolute saturation deficit (mm of mercury) replaces evaporation.	$\frac{P}{D}$
1928	E. Reichel	Inserts the number of days with precipitation (N) in the formula of deMartonne.	$\frac{NP}{T + 10}$
1931	C.W. Thornthwaite	Precipitation effectiveness. Monthly precipitation to evaporation ratios determined, summed, and multiplied by 10 to eliminate fraction, (where n is an individual month, and T is the mean monthly temperature). For stations where evaporation data were not available, a formula using only precipitation and temperature data was provided. *(Note:* Formulae use English units.)	$\left\{ \sum_{n=1}^{12} \frac{P_n}{E_n} \right\} 10$
1932	V.B. Shostakovitch	t is the mean temperature during the growing period.	$\frac{P}{t10}$
1933	L. Emberger	An attempt to incorporate the effect of the seasonality of temperature on aridity. M is the mean maximum temperature of the warmest month and m is the minimum temperature of the coldest month.	$\frac{100P}{(M + m)(M - m)}$

Table A27 (Continued)

Year	Author	Remarks	Formula
1934	W. Gorozynski	Aridity coefficient. C is the cosecant of latitude, T_r is the difference between the means of the hottest and coldest months, and P_r is the difference between the greatest and least annual precipitation totals over 50 years. The coefficient increases with increasing aridity with its maximum value near 100. *(Note:* formula uses English units.)	CT_rP_r
1937	G.T. Selianinov	Effectiveness of precipitation in the growing season. Only mean monthly temperatures above 10°C are summed.	$\frac{P10}{\sum_{n=1}^{12} T_n}$
1941	N.N. Ivanova	Calculation of a precipitation "potential" evaporation ratio using the formula at right where t is the mean monthly temperature and a is the mean monthly relative humidity.	$\frac{P}{E}$ $E = 0.0018(25 + t)^2(100 - a)$
1942	E. de Martonne	Modification of earlier work incorporating a representation of the temperature (T_d) and precipitation of the driest month (P_d)′	$\frac{P}{T + 10} + \frac{(12P_d/(T_d + 10))}{2}$
1947	N.V. Bova	Inclusion of soil moisture conditions in a precipitation/temperature ratio. H is the initial moisture content of the soil.	$\frac{H + P}{\sum_{n=1}^{12} T_n}$
1948	C.W. Thornthwaite	Represents a water balance approach to aridity where I_h is the Humidity Index, s is the surplus moisture in the humid season, n is the water deficiency in the dry season, I_a is the Aridity Index, and I_m is the Moisture Index. Later modifications were made to this work.	$I_h = 100\,s/n$ $I_a = 100\,d/n$ $I_m = I_h - 0.6I_a$ $I_m = \frac{100s - 60d}{n}$
1948	V.P. Popov	Index of Aridity. Σ_g is the annual effective precipitation, $t - t'$ is the mean annual wet bulb depression, and r is a factor based on daylength.	$\frac{\Sigma_g}{2.4(t - t')r}$
1949	J.A. Prescott	Refinement of earlier formulae using precipitation and saturation deficit. *Note:* This method uses English units.	$\frac{P}{0.7D}$
1950	A.A. Skvortsov	E_a, actual evaporation, compared to E_{st}, "standard" evaporation measured from a water surface.	$\frac{E_a}{E_{st}}$
1951	R. Capot-Rey	P and T refer to the mean annual precipitation and evaporation while p and t refer to the precipitation and evaporation of the wettest month.	$\frac{100\,\frac{P}{e} + 12\,\frac{P}{e}}{2}$
1951	M.I. Budyko	Radiational Index of Dryness. R is the mean annual net radiation and L is the latent heat of vaporization for water. This is the first index using a radiation balance approach.	$\frac{R}{LP}$
1952	S.J. Kostin	Precipitation versus potential evapotranspiration for the same period.	$\frac{P}{PE}$
1953	P. Meigs	Use of Thornthwaite's Moisture Index to classify and map the dry lands of the Earth. No formula used.	

Table A27 (*Continued*)

Year	Author	Remarks	Formula
1955	H. Gaussen	Classification based on the duration and severity of dry months. A dry month is defined by the conditions at right. Other factors considered by Gaussen's definition of aridity include number of rainy days, humidity, mist, and dew.	$P \leq 2T$
1957	F.R. Bharucha and G.Y Shanbhag	A reuse of the *P/E* index using the formula at right. E is the mean 24-hour evaporation in inches, B is the mean wind velocity in miles per hour, h is the mean relative humidity in percent, and e is the mean vapor pressure in inches of mercury.	$E = (1.465 - 0.0186B)$ $(0.44 + 0.11BW)\dfrac{100}{h} - 1e$
1960	P. Meigs	Revision of 1953 maps. This work has become the most widely used identification of the world's arid regions.	
1962	V.M. MeherHomji	Index of Aridity–Humidity. S is the "precipitation quantity factor" and X is the length of the day period.	$S + X$
1965	C. Troll	Defined arid climates on the basis of number of months that the expression at right holds true.	$P > PE$
1967	C.C. Wallen	Interannual variability (V_I), where n is a particular year in a series of N years. The second equation is an empirical one that describes the arid margin of dryland farming.	$V_I = \dfrac{100\sum (P_n - 1 - P_n)}{\overline{P}(N - 1)}$
1967	J. Cocheme and P. Franquin	Matches water availability to a crop's growth cycle through a comparison of the values of precipitation and evapotranspiration *(ET)*. Can be used for any growing period.	P vs. ET $V_I = 0.07\overline{P} + 22$
1968	US Army	World Desert Classification. Based on rainy days per month with a rainy day defined as any day with greater than 0.1 inch of precipitation. Months are categorized in four categories by the categorization of the cumulative number of wet months in a year. Used with respect to men and military equipment.	
1969	H. Lettau	Approaches aridity from the standpoint of surface energy and moisture fluxes. B is the Bowen Ratio (cf. the ratio of sensible to latent heat fluxes) and C is the annual water surplus divided by the precipitation. The formula is equivalent to Budyko's Radiational Index of Dryness.	$(1 + B)(1 - C)$
1970	W.K. Sly	The ratio of growing-season precipitation to total amount of water required by the crop if lack of water is not to limit production. P is the growing season precipitation, SM is the start of the growing season, and IR is the calculated irrigation requirement during the growing season.	$\dfrac{P}{P + SM + IR}$

Table A27 (*Continued*)

Year	Author	Remarks	Formula
1971	G.H. Hargreaves	Moisture Available Index (MAI). For a specified period the ratio of the monthly rainfall total expected with a 75% probability to the estimated potential evapotranspiration. Values of 1.00 to 0.00 were considered increasingly moisture-deficient.	$\frac{P_p}{PE}$
1979	UNESCO	Map of the World Distribution of Arid Regions. Based on the ratio of precipitation to evapotranspiration with evapotranspiration being determined by Penman's method. This work was intended to replace Meigs's 1960 work.	$\frac{P}{ET}$
1980	R.P. Sarker and B.C. Biwas	Modification of MAI to consider weekly periods, various levels of rainfall total probabilities so that P_A is the assured rainfall of a period and PE is the potential evapotranspiration for the same period.	$\frac{P_A}{PE}$

Notes: Dates given are first appearance in the literature. All formulae are in metric units unless otherwise noted. Symbols have been modified from original sources for purposes of comparison.

His concepts have gained wide use because of the simplicity of their data requirements and their general agreement with world vegetation patterns. However, some engineers and agriculturalists have criticized his methods as too general for use in specific applications. The formulae have been found to produce unreliable results in certain tropical locales.

Budyko (1951) offered a new approach by considering the heat and water balance equations of the Earth's surface. His Radiational Index of Dryness was the ratio of the mean annual net radiation (i.e. the radiation balance) to the product of the mean annual precipitation times the latent heat of vaporization for water. The warm dry conditions synonymous with arid regions are well characterized by Budyko's index. In practical terms the Radiational Index of Dryness is the number of times the net radiative energy income at the surface can evaporate the mean annual precipitation. Although a number of writers have preferred Budyko's method of calculating aridity, a major limitation in application is the lack of long-term radiation records at many observation stations.

Other indexes have tended to be refinements and hybridizations of the above notions. Of recent interest has been the use of aridity indexes to define the agricultural boundary between arid and semiarid climates. UNESCO, FAO, and WMO are in accord that the boundary should be drawn where lack of water makes dryland farming impossible. Thus, aridity indexes are gaining increased importance in the planning of water supplies for crops.

Meigs's maps (1953, 1960) have been the most widely cited classification of aridity. Meigs used Thornthwaite's Moisture Index to define aridity. The 1 : 2 500 000 Map of the World Distribution of Arid Regions (UNESCO, 1979) has been produced to refine Meigs's maps. In this latter work approximately one-third of the world's continental surface is classified as having some degree of aridity.

Although UNESCO's 1979 map continued use of the ratio of precipitation to evapotranspiration, evapotranspiration was calculated by the more-favored Penman method. Calculation of aridity indices usually includes an input of evapotranspiration, The present international consensus is to estimate reference evapotranspiration using the Penman–Monteith formula (Allen et al., 1998). This formula is state-of-the-art but needs relatively esoteric atmospheric and soil input such as solar radiation and ground heat flux; if such data are not available locally, they can be estimated. An excellent explanation and commentary of operational drought-related aridity indices was compiled by Heim Jr. (2002).

Traditionally, climatologists and agriculturalists have used long-term weather data from standard weather shelters to create maps of aridity at Earth's surface. The difficulties of interpolating between observation points have created profound uncertainties in areas where data are sparse. For instance, there has never been a worldwide map of Thornthwaite's Moisture Index. The advent of satellites with continuous coverage of immense areas over a course of years has had a profound impact in the use of aridity indices. Recent advances in the archiving and collation of data have allowed worldwide *monitoring* of aridity as opposed to hindsight assessments.

The most commonly used satellite measure is the Normalized Difference Vegetation Index (NDVI). Derived from the Advanced Very High Resolution Radiometer (AVHRR) on the NOAA polar orbiter series, the NDVI at a location is closely related to the proportion of photosynthetically absorbed radiation that can be calculated from a ratio of reflectances in visible (0.58–0.68 μm) and near-infrared (0.725–1.1 μm). AVHRR channels:

$$(\mathrm{CH2} - \mathrm{CH1}) / (\mathrm{CH2} + \mathrm{CH1})$$

Channel 1 (CH1) is the reflectance in the visible and Channel 2 (CH2) is the reflectance in the reflective infrared. CH1 is sensitive to chlorophyll's absorption of incoming radiation, and CH2 is in a portion of the spectrum in which the mesophyll structure in leaves causes great reflectance (Tucker et al., 1991). As the NDVI values increase, this infers increasing amounts of biomass. Active biomass is largely controlled by climate, so NDVI is essentially an aridity index when time series of values are calculated over area. Multiyear data sets are needed so as to sort the phonological effects of green-up and senescence from atmospheric variability.

Near-real-time monitoring of aridity to assess drought is now possible. Surface and satellite measures of short-term drought/aridity can be combined to provide operational assessments. An example of this sort of work is given by Svoboda et al. (2002). By using a blend of the Palmer Drought Severity Index, CPC Soil Moisture Model Percentiles, USGS Daily Streamflow Percentiles, Percent of Normal Precipitation, the Standardized Precipitation Index, and the Satellite Vegetation Health Index, a weekly Drought Monitor index value is calculated for each US climate division. The results are mapped and widely distributed.

As latter-day aridity monitoring and research continues, the climatological prospects are exciting – "intellectual descendants" of the aridity indices of the early 1900s are providing useful decision support to policymakers. As time progresses and time-series of these products achieve climatological proportions, academic analyses should offer unprecedented dynamism to our concepts of aridity.

Stephen J. Stadler

Bibliography

Allen, R.G., Pereira, L.S., Raes, D., and Smith, D., 1998. Crop evapotranspiration – guidelines for computing crop water requirements. FAO irrigation and drainage paper no. 56. Rome: FAO.

Budyko, M.I., 1951. O. Klimaticheskikh Factorakh Stoka (On climatic factors and runoff). *Problemyfiz. Geog.*, **16**: 41–48.

Dzerdeevskii, B.L., 1958. On some climatological problems and microclimatological studies of arid and semiarid regions in the U.S.S.R. In *Climatology and Microclimatology: Proceedings of the Canberra Symposium*. Paris: UNESCO, Arid Zone Research, pp. 315–323.

Hare, F.K., 1977. Climate and desertification. In Secretariat of the United Nations Conference on Desertification, ed., *Desertification: Its Causes and Consequences*. Oxford: Pergamon Press, pp. 63–168.

Heim, R., Jr, 2002. A review of twentieth century drought indices used in the United States. *Bull. Amer. Met. Soc.*, **83**(8): 1149–1165.

International Crops Research Institute for the Semi-Arid Tropics, 1980. *Climatic Classification: A Consultants Meeting*. Patancheru, India: IRCISAT.

Köppen, W., 1918. Klassification der Klimate nach Tempertur, Niederschlag and Jahreslauf. *Petermanns Geog. Mitt.*, **64**: 193–203, 243–248.

Köppen, W., 1936. Das Geographische System der Klimate. In Köppen, C.W., and Geiger, R., eds., *Handbuch der Klimatologie*, vol. 3. Berlin: Gebrüder Bornträger.

Meigs, P., 1953. *World Distribution of Arid and Semiarid Homoclimates*. Arid Zone Programme, vol. 1. Paris: UNESCO, pp. 203–210.

Meigs, P., 1960. *Distribution of Arid Homoclimates: Eastern Hemisphere: Western Hemisphere*. United Nations Maps No. 392 and No. 393, Revision 1. Paris: UNESCO.

Svoboda, M., LeComte, D., Hayes, M. et al., 2002. The drought monitor. *Bull. Am. Met. Soc.*, **83**(8): 1181–1189.

Thornthwaite, C.W., 1931. The climates of North America. *Geog. Rev.*, **21**(3): 633–655.

Thornthwaite, C.W., 1948. An approach toward a rational classification of climate. *Geog. Rev.*, **38**(1): 55–94.

Tucker, C.J., Newcomb, W.W., Los, S.O., and Prince, S.D., 1991. Mean and inter-year variation of growing-season normalized difference vegetation index for the Sahel 1981–1989. *Int. J. Remote Sens.*, **12**: 1113–1115.

UNESCO, 1979. *Map of the World Distribution of Arid Regions*, MAB Technical Note 7. Paris: UNESCO.

Cross-references

Arid Climates
Desertification
Deserts
Drought
Water Budget Analysis

ART AND CLIMATE

"Art and Climate" is the title of an article published by Richard Wagner, the famous German musician, in 1841. Wagner explains in the introduction that his opinions on the future of Art had been criticized for failing to take into account the *influence of Climate upon man's capacity for Art.* Broadly this criticism suggested that northern Europeans had a poorer capacity for art than those who were blessed with the Ionic skies of the warmer climates of the Mediterranean. Wagner was not impressed with this criticism and set out to prove in the article that "Everywhere, in every climate, will these works of Art be inspired by native skies: they will be beautiful alike and perfect". However, many of Wagner's ideas have been controversial and considered almost racial and linked to what Livingstone (2002) has called moral climatology. Hence we have to be careful and state that the quality of art in a region is not in any way determined by climate. Climatic determinism will undoubtedly influence the content but not quality of art. Climate will therefore influence art but can art influence climate? Oscar Wilde, writing in 1889, certainly thought so:

> At present, people see fogs, not because there are fogs, but because poets and painters have taught them the mysterious loveliness of such effects. There may have been fogs for centuries in London. But . . . They did not exist till Art had invented them (Wilde 1889: 925)

The climate of a region can be considered to be a restraining influence on the weather – keeping it within a season's allowable array. No such simple definition can be offered for "art", a term derived from the Latin *ars* that, like the equivalent Greek word, also means science, skill, craft, ruse, etc. Here, art is defined as the manifest expression of the human experience in response to stimuli from the outer and inner world.

These expressions assume a multitude of forms, but only those that have significant relationships to climatic features as stimuli are considered here. Nevertheless, it should be mentioned that in architecture, e.g., the thickness of the walls of old houses in Europe is a function of the continentality of the region (Landsberg, 1958); or a bridge over the Oreto river at Palermo, Sicily, built in AD 1113, indicates that it originally spanned a much larger river, i.e. during a moister period in the Mediterranean area than prevails in our time (Lamb, 1968). Outdoor sculpture, an art related to architecture, can suffer from the ravages of wind, hydrometeors, and air pollution.

Another powerful medium for expressing human experience is the "international language" of music, vocal and instrumental, which is not limited to titles or texts that refer to climatic features, such as "Seasons" (Vivaldi, Haydn, Tchaikowsky, Glazunov), "Nuages" (clouds) by Debussy, or Brahms' "Regenlied" (rain song). There is also musical imitation of weather sounds such as wind, thunder, even rain and lightning as, for example, in the fourth movement of Beethoven's sixth symphony (Neuberger, 1961; Burhop, 1994).

A much wider range of atmospheric imagery is used in language, i.e. written or verbal prose or poetry, including drama and comedy (Aristophanes, 423 BC) and pictorial art using various media, but excluding sculpture.

Language

The spoken word

When communicating with one another, people express not only their opinion about the topic of conversation, but in their language also express other experiences in symbolic form for the purpose of emphasis or as circumscription of situations, happenings, or emotions. Considering our continuing exposure to atmospheric properties and phenomena, it is not surprising that much of our idiomatic speech involves meteorological imagery. Phrases such as thunderous applause, lightning speed, whirlwind courtship, know which way the wind blows, to be under a cloud, hazy recollection, foggy notion, snow-white, thunderstruck, etc., involve the appropriate properties of the pertinent meteorological phenomena. Similar idiomatic expressions are also used in French, German, Italian, Turkish, and many other languages (Neuberger, 1961).

The written word

As in spoken language, meteorological imagery abounds in the literature of Europe, the Middle East and the Far East. Starting with the Bible, through classical Greek and Roman literature, and from the Renaissance (Heninger, 1968; Janković, 2000) to the present time, with parallels in the Asian literature, we find weather imagery and weather and climatic descriptions. They are used in prose and poetry, in drama and comedy, thereby providing, literally and figuratively, an "atmosphere" for the actions and events described or as substitute expressions of human emotions. Bone (1976) examines clouds in the poetry of Wordsworth, Byron, Shelley and Keats. Three anthologies of poetry (one in German) revealed that 1152 out of 2563 poems (i.e. 45%) contained references to meteorological elements.

It appears that the extent to which weather images or descriptions are used in writing, is linked to the severity of weather and climate; thus, one finds many more references to weather in the British, Scandinavian, German, and especially Russian literature than in French and that of the Mediterranean countries in which milder climates prevail. Heninger (1968), in his extensive analysis of a large number of meteorological references in the literature of England, also cites descriptions of, and literary reactions to, air pollution in London and its environs, resulting from the domestic and industrial uses of coal. The employment of coal as fuel started in the thirteenth century, and due to the resultant smoke has led to a higher frequency, greater density, and longer duration of fogs. Early writers have also remarked on the deleterious effects of smoke on people, plants, and buildings (Brimblecombe and Ogden, 1977; Brimblecombe, 1988, 2000). Monet painted 95 images of the London smog (Thornes and Metherell, 2003).

Literature written before the establishment of observational networks in the nineteenth century can also give valuable clues to the climate and its variations over time in different regions. Chronicles written by the ancient Egyptians and Babylonians always included special meteorological and climatological events such as advances or retreats of glaciers, lake or river freezes, floods, storms, hail, heavy rains, etc. (Lamb, 1967, 1968, 1995; Watson, 1984; Durschmied, 2000). In the literature of ancient Greece, the epics of Homer, the writings of Herodotus, of Hippocrates (460–377 BC), who could be called the first bioclimatologist, and of others indicate that colder and wetter periods than now occurred over most of Europe throughout the first millennium BC (Frisinger, 1977).

Hundreds of references to climatological and meteorological phenomena can be found in the works of Shakespeare. For example, in Hamlet, Act I, Scene I, line 63 reads: "He smote the sledded Polacks on the ice"; this undoubtedly refers to the deep freezes of the waters east and south of Denmark, as well as large portions of the Baltic Sea in 1589–1590. This was part of a longer cold epoch that also featured significantly during the Thirty Years' War (1618–1648).

An interesting point was raised by Bonacina (1939) when he compared written descriptions with paintings. Words can depict as many details of an atmospheric event as can paintings, but a description can also report changes or sequences of such events. Pictorial representations reproduce only a moment in an event; however, some Medieval and Renaissance artists tried to overcome part of this limitation by putting non-simultaneous aspects of a story on the same canvas.

Pictorial arts

General remarks

Although this category of the arts includes etchings, drawings, cave paintings, and pictorial decorations of pottery (especially those of classical Greece), only murals and paintings in the most usual sense of the term will be considered here. This is not to say that the other media cannot, or do not, represent, or at least give clues to, climatic features; but such is relatively rare. In drawings there are no colors by which to judge the condition of the sky or, in prints and pottery, the color range is very limited. Nevertheless, there is among the Tassili Frescoes in the caves of southeastern Algeria the depiction of pelican heads (Lhote, 1961) and of a canoe, probably used for hippopotamus hunting, that indicates the existence of lakes in about 3500 BC on what is now part of the African Sahara (Lamb, 1977). Also some decorated ancient Greek pottery shows ships with billowing sails, implying wind.

Excluded from consideration here are the murals of the ancient Greeks and Romans; there are too few of them from which to draw significant conclusions with respect to climate. Yet, according to the late art historian, Dr H.W. Janson, (personal communication, 1968), there is an

> almost complete lack of any clouds in ancient Roman painting. There are plenty of landscape backgrounds, but the skies are almost invariably cloudless. Suddenly, from the 4th c. AD on, clouds begin to appear in large quantity . . . the change from no-clouds to clouds occurs in a few decades.

This art–historic fact seems to correlate with the increase of nocturnal cloudiness in the zone between 30°N and 50°N latitudes from AD 300 to 500 as calculated from the frequency of discovery of comets in Europe and elsewhere. As in Roman paintings, the classical Greek and Etruscan frescoes and later the Byzantine school of painting contain only an occasional sky background. In general, Western art during the Middle Ages showed a preference for gold backgrounds in lieu of skies. It is only in the transition period to the Renaissance, starting perhaps with the turn of the fourteenth century, that artists seemed to become more aware of the pictorial opportunities of their natural environment; the awareness of nature being the hallmark of the Renaissance spirit.

Paintings

A visit to any art gallery, excepting those that exhibit abstract art exclusively, clearly shows that in every century many artists have chronicled almost everything in their own environment: fauna and flora, architecture, furniture, foods, fashions, weapons, utensils, tools, toys and games, sports equipment, and musical instruments.

Considering the powerful influence of the atmospheric environment on all life forms, we can expect that artists also became chroniclers of the climates they experienced. The expression of climatic features in art can be achieved in two mutually nonexclusive ways: (1) directly in pictorial representation of clouds, frozen ponds, snowy landscapes, etc.; or (2) indirectly by images of people wearing heavy clothes, indicating low temperatures, or of a flowing scarf, billowing sails, waves on bodies of water, and the drift of smoke, all indicating wind. An example of the first category is "Storm over Taos" by John Marin (1872–1953). This painting shows a forcefully executed sky with a towering thundercloud on the left, a descending shower in the middle, and zig-zag lightning on the right (Figure A52). This watercolor also shows that modern painters have not abandoned the representation of nature. An example of the second category is "Lady at the Harpsichord" by Jan Miense Molenaer (1610–1668), painted between 1635 and 1640. The lady's attire is made of very heavy materials; it must have been quite cold, indeed. In order to avoid contact with the cold tile floor her feet are propped up on a footstool with a ceramic brazier, presumably containing hot coals (Figure A53). Another interesting feature is the landscape with clouds painted on the inside of the spinet cover by which the artist brings the outdoors into the room. Many other artists similarly have painted indoor scenes with windows or open doors through which a view of sky and clouds was admitted.

It appears that artists have used atmospheric imagery in several ways: as a decorative or incidental feature, as a primary subject, and/or as a symbolic support of or contrast to the emotional content of the human scene.

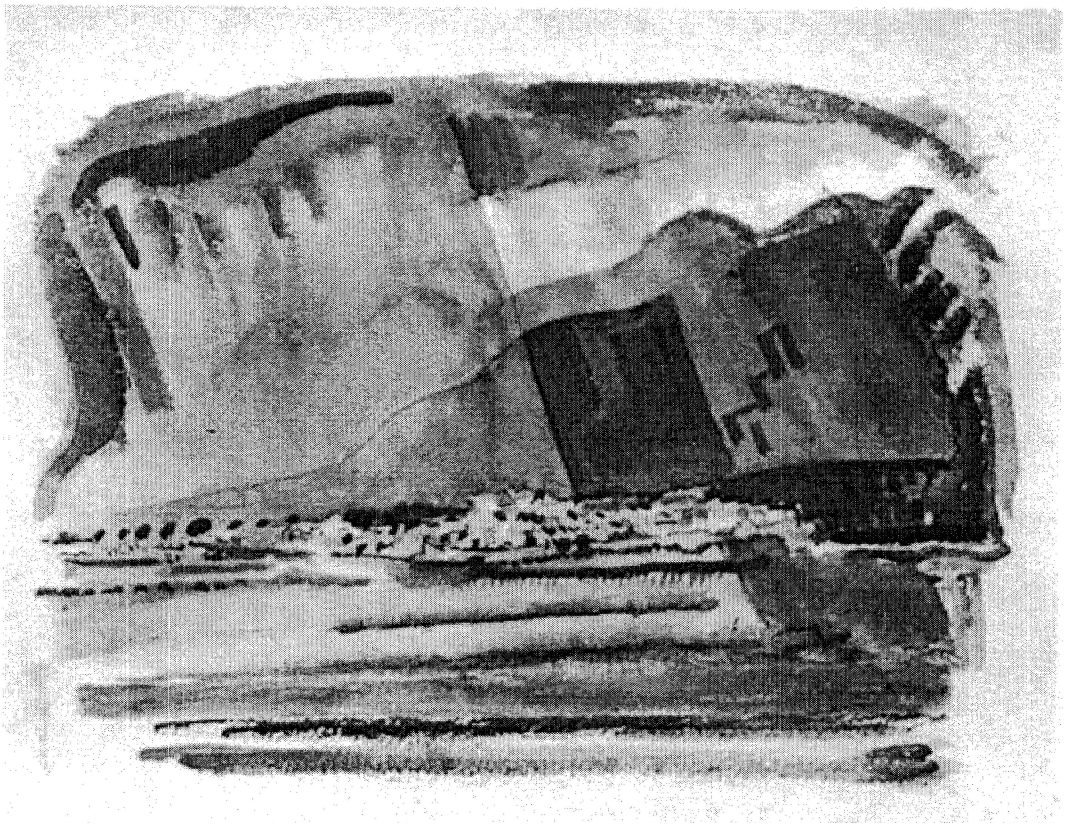

Figure A52 "Storm over Taos", by John Marin (courtesy of the National Gallery of Art).

Figure A53 ″Lady at the Harpsichord″, by Jan Miense Molenaer (courtesy of Fotocommissie Rijkmuseum Amsterdam).

An example of the first category is seen in Molenaer's painting mentioned above; the landscape inside the harpsichord cover is merely a decorative element. The painting by John Marin is representative of the second category, as the title indicates. The title of a painting, however, cannot be considered the main criterion for the subject category. For instance, "Breezing Up", by Winslow Homer (1836–1910), while showing a large amount of the canvas covered with an almost overcast sky and an agitated ocean, is basically a scene of human activity, namely, three boys and a man in a sailboat (Figure A54). For the purpose of this article, any painting in which the sky and/or other atmospheric phenomenon is the dominant feature can be considered a meteorological or climatological painting. The "Skating Scene", by the American painter John Tooe (1815–1860), belongs clearly to the second category, as the overcast sky, the snow-covered landscape, and the frozen creek dwarf the skating scene proper (Figure A55). "Madonna and Child", by Giovanni Bellini (*ca.* 1430–1516), shows a sunlit strip of landscape in the middle and a few bright cumuliform clouds on the upper left; but then above the Madonna's head spreads an ominous dark thundercloud, a symbolic reminder of the future tragedy (Figure A56). This type of example can be found in innumerable religious paintings (Neuberger, 1961).

Many authors have written about the artist's perception of his or her climatic environment (Lamb, 1967; Botley, 1970; Gedzelman, 1989; Neuberger, 1970; Spink, 1970; Thornes, 1979, 1999; Burroughs, 1981; Walsh, 1991). A great deal of thought was given, not only to the esthetic aspects of clouds in landscapes, but also to the sudden and substantial increase of snowy landscapes in the sixteenth century, which coincided with the emergence of the "Little Ice Age". The first attempt at

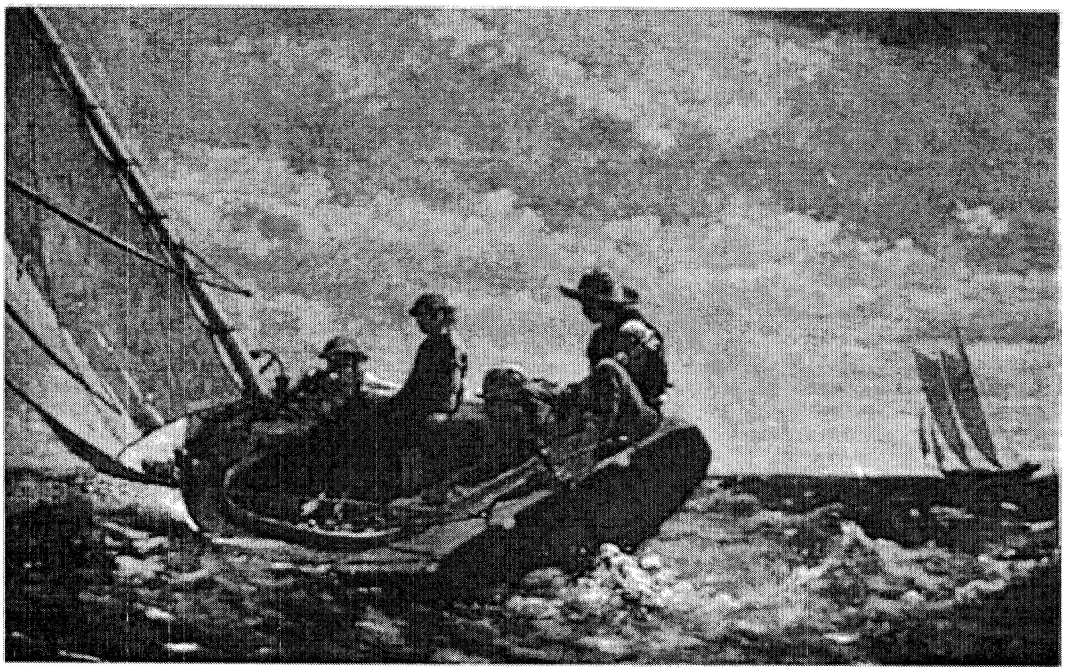

Figure A54 "Breezing Up", by Winslow Homer (courtesy of the National Gallery of Art).

Figure A55 "Skating Scene", by John Toole (courtesy of the National Gallery of Art).

extracting quantitative information of climatic changes from paintings with respect to cloudiness was made by Lamb (1967); he demonstrated such changes by analyzing the amount of sky cover in 200 paintings of Dutch and British artists. He used only summer scenes painted between 1550–1568, 1590–1700, 1730–1788, 1790–1840, and 1930–1939; with such a small and biased sample the statistical results become uncertain, although they are supported by other evidence. In order to test the hypotheses that the average climatic features derived from the paintings of many artists living in the same climatic epoch should be different for different climatic regions, and that such differences should exist for different climatic epochs, Neuberger, in 1967, evaluated 12 284 paintings in 41 art museums in 17 cities of nine countries.

Figure A56 "Madonna and Child", by Giovanni Bellini (courtesy of the National Gallery of Art).

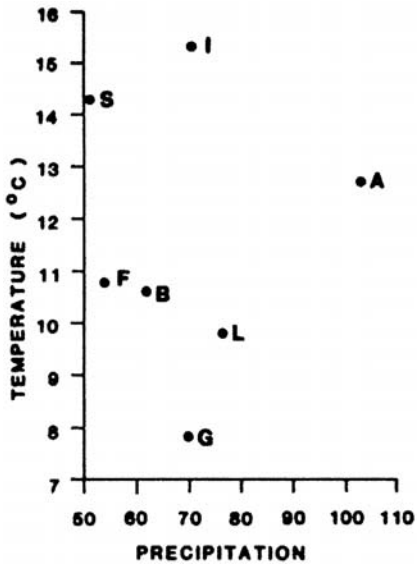

Figure A57 Mean regional annual temperatures and precipitation (in cm) for the period 1951–1960.

The regional climatic differences

For determining the location of the artists, the art–historic classification according to countries and schools was the only method available. This does not account for the travels of many artists or their move to different countries and climates. Vincent Van Gogh (1853–1890), though considered a Dutch painter, moved to England, Belgium, northern France, and finally southern France, where he produced a great many paintings during the last three years of his life. This fact, together with the differences in style and idiosyncrasies of individual artists living in the same region at the same time and in the same climate, will tend to diminish the average differences. Another "handicap" is the fact that the indoor climates of different art galleries, as well as the age of the paintings, may alter, to a lesser or greater degree, the colors of the skies represented. These and other factors that operate against the verification of the above hypothesis will result in minimizing the statistical differences (Neuberger, 1970).

The regions

Only the following regions (art schools) were involved in Neuberger's study. *American,* which is essentially the eastern seaboard from Richmond, Virginia, to Boston, Massachusetts, where 90% of the artists surveyed lived and worked. For this region the climate of New York City is considered representative, although the actual climate is different at both ends of the region. Finer detail of the climate did not seem to be warranted in view of the other factors mentioned above. *British,* with London representing the climate. *French,* with Paris representing the regional climate, although the same objection may be raised as in the case of New York City. *Low Countries,* combining Holland, represented by DeBilt, and Belgium, represented by Uccle: this combination is permitted in view of the great similarity of the climates as well as of the cultural aspects. *German,* including Austria, Switzerland and relatively few paintings from what is now the Czech Republic and Slovakia and adjacent countries – in other words, the central European region with Görlitz representing the regional climatic center. *Italian,* with Rome representing the climate. *Spanish,* represented by Madrid.

Figure A57 shows the regional differences of mean annual temperatures and precipitation for the seven regions, abbreviated with their initials, for the period 1951–1960. As will become evident in the evaluation of the paintings, the apparent similarity of the British and French climates is not always found in the paintings, largely because of the influence of the paintings by artists in southern France.

Climatic features in paintings

All paintings exhibited in each of the art galleries visited were evaluated with respect to the above-mentioned seven regions, the century and decade of the painting, the artist's name, the percent of canvas area covered by sky, the prevalent type and amount of clouds, the sky color (pale blue = 1; medium blue = 2; deep blue = 3), the visibility, i.e. the apparent transparency of the air painted in the picture (poor = 1; medium = 2; good = 3), and several other items. The qualitative values of sky color and visibility were subsequently converted into percentages by statistical means, so that the range from 0% to 100% would represent a very pale-blue to a

very deep-blue sky and a dense fog to a very clear atmosphere, respectively.

With respect to sky color and visibility, the possible effects of aging of the painting, its illumination in the museum, and of the technique used by the painter were anticipated at the start. Pointillists, like the French artists Seurat (1859–1891) and Signac (1863–1935), would produce more or less hazy-looking atmospheres in their paintings. However, since these and other influences would tend to negate the hypothesis, they were considered tolerable. It should be noted that, for the statistical evaluations, 325 works painted before the year 1400 were eliminated, chiefly because they had gold backgrounds or showed no sky or other climatic features; thus, the total number of paintings was reduced to 11 959. Although this seems to be a substantial statistical population, in reality it is only a minuscule sample of the total output by all the artists of Western culture, which must amount to hundreds of thousands of paintings. A hundred collections in the United States alone hold 43 143 works of American painters.

Regional differences in blueness of sky

In Table A28 the average blueness in percentages and the ratios of frequencies of deep-blue (*d*) to pale-blue skies (*p*) are presented for a total of 4411 paintings; the ratio *d/p* amplifies the regional differences by disregarding the medium-blue category. There is no significant difference between regions A, L, and F, but region B has by far the fewest deep-blue skies in its paintings. Central European paintings (region G) have 30 more deep-blue than pale-blue skies, and the Mediterranean regions S and I show a large predominance of deep-blue skies.

Regional differences in visibility

The average visibilities in percentages are given by regions for a total of 5601 paintings in Table A29. The results are similar to those in Table A28 in that there is little difference between the regions A, L, and F. The British region has the greatest opacity of the painted atmosphere, and central and southern European paintings show the highest transparency of the air. The statistical significance levels are 0.1% for all pairs of regions, except for A-L and F-S, and no significance for the difference between G and S.

Regional differences in painted clouds

Of each of the 5805 paintings with clouds, only the dominant cloud type was recorded according to the four commonly used categories: high, middle, low, and convective clouds. In Table A30 the relative frequencies of each of the four cloud families are shown. The highest frequency for each region is in boldface type. The average frequencies for all regions combined are 8% for high, 35% for middle, 25% for low, and 32% for convective clouds, showing the artists' preference for middle and convective clouds. A notable exception is seen in the artists of the British region who show a significant preference for low clouds.

The cloud amounts were estimated in the four categories: (1) clear (no clouds); (2) scattered (one-half or less of the sky area covered by clouds); (3) broken (more than one-half of the sky area covered by clouds); and (4) overcast (no blue sky visible). Table A31 gives the relative frequencies (percentages) of 6483 paintings in the four categories by region.

Table A28 Average blueness of painted skies by region

	Region						
	A	B	L	F	G	S	I
Blueness (%)	40	35	44	45	54	79	70
Ratio *d/p*	0.5	0.3	0.6	0.7	1.3	8.1	3.9

Table A29 Average visibility by region

	Region						
	A	B	L	F	G	S	I
Visibility (%)	37	33	38	36	40	42	54

Table A30 Average frequencies of cloud families by region

	Region						
	A	B	L	F	G	S	I
High clouds	5	5	5	9	11	6	9
Middle clouds	**43**	23	**32**	**36**	**33**	**38**	**43**
Low clouds	30	**40**	27	27	27	28	14
Convective clouds	22	32	36	28	29	28	34

Table A31 Relative frequencies of cloudiness categories by region

	Region						
	A	B	L	F	G	S	I
Clear	5	0	7	9	16	13	12
Scattered	16	4	11	10	16	13	24
Broken	**47**	**48**	**44**	**49**	**42**	**38**	**42**
Overcast	32	**48**	38	32	26	36	22

All regions show a maximum in the "broken" category, except that British painters avoided clear skies and showed as many overcast as broken skies. All regional differences are significant at the 1% or better level.

The average cloudiness for each region was statistically converted into percent cloudiness from the percent frequencies in Table A31. The results again show that the British painters have the greatest preference for very cloudy skies, whereas the Mediterranean painters prefer skies with considerably less cloudiness, as is evident from Table A32. The differences among the regions are significant at better than the 1% level.

Painted versus observed visibilities by region

Although Table A29 established regional differences in visibility painted, the question arises concerning the extent to which these visibilities correspond to the climatically prevailing visibilities. Actual observations at the stations shown in Figure A57 are available only since 1850, so that, for comparison, only the painted data for the period 1850–1967 are usable. Because the

painted visibilities were estimated in only three categories, the observed visibilities, which were recorded in different codes at the various stations, were also converted into three classes: 1 = visibilities less than 2.5 miles; 2 = those between 2.5 miles and 11 miles; 3 = those larger than 11 miles. Both sets of data were then expressed in percentages. Only 1677 paintings were available for the seven regions in the period 1850–1967. Table A33 shows that the observed data have a larger range and greater differences between regions. Both sets show minimum visibility for the Low Countries and maximum visibility for the Mediterranean regions. Nevertheless, considering the relatively small statistical sample and the coarseness of the estimates of painted transparency of the air, the fact that British painters paint a more transparent air than do the American and Low Countries artists seems to be supported by actual observations.

Painted versus observed cloudiness by region

For the comparison of painted with actually observed cloudiness, 1848 paintings were available for the period from 1850 to 1967. Figure A58 shows the observed versus the painted average cloudiness for each region. Although the artists exaggerate cloudiness, with the exception of the Italian painters, there is an excellent linear relationship between painted (P) and observed (O) averages with a correlation coefficient of 0.95 ± 0.03 and a regression equation $O_c = 0.5P + 26$ (O_c and P in percents). When we use the equation to compute O_c, we obtain the values in Table A34 in which the actually observed cloudiness averages (O) and the differences $O_c - O$ are given. These differences are well within the accuracy of the observations.

In summary, the quality of the relationships between the actually observed and the painted regional averages of visibility and cloudiness in the period from 1850 to 1967 permits the conclusion that the collective experience of climatic features by artists in a given region finds its expression in paintings that correspond well to the actually observed average values.

Table A32 Average percent cloudiness by region

	Region						
	A	B	L	F	G	S	I
Cloudiness	72	85	75	72	63	69	62

Table A33 Observed and painted visibilities in percent by region for the period 1850–1967

	Region						
	A	B	L	F	G	S	I
Observed	47	53	42	58	54	93	90
Painted	38	42	36	38	38	63	78

Table A34 Cloudiness (O_c) computed from the linear relationship between painted and actually observed (O) values

	Region						
	A	B	L	F	G	S	I
O_c (%)	60	68	65	62	61	51	44
O (%)	56	68	66	62	62	48	47
$O_c - O$	4	0	−1	0	−1	3	−3

Climatic changes in paintings

The last major ice age ended about 12 000 years ago. However, the warming trend during the postglacial period was not a steady, continuous process but had intermittant relapses into colder periods. The so-called Little Ice Age was the latest and probably the best-documented excursion of climate that affected the entire northern hemisphere (Lamb, 1967). There is disagreement as to when it started. It seems to have emerged slowly with the beginning of the sixteenth century, although there were some precursors of it in the preceding century. The end can be dated more easily, as a warming trend set in by 1850. In general, the Little Ice Age was an epoch of frequent wet and cold years. Southward displacement of storm tracks brought snow and ice into the Mediterranean regions and rapid advances of Alpine glaciers and other climatic disasters occurred all over Europe (Neuberger, 1970).

Lamb (1967) has found from his brief survey of Dutch and British paintings that cloudiness increased from around the middle of the sixteenth century. With the large volume of data used here in Tables A28, A29, A30, and A32, averages combining the data of all regions were calculated for three epochs: the preculmination period of the Little Ice Age from 1400 to 1549; the culmination period of the Little Ice Age from 1550 to 1849; and the postculmination period from 1850 to 1967. In Figure A59 these averages show that there was a substantial paling of the blue color of painted skies toward the culmination period, but no recovery afterwards. The same trend is true for visibility. The failure of sky blueness and visibility to improve in the last epoch is in part due to the effects of the techniques of impressionism, which created a hazy atmosphere by the uncertain contours resulting from short brush strokes. This method reached its extreme in pointillism. On the other hand, this trend should have been counteracted by expressionism with its bold colors and sharp contours. It seems reasonable to assume that in the postculmination period the progressive industrialization, with its attendant air pollution, diminished both the blueness of the sky and the transparency of the air. The combined frequencies of low and convective clouds, both of which may lead to

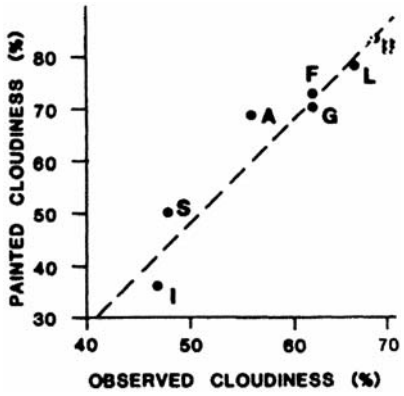

Figure A58 Relationship between the average regional cloudiness as observed and painted for the period 1850–1968.

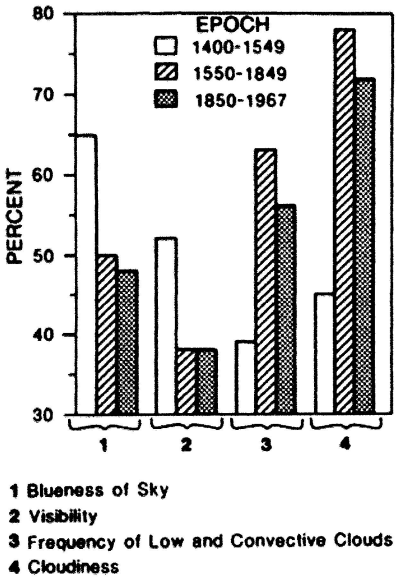

Figure A59 Averages for all regions of climatic features painted in the preculmination period, the culmination period, and the postculmination period of the Little Ice Age.

precipitation, show a strong increase from the first to the second epoch and a reduction in the third epoch. Similarly, the cloudiness has a large rise and a subsequent small decline, the latter probably being caused, at least to some extent, by human activities.

In conclusion, the collective climatic experience of artists in a given region at a given time is reflected in their paintings, notwithstanding the individual artist's techniques and intentions, or awareness of his or her surrounding climate. Subsequent physical and chemical effects of the climate on paintings are also reflected by the intensity and hue of the paint on the canvas. The importance of climate in the appreciation of landscape painting is now established and features in several recent art exihibitions such as "Impressionists in Winter" (Moffett, 1998); "Constable's Clouds" (Morris, 2000); "Holland Frozen in Time" (van Suchtelen, 2001).

Hans Neuberger and John E. Thornes

Bibliography

Aristophanes, 423 BC. *The Clouds*, ed. K. J. Dover. (Oxford: Clarendon Press, 1968).

Bonacina, L.C.W., 1939. Landscape meteorology and its reflection in art and literature, *Quarterly Journal of the Royal Meteorological Society*, **65**: 485–497.

Bone, J.D., 1976. Clouds in the poetry of four romantics. *Catalogue of the Cloud Watchers Exhibition*, Coventry City Art Gallery, Coventry, UK.

Botley, C.M., 1970. Climate in art. *Weather*, **25**: 289.

Brimblecombe, P., 1988. *The Big Smoke, A History of Air Pollution in London since Medieval Times*. London and New York: Methuen.

Brimblecombe, P., 2000. Aerosols and air pollution in art. *Proceedings of the Symposium on the History of Aerosol Science*, Vienna.

Brimblecombe, P., and Ogden, C., 1977. Air pollution in art and literature. *Weather*, **32**: 285–291.

Burhop, N.G., 1994. The Representation of Weather in Music. Unpublished MSc thesis, School of Geography, Earth and Environmental Sciences, University of Birmingham, UK.

Burroughs, W.J., 1981. Winter landscapes and climatic change. *Weather*, **36**: 352–357.

Durschmied, E., 2000. *The Weather Factor: How Nature has Changed History*. London: Coronet Books.

Frisinger, H.H., 1977. *The History of Meteorology to 1800*. History Monograph Series. New York: American Meteorological Society, Science History Publications.

Gedzelman, S.D., 1989. Cloud classification before Luke Howard. *Bulletin of the American Meteorological Society*, **70**: 381–395.

Heninger, S.K., 1968. *A Handbook of Renaissance Meteorology*. New York: Greenwood Press.

Janković, V., 2000. *Reading the Skies: a cultural history of English weather 1650-1820*. Manchester: Manchester University Press.

Lamb, H.H., 1967. Britain's changing climate. *Geography Journal*, **133**: 445–466.

Lamb, H.H., 1968. The climatic background to the birth of civilization. *Advances in Science*, **25**: 103–120.

Lamb, H.H., 1977. *Climate: Present, Past and Future*, vol. 2. New York: Barnes & Noble.

Lamb, H.H., 1995, *Climate, History and the Modern World*. London: Methuen.

Landsberg, H., 1958. *Physical Climatology*. DuBois, PA: Gray Printing.

Lhote, H., 1961. Rock art of the Maghreb and Sahara. In Bandi, H.G., et al. eds., *The Art of the Stone Age*. New York: Crown, pp. 99–152.

Livingstone, D.N., 2002. Race, space and moral climatology: notes towards a genealogy. *Journal of Historical Geography*, **28**: 159–180.

Moffet, C.S., 1998. *Impressionists in Winter*. Washington, DC: Philip Wilson.

Morris, E., 2000. *Constable's Clouds*. Edinburgh: National Gallery of Scotland.

Neuberger, H., 1961. Meteorological imagery in language–music–and art. *Mineral Ind.* **29**: 1–8.

Neuberger, H., 1970. Climate in art. *Weather*, **25**: 46–56, 61.

Spink, P.C., 1970. Climate in art. *Weather*, **25**: 289.

Suchtelen van, A., 2001. *Holland Frozen in Time*. Zwolle, Holland: Waanders.

Thornes, J.E., 1979. Landscape and clouds. *Geography Magazine*, **51**: 492–499.

Thornes, J.E., 1999. *John Constable's Skies*. Birmingham: University of Birmingham Press.

Thornes, J.E., and Metherell, G., 2003. Monet's "London Series" and the cultural climate of London at the turn of the twentieth century. In Strauss, S., and Orlove, B.S., eds., *Climate, Weather and Culture*. Oxford: Berg.

Wagner, R., 1841, *Kunst und Klima* (Art and Climate). *Samtliche Schriften und Dichtungen*, **3**: 207–221.

Walsh, J., 1991. Skies and reality in Dutch Landscape. In Freeberg, D., and de Fries, J., eds., *Art in History, History in Art*, ed by Chicago: University of Chicago Press.

Watson, L., 1984. *Heaven's Breath: a natural history of the wind*. London: Coronet Books.

Wilde, O., 1889. *The Decay of Lying*. In *The works of Oscar Wilde*, 1987 edition, Leicester: Galley Press.

Cross-references

Cultural Climatology
Literature and Climate

ASIA, CLIMATES OF SIBERIA, CENTRAL AND EAST ASIA

Central Asian, Siberian, and East Asian mega climatic regions, located on the world's largest and most physically diverse continent, are experiencing a period of marked climatic change. The impact of climatic change is affecting the lives of nearly

two billion people. With more climatic types than any other continent, and with one-third of the world's land mass, any perturbation of Asian weather and climate is biophysically and socioeconomically important. Containing the highest point above sea level and the coldest inhabited place on earth, Asia's location and geomorphology contribute much to climatic diversity. Major variations of climatic types are defined by receipt of solar energy, moisture from the Atlantic Ocean in the west and the Pacific Ocean in the east, and the powerful Siberian Winter High Pressure Cell. A decrease in temperature occurs from south to north, with an increase in continentality from west to east. Latitudinal variations of climate are significant.

Asian climates

Using the Köppen climatic classification, north and east Asia may be divided into three major climatic realms: Siberia or Northeast Asia in the north (Dfb, Dfc, Dwa, Dwb, Dwc, Dwd, and ET); Central Asia or Desert Asia in the west and center (BS and BW); and East Asia or Monsoon Impacted Southeast Asia (Cfa and Cw). Siberia or Northeast Asia is the largest. A complex set of interactive climatic controls and many multifaceted physiographic features influence local climates and give distinctive regional climatic character to places (Figure A60). One of the most impacting and heat-determining factors is the length of day and night at different latitudes, particularly in Siberia and Central Asia (Table A35).

Siberia extends from the Ural Mountains in the west to the Pacific Ocean in the east. It is bounded on the north by the cold Arctic Ocean and on the south by Central Asia and South Asia. The climate of Siberia is one of the most continental on Earth, with great seasonal changes. The average frost-free period is only 75–82 days. Average annual precipitation ranges from 250 mm to over 2000 mm. During the winter Siberia is divided into two climatic parts: the northwest, dominated by frequent storms, high winds, and snow; and the southeast, dominated by clear skies and calm weather. A major part of Siberia is underlain by continuous permafrost, up to 1600 meters deep and extremely cold (−12°C). These factors impact temperature efficiency and moisture effectiveness in this region. The seasonal snow-melt layer is dynamical in space and time, impacts heat energetic conditions, and serves as diagnostic criteria for estimating global change or climate. Since the late 1960s a decrease in snow cover, a reduction in annual duration of lake and river ice cover, a temperature decrease, and significant changes in precipitation, cloud cover, temperature ranges, and drought frequency have occurred (Dando et al., 2003).

Along with a change in Siberia's climate, and an increase in urban conglomeration, urban climates have impacted all biophysical processes. Increased atmospheric humidity, increased absolute humidity, and extensive use of firewood and low-quality coal for heating and for power have induced a phenomenon that is detrimental to all cultural and physical activities – urban fog (Table A36).

East Asia, recording atypical weather perturbations, including persistent drought in normally moist areas and devastating floods in normally dry regions, is experiencing an unusually strong manifestation of global warming. Changes in high-pressure cell positions and characteristics, shifts in low-pressure cell locations and intensities, and a variation of jet stream seasonal paths have modified weather patterns. Warming of the atmosphere has increased evaporation, increased specific humidity, intensified drought, increased the amount of moisture in air masses, and increased the amount of moisture and energy in the air for rainstorms, snowstorms, typhoons, and tornadoes. Concomitantly, extreme cold temperatures in early winter, followed by anonymously warm temperatures in late winter, have disrupted natural processes in eastern Mongolia and northeastern China. Changes in precipitation regimes in spring, summer, and autumn in China and Japan have enhanced the potential for flooding. A combination of human activities that modify climatic elements and controls and natural causes of climatic change could lead to large-scale weather-related disasters and to a redefinition of the traditional boundaries of East Asia's climatic regions (Figure A61).

Table A35 Maximum lengths of day and night at different latitudes (excluding twilight)

North latitude	Daylight (in days)	Darkness (in days)
90°	189	176
85°	163	150
80°	137	123
75°	107	93
70°	70	55
67°38'	54	under 24 hours
60°	18 hours 27 minutes	18 hours 27 minutes
50°	16 hours 18 minutes	16 hours 18 minutes

Source: Kriuchkov, 1973 and Lounsbury, 1973.

Table A36 Number of days with urban fog in selected Siberian cities

1.	Anadyr	33	Evenly distributed annually
2.	Bratsk	97	Fall and winter primarily
3.	Irkutsk	102	Primarily in winter
4.	Novosibirsk	31	Primarily in late fall
5.	Petropavlovsk-Kamchatskii	48	Primarily in summer
6.	Salekhard	48	Primarily in winter
7.	Surgut	47	Primarily in winter
8.	Verkhoiansk	56	Primarily in winter
9.	Yakutsk	62	Primarily in winter

Source: Field work, interviews, archival research, and Kriuchkov, 1973.

Climatic changes

In the 1999–2002 period a severe drought persisted across a large part of Central Asia, portions of south and southwest Asia, including Afghanistan, Iraq, Iran, Saudi Arabia, Syria, Israel, Turkmenistan, Uzbekistan, Kazakhstan, Tajikistan, Pakistan, and parts of India (Lawton, 2002). At the time it was the largest contiguous region of severe drought in the world. The International Research Institute for Climatic Prediction considered this widespread drought a "grave humanitarian crisis". Scientists from the Ohio State University analyzing ice cores from glaciers in Central Asia noted a warming in this region over the past 50 years. At one site the recent warming and drying trend exceeded anything observed in the past 12 000 years. Current global warming has exceeded the normal range of climatic variations during the last 5000 years (Jones, 2001). Warming trends in Central and Desert Asia are not just natural fluctuations that will reverse quickly. Concomitant with the Pacific (SO) and North Atlantic Oscillations (NAS), humans have contributed to climatic changes in Central Asia. Drying of the Aral Sea is one of the best-known environmental disasters

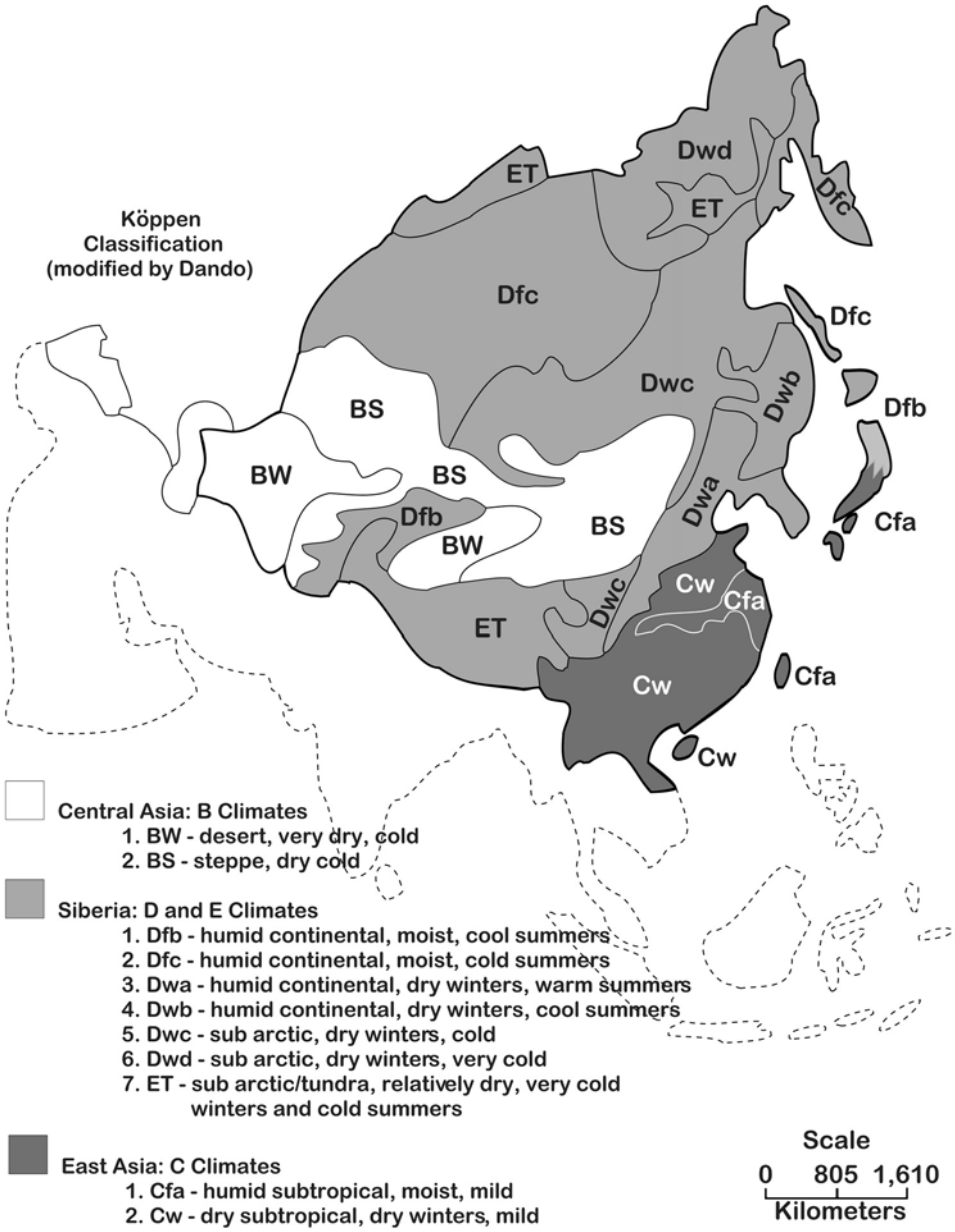

Figure A60 Asian climates (2003). Anna R. Carson 2003.

caused by humans in the past three or four decades. There is widespread agreement in the scientific community that, with the reduction in Aral Sea level, the regional climate has changed for the worst and become more extreme.

Climatic elements

The unequal distribution of solar radiation over Asia is the primary factor in Asia's multifaceted weather and climate. In Asia's tropical belt the sun remains high with little seasonal variation, and this accounts for continuous warm to hot year-round temperatures. In Asia's mid-latitudes, solar radiation receipts exhibit a strong seasonal maximum and a strong seasonal minimum which are reflected in greater seasonal variations in temperature than the tropical belt. And in Asia's high latitudes there is a period of limited to no solar radiation received at the surface of the Earth, resulting in a season with extremely low temperatures in the winter or low sun period (Figures A62 and A63). Total solar radiation received at the Earth's land – sea surface during the entire year in kcal/cm^2 per year ranges from 140 to 180 in Asia's tropical belt, 160 to 120 in Asia's mid-latitudes, and 100 to 60 in Asia's high latitudes. Maximum solar radiation received at the Earth's surface occurs in the steppe and desert regions of west-central Asia. Transformation of available solar

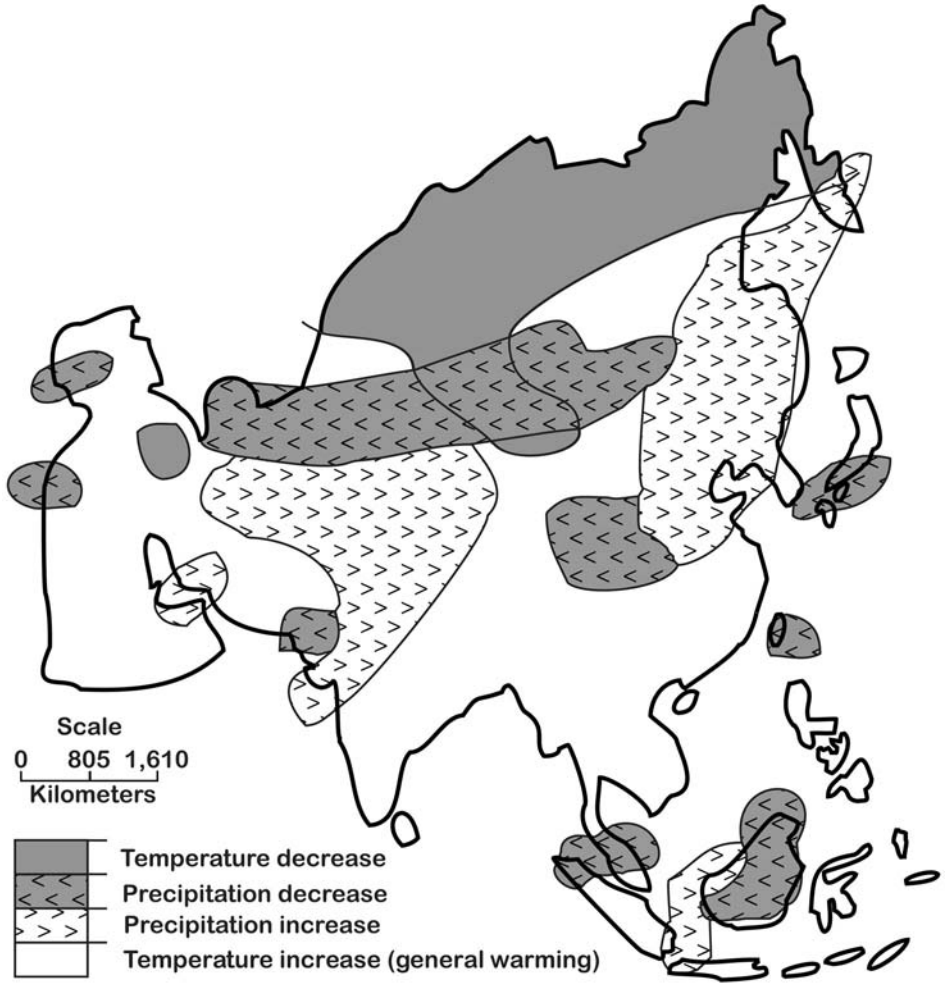

Figure A61 Trends in temperature and precipitation change: 1901–1998. Anna R. Carson 2003.

radiation is an essential ingredient of the process that produces Asia's climate – particularly temperature ranges (Borisov, 1965).

Temperature

Northern Asia, specifically Siberia, is climatically isolated from moist tropical air masses and records the greatest mean annual temperature range on earth (Table A37). At Verkhoyansk, in the valley of the Yana River, January temperatures average −49°C, July temperatures average +15°C, and the absolute temperature range is 103°C. Oymyakon, located in the same physiogeographic region, records an absolute temperature range of 104°C. Siberian winter low temperatures are proverbial, and for most of Siberia the January mean annual temperature is less than −25°C. In contrast, much of southwestern Asia is subject to moderate heat (Arakawa, 1969).

The temperatures of eastern China resemble those of the eastern United States. Winter cP and cA air masses from Siberia are more powerful and colder than those that move south from Canada. Summer mT air masses from the South

Table A37 Average annual temperatures at selected Siberian stations (in °C)

Station	Latitude (N)	Longitude (E)	Average annual Temperature
Salekhard	66°31′	66°35′	−6.6
Surgut	61°17′	72°30′	−4.0
Tiumen'	57°10′	65°32′	+1.0
Novosibirsk	54°58′	82°56′	−0.4
Igarka	67°27′	86°35′	−8.5
Eniseisk	58°27′	92°10′	−1.9
Bratsk	56°04′	101°50′	−2.7
Irkutsk	52°16′	104°19′	−1.1
Verkhoiansk	67°33′	133°25′	−16.0
Takutsk	62°01′	129°43′	−10.3
Baunak	54°43′	128°52′	−5.0
Nerchinsk	52°02′	116°31′	−3.8
Anadyr Petropavlovsk	64°27′	177°34′	−8.1
Kamchatskii	52°33′	158°43′	+0.6
Sovetskaia Gavan'	48°58′	140°17′	−0.5

Source: Nuttonson, 1950, appendices.

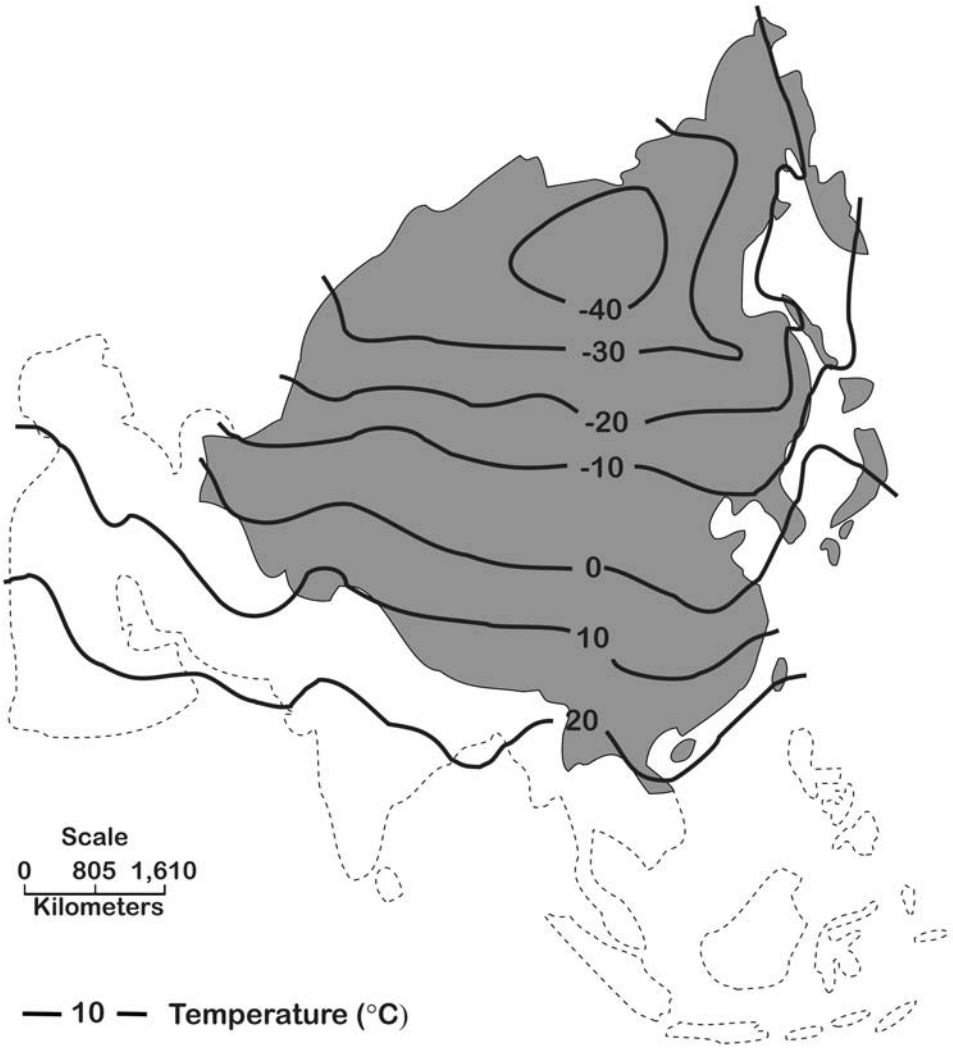

Figure A62 Average temperature: January. *Source: Geograficheski Atlas,* 1959, Moskva, p. 14; *Preroda i Resoursi Zemli,* 1999, Moskva and Vienna, p. 52. Anna R. Carson 2003.

China Sea are stronger than mT air masses from the Gulf of Mexico. China extends farther north to south than the United States and has a wider range of climates and temperature regimes. China extends from 18° to 53° north latitude. This is the equivalent distance from Puerto Rico to Labrador. Concomitantly, no simple summary can give adequate insights into Japan's temperature regimes. The Japanese islands extend for 1400 kilometers or more and are surrounded by temperature-modifying ocean and seas. Irregularities in island topography induce sharp vertical temperature contrasts. The winter monsoon typically brings cold air masses and low temperatures from Siberia, while the summer monsoon brings warm, moist maritime air masses and warm, mild temperatures to Japan. The normal January temperature gradient is slightly more than 2°C per degree of latitude; the normal July temperature gradient is less than 1/2°C per degree of latitude.

Asia's spatial temperature differences and ranges are greatest in winter, least in summer, and more extreme in all seasons within the land-locked core, rather than the south and eastern maritime periphery (Figures A62 and A63). Winter isotherms reflect the influence of ameliorating ocean currents, mountain barriers, altitude above sea level, high-pressure cells, and solar radiation. Summer isotherms reflect solar radiation and latitude, along with altitude (Global Change, A and B, 1999).

Precipitation

Precipitation receipts, in general, increase from north to south and from the southwest to the southeast. Throughout most of Siberia the annual average precipitation is scarcely 250 mm and in parts of Central Asia, the Tarim Basin, and the Gobi Desert, less than 100 mm. In east China there are regions that receive

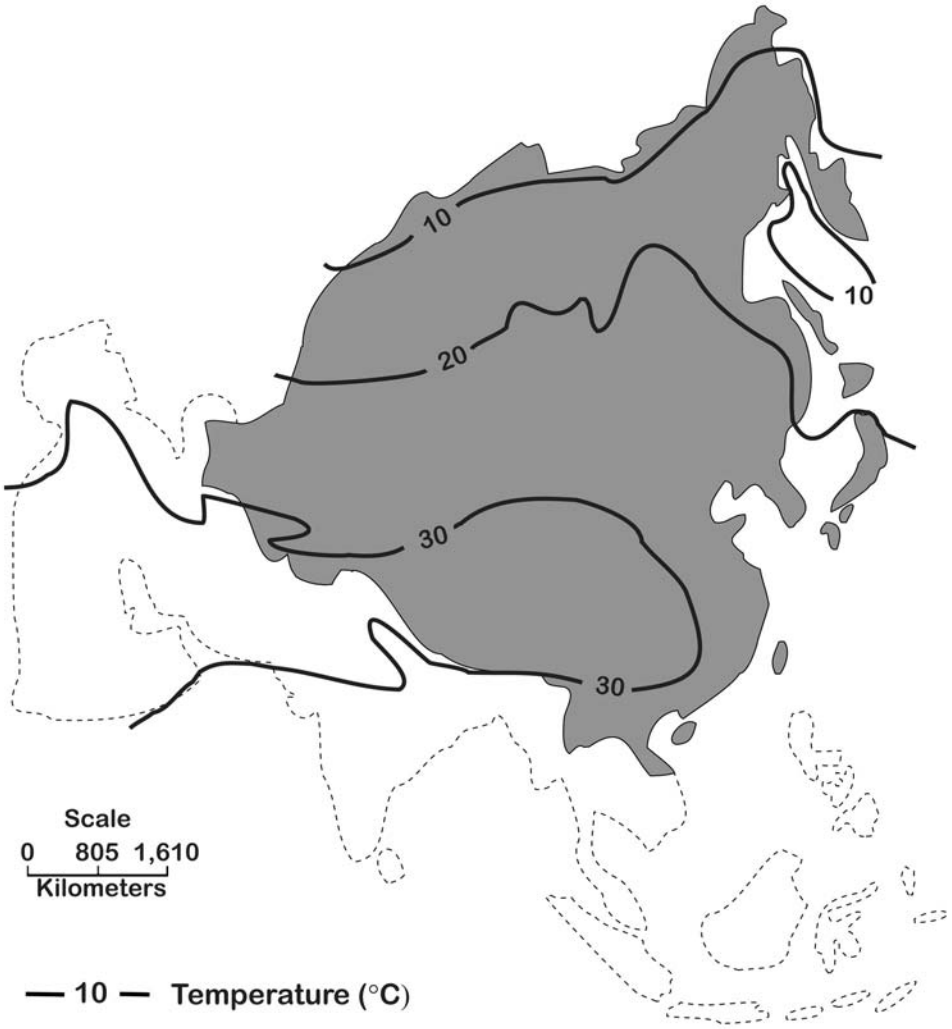

Figure A63 Average temperature: July. *Source: Geograficheski Atlas,* 1959, Moskva, p. 14; *Preroda i Resoursi Zemli,* 1999, Moskva and Vienna, p. 52. Anna R. Carson 2003.

more than 2000 mm per year (Figure A64). A small part of China, north of Nepal, receives over 3000 mm annually. Seasonal distribution of precipitation becomes of greatest importance, for the summer heat and continental character of Asia affect precipitation effectiveness and thermal efficiency. In insular and island-studded southeast and east Asia, where there is limited or no frost, rainfall is relatively evenly distributed throughout the year (Cfa and Dfb). Interior and rainshadow locations in south and east Asia experience a distinct dry season in the low-sun period or winter (CW, Dwa, and Dwb). Mediterranean Sea-influenced west Asia and the dry eastern coastal region of the Caspian Sea receive most of their precipitation in winter, at least three times as much precipitation in the wettest winter month as the driest month of summer (Cs). Precipitation in the dry realms of southwest Asia, Central Asia, Tarim Basin, and the Gobi Desert is minimal and erratic, but most of the precipitation is secured in summer from violent convective showers (BW) or a combination of violent convective showers and frontal activity (BS). And in the subarctic and arctic areas of Siberia (Dwc, Dwd, and ET), summer is the season of maximum temperatures, highest specific humidity, deepest penetration of maritime air masses under the influence of the summer monsoon, and is the period of maximum precipitation (Figures A62 and A63). Asia's central dry realm separates Asia's eastern warm-to-hot wet belt from Asia's north and northeastern cool-to-cold limited precipitation belt (Griffiths and Driscoll, 1982).

Barnaul – an example of a precipitation regime impacted by continentality

Barnaul is located in Siberia, west of the Ural Mountains, in the extreme eastern portion of the zone of the Russian forest steppe. Barnaul's maximum monthly precipitation falls in July that is also the warmest month of the year. Precipitation is

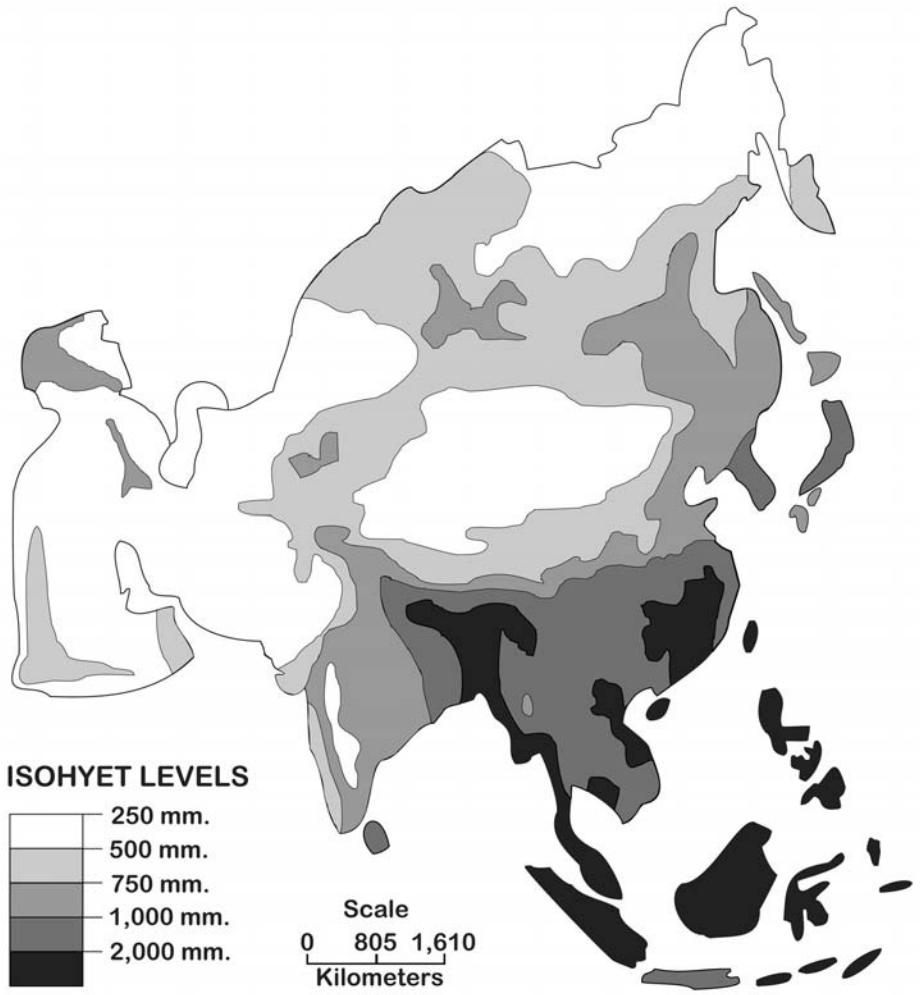

Figure A64 Asian precipitation. *Source: Geograficheski Atlas,* 1959, Moskva, p. 16; *Preroda i Resoursi Zemli,* 1999, Moskva and Vienna, p. 56; *Oxford Economic Atlas of the World,* 4th edn, 1972, p. 2. Anna R. Carson 2003.

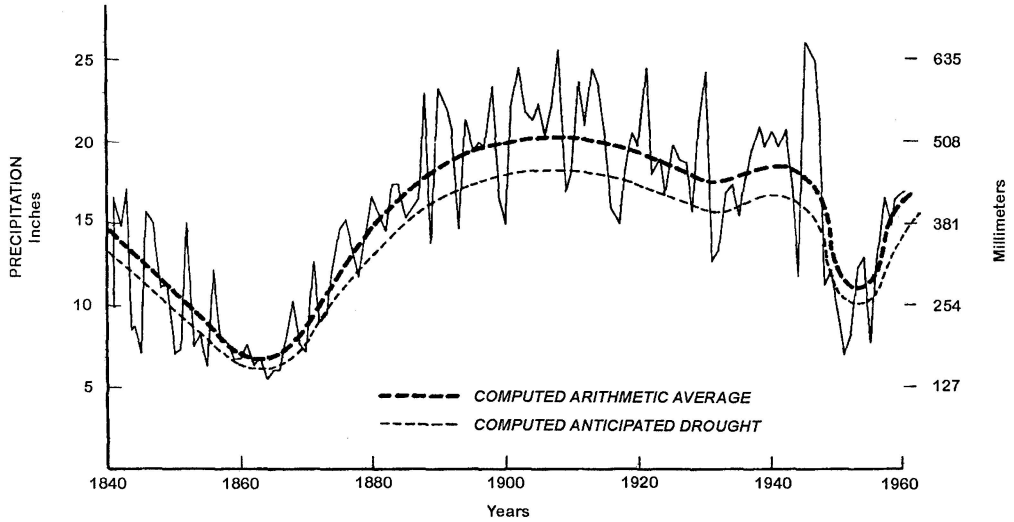

Figure A65 Barnaul – variation in precipitation, 1840–1960. *Source:* A.M. Shulyin, *Izv. AN USSR, serila geogr.*, 1963, no. 2, p. 168. Anna R. Carson 2003.

marginal for agriculture and for supplying moisture for economic development. Droughts are common, occurring once every 4 years on the average (Figure A65). A review of the climatic records for Barnaul from 1890 to 1966 shows that droughts were recorded in 1900–1902, 1904–1905, 1909–1910, 1917, 1920, 1923, 1927, 1929, 1931–1932, 1934, 1939, 1945, 1951–1952, 1955, and 1962–1963 (Figure A65). Analysis of precipitation data for Barnaul reveals a tendency toward the repetition of very moist years when all four seasons are wet or three seasons very wet and then a dry or very dry year or two followed by an average year or two.

Sukhovei – an Asian atmospheric enigma

Hot desiccating winds at times become associated with droughts, but these hot, dry winds or *sukhovei* can occur when there is no drought and can cause death to plants even when there are adequate reserves of moisture within the soil.

Sukhovei are hot, dry masses of air that envelop plants, increase evapotranspiration rates by factors of 2–3 to 20 times, and injure or destroy crops. Air in a *sukhovey* is so devoid of moisture that, in general, the relative humidity is less than 30% and, in many cases, less than 20% for an extended period of time. In a drought there are day and night variations in relative humidity, and at night dew may even form. In a *sukhovey* the relative humidity varies very little during the entire day/night period, and evaporation takes place continuously. The majority of cultivated plants cannot endure desiccation of their tissues; therefore the moisture lost to the atmosphere must be replaced by an inflow of moisture from the roots. Plants, unable to compensate for losses as a result of increased evaporation, lose turgescence, wilt, and die.

Sukhovei winds may reach speeds in excess of 70 miles per hour, but the usual velocity is from 7 to 11 miles per hour. Plant transpiration is increased by the most moderate wind speeds via the removal of water vapor from the apertures of the stomatal apparatus. Even wind with a velocity of 4–5 miles per hour increases plant transpiration threefold. When *sukhovei* winds achieve great speed they often turn into dust storms or so-called "black storms", which remove vast amounts of unconsolidated material and even small plants over great distances. As much as 5 inches of soil have been removed from various steppe regions in one year by dust storms. *Sukhovei* winds may last for an hour or two, or they may last for several days, but the end result is the same: dry winds increase evaporation and disrupt the water balance (the ratio of the water inflow from roots to that transpired to the atmosphere) of the plant tissue.

The origin of *sukhovei* remains an enigma, but there is a general agreement that both droughts and *sukhovei* develop under the south-central edge of displaced anticyclones, anticyclones 10° to 20° north from their usual summer position. Displaced anticyclones with diverging, clockwise air masses are characterized by little cloud cover, low relative humidity (dropping, in some instances, to 10–17%), and the absence of rainfall. Intense solar radiation and very high temperatures create moisture deficits and desiccation of the soil.

Basic atmospheric circulation

Air masses

The basic atmospheric circulation features involved in giving regional character to Asia's climates are the movement of air masses, transformation of air mass properties, and interactions between them along fronts. Asian air masses show great contrasts in temperature, moisture, and density. At any particular site the properties of air masses depend not only upon the nature of the source region but also the modification the air mass experienced en route from the source region. En route air mass modifications are of great importance in determining the nature of weather associated with an air mass (Lydolph, 1977; Takahashi and Arakawa, 1981). Some typical characteristics of air masses and their source regions are as follows:

1. Continental Arctic (winter) air masses are stable, intensely cold (−55° to −35°C), extremely dry, with inversions; cA air masses enter Siberia from the Arctic seas and at times penetrate to the Pacific Ocean; they are associated with clear skies, low temperatures, and dense air.
2. Continental polar (winter) air masses are very stable with strong temperature inversions and are cold (−35° to −20°C) and dry; they spread to the north and to the south of the "great ridge" of high pressure in Siberia and Outer Mongolia at approximately the 50th parallel and dominate the weather of the entire continent; generally cP air masses produce clear, cold, and cloudless weather.
3. Maritime tropical (winter) air masses are, for the most part, unable to penetrate eastern Asia in winter due to the intensity of the great Siberian High Pressure Cell; mT air masses that influence the weather in central Asia in winter circulate around the eastern edge of the Azores – Bermuda High Pressure Cell where upper level subsistence is strong; mT air masses are cool, dry, and stable in winter.
4. Maritime polar (winter) air masses have great difficulty penetrating deep into the Asian continent in winter, for the Siberian High Pressure Cell and strong outflowing winds in eastern Asia inhibit mP incursions. The mP air masses basically are conditionally stable, cool (0–10°C) and moist; they have significant influence upon the weather of maritime eastern Siberia, Manchuria, and Korea.
5. Continental polar (summer) air masses are, in general, stable or conditionally stable, cool (5–15°C) and somewhat moist; east and south Asia are so dominated by mT air in summer that cP air contributes little to the weather of that region.
6. Maritime polar (summer) air masses are a contributing factor to the summer weather of Manchuria, eastern Siberia, and Japan, and are, in most cases, stable to conditionally stable, mild (2–14°C), and humid; conflicts between mP and mT air masses in summer lead to the formation of a semi-stationary front in northeast Asia with associated overcast and drizzly weather.
7. Maritime tropical (summer) air masses initially are conditionally stable and very moist; mT air masses provide moisture for the summer monsoon and in spring invading mT air meets cP air in central and south China producing very active cyclogenesis; mT air masses dominate the weather of eastern Asia during the high-sun period.
8. Continental tropical (summer) air masses develop over southwest Asia in summer and are conditionally stable, dusty, very hot (30–42°C), and hold moisture; cT air flows north and northwest in summer into western Asia, advecting heat and absorbing moisture en route, plus contributing a characteristic opalescent haze to the local climates.

Asian air masses show great contrasts in temperature, moisture, and density. At any particular site, properties of air masses depend not only upon the nature of the source region but also the

modification the air mass experienced en route from the source region. En route air mass modifications are of great importance in determining the nature of weather associated with an air mass (Lydolph, 1977; Takahashi and Arakawa, 1981).

Siberian high-pressure cell

General atmospheric circulation over Asia is controlled by centers or cells of high or low pressure whose axes are, in general, east–west and whose pressure centers vary drastically from winter to summer. In winter an extensive and well-developed high-pressure cell, centered over Mongolia, dominates the weather over most of east Asia (Figure A66). Triangular in shape, with the apex extending in the west to the Caspian Sea and the base anchored in the northeast near the Verkhoyansk Mountains of Siberia and in the southeast near the Chin Ling Mountains of east-central China, the Siberian High effectively blocks penetration of moisture-bearing, moderating maritime air masses in winter. Acting as a wedge forcing air masses to skirt northeasterly from the Black Sea across much of northern Siberia and to flow southerly along the Kamchatka Peninsula toward northern Japan, this intense high-pressure cell generates continental, land-trajectory, dry, cool, low-level air masses which surge from the north and northeast to the southwest across all of south and east Asia. The Siberian High, whose core and area of highest pressure is focused upon Lake Baikal, pulsates in intensity and breaks at times into smaller high-pressure cells of less intensity. February marks the height of the Siberian High's dominance of the winter circulation over Asia. The Siberian High weakens and shifts its center westward into a position over northeastern Central Asia in April, then dissipates in May. The weather map of Asia begins to be dominated by an intensive, thermally induced low-pressure cell over southwestern Asia and focused upon the tip of the Arabian Peninsula, the Iranian Plateau, and the Thar Desert of Pakistan (Davydova et al., 1966).

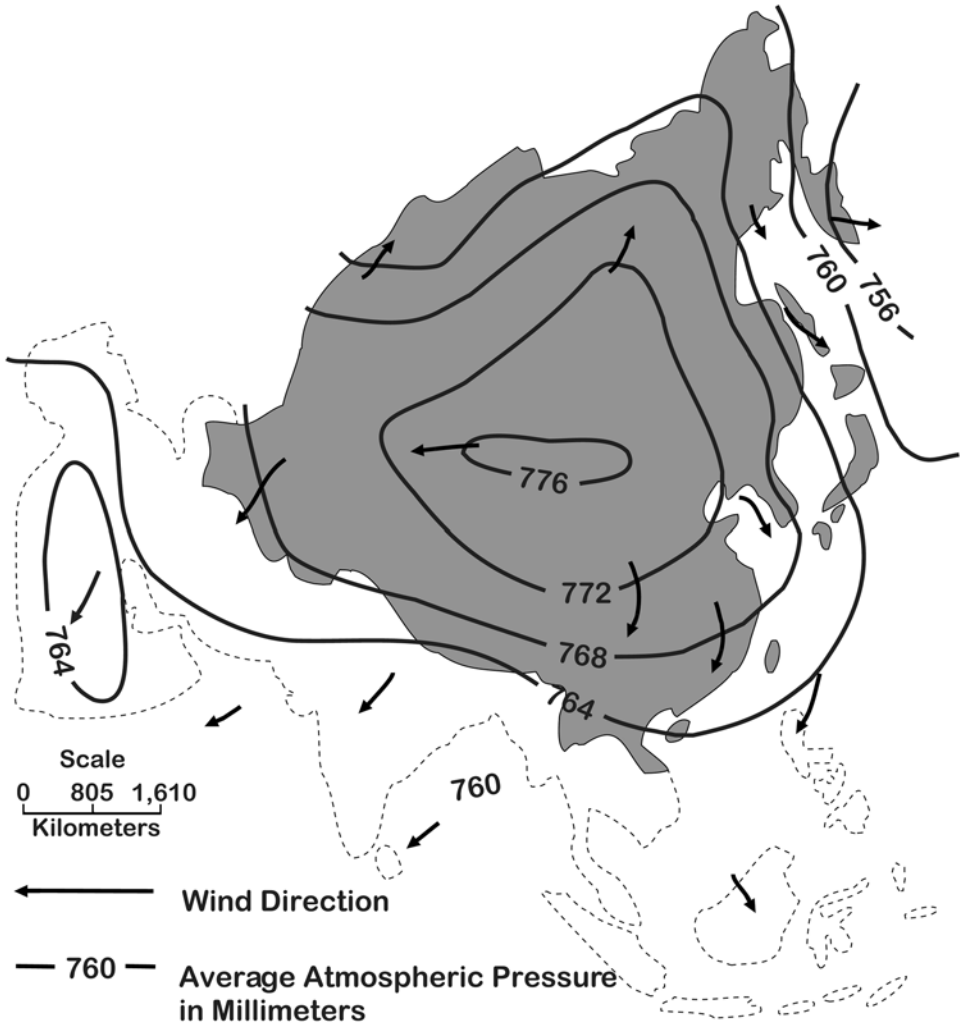

Figure A66 Atmospheric pressure and winds: January. *Source: Geograficheski Atlas*, 1959, Moskva, p. 15; *Preroda i Resoursi Zemli*, 1999, Moskva and Vienna, p. 51. Anna R. Carson 2003.

Southwest Asian low

In summer, east Asia's weather is dominated by a large, deep, thermally induced low-pressure cell that extends from the Arabian Peninsula to central China and from central India to Central Asia – centered approximately 30°N latitude and 70°E longitude (Figure A67). A complex cell, the Southwest Asian Low experiences east–west locational oscillations and occasional intense pressure deepening. This low in summer has the effect of interrupting the subtropical high-pressure system in the northern hemisphere by dividing the globe-girdling zonal band into two distinct large oceanic cells. One intense depression, the Southwest Asian Low, induces a radical change in prevailing winds and storm tracts during the high-sun period. Air masses from the stable eastern end of the Azores–Bermuda High Pressure Cell skirt this low from a north to northwesterly direction across the eastern rim of the Arabian Peninsula; less intense air masses from the northern quadrant of the Azores–Bermuda High sweep eastward across Turkey and into the northern extremities of Central Asia. Air masses and storms spawned under the western unstable quadrant of the Hawaiian High sweep from the south and southeast in a northerly trajectory across Japan, extreme eastern China, and the Russian Maritime Provinces. But the most constant and climatically significant air masses and storms are advected to this intense low-pressure cell as southwesterly trade winds spawned from a semipermanent high-pressure cell in the southern hemisphere over the Indian Ocean. In India and east Asia this modification of the general planetary wind system in summer constitutes the Asian monsoon (Tsuchija, 1964; Chang, 1967).

Frontal dynamics

Frontal zones and wind systems conform to the location and circulation of major air masses. In winter three major zones of cyclonic activity are distinguished over Asia. One zone is located

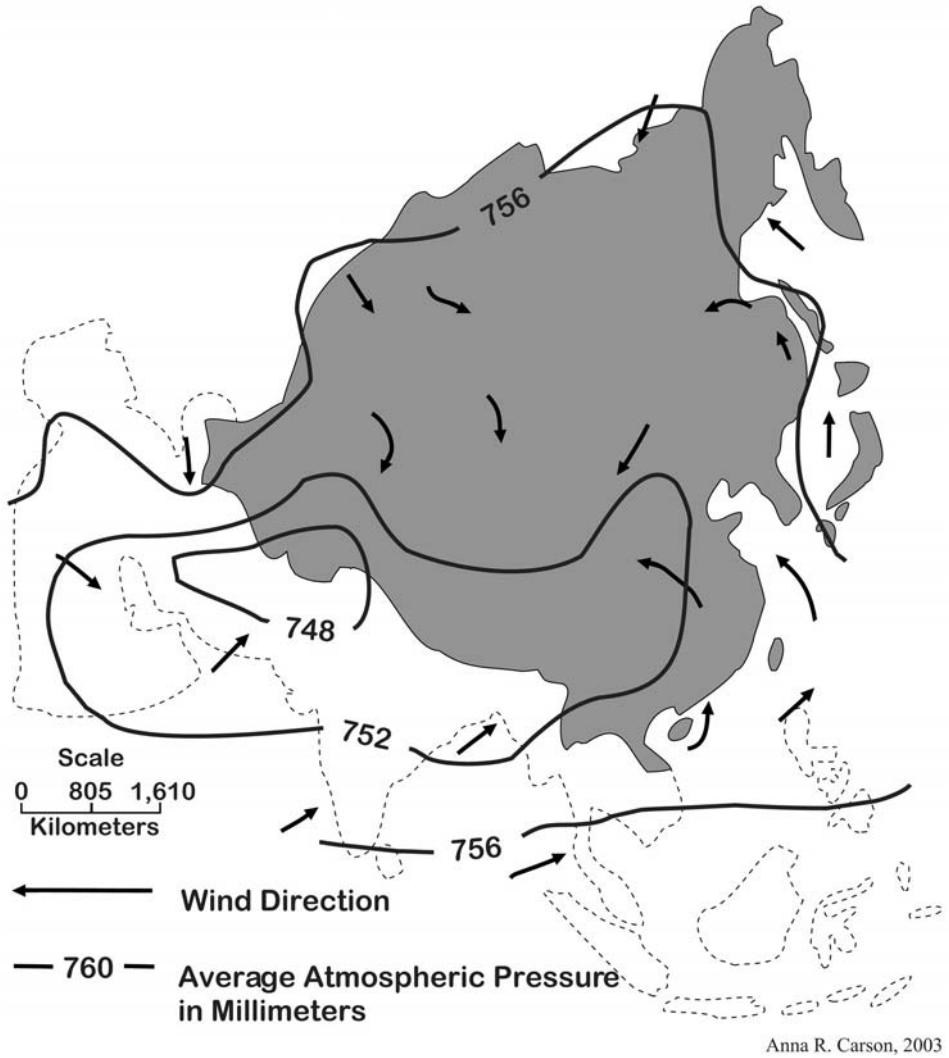

Figure A67 Atmospheric pressure and winds: July. *Source: Geograficheski Atlas*, 1959, Moskva, p. 15; *Preroda i Resoursi Zemli*, 1999, Moskva and Vienna, p. 51. Anna R. Carson 2003.

along the Asiatic Arctic Front, well above the Arctic Circle in northern Siberia, extending along the shores of the continent. This front fluctuates greatly and Arctic air masses, at times, penetrate east-central Asia. The second zone is along the Southwest Asian Polar Front that develops in winter over the Mediterranean Sea and extends to the Caspian Sea. The third zone is along the East Asian Polar Front that aligns itself in a northeasterly path from extreme south Asia toward Japan. Along these winter frontal zones, and moving at various directions and speeds, depressions and anticyclones impart to the climates of Asia that special character by which one area differs from another.

During summer, three major zones of pronounced cyclonic activity can be identified. The first is the southward-displaced Asiatic Arctic Front that at times extends east–west across northwestern Siberia along the 70°N parallel. A second zone of pronounced cyclonic activity is the Asian Polar Front that normally extends from the eastern tip of Lake Balkash in Central Asia, over Mongolia, to the northernmost bend of the Amur River along the 50°N latitude. This oscillating and at times southward-dipping Asiatic Polar Front zone has been called the "barometric backbone of Asia" in summer or the "great ridge", for a large number of anticyclones is observed each year between 50° and 55°N latitude. The third major zone is along the South Asian Intertropical Front. Extending over China at approximately 25°N latitude, the South Asian Intertropical Front is well defined in some locations, but in others it is weak or absent. In this belt, convergence of surface winds result in large-scale lifting of warm, humid, relatively unstable air, producing numerous weak, rain-generating disturbances (Trewartha, 1981). Along major frontal zones are found pronounced horizontal variations in temperature, humidity, and stability – usually jet streams. Strong, narrow jet stream currents, thousands of kilometers long, hundreds of kilometers wide, and several kilometers deep, are concentrated along a nearly horizontal axis in the upper troposphere or stratosphere, producing strong vertical and lateral shearing action.

Jet streams

Three distinct jet systems, the Polar Front Jet, the Subtropical Jet, and the Tropical Easterly Jet, have a major impact upon weather and climate in Asia. Latitudinal location of these jet systems, especially the Polar Jet, shifts considerably from day to day and from season to season, often following a meandering course. But in general, the Polar Front Jet gives rise to storms and cyclones in the middle latitudes of Asia, the Subtropical Jet noted for a predominant subsidence motion gives rise to fair weather, and the Tropical Easterly Jet is closely associated with the Indian monsoon. Over most of Asia the Polar Front Jet and the Subtropical Jet are most intense on the eastern margin of the continent and are best developed during winter and early spring. Jet stream wind speeds up to 500 km/h have been encountered over Japan. The Subtropical Jet, at times in winter, forms three planetary waves with ridges over eastern China and Japan. It frequently merges with the Polar Front Jet producing excessively strong jet wind speeds. During summer the Subtropical Jet loses its intensity and is mapped only occasionally.

East Asian monsoon

The East Asian monsoon is a gigantic multifactored, multifaceted, complex weather system, composed of diverse heat and moisture cycles intimately related to local topography, modified air masses, quasistationary troughs and ridges, and jet streams. Weather over most of eastern Asia during winter is dominated by the Siberian High-Pressure Cell and outflowing continental air masses. Low-level air flow is mainly from the north and is cold, dry, and stable. Successive waves of cold northeasterlies commence in late September and early October, progressing farther and farther southward, reaching the south China coast by late November or early December. In the higher midlatitudes of Asia during the low-sun period, a steep north–south pressure gradient persists. During March and April the Siberian High gradually weakens, and incursions of moist maritime tropical air from the south and east replace the cold-to-cool northeasterlies, producing widespread stratus clouds, fog, and drizzle that may persist for days (Das, 1968).

In summer a combination of the deep and elongated Southwest Asian Low-Pressure Cell extending from the Arabian Peninsula to China, and the South Asian Intertropical Front, reaching its maximum poleward displacement, sets the stage for a marked seasonal reversal of air flow. Warm, moist, and conditionally unstable southwesterly maritime air masses from relatively cooler oceanic source regions eventually overcome blocking atmospheric conditions, and flow northwestward over China and Japan. Considerable convective activity develops over land, and heavy showers and thunderstorms contribute largely to the summer rainfall maximum of the region. Characteristics and attributes and onset and duration of the monsoon are site-specific. Duration of the summer monsoon in China varies between north and south. Dates of monsoon onset and percent of annual average rainfall received have been a focus of numerous studies in the past century. A synthesis of these studies is given in Table A38.

In all cases low-level wind patterns and resultant weather in summer are complicated by topography. Distance from air mass source regions, moisture content of air masses, and orographic barriers and atmospheric disturbances associated with cyclonic or inter-air mass convective activity determine distribution and quantity of precipitation. There is a pronounced difference between the East Asian and South Asian monsoonal weather. The East Asian winter monsoon is much stronger than the South Asian winter monsoon, and the East Asian summer

Table A38 Dates, duration and percent of rainfall by region

Location	Dates	Duration	Rainfall
1. South China	Mid-April; end October	6½ months	75–90%
2. South Central China	Mid-May; mid October	5½ months	60–80%
3. North Central China	June; end August	3 months	60–75%
4. North China/Mongolia	June; end August	3 months	Less than 60%

monsoon is much weaker than the South Asian summer monsoon (Trewartha and Horn, 1980).

Storms

Local winds

Owing to the great variety in relief and exposure, Asia is subject to numerous local winds and their associated weather. Ubiquitous in Asia are the warm, dry, gusty, downslope *foehn* winds generated, in most cases, by passing atmospheric disturbances in highland or mountainous areas. For example, in Central Asia and Siberia, *foehn*-like winds experienced along the Caspian Sea are locally called *germich*; in Uzbekistan, *Afghanets*; in Tadzhikistan, *harmsil*; in and near the great Fergana Valley, *ursatevskiy* and *kastek*; and along the Kazakh–Chinese border at the Dzhungarian Gate east of Lake Balkhash, *evgey*. Winds are given a medley of names, and the largest and most pronounced are a major contributing factor responsible for the broad aspects of Asia's climate (Critchfield, 1983).

For each season of the weather year, representative winds of local significance have been identified and named:

1. Summer – A hot, strong, and constant northerly summer wind carrying considerable dust and obscuring the atmosphere is called *karaburan* in the Tarim Basin of Sinkiang and northwestern China and *chang* in Turkmenia. At times, on the southern edge of a modified Arctic air mass that advects into southern Siberia and Central Asia, hot, dry moisture-absorbing *sukhovei* winds eliminate local cloud cover, permit intense solar radiation to strike the Earth and reduce relative humidity at the surface to a very low value both day and night.
2. Fall – Cold and often very dry northerly or northeasterly winds, preceded by a cold front, often blow with great strength and violent gusts down from the mountains and high plateaus of northern Siberia and the Caucasus. *Bora* is the term identifying this type of wind in the region between the Black and Caspian seas, and *sarma* and *kharanka* are bora-type winds in the Lake Baikal region of southern Siberia.
3. Winter – Very cold northerly or northeasterly gale-force winds, often blowing at temperatures below −20°C and accompanied by falling or drifting snow, are generated from the back side of winter depressions in Siberia and Central Asia. The sensation of cold temperatures is increased by the low wind-chill factor associated with a *buran* or a *purga*, and the break in the comparative calm associated with the Siberian High-Pressure Cell.
4. Spring – Continental depressions passing eastward over central China and the Yellow Sea in spring and early summer bring heavy overcasts, high humidity, and rain to China and Japan. *Bai-u*, *mai-yu*, or *plum rains*, as they are called, are an extended period of unstable weather caused by stagnation of the polar front.

Thunderstorms and tornadoes

Thunderstorms reach their maximum development in Asia over lowlands in summer. Most thunderstorms are ordinary convective cumulonimbus clouds within maritime tropical air masses that produce localized precipitation. Air mass thunderstorms, randomly scattered, are initiated primarily by daytime solar heating of land surfaces. Frontal and orographic thunderstorms have distinct patterns and movements, for they are triggered in a place or zone where unstable air is forced upward. Severe thunderstorms may produce hail, strong surface winds, and tornadoes. Convective thunderstorms develop more frequently here because of strong insolation and low wind velocities. Clouds of convective thunderstorms reach elevations of 12 000 meters or more, and rainfall associated with these cells is short in duration, intense, and localized. Very few thunderstorms are observed over the tundra regions of Siberia – less than five per year. Thunderstorm activity is a summer phenomenon in China, much of Central Asia, Singkiang, Mongolia, the Maritime Provinces of the Far East, and Siberia. They commence during the fall transitional period, are more prevalent in winter, and decline in number during the spring transitional period.

The most destructive spin-off of a thunderstorm is the tornado, an extremely violent rotating column of air that descends from a thunderstorm's cloud base and can cause great destruction along a narrow track. An Asian tornado travels in a 150–500 meter wide, approximately several kilometers long, straight track, at speeds ranging between 50 and 100 kph. Although one of the least extensive, it is the most violent of all Asian storms. As the whirling mass of unstable air gains force, a rotating column of white condensation is formed at the base of the cloud. Dirt and debris sucked into this whirlwind darken the column as the column of air reaches the ground. A notable feature of the climate of Asia is the relative infrequency of tornadoes, particularly as compared to central and eastern North America at similar latitudes. Although records are inadequate, there are sufficient data to conclude that tornadoes occur on the order of once every 3–5 years in the northern Caspian Sea area and Central Asia during May, June, and July and two to five or more annually in China and Japan during August and September.

Tropical cyclones

One of the most powerful and destructive types of cyclonic storms is the tropical cyclone (Hsu, 1982). Referred loosely to any pressure depression (near 1000 mb) originating above warm oceans in tropical regions, tropical cyclones form an important feature of the weather and climate of south and east Asia – particularly from July to October. Different terms are used worldwide to describe this tropical storm: *typhoon* in the western Pacific; *baquios* or *baruio* in the Philippines; *tropical cyclone* in the Indian Ocean; *willey-willeys* in Australia; *hurricane* in the eastern Pacific and Atlantic; *cordanazo* in Mexico; and *taino* in Haiti.

Organization and development of tropical cyclones are not fully understood, and they are under intensive study. Formation of this type of storm is associated with warm ocean surfaces not less than 27°C, located between 5° and 10°N latitude, light to calm initial winds, and waves or troughs of low pressure deeply embedded in easterly wind streams converging into an unstable atmospheric zone. Large quantities of latent heat released through condensation are converged and transferred to higher levels, deepening the pressure center and intensifying the storm. An almost circular storm of extremely low pressure, into which winds spiral with great speed, is formed. Asian tropical cyclones travel slowly at speeds of 16–48 kph, cut a destructive storm path 80–160 km wide, and winds in the wall cloud area achieve speeds in excess of 200 kph. Passage of a tropical cyclone over

water and land is associated with strong winds and heavy rainfall. Storm tracks vary annually and no two recorded tracks have been exactly the same. Despite all irregularities, most tropical cyclones have a tendency to move westward, then poleward, finally turning eastward, toward higher latitudes under the influence of both internal circulation and external steering currents, penetrating into the belt of westerly winds. This awesome tropical storm contributes between 25% and 50% of the annual precipitation received in many tropical weather stations. Flooding, destructive wind force, and storm surge are responsible for much property damage and for human casualties.

Occurrence of tropical cyclones is restricted to specific seasons depending upon the geographical location of the storm-affected region. The Observatory of Hong Kong reports that 83% of the annual total recorded in Hong Kong occur between June and November. Approximately 50% of these severe tropical storms attain typhoon intensity. From mid-November to April, very few tropical storms pass over the coasts of China and Korea, but in the warm July through October period numerous tropical depressions, tropical storms, severe tropical storms, and tropical cyclones (typhoons) are experienced. In the 1884–1955 period at least 438 tropical cyclones crossed various sections of the Chinese and Korean coasts. Japan's tropical cyclone season begins in June and ends in November, reaching its peak occurrence in September. In the 1918–1947 period 85 typhoons were reported in Japan. The tropical cyclone season is slightly longer in the Philippines, extending from June to December. Almost 90% of all tropical cyclones in the 1948–1962 period were noted in the summer and fall seasons. Tropical cyclones usually weaken over land, and few penetrate and persist more than 500 km inland. The rise in sea level, when combined with high tides, accounts for more damage and loss of life in Asia than violent wind (Riehl, 1979).

Prospectus

Continentality, as a climatic control or factor, is best manifested in the extremes found in the climates of Central Asia, Siberia, and East Asia. The land-dominated interior climates present striking contrasts to the maritime-impacted coastal and island areas. Winters are much colder than corresponding latitudes in western Europe and North America; also, those regions where continentality is a climatic factor are the regions where climatic change is most noticeable. Vegetal, agricultural, and biotic zones have advanced 10 km northward in some climatic regions. This is best revealed in satellite remote sensing images of Central Asia and Siberia. In the past 20 years Asian temperatures have remained above the long-term averages (Figures 3 and 4). An annual change in temperature of only a few degrees centigrade affects the climates of Asia sufficiently to render marginal agricultural regions unacceptable for food production and to wreak havoc on local food supplies (Bryson and Murry, 1977). Moreover, a combination of human activities that modify climatic elements with natural causes of climatic change could lead to more frequent or more severe changes in Asia's climatic regions (Christianson, 1999). For those struggling to secure a meager existence from a hectare or two of land in Asia, and for the urban dweller seeking water to maintain bodily functions, any climatic change disrupts lifestyles – because humans and human institutions are adjusted to precisely the climate and weather that prevail (Budyko, 1977; Dando, 1980; Martens, 1999).

William A. Dando

Bibliography

Arakawa, H. (ed.), 1969. *Climates of Northern and Eastern Asia*. World Survey of Climatology, vol. 8. Amsterdam: Elsevier.

Borisov, A.A., 1965. *Climates of the U.S.S.R.* R. A. Ledward (trans.). Chicago: Aldine, pp. 1–28.

Bryson, R., and Murry, T., 1977. *Climates of Hunger*. Madison: University of Wisconsin Press, pp. 123–156.

Budyko, M.I., 1977. *Climatic Changes* (American Geophysical Union trans.). Washington, DC: American Geophysical Union, pp. 197–245.

Chang, J., 1967. The Indian Summer Monsoon. *Geographical Review*, **57**: 372–396.

Christianson, G., 1999. *Greenhouse: the 200-year story of global warming*. New York: Walker & Company.

Critchfield, H., 1983. *General Climatology*. Englewood Cliffs, NJ: Prentice-Hall, pp. 88–101.

Dando, W., 1980. *The Geography of Famine*. London: Edward Arnold.

Dando, W.A., Carson, A.R., and Dando, C.Z., 2003. *Russia*. Philadelphia: Chelsea House, pp. 30–35.

Das, P., 1968. *The Monsoons*. New York: St Martin's Press.

Davydova, M., Kamenskii, A., Nekiukova, N., and Tushinskii, G., 1966. *Fizicheskaia Geografiia SSSR*. Moskva: Prosveshchenie, pp. 57–82, 439–704.

Davydova, M., Kamenskii, A., Nekiukova, N., and Tushinskii, G., 1999A. Global change: a review of recent anomalies. *Global Change*, **5**(1): 6–7.

Davydova, M., Kamenskii, A., Nekiukova, N., and Tushinskii, G., 1999B. Russia plagued by heat and drought. *Global Change*, **5**(3): 7.

Griffiths, J., and Driscoll, D., 1982. *Survey of Climatology*. Columbus, Ohio: Charles E. Merrill, pp. 162–172.

Hsu, S.I., 1982. *Tropical Cyclone in the Western North Pacific*. Occasional Paper No. 24. Hong Kong: Chinese University of Hong Kong, Department of Geography, vol. 2.

Jones, P., 200l. "The Travails of a Warmer World." Presentation by Dr. Jones, University of East Anglia, Intergovernmental Panel on Climatic Change, Washington, DC.

Kriuchkov, V., 1973. *Krainii Sever: Problemy Ratsional'nogo Ispol'zovaniia Pirodnykh Resursov*. Moskva, Mysl, p. 15.

Lawton, J., 2002. Rebuilding in Afghanistan. *Saudi Aramco World*, **53**(6): 16.

Lounsbury, J.F., 1973. *A Workshop for Weather and Climate*. Dubuque: William C. Brown, p. 124.

Lydolph, P.E., 1977. *Climates of the Soviet Union*. World Survey of Climatology, vol. 7. Amsterdam: Elsevier.

Martens, P., 1999. How will climatic change affect human health, *American Scientist*, **87**(6): 534–541.

Nuttonson, M.Y., 1950. *Agricultural Climatology of Siberia*. Washington, DC: American Institute of Crop Ecology, appendices.

Nuttonson, M.Y., 1999. *Preroda i Resoursi Zemli*. Moskva and Vienna: Geographical Institute Ed. Holzel, pp. 51–56.

Riehl, H., 1979. *Climate and Weather in the Tropics*. London: Academic Press, pp. 459–496.

Takahashi, K., and Arakawa, H., (eds.), 1981. *Climates of Southern and Western Asia*. World Survey of Climatology, vol. 9. Amsterdam: Elsevier.

Trewartha, G.T., 1981. *The Earth's Problem Climates*, 2nd edn. Madison: University of Wisconsin Press, pp. 173–254.

Trewartha, G., and Horn, L., 1980. *An Introduction to Climate*. New York: McGraw-Hill, pp. 123–128.

Tsuchija, I., 1964. *Climate of Asia*. World Climatology, vol. 1. Tokyo: Kokon Shoin, p. 577.

Cross-references

Asia, Climate of South
Asia, Climate of Southwest
Climate Classification
Continental Climate and Continentality
Siberian (Asiatic) High
Taiga Climate
Tundra Climate

ASIA, CLIMATE OF SOUTH

South Asia, which mainly includes India, Pakistan, Bangladesh, Sri Lanka, Nepal, and Bhutan in this article, is located between about 5° and 37°N, in tropical and equatorial latitudes, with the Indian Ocean to the south, the Great Himalayas and Karakoram to the north, the Baluchistan highlands to the west, and the meridional chains of mountains in Indochina to the east. The distinct geographical features in South Asia restrict the horizontal exchange of oceanic and continental airmasses and modify the climate to a characteristic pattern. Besides great mountains and upland systems there are also lowland depressions. Numerous bays and gulfs enhance the influence of the ocean. In winter a warm, westward-flowing current reaches eastern Sri Lanka, from where it diverges northward, affecting the southeast coast of India. During the summer a warm current in the Indian Ocean reaches the west coast of India and flows southward; from south of Sri Lanka the current moves east (Martyn, 1992).

South Asia mainly consists of four climate zones. The northern Indian edge, as well as the upland and mountainous part of Pakistan, has a dry continental, subtropical climate. The far south of India and southwest Sri Lanka are located in the zone of equatorial climates. The rest of the areas lie in the tropical zone, with hot semi-tropical climate in northwest India, cool-winter hot tropical climate in Bangladesh, and semiarid tropical climate in the center of the peninsula. The last two tropical climate zones are greatly affected by monsoon circulations (Martyn, 1992; Rao, 1981; Papadakis, 1966). In addition, mountain climate occurs in the Himalayas. Climates there vary with elevation, from permanent ice caps at high elevation to subtropical climate at lower lands.

The most important climate feature in the region is the southwest monsoon, which lasts for 4 months, from June to September. In this southwest monsoon period the precipitation is one order of magnitude more than during the rest of the year. Because temperatures in the South Asian monsoon region drop dramatically in June and July, due to the monsoon onset, March to May becomes the warmest period.

In this article the observational data for precipitation are from the rain gauges station data over land and the data are interpolated to 1° resolution (Xie and Arkin, 1997), covering 1948–2003. The surface temperature data are from the National Center for Environmental Prediction (NCEP), the Climate Analysis Center, and the Climate Anomaly Monitoring System station data achieve (CAMS, Ropelewski et al., 1985); they include data from 1948 through June 2003. The NCEP/National Center for Atmospheric Research (NCAR) Global Reanalysis data from 1948 to 2003 (Kistler et al., 1999) are used for circulation and radiation figures.

Radiation

Although the sun's altitude is high during the entire year, and the amount of daylight varies little during the year for the area south of 30°N (Martyn, 1992), the solar radiation still exhibits high seasonality and great spatial variability (Figure A68). Annual mean solar radiation amounts decrease eastward, from 290 W m^{-2} in Baluchistan to less than 240 W m^{-2} in Bangladesh. Annual mean downward long-wave radiation at the surface decreases northward, which is consistent with the temperature gradient and water vapor quantity, with the two coasts having the highest long-wave radiation (about 390–400 W m^{-2}) due to cloudiness.

January solar radiation is about 240–250 W m^{-2} in the southern peninsula and western Sri Lanka, and drops to 220 W m^{-2} in the northern peninsula and eastern Sri Lanka. Much lower solar radiation is received in the northwest subcontinent and northeast Bangladesh, with north Pakistan having the lowest (Figure A68a). The long-wave radiation shows a clear zonal pattern, with high gradients in the Himalayas associated with topography (Figure A68c). In July the solar radiation decreases southeastward from northwest South Asia. Pakistan and northwest India receive the most solar radiation, between 300 and 360 W m^{-2}. In northeast India and Bangladesh the solar radiation decreases southward from 300 to 200 W m^{-2}. The southern continent has less solar radiation, especially along the west coast of India, due to the cloudiness in these regions (Figure A68b). There are two very high downward long-wave radiation centers over the Indian Ocean, located at both sides of the Indian peninsula and associated with heavy rain in these two areas. Apart from the areas influenced by these two centers, in other parts of the peninsula and Sri Lanka it is quite uniform, between 410 and 420 W m^{-2} (Figure A68d).

Circulation

A characteristic feature of the South Asian climate is the atmospheric circulation associated with the monsoon evolution. The extensive Eurasian continent and the Indian and Pacific Oceans play an important role in monsoon formation. In the winter the northeast monsoon prevails and sea-level pressure decreases to the south. The Intertropical Convergence Zone (ITCZ), associated with the equatorial low-pressure belt, runs across the entire Indian Ocean along 10°S latitude. The cold air from the Siberian High, which is centered at 45°N and 105°E, approaches eastern India and the Bay of Bengal starting in October. Since the barrier of Tibet and the Himalayas blocks the advance of cold polar air, low-level northeast winds only run across the Bay of Bengal and reach northeast India. The pressure gradient is strong to the north of the Himalayas but weak over the Indian Peninsula. From October to May the southern branch of the westerly jet stream, usually flowing between 28° and 30°N, crosses the Himalayas. This westerly wind in the upper troposphere is strongest in January and gradually slackens.

Meanwhile, in western South Asia, cold air from Iran and Afghanistan reaches Pakistan and northern India. Cyclonic disturbances are more frequent over the western Himalayas and Karakoram from early November to the end of May because of strong vertical wind shear in the basic current (Hamilton, 1979). They reach the Ounjab, Rajasthan, and even Patna on the Ganges Plain. They bring clouds and precipitation in November and December, and cold weather, thunderstorms, and precipitation in the normally hot, dry period from March to May (Lockwood, 1974; Martyn, 1992).

Development of low pressure due to increased heating over land starts for South Asia in March. Heat lows are usually found in an area extending from Somalia across southern Arabia to Pakistan and northwest India between May and September, and are most intense in July. Middle tropospheric subsidence is considered to affect the heat low (Hamilton, 1979). The distribution of sea-level pressure, as well as

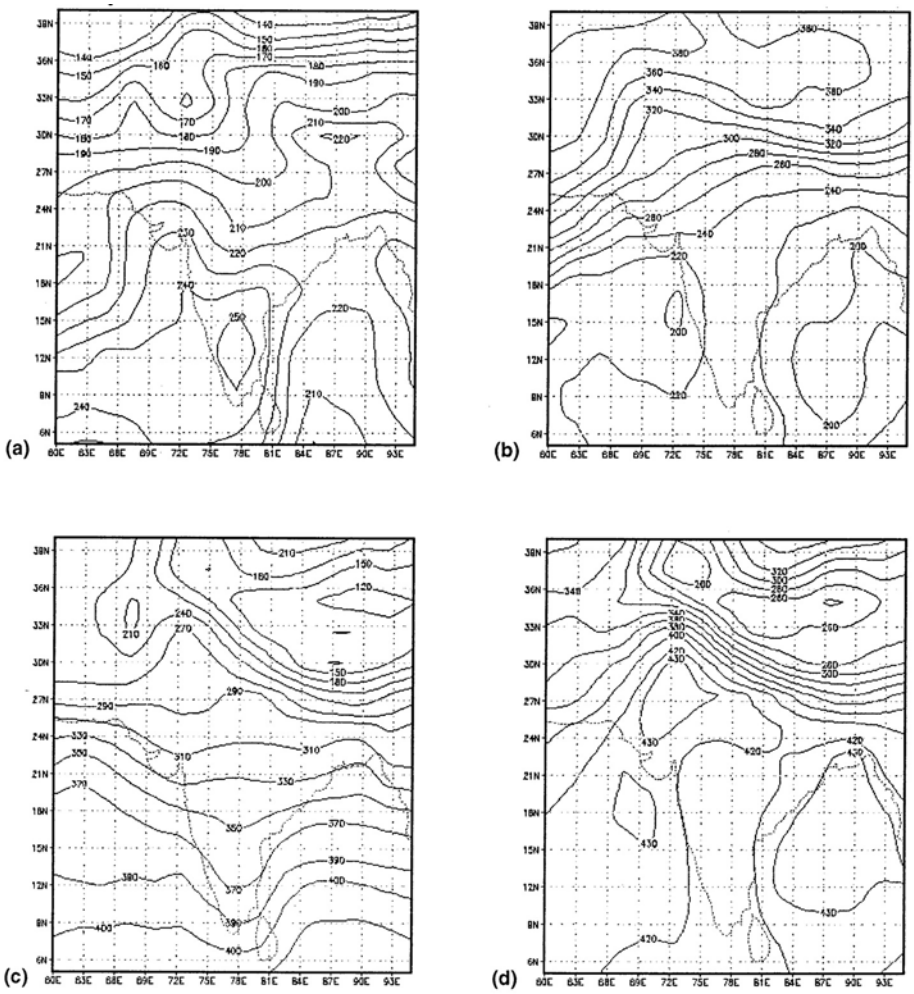

Figure A68 Monthly mean radiation flux at the surface ($W\,m^{-2}$): (**a**) January mean downward short-wave radiation; (**b**) July mean downward short-wave radiation; (**c**) January mean downward long-wave radiation; (**d**) July mean downward long-wave radiation.

low-level air flow over the Indian subcontinent, experiences a complete reversal from January to July (Figures A69a and A69b). Earlier northeasterlies are replaced by westerlies in April with the core of a subtropical jet stream at 200 mb near 27°N. This jet gradually weakens from an average speed of about $40\,m\,s^{-1}$ in March to about $25\,m\,s^{-1}$ in May (Hamilton, 1979; Keshavamurty and Rao, 1992).

In the summer the low pressures are centered over Pakistan, northwest India, and the Ganges Plains. The Indian Ocean high is strong and centered at 30°S and 60°E. At the beginning of June, as the jet stream disappears above the southern border of the Tibetan Plateau, the low over Pakistan deepens and the ITCZ moves in. The change in the direction of circulation to southwest occurs suddenly (called the burst of the monsoon) because of the very steep horizontal northward pressure gradient. The southwest monsoons, carrying enormous quantities of moisture from the Indian Ocean, reach the coast of India (Figure A69b). The monsoon circulation dominates South Asia. Because wind now blows off the sea, the summer monsoon contains far more water vapor than the winter monsoon. The depth of the summer monsoon over the Indian Peninsula decreases northwards (Martyn, 1992). Humidity, cloudiness, and precipitation all increase in the summer, but the increase of temperature is checked. When the monsoons change direction during the summer, cyclonic activity increases rapidly over very warm seas and oceans and is extremely violent over the Bay of Bengal.

Monsoon depressions form in the Bay of Bengal from June to September, move west/northwest, and reach at least the central parts of the subcontinent before weakening or disappearing. They are usually moderately vigorous, with surface winds below $20\,m\,s^{-1}$ and a central pressure range from 2 to −10 mb below normal. Many depressions are probably of a baroclinic type (Koteswaram and George, 1958) and usually exist in the presence of a large zonal wind shear between the upper and lower troposphere. Monsoon depressions are an important summertime precipitation agency between 18°N and 25°N. They bring widespread rains in the southwest quadrant, with many heavy rainfall events. As a depression moves over land it usually weakens due to frictional dissipation of energy and a reduction of

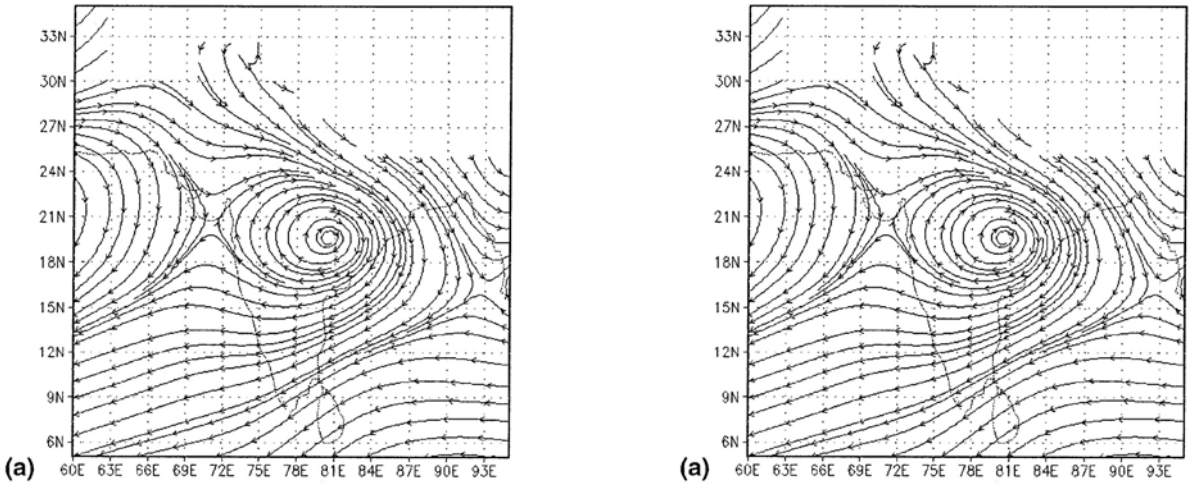

Figure A69 Monthly mean streamline at 850 mb: (**a**) January; (**b**) July.

moisture intake. Eventually, most depressions merge into the monsoon trough over northwestern India (Hamilton, 1979).

The transition of a summer circulation to a winter circulation is of shorter duration than the reversion from winter circulation to summer circulation. The transition comes suddenly over the Himalayas as the circumpolar westerlies begin to intensify and move south. A subtropical westerly jet stream develops at the northwestern end of the Himalayas, thereafter extending southeastward. By mid-October the jet is fully established south of the Himalayas. A winter circulation develops north of 25°N by early November (Yeh et al., 1959; Hamilton, 1979).

Surface temperature

The isotherms in January generally are parallel to the latitudes except near the coasts. January mean temperatures in northern South Asia are about 10°C, which is not as cold as most parts of Asia because the Himalayas and Sulaiman block the inflow of masses of cold air from the north. On the Indian Peninsula, south of 18–20°N in the east, the temperatures exceed 20°C and can reach 24–27°C on the equator (Figure A70a). In Kashmir the mean temperature can be 1°C at Srinnagar (1666 m) and −15.7°C at Dras (Martyn, 1992), where below-zero temperatures are usual from November to April.

Land becomes progressively heated after January. The warmest period of the year precedes the monsoon from March to mid-June. In the far north the warmest month is July Figure A70b), and the warm season begins earlier southward; for instance, in southern India it begins in April. During the warm period the mean temperatures in the northern Deccan exceed 35°C (and even reach 38–42°C), and in the interior of the peninsula they reach 33°C. Because of the greater moisture brought in with the sea breezes, coasts are not hotter in the afternoon hours than the peninsular interior. The west coast of India is about 5°C cooler than the east coast.

In July the southwest monsoon is established over India and the cloudiness is heavy. Monthly mean temperatures over much of Indian Peninsula are quite uniform, around 27°C (Figure A70b). However, temperatures of over 30°C are recorded in the Great Indian Desert, and may reach 32–36°C. Temperatures in the Himalayan mountain valleys are from 24°C at elevations of 1700 m to 17°C at 3500 m (Martyn, 1992). Absolute maximums in some interior regions even exceed 40°C. The summer monsoon season is the second cooler period in the year because clouds and rain prevent the temperature from rising too much during the day. Once the monsoon ends the temperatures rise and a second annual maximum is attained. This is not as high as the pre-monsoon maximum because of the greater quantity of moisture in the air and the sun's lower altitude. Monthly mean temperatures over the entire subcontinent in October are generally within the range of 27–29°C. This is the month of the most equable distribution of temperature on the Indian Peninsula. The range of annual temperature variation is about 1–5°C for most parts of the region.

Near-surface humidity and cloudiness

In January the relative humidity on the southern peninsula is higher than 50–60%, and even 70% on the coasts. A maximum relative humidity of over 80% in Sri Lanka and Hhasi-Janitia Hills in northeast India has been recorded. The driest areas are the Indus Plain and the adjacent areas of Pakistan and western India. In the western Himalayas the humidity is high when temperatures are very low, but becomes lowest in May–July. From March to mid-June (the warm months) the relative humidity is under 30–40% on the Indus Plain, in the Punjab, Rajasthan, and at the western end of the Ganges Plain, and under 50% on the Deccan Plateau and in central Burma (Martyn, 1992). In July the areas most affected by the monsoon have relative humidity of over 80%, while the southwest coasts of India, the Khasi-Janta Hills, and some sections of the Himalayas even reach above 90%. However, there are areas in Pakistan still with relatively low humidity. On the Coromandel Coast and in eastern Sri Lanka the relative humidity reaches the lowest value in a year (Martyn, 1992). In the driest regions of Rajasthan the relative humidity does not exceed 60%, and in central India it does not reach 80%. In the eastern Himalayas, where the effects of the monsoon are strong, there are two wet

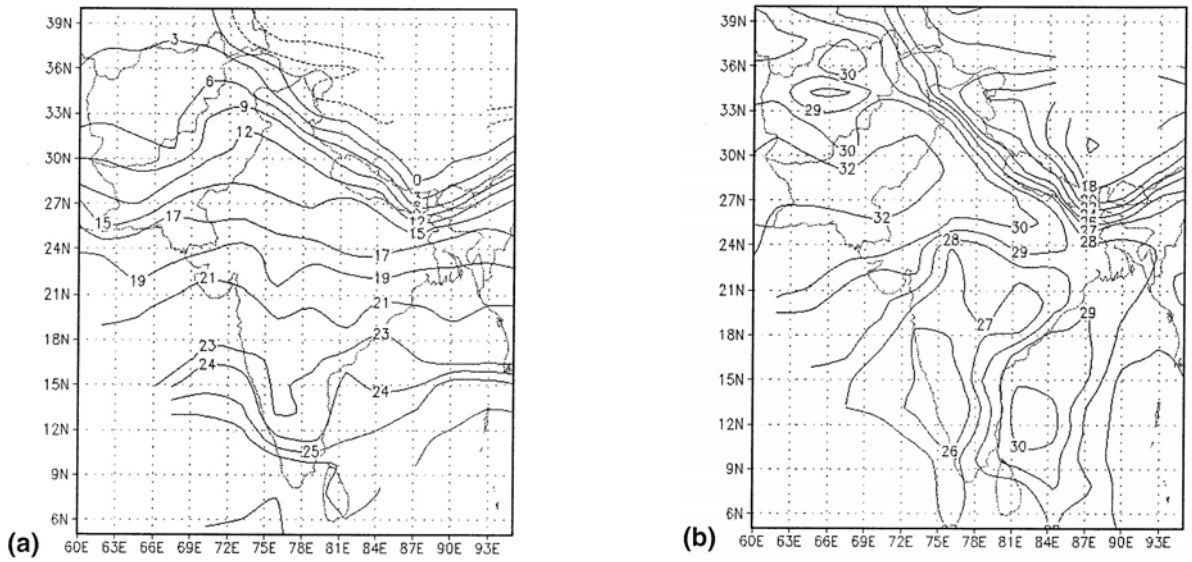

Figure A70 Monthly mean surface temperature: (**a**) January; (**b**) July.

periods, one in January and February and one from May through October, while two dry periods remain between these two wet periods.

The cloudiness and its annual variation are varied; they depend on atmospheric circulation and topography. With the arrival of the summer monsoon, which carries a huge amount of moisture from the Indian Ocean, South Asia becomes one of the most overcast parts of Asia, normally over 80%. Cloudiness even reaches 90% in western India in the upper reaches of the Godavari and the windward slopes of the Khasi-Jaintia Hills. The southern and northern parts of the region have greatest cloud cover from June to August, and from July to August, respectively. During the rest of the year the cloudiness is much less. In the west the cloudiness is 10–22% during the November–April period. In the east on the Bay of Bengal the lower cloudiness is about 22–45% during January–March. In January it is scanty (under 30% or even lower) in most parts of South Asia; but in the far north of India, where a westerly circulation is frequent, cloudiness is greatest (Martyn, 1992).

Precipitation

Precipitation attracts much more attention than any other aspect of Indian subcontinent meteorology. Precipitation in South Asia exhibits strong spatial variability. Pakistan and northwest India, where there is very little water vapor in the air and little precipitation due to limited evaporation and to dry air currents, have the most arid areas in South Asia. Annual precipitation is less than 250 mm in the driest parts of these areas (Figure A71a). Despite considerable low-level convergence into the low-pressure areas, there are very little clouds and precipitation because of extremely low humidity and/or because of stable inversion (Hamilton, 1979). From the east coast of India the precipitation decreases inland south of 17°N. The interior of the peninsulas, especially the lee side of the Western Ghats, has low precipitation, less than 1000 mm per year. Low precipitation is also found in the upper basin of the Bhima River (around 18°N) and its tributaries. In northern India there is a low precipitation strip from about 28°N and 75°E to 25°N and 87°E; but topographic effects and monsoons produce significant precipitation along the Himalayas.

In monsoon areas the precipitation exceeds 1000 mm per year. Maximums of precipitation coincide with higher elevations in the Ghats and the eastern Himalayas. In the Khasi-Jaintia Hills the precipitation can reach as much as 11 000 mm per year. On the Malabar Coast and at the southern end of the Western Ghats in India the value reaches more than 3000 mm per year. In Sri Lanka the annual precipitation is also affected by monsoons and is higher than 1300 mm per year; in the southwest it exceeds 2200 mm per year. The pattern of rainy days is similar to that of annual precipitation. The highest number of rainy days (200 per year) is recorded in southwest Sri Lanka. The rainy days number about 170 per year in the eastern Himalayas and about 150 on the Malabar Coast. The interior regions of India have rain on 5–80 days per year, while in the Great India Desert it falls on less than 5 days (Martyn, 1992; Rao, 1981).

The precipitation in South Asia is linked to seasonal changes in the atmospheric circulation. Rains develop over southern India and the southern Bay of Bengal in May–June (Webster et al., 1998). The abrupt northward jump appears with the onset of the South Asian summer monsoon. Based on analysis of various data sets it was found that the South Asian monsoon onset was associated with the reversal of the meridional gradient of upper tropospheric temperature south of the Tibetan Plateau (Flohn, 1957; Li and Yanai, 1996).

The monsoons bring most of the region's precipitation (Figure A71c). On the Indian Peninsula north of 13°N the rainy season begins in mid-June and lasts until September; in Bangladesh it lasts until October. The monsoon usually advances from two locations – one from the Bay of Bengal to central India and southern India in June and reaching northwest India by early July, and the other one over the Arabian Sea 1 month later. This progression of monsoons is associated with large-scale ascent through the troposphere with strong lower tropospheric convergence and upper tropospheric divergence. The periods of maximum thunderstorm frequency precede and

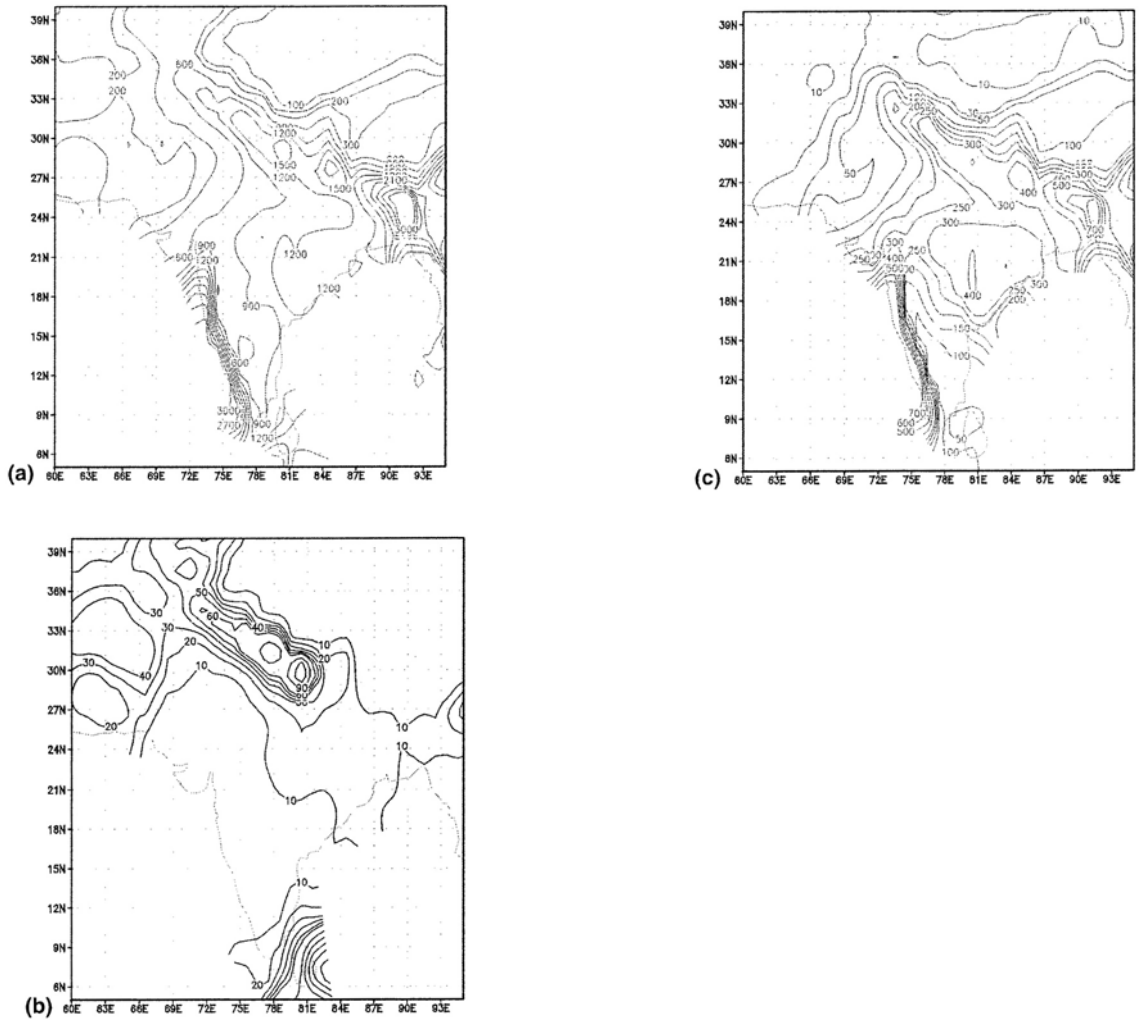

Figure A71 Precipitation: (**a**) Annual mean (mm year^{-1}); (**b**) January mean (mm month^{-1}); (**c**) July mean (mm month^{-1}).

follow the summer rains (Hamilton, 1979). In most parts of South Asia the spatial distribution of annual precipitation is similar to that in this period. The southwest monsoon rain provides water for agriculture in the world's very populous regions.

Orographic influence is dominant as onshore winds blow to the Western Ghats and the Khasi-Jaintia Hills. The main impact of the southwest monsoon is in a 250-km long stretch of the Himalayas between 87 and 90°E. Not only do the Himalayas receive heavy rains, but also the plains adjoining the foothills receive more rain than the plains further south. Even in north Pakistan the precipitation also ensues from monsoons from June to September. A trough (the monsoon trough) extends east-southeastward from Indo-Pakistan heat low to the northern part of the Bay of Bengal near 25°N in June and July and shifts a little further north in July–August, by which time it dominates weather over the Indian subcontinent. It retreats southward and disappears in September as a near-equatorial trough near 10°N. The position of this trough is an index of the activity of the monsoon over the subcontinent. If the trough is in a normal position it will be a normal monsoon year. When the trough shifts to the foothills of the Himalayas this indicates a break situation (Rao, 1981; Hamilton, 1979).

Temporal variations in precipitation are associated with shifts of position in large-scale upper tropospheric circulation, the low-level monsoon trough, and the development of synoptic disturbances. The precipitation maximum occurs in May–August (some areas extend to September). Rain is very heavy, especially at the start of the monsoon season and during tropical cyclones. Along the Coromandel Coast the rains begin in July, sometimes even in August. There is rain on more than 20 days in a month. In some areas, rainy days reach 25–28. However, it is very dry on the southeast tip of the peninsula. In the northwestern parts of the subcontinent the precipitation also decreases progressively westward.

A seasonal reversal of winds at lower levels, the displacement of the monsoon airmass by the continental airmass, and development of anticyclonic flow indicate withdrawal of the monsoon. From mid-September, as the surface temperature falls, the atmospheric pressure over the Indus and Ganges Plain rises rapidly and becomes higher than that over the Bay of Bengal. In October the ITCZ lies at 10°N and only affects

southern India. Southern India and southwest Sri Lanka have two rainy seasons due to the movement of the ITCZ. The first one is from May to July, and the second one is from October to November. In addition, tropical cyclones have prolonged heavy rainfall on the Coromandel Coast in fall. The turn of the monsoons is the time when tropical cyclones develop over the Bay of Bengal. In the Bay of Bengal, based on 70-year records, 15% of cyclones arise in April and May, and 38% arise in October and November (Rao, 1981). Fall cyclones are much stronger than the pre-monsoon ones. Some are listed as severe cyclonic storms with winds of 48 knots or more. The most violent cyclones over the Bay of Bengal cross the central Deccan along the Krishnai river valley. Others turn to blow up the eastern coast toward Bangladesh. Considerable flood damage has occurred in the Ganges delta. Apart from this, the cyclones are accompanied by high winds, tidal waves, and heavy rain. There can be disastrous flooding.

The winter precipitation over South Asia is only a small fraction of the annual amount, except in Kashmir and its surroundings (Figure 71b). During winter in Kashmir, Karakoram, cyclonic precipitation is dominant. On the east coast of Sri Lanka the rainfall is still more than 30 mm per month, decreasing to 15 mm per month along the west coast.

Impact of the Himalayas/Tibetan Plateau on the South Asian climate

The northern edge of South Asia is bounded by the Himalayas, which run along the southern periphery of the Tibetan Plateau; it extends over the latitude–longitude domain of 70–105°E, 25–45°N, with a mean elevation of more than 4000 m above sea level. Strong contrast exists between the eastern and western parts of the Plateau in both land surface features and meteorological characteristics.

The sharp edge of the Himalayas and the vast and high Plateau force the large-scale airflow to go around rather than over it. This effect is clearly seen in the flow features well above the Plateau. The mid-tropospheric westerly jet stream is situated to the south of the Plateau before the onset of the summer monsoon, but it suddenly jumps to the north side with the monsoon onset. Earlier, the thermal influences of the Tibetan Plateau were inferred from the presence of a huge upper tropospheric anticyclone above the Plateau in summer (Flohn, 1957) and from the pronounced diurnal variations in the surface meteorological elements along the periphery of the Plateau (Yeh and Gao, 1979).

During winter the Tibetan Plateau is a cold source; it acts as a heat source from March until October. The elevated heat source above the Plateau acts to warm the mid-upper tropospheric air, and the temperature over the Plateau in summer exceeds that over the Indian Ocean (Yanai et al., 1992). This meridional gradient of temperature, appearing in May–June, is crucial for the onset of the South Asian monsoon. Concurrent with the reversal of the temperature gradient, the rain belt associated with the ITCZ over the Indian Ocean suddenly moves onto the Indian subcontinent and reaches the foot of the Himalayas

With the cooling of the Plateau surface the westerly jet stream retreats to the south side of the Plateau in late October; this is just after the end of the southwest monsoon in India and almost concurrent with the commencement of the northeast winter monsoon over southeast India (Matsumoto, 1992).

Y. Xue and M. Yanai

Bibliography

Flohn, H., 1957. Large-scale aspects of the "summer monsoon" in South and East Asia. *Journal of the Meteorological Society of Japan*, **75**: 180–186.

Hamilton, M.G., 1979. *The South Asian Summer Monsoon*. London: Edward Arnold.

Keshavamurty, R.N., and Rao, M.S., 1992. *The Physics of Monsoons.* New Delhi: Allied Publishers.

Kistler, E., Kalnay, E., Collins, W., Saha, S., et al. 1999. The NCEP/NCAR 50-year Reanalysis. *Bulletin of the American Meteorological Society*, **82**: 247–268.

Koteswaram, P., and George, C.A., 1958. On the formation of monsoon depression in the Bay of Bengal. *Indian Journal of Meteorology and Geophysics*, **9**: 9–22.

Li, C., and Yanai, M., 1996. The onset and interannual variability of the Asian summer monsoon in relation to land-sea thermal contrast. *Journal of Climate*, **9**: 358–375.

Lockwood, J.G., 1974. *World Climatology: an Environmental Approach.* London: Edward Arnold.

Matsumoto, J., 1992. The seasonal changes in Asian and Australian regions. *Journal of the Meteorological Society of Japan*, **70**: 257–273.

Martyn, D., 1992. *Climates of the World. Developments in Atmospheric Science*, vol. 18. Amsterdam: Elsevier.

Papadakis, J., 1966. *Climates of the World and their Agricultural Potentialities*. Buenos Aires: Cordoba.

Rao, Y.P., 1981. The climate of the Indian subcontinent. In Takahashi, K., and Arakawa, H., eds., *Climates of Southern and Western Asia.* Amsterdam: Elsevier, pp. 67–117.

Ropelewski, C.F., Janowiak, J.E., and Halpert, M.F., 1985. The analysis and display of real time surface climate data. *Monthly Weather Review,* **113**: 1101–1107.

Webster, P.J., Magana, V., Palmer, T.N., et al. 1998. Monsoons: processes, predictability, and the prospects for prediction. *Journal of Geophysical Research*, **103**(C7): 14,451–14,510.

Xie, P., and Arkin, P.A., 1997. Global precipitation: a 17-year monthly analysis based on gauge observations, satellite estimates and numerical model outputs. *Bulletin of the American Meteorological Society*, **78**: 2539–2558.

Yanai, M., Li, C., and Song, Z., 1992. Seasonal heating of the Tibetan Plateau and its effects on the evolution of the Asian summer monsoon. *Journal of the Meteorological Society of Japan*, **70**: 319–351.

Ye, D. (Yeh, T.C.), and Gao, Y.-X., 1979. *The Meteorology of the Qinghai-Xizang (Tibet) Plateau*. Science Press: Beijing (in Chinese).

Yeh, T.C., Dao, S.Y., and Li, M.T., 1959. The abrupt change of circulation over the northern hemisphere during June and October. *The Atmosphere and the Sea in Motion*. New York: Rockefeller Institute, pp. 249–267.

Cross-references

Asia, Climates of Siberia, Central and East Asia
Asia, Climate of Southwest
Climate Classification
Intertropical Convergence Zone
Monsoons and Monsoon Climate
Tropical and Equatorial Climates

ASIA, CLIMATE OF SOUTHWEST

The region commonly referred to as southwest Asia reaches from the mid-latitudes to the tropics and encompasses a swath of land stretching zonally from the eastern shores of the Mediterranean Sea to the Himalayan Mountains and meridionally from the Caspian Sea to the Arabian Sea (roughly 26°E to 70°E and 12°N to 42°N). In addition, this area includes the Gulf of Aden, the Arabian (Persian) Gulf, and the Red Sea. The

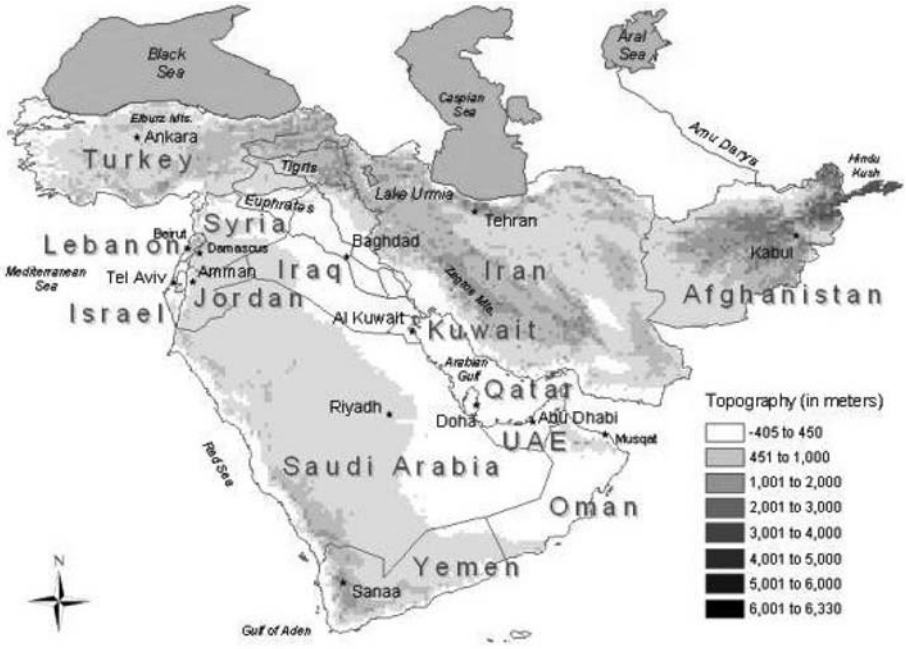

Figure A72 Topographic map of southwest Asia in meters above sea level. Topographic data were provided by the United States Geological Survey (USGS) Land Processes Distributed Active Archive Center (DAAC) established as part of NASA's Earth Observing System (EOS) Data and Information System (EOSDIS) and are available at http://edcdaac.usgs.gov/main.html. GTOPO30 is a global digital elevation model (DEM) with a horizontal grid spacing of 30 arc seconds (approximately 1 kilometer).

countries within this region include: Afghanistan, Bahrain, Iran, Iraq, Israel, Jordan, Kuwait, Lebanon, Oman, Qatar, Saudi Arabia, Syria, Turkey, the United Arab Emirates (UAE) and Yemen (Figure A72).

Location and topography

Southwest Asia is bordered by seven bodies of water: the Mediterranean, the Red, the Arabian, the Caspian and the Black Seas, the Gulf of Aden, and the Arabian (Persian) Gulf. There are three major plateaus:

1. The Iranian Plateau: with the Elburz mountain range bordering it to the north and the Zagros mountain range bordering it to the west.
2. The Anatolian Plateau: with the Septus and Pentus mountain ranges bordering in the north and the Toros mountain range bordering in the south.
3. The plateau of the Arabian Peninsula, which is characterized by a vast desert area including the Arabian, Syrian, and Iranian deserts.

Climatic classification

Southwest Asia is a region of diverse climates and is generally divided into three main climate types: arid, semiarid, and temperate. According to the Köppen classification system, a system of climate classification using latitude band and degree of continentality as its primary forcing factors, Central Asia is a predominantly B-type climate regime. This implies that 70% or more of the annual precipitation falls in the cooler half of the year (October–March in the northern hemisphere). Based on the Köppen–Geiger classification, which factors in seasonal distribution of rainfall and the degree of dryness/coldness of the season, southwest Asia can further be divided into five climatic types (Figure A73). These climatic types are are listed in Table A39.

General circulation

Southwest Asia lies at the boundary of three competing climate regimes. These three systems are: (1) the cold Siberian High in winter over Central Asia, (2) the monsoon Asian Low in summer over India , and (3) eastward propagating secondary low-pressure systems traveling through the Mediterranean and adjacent areas during non-summer seasons. Overall, the climate of northern southwest Asia is governed by extra-tropical synoptic scale disturbances while the climate of southern southwest Asia is governed by smaller-scale seasonal thermodynamics.

Airmasses

Polar continental air (cP)

Polar continental air (cP) is formed over Central Asia in winter and is characterized by extremely low temperatures in a shallow surface layer with a significant inversion reaching to 1500 m. The cP airmasses are stable in their source regions – the central parts of Asia and North Africa – but are modified upon entering southwest Asia. As an example, when cP air enters southwest Asia via the Caspian Sea the surface inversion is destroyed by heating from below, resulting in increased

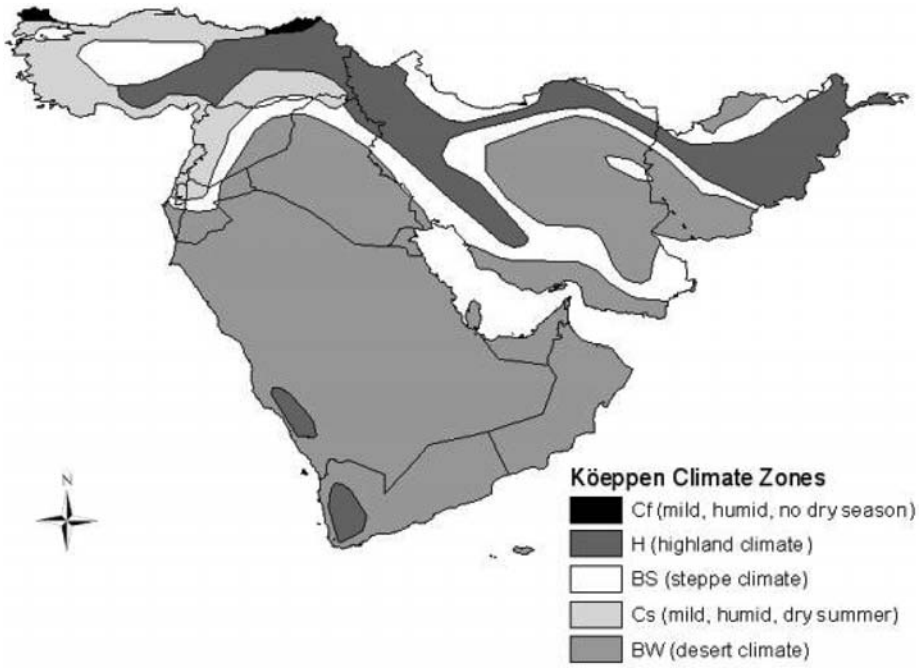

Figure A73 Köppen classification zones for southwest Asia. Köppen data were obtained through the Center for International Development at Harvard University and are available at http://www2.cid.harvard.edu/ciddata/geographydata.htm

Table A39 Köppen–Geiger climatic types for southwest Asia

Type	Winter	Summer	Location
Cs	Temperate, rainy	Hot, dry	Coast of Turkey, Syria, Lebanon and Israel
Cf	Temperate, rainy	Warm, rainy	Interior parts of the Anatolian Plateau
H	Temperate, rainy	Dry	Mountain ranges in southwest Arabian Peninsula
BW	Arid	Arid	Desert areas of Arabian Peninsula, Iran, Syria and Iraq
BS	Semi-arid	0.1/2.9	Arabian Peninsula, Oman, Jordan, Syria, Israel, Iraq and Iran

cloudiness due to the absorption of moisture. The cP airmasses are shifted north of 50°N in summer and hence do not influence the climate of the region.

Tropical maritime (mT)

The source region for tropical maritime (mT) airmasses is the southern portions of the oceans.

Polar maritime air (mP)

In winter polar maritime (mP) airmasses invade the Anatolian Plateau and the Black Sea and tend to be modified because of the long stretches across land. These airmasses tend to be more humid than cP airmasses and they follow the migrating low-pressure systems across Europe – losing most of their moisture upon orographic uplift. The mP airmasses are not present in the summer.

Tropical continental air (cT)

Formed over the dry land areas of central Asia and the African Sahara in summer, late spring, and early fall when surface heating is pronounced, tropical continental (cT) airmasses precede the "khamsin" dust storms occurring in late spring/early fall. These dust storms are very hot and dry and frequently proceed eastward through the Sinai or the northern Red Sea.

The characteristic airmasses of southwest Asia are cP, cT and mP in winter and cT and mT in summer – with each of these airmasses having a different source region.

Winter

The following section describes general climate conditions during the winter season in terms of sea-level pressure, temperature and precipitation. Average winter (December through February; DJF) total precipitation and average winter temperature are presented in Figure A74 and Table A40.

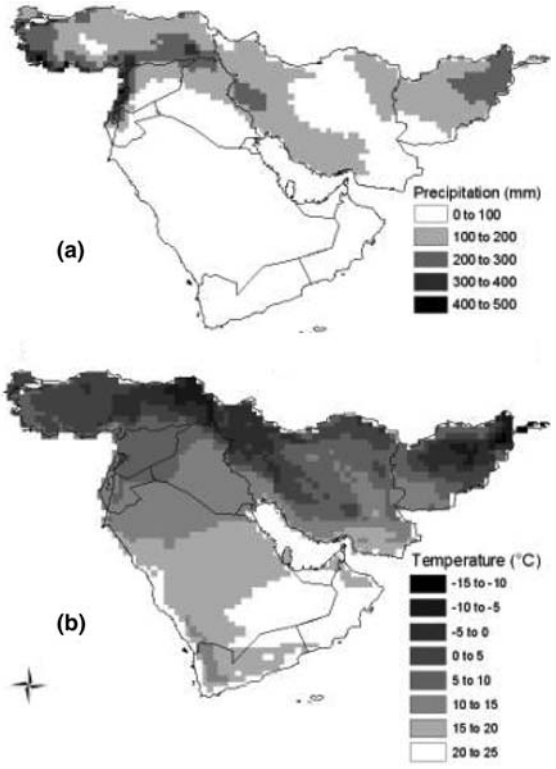

Figure A74 Average total winter precipitation is shown in (**a**) and average winter temperature is shown in (**b**). Monthly temperature and precipitation data (New et al., 2000) have a resolution of 0.5° × 0.5° and are averaged over the period 1901–1998.

Table A40 Mean average temperature (*T*) in °C and total precipitation (*P*) in mm/day for summer and winter (S/W)

Country	*T* (S/W °C)	*P* (S/W mm/day)
Afghanistan	24.1/3.3	0.8/5.9
Bahrain	NA/NA	NA/NA
Iran	27.4/7.4	0.3/3.6
Iraq	31.7/10.8	0.0/3.3
Israel	26.0/13.1	0.1/2.9
Jordan	26.0/10.4	0.1/2.8
Kuwait	35.7/14.7	0.0/1.4
Lebanon	23.9/9.8	0.0/10.1
Oman	29.0/21.4	1.2/1.5
Qatar	35.0/19.0	0.0/1.5
Saudi Arabia	31.7/17.5	0.40/1.0
Syria	27.6/8.0	0.02/4.3
Turkey	20.6/1.6	1.4/6.1
Yemen	26.7/19.3	2.6/1.3

Pressure

The general features of mean sea-level pressure in winter can be summarized as follows:

1. *Siberian and Azores High*: the northern portion of an anticyclonic ridge over the region is an extension of the Siberian High. This ridge results in northeast surface winds over the Black and Caspian Seas. The southern portion is related to the Azores High which extends over the southern half of the Arabian Peninsula and is associated with an easterly current thought to be related to the easterly trade winds or to the northeast monsoons which prevail over India in winter. The intensity of this ridge is directly related to the passage of mid-latitude winter storms entering into the Mediterranean – these will be discussed next.
2. *Mid-latitude storms*: these depressions enter into the Mediterranean from the Atlantic via different tracks. These tracks include (a) northern Spain, (b) southern France, and (c) straits of Gibraltar. Some are secondary low-pressure systems, meaning they further develop upon entering into the Mediterranean – mainly the Gulf of Genoa, over Cyprus and in the Adriatic Sea. Orographic depressions are created on the lee side of the Alps in Switzerland and Atlas Mountains over North Africa. In general the Mediterranean low-pressure systems travel only 20–30 miles inland; however, when these low-pressure systems come in contact with the Caspian Sea and Arabian Gulf they are strengthened and have enough energy to penetrate into Iraq, Iran, and Afghanistan – providing the major source of rain to this region. Overall, it is the Mediterranean depressions which carry most of the precipitation to the northern half of southwest Asia – the area of greatest precipitation being the coastal regions of the Black, Caspian, and Mediterranean Seas.
3. *Subtropical jet*: the 200 mn upper-level winds show an axis of strong westerly winds centered at approximately 23–27°N – this is the subtropical jet. Upper tropospheric divergence around the jet – together with low-level convergence – is considered a major factor in the development of the convective activity in non-summer seasons. The high cloud base and dryness over Saudi Arabia does not allow precipitation to fall to the surface; strong gusts, sandstorms and thunderstorms are observed. Upper tropospheric divergence, coupled with lower-level convergence, is also considered an important precursor for the development and maintenance of small-scale systems such as desert depressions.
4. *Polar jet:* along with the subtropical jet stream, a permanent feature of the upper tropospheric flow pattern in fall, winter, and spring, southwest Asia is also invaded by active branches of the polar jet which is associated with the passage of low-pressure systems generated in the Mediterranean.

Temperature and precipitation

In southwest Asia the precipitation primarily falls from winter storms moving eastward from the Mediterranean, with the high mountains of the region intercepting most of the water and the interior high plains left with large stretches of barren desert. This wintertime precipitation generally occurs between the months of November and April, with the peak between January and March. Much of the precipitation falls as snow in the higher elevations and the timing and amount of snowmelt is an important factor in the irrigated agriculture prevalent in the region.

Summer

The following section describes general climate conditions during the summer season in terms of sea-level pressure, temperature and precipitation. Average summer (June through August; JJA) total precipitation and average summer temperature are presented in Figure A75 and Table A40.

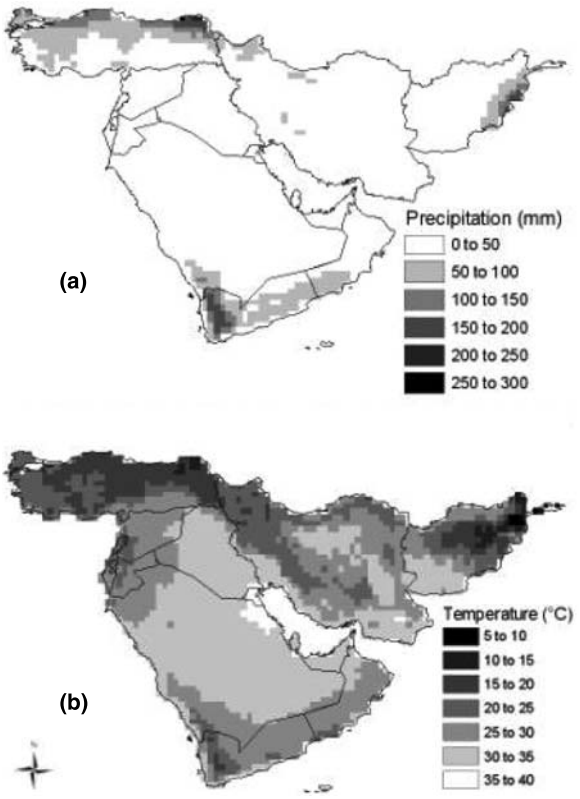

Figure A75 Average total summer (JJA) precipitation is shown in (**a**) and average summer temperature is shown in (**b**). Data used are same as in Figure A24.

Pressure

1. *Indian monsoon*: in summer the western branch of the Asian Low dominates southwest Asia which is approximately centered over 30°N. While appearing essentially fixed in time and space over the Arabian/Persian Gulf in the daily series of SLP, synoptic charts reveal zonal variability in the western branch – sometimes extending all the way into the eastern Mediterranean. During such an event, warm subtropical air will advect over the eastern Mediterranean region resulting in intense heat waves. The basic theory of these summer heat waves relies on the latitudinal elongation of the monsoon low over the Arabian/Persian Gulf or to an overall strengthening of the low.
2. *Quasi-stationary surfaces*: the summer season marks a time of generally stable conditions lacking significant daily variability. This allows for the emergence of quasi-stationary surfaces of separation between two unique air streams; namely the subtropical front and the intertropical front.

Temperature and precipitation

Very little rain falls in most of southwest Asia during the summer season. However, in eastern Pakistan the primary rainfall season is summer, associated with the northernmost advance of the Asian monsoon, which results in a summertime maximum in precipitation in the northern mountain regions of Pakistan but generally suppresses rainfall over Iran and Afghanistan. Dust storms occur throughout the year in the desert high plains. Such storms are prevalent through much of the region in summer, often associated with the "wind of 120 days", the highly persistent winds of the warm season which blow from north to south.

Observational records

Lack of meteorological observations continues to pose a problem for long-term climate monitoring aimed at "clarifying the climate picture", making it difficult to cleanly differentiate between different climatic regimes.

Global warming

According to the Third Assessment Report (Working Group II) of the Intergovernmental Panel on Climate Change continuing emissions of greenhouse gases are likely to result in significant changes in mean climate and its intraseasonal variability in Asia (IPCC, 2001). General circulation models (GCM) suggest that the area-averaged annual mean warming over Asia would reach about 3°C by 2050 and 5°C by 2080. When the cooling effects of sulfate aerosols are added to the models, surface warming is reduced slightly, reaching 2.5°C by 2050 and 4°C by 2080. Seasonally speaking, warming over Asia is expected to be higher during northern hemisphere (NH) winter. Both the annual mean and winter season minimum temperature is expected to rise more than the maximum temperature in Asia, leading to a decrease in the diurnal temperature range (DTR) over these time periods. During summer, however, DTR is expected to increase, suggesting a rise in average summertime maximum temperature. When compared with other regions, the summertime DTR increase is expected to be significantly higher.

All GCM project an enhanced hydrological cycle resulting in rainfall increases over Asia due to continued growth in the emissions of greenhouse gases. A 7% increase is projected by 2050 and an 11% increase is projected by 2080. When the cooling effects of sulfate aerosols are added to the models the projected increase in precipitation is reduced to 3% in 2050 and 7% in 2080. As with temperature, precipitation increases are expected to be greatest during the NH winter. A decline in summer precipitation is expected in southwest Asia. Because this area already receives so little precipitation, severe water-stress conditions resulting in expansion of the deserts are a possibility – when factoring in both the rise in temperature and loss of soil moisture. Increased temperatures can also affect the amount and timing of snowmelt and river flow in southwest Asia. In addition, global warming could affect the role the tropical oceans play in the climate of the region as well as the character of winter storms that currently supply the majority of cold season precipitation.

Overall, southwest Asia appears to be highly vulnerable to anticipated climate change projections. Water stress is expected to be high with significant negative impacts on the agricultural sector. Agricultural productivity in southwest Asia is likely to suffer severe losses due to increases in temperature, soil moisture depletion, and the increased potential for severe drought – ultimately increasing the potential for food insecurity and famine. Adaptation strategies identified for southwest Asia include: (1) transition from conventional crops to intensive greenhouse agriculture, (2) improve conservation of freshwater

supply for times of enhanced water stress, and (3) protect lakes and reservoirs.

Bibliography

CID, 1999. CID Geography Datasets: Köppen–Geiger Climate zones, Center for International Development at Harvard University, Cambridge, MA, USA. Available online at http://www.cid.harvard.edu/cidglobal/economic.htm.

IPCC, 2001. Asia. In McCarthy, J.J., Canziani, O.F., Leary, N.A., Dokken, D.J., and White, K.S., eds., *Climate Change 2001: Impacts, Adaptation, and Vulnerability. Contribution of Working Group II to the Third Assessment Report of the Intergovernmental Panel on Climate Change*. Cambridge, New York: Cambridge University Press.

New, M.G., Hulme, M., and Jones, P.D., 2000. Representing twentieth-century space–time climate variability. Part II: Development of 1901–1996 monthly grids of terrestrial surface climate. *Journal of Climate*, **13**: 2217–2238.

Takahashi, K., and Arakawa, H., 1981. Climate of southern and western Asia. In Landsberg, H.E., ed., *World Survey of Climatology*, vol. 9. Amsterdam: Elsevier, pp. 183–256.

USGS, Global 30 Arc-second Elevation Dataset, Land Processes Distributed Active Archive Center (LPDAAC), EROS Data Center, Sioux Falls, SD, USA. Available online at http://edcdaac.usgs.gov.

Heidi M. Cullen

Cross-references

Airmass Climatology
Asia, Climate of South
Climate Classification
Deserts
Extratropical Cyclones
Mediterranean Climates
Monsoons and Monsoon Climate

ATMOSPHERE

The atmosphere is the envelope of air surrounding the Earth. It consists of a physical mixture of gases and particle matter. Based on its temperature structure, the atmosphere can be divided into several sections. Below about 12 km is the *troposphere*, where the majority of the world's weather occurs and the temperature broadly decreases from about 15°C at the Earth's surface to −54°C at the top. Almost all of the processes of vertical transfer of atmospheric properties through turbulence and mixing occur in the troposphere.

Above the troposphere the temperatures increase to a level of about 50 km, in the region called the *stratosphere*. Here the atmosphere is very stable and contains layers of gaseous and particle matter, mainly of volcanic origin. The troposphere and the stratosphere are separated by the *tropopause*, which is located where temperatures suddenly begin to increase with altitude. Above the stratosphere is the *stratopause*, which separates the stratosphere from the *mesosphere* (48–78 km), where temperatures decrease with altitude again. Above the mesosphere is the *thermosphere* (above 80 km), another stratum in which temperature increases with altitude, where the thin outer layers of the atmosphere are directly interacting with emissions from the sun. Both the mesosphere and thermosphere contain gaseous atoms and ions in very rarefied concentrations.

Table A41 Physical characteristics of the atmosphere at sea level

Descriptor	Value	Units
Pressure	1013.25	hPa
Temperature	283	K
Density	1.29×10^{-3}	g/cm
Molecular weight (dry air)	28.966	—

Table A42 Average dry air composition below 25 km (after Barry and Chorley, 1987)

Gaseous component	Chemical symbol	Percentage volume
Nitrogen	N_2	78.08
Oxygen	O_2	20.94
Argon	A	0.93
Carbon dioxide	CO_2	0.034*
Neon	Ne	0.0018
Helium	He	0.0005
Ozone	O_3	0.00006

* Variable and presently increasing in concentration on a global scale.

Table A41 presents the average physical characteristics of the atmosphere at sea level. This part of the atmosphere is where the greatest interactions with the Earth's surface occur, and is defined as the *boundary* (or *mixing*) *layer*. Above the surface both atmospheric density and pressure decrease logarithmically. Thus, approximately half the mass of the atmosphere is situated below an altitude of 5.6 km, and the pressure at this altitude is about 500 hPa.

The atmosphere itself is not a chemical compound, but contains a wide variety of chemical compounds and individual gas molecules as part of its composition. The composition is not constant, but is highly variable between locations and over time. In terms of content it is dominated by four gases: nitrogen, oxygen, argon, and carbon dioxide, as shown in Table A42. All of these gases are stable in concentration except carbon dioxide and ozone. Carbon dioxide is a major greenhouse gas, and is controversially linked to the rise in global air temperatures over the past century. Ozone occurs naturally as a layer in the stratosphere, between 10 and 50 km and peaking in concentration around 25 km. Its major role is to protect the Earth's surface from harmful ultraviolet radiation from the sun. The ozone layer is threatened by partial destruction as a result of chemical reactions with chlorofluorocarbon emissions from human activities.

The most important gas not included in Table A42 is water vapor. Concentrations range from almost 0% by volume over the driest regions of the Earth (deserts and polar ice caps) to about 4% in the hot tropical regions. A greenhouse gas, water vapor, is an essential part of the hydrologic cycle and is crucial to the maintenance of life on Earth. It is the only compound that can exist naturally in all three states at one location.

The troposphere and lower stratosphere also contain spatially inhomogeneous quantities of particles, dust, and aerosols. Particle matter in the stratosphere originates mainly from volcanic explosions, and through scattering of shortwave radiation may create spectacular sunsets and affect global temperatures for periods of up to 2 years. In the troposphere, particle matter originates from sea spray, windblown surface material, air pollution emissions, and chemical reactions. Particles form

condensation nuclei for clouds, affect visibility through short wave radiation scattering, and are often responsible for pollution episodes in major cities around the globe.

Howard A. Bridgman

Bibliography

Barry, R.G., and Chorley, R.J., 1987. *Atmosphere, Weather and Climate*, 5th edn. London: Methuen.
Goody, R., 1995. *Principles of Atmospheric Physics and Chemistry.* New York: Oxford University Press.
Lutgens, F.K., and Tarbuck, E.J., 2001. *The Atmosphere*, 8th edn. Upper Saddle River, NJ: Prentice-Hall.
Wayne, R.P., 1999. *Chemistry of Atmospheres*, 3rd edn. New York: Van Nostrand.

Cross-references

Aerosols
Air Pollution Climatology
Atmospheric Nomenclature
Greenhouse Effect and Greenhouse Gases
Precipitation

ATMOSPHERIC CIRCULATION, GLOBAL

Global atmospheric circulation consists of the observed wind systems with their annual and seasonal variations, and is the principal factor in determining the distribution of climatic zones, while variations in the atmospheric and oceanic circulations are responsible for many of the observed longer-term fluctuations in climate. The two major controls on the global wind circulation are inequalities in radiation distribution over the Earth's surface and the Earth's rotation. Global radiation distribution, together with gravity, drives the global atmospheric circulation, whereas the Earth's rotation determines its shape. Basically, the mean surface circulation consists of easterly winds with equatorial components in the tropics and westerly winds with poleward components in middle latitudes, the corresponding meridional flows aloft being reversed. Weak surface easterlies are observed in polar regions, and extensive areas of calms in the equatorial and also the subtropical regions. Strong, westerly winds are found in the upper troposphere poleward of about 25°N and 25°S.

Causes of the global atmospheric circulation

Radiation distribution

The planet Earth receives energy from the sun in the form of short-wave radiation, while radiating an equal amount of heat to space in the form of longwave radiation. This balance of heat gain equaling heat loss applies only to the planet as a whole over several annual periods; it does not apply to any specific area for short periods of time. The equatorial region absorbs more radiation than it loses, while the polar regions radiate more heat than they receive. (The distribution of radiation over the Earth's surface is reviewed by Lockwood, 1979, 1985.) However, the equatorial belt does not become warmer during the year, nor do the poles become colder. This is because heat flows from the warm regions to the cold regions, maintaining the observed temperatures. An exchange of heat is brought about by the fluid motions in the atmosphere and oceans, thus forming the observed circulation of the atmosphere and oceans.

If the Earth's surface were homogeneous, and the planet was not rotating, the imposition of a theoretical latitudinal (north-south) heating gradient, with cold poles and a warm equator, would probably result in a single circulation cell in each hemisphere with an upward limb at the equator and downward limbs at the poles. Such cells would be energetically direct cells because they result from a direct transformation of potential to kinetic energy. They are often referred to as Hadley cells in tribute to the eighteenth-century scientist who first suggested their possible existence. In reality, on an Earth with one face always toward the sun, the equatorial segment of the sunward face would be extremely hot and the dark face extremely cold. The temperature gradient would be from the daylight to the dark face, not from equator to pole, with a corresponding circulation cell between the two faces. The Earth's rotation smears the region of strong solar tropical heating zonally around the whole globe and generates the observed equator – polar temperature gradients.

The Earth's rotation

The real Earth rotates, and this makes the existence of simple Hadley cells extending from equator to pole impossible, since the rotation generates east–west motions in the atmosphere. To an observer on the rotating Earth it appears as if a force is acting on moving air particles that causes them to be deflected from their original path, and this apparent force-per-unit mass is termed the Coriolis force. The Coriolis force turns the wind to the right in the northern hemisphere and to the left in the southern hemisphere. Therefore, in the northern hemisphere, the upper poleward current of the Hadley cell assumes a strong eastward component (westerly wind) and the lower equatorial current assumes a westward component (easterly wind). For a given heating gradient the turning of the wind tends to reduce the efficiency with which a single cell can transport heat poleward. For a sufficiently large rotation rate a balance cannot be maintained, and the imposed latitudinally dependent heating would cause the meridional temperature gradient to increase with time, while remaining circularly symmetric about the pole. However, there comes a time when small meridional displacements of a suitable east–west size can become dynamically unstable and grow, the process being an example of baroclinic instability.

Baroclinic instability

The growth of these wave disturbances under baroclinic instability is characterized by the ascent of warmer airmasses and descent of colder airmasses, causing a decrease of potential energy and an associated release of kinetic energy. Potential temperature increases with height; thus this ascent and descent of airmasses takes place in a manner described by the term slantwise convection. In the normal atmosphere equal potential temperature (isentropic) surfaces slope upward from lower to higher latitudes, and in slantwise convection the trajectories of individual air particles are tilted at an angle to the horizontal that is comparable with, but less than, the slope of the isentropic

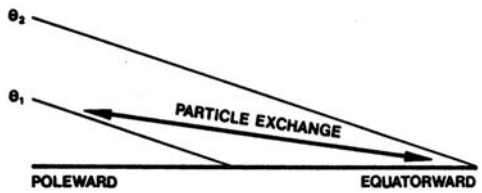

Figure A76 Height–latitude cross-section of the troposphere showing potential temperature θ increasing equatorward and upward. The system is stable for vertical convection, but energy can be released if particles are exchanged by slantwise convection along the thick solid arrow.

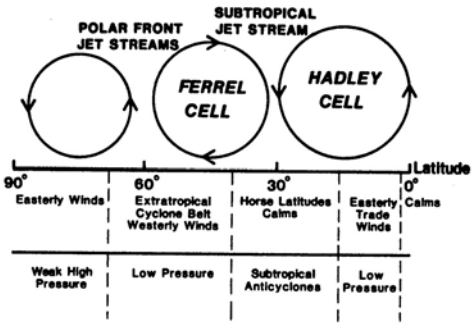

Figure A77 A schematic representation of the mean meridional circulation of the northern hemisphere.

surfaces (Figure A76). Therefore, while an air parcel may be prevented from rising vertically because the prevailing lapse rate is less than the appropriate adiabatic lapse rate, poleward travel brings it to an environment more dense than itself, enabling it to rise. Air at higher levels and higher latitudes may similarly descend by equatorward movement. Further details may be found in Lorenz (1967), Barry and Carleton (2001), and Houghton (2002).

Mean global atmospheric circulation

Mean meridional circulation

Disturbances with the dimensions of about five to eight waves about the pole will grow fastest under baroclinic instability. At the surface, anticyclones in this size range that develop will grow and ultimately move equatorward, finding final residence in the subtropics. Similarly, surface low-pressure systems develop and move poleward. The resultant mean meridional circulation is no longer simple. The single equator-to-pole direct cell postulated by Hadley to exist if the Earth did not rotate is contracted equatorward, so that the poleward descending limb coincides with the axis of the surface subtropical anticyclones (Figure A77). In the tropics baroclinic instability is virtually non-existent because of the weak Coriolis force, so that direct mean meridional circulation (the Hadley cell) is still the most efficient means for effecting a poleward heat transfer. In mid-latitudes unstable wave motion is the most efficient means for poleward heat transfer. An energetically weak indirect mean meridional circulation, known as the Ferrel cell, exists in middle latitudes.

Subtropical jet streams

A schematic representation of the mean meridional circulation in the northern hemisphere during winter is shown in Figure A77. The simple Hadley cell circulation is clearly seen south of 30°N. Eastward angular momentum is transported from the equatorial latitudes to the middle latitudes by nearly horizontal eddies, 1000 km or more across, moving in the upper troposphere and lower stratosphere. Such a transport, together with the dynamics of the middle latitude atmosphere, leads to an accumulation of eastward momentum between 30° and 40° latitude, where a strong meandering current of air, generally known as the subtropical westerly jet stream, develops. The cores of the subtropical westerly jet streams in both hemispheres and throughout the year occur at an altitude of about 12 km. The air subsiding from the jet streams forms subtropical anticyclones. More momentum than is necessary to maintain subtropical jet streams against dissipation through internal friction is transported to these zones of strong winds. The excess is transported downward to maintain the eastward-flowing surface winds of the middle latitudes against ground friction. The supply of eastward momentum to the Earth's surface in middle latitudes tends to speed up the Earth's rotation. Counteracting such potential speeding-up of the Earth's rotation, air flows from the subtropical anticyclones toward the equatorial regions, forming the so-called trade winds. The trade winds, with a strong component directed toward the west, tend to retard the Earth's rotation, and in turn gain eastward momentum.

Mean surface winds

An idealized mean surface wind circulation with associated pressure distribution, as shown in Figure A78, may be described as follows:

1. The equatorial trough. A shallow belt of low pressure on or near the equator with light or variable winds.
2. The trade winds. Between the equatorial trough and latitudes 30°N and 30°S are northeast winds in the northern hemisphere and southeast winds in the southern hemisphere.
3. The subtropical anticyclones. Ridges of high pressure between about latitudes 30–40°N and S, associated with light, variable winds.
4. The westerlies. Belts of generally westerly winds, southwest in the northern hemisphere and northwest in the southern hemisphere, between about latitudes 40–60°N and S.
5. The temperate latitude low-pressure systems. Variable winds converging into low-pressure belts at about 60°N and 60°S, the subpolar low-pressure area.
6. The polar anticyclones. Regions of outflowing winds with an easterly component, diverging from weak high-pressure systems near the poles.

Further detailed descriptions of mean atmospheric circulation patterns may be found in the textbooks listed in the Bibliography.

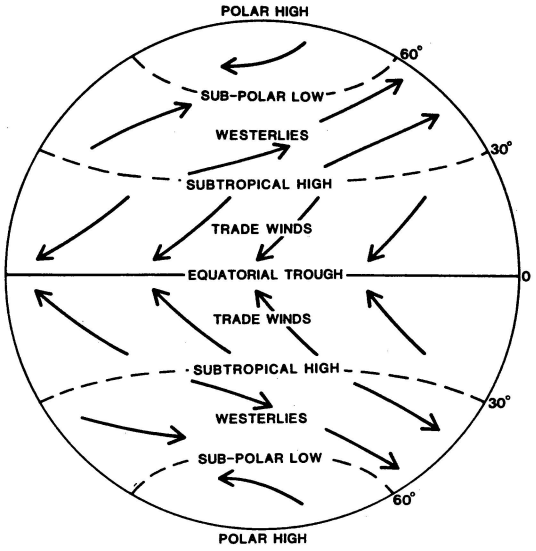

Figure A78 Idealized mean surface wind circulation.

Tropical circulation patterns

The mean surface winds in the tropics are directed predominantly toward the equator within latitudes 30°N and 30°S. Such motions can persist only if some force accelerates the air in that direction, and the only force in the atmosphere known to produce accelerations of large-scale windfields is the pressure force. Therefore, high pressure must exist in the subtropics and low pressure in the equatorial zone, with the resulting pressure gradients driving the mean winds. The average latitude of the equatorial low-pressure trough is about 5°S in the northern winter and 15°N in the southern winter. The annual mean latitude is about 5°N, so the meteorological southern hemisphere is larger than the northern hemisphere. This is largely a result of the differing ocean/continent configurations of the hemispheres (McGregor and Nieuwolt, 1998).

The trade winds

Between the equatorial low-pressure trough and the subtropical high-pressure belt lie two belts of tropical easterlies, each with an equatorial meridional flow. These wind systems are known as the northeast trade winds in the northern hemisphere and the southeast trade winds in the southern hemisphere. There tends to be a certain monotony about the weather of the trade winds since their extreme steadiness reflects the permanence of the subtropical anticyclones, which are inclined to be the most intense in winter, making the trade winds strongest in winter and weakest in summer. Figure A79 shows that all tropical oceans except the northern Indian Ocean have extensive areas of trade winds. Each trade wind region contains definite centers of resultant high wind speed that reach 6–8 m/s. In contrast, wind speeds are low in the subtropics and in the equatorial trough zone. According to Riehl (1979), when wind speed is averaged without regard to direction, an almost uniform value of 7 m/s appears everywhere except within the equatorial trough.

During the summer of 1856 an expedition under the direction of C. Piazzi-Smyth visited the island of Tenerife in the Canary Islands to make astronomical observations from the top of the Peak of Tenerife. On two of the journeys up and down the 3000 m mountain, Piazzi-Smyth carefully measured the temperature, moisture content, direction, and speed of the local trade winds. He found that an inversion was often present, and that it was not located at the top of the northeast trade regime, but was situated in the middle of the current; thus, it could not be explained as a boundary between two airstreams from different directions. He also noticed that the top of the cloud layer corresponded to the base of the inversion. These observations by Piazzi-Smyth have been confirmed many times and the trade-wind inversion is now known to be of great importance in the meteorology of the tropics. Broad-scale subsidence in the subtropical anticyclones is the main cause of the very dry air above the trade-wind inversion. The subsiding air normally meets a surface stream of relatively cool maritime air flowing toward the equator. The inversion forms at the meeting point of these two airstreams, both of which flow in the same direction, and the height of the inversion base is a measure of the depth to which the upper current has been able to penetrate downward.

Subsidence is most marked at the eastern ends of the subtropical anticyclonic cells; that is to say, along the desert cold-water coasts of the western edges of North and South America and Africa, and it is here that the trade-wind inversion is at its lowest. Normally, as the trade winds approach the equator, the trade inversion increases in altitude and conditions become less arid. Over the oceans the intense tropical radiation evaporates water that is carried aloft by thermals and eventually distributed throughout the layer below the trade inversion. The result is that the layer below the inversion becomes more moist as the trade wind nears the equator and the continual convection in the cool layer forces the trade inversion to rise in height.

The equatorial trough

Trade winds from the northern and southern hemispheres meet in the equatorial trough, a shallow trough of low pressure generally situated near the equator. Its position is clear-cut in January (except in the central South Pacific), and in July the trough can be located with ease over Africa, the Atlantic, and the Pacific to about 150°E. The equatorial trough shows a marked tendency to meander with longitude; in January it ranges from 17°S to 8°N, in July from 2°N to 27°N. This is largely the result of wide oscillations in the monsoon regions that cover the whole of southern Asia and North Africa in the northern summer, and southern Africa and Australia in the southern summer. The excursions into the southern hemisphere are smaller than those into the northern hemisphere, because the more constant westerly circulation of the southern hemisphere's middle latitudes constrains the equatorial trough to near the equator. Over southern Asia and the Indian Ocean the mean seasonal positions are around 15°N and 5°S, a difference of 20° latitude. In contrast, the trough is quasistationary over the oceanic half of the Pacific and Atlantic, where seasonal displacement is restricted to 5° latitude or less. Winds in the equatorial trough generally are calm or light easterly. Over some areas, such as the Indian

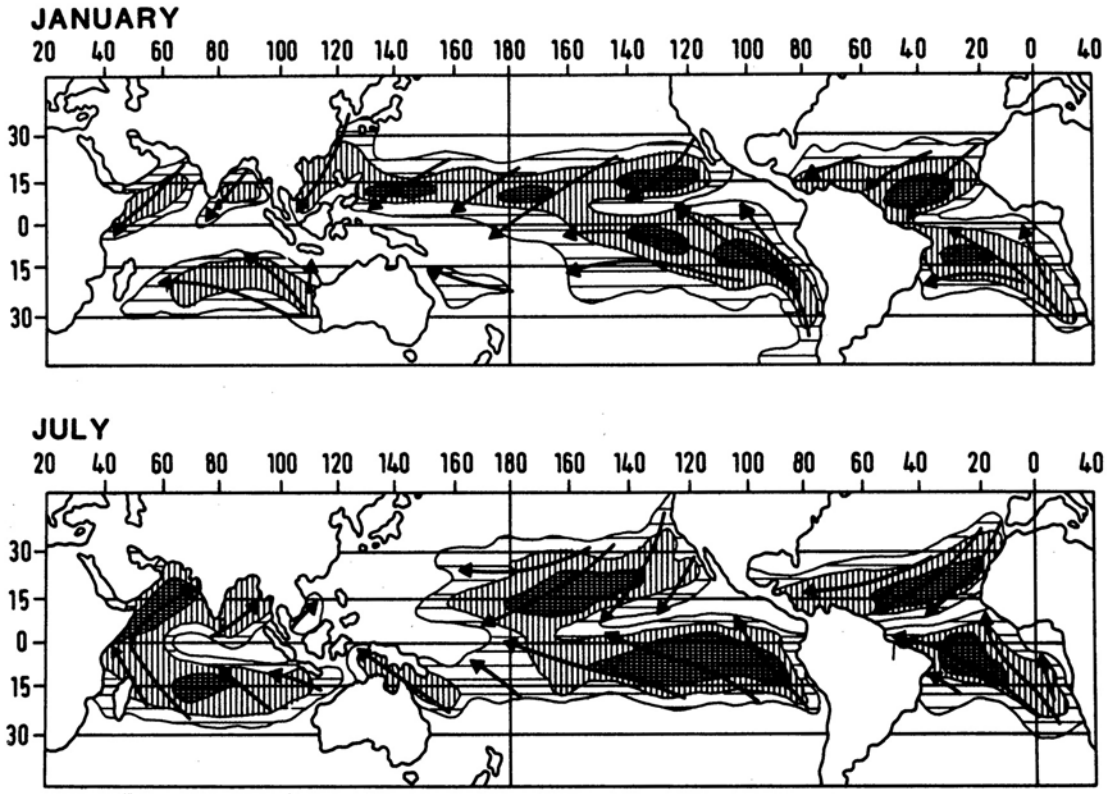

Figure A79 The trade-wind systems of the world in January and July. The isopleths are in terms of relative constancy of wind direction and enclose shaded areas where 50%, 70%, and 90% of all winds blow from the predominant quadrant with Beaufort force 3 or more (over 3.4 m/s) (after Crowe, 1971).

Ocean and Southeast Asia, the structure of the trough is complex and westerlies may be found.

The Walker circulation and the Southern Oscillation

Dietrich and Kalle (1957) have mapped the difference between the sea-surface temperature and its average value along the part of each latitude circle situated over the oceans. If cold-water regions are defined as ocean areas with sea surface temperatures below the latitudinal average, by far the most extensive cold-water area is the South Pacific cold water stretching about 85° westward from the coast of South America. In contrast the South Atlantic cold water continues westward from the coast of Africa by only about 40° longitude.

Bjerknes (1969) believes that when the Pacific cold ocean water along the equator is well developed, the air above will be too cold to take part in the ascending motion of the Hadley cell circulation. Instead, the equatorial air flows westward between the Hadley cell circulations of the two hemispheres to the warm western Pacific, where, having been heated and supplied with moisture from the warmer waters, the equatorial air can take part in large-scale, moist adiabatic ascent. In Indonesia huge cloud clusters with a diameter of more than 600 m develop each day, giving an area-averaged rainfall of around 2200 mm per year. This is equivalent to a release of latent heat of about 170 $W m^{-2}$, much more than the net radiation near the surface. The resulting thermally driven

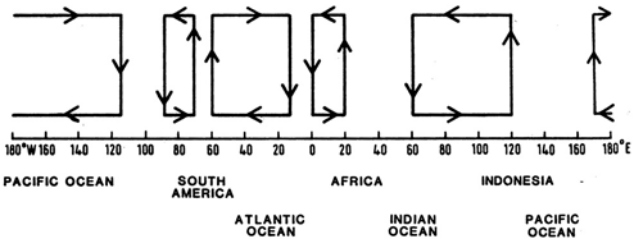

Figure A80 Schematic representation of the Walker circulation near the equator during the northern winter.

circulation (Figure A80) between an equatorial heat center – the maritime continent of Indonesia – and a cooling area in the eastern Pacific is often known as a Walker circulation. As shown in Figure A80, the equatorial Atlantic is analogous to the equatorial Pacific in that the warmest part is in the west, at the coast of Brazil. West–east contrasts of water temperature in the Atlantic are much smaller than in the Pacific, so the potential for a Walker-type circulation is less. Nevertheless, in January a thermally driven Walker circulation may operate from the Gulf of Guinea to the Andes, with the axes of the circulation near the mouth of the Amazon.

Sir Gilbert Walker described in his papers in the 1920s and 1930s what he named the Southern Oscillation. The Southern Oscillation is dominated by an exchange of air between the Southeast Pacific subtropical high and the Indonesian equatorial low, with a period that varies between roughly 1 and 5 years. The Southern Oscillation may be defined in terms of the difference in sea level pressure between Darwin, Australia and Tahiti. Records are available, with the exception of a few years and occasional months, from the late 1800s. During one phase of this oscillation the trade winds are intense and converge into the warm western tropical Pacific, where rainfall is plentiful and sea-level pressures low. At such times the atmosphere over the eastern tropical Pacific is cold and dry. During the complementary phase the trade winds relax, the zone of warm surface waters and heavy precipitation shifts eastward, and sea-level pressure rises in the west while it falls in the east. The latter phase is the more unusual and in the eastern Pacific has become known as El Niño, while vigorous episodes of the former are often termed La Niña. The combined atmospheric/oceanic conditions that give rise to these changes in rainfall across the Pacific and neighbouring areas are referred to as El Niño Southern Oscillation (ENSO) events. The El Niño phenomena are associated with extreme negative Southern Oscillation values, but for much of the time the series exhibits continuous transitions from high to low values with most values being positive. ENSO is important climatologically (Glantz, 1996; Diaz et al., 2001) for two main reasons. First, it is one of the most striking examples of interannual climatic variability on an almost global scale. Secondly, in the Pacific it is associated with considerable fluctuations in rainfall and sea surface temperature, and also with extreme weather events around the world.

Monsoon climates of southern Asia

Originally the term monsoon was applied to the surface winds of southern Asia that reverse between winter and summer, but the word is now used for many different types of phenomena, such as the stratospheric monsoon, the European monsoon, etc. The "classic" characteristics of a monsoon climate are mainly to be found in the Indian subcontinent, where over much of the region the annual changes may conveniently be divided as follows:

1. The season of the northeast monsoon:
   (a) January and February, winter season
   (b) March to May, hot weather season.
2. The season of the southwest monsoon:
   (a) June to September, season of general rains
   (b) October to December, postmonsoon season.

Halley proposed the first explanation of the Asiatic monsoon in a memoir presented to the Royal Society in 1686. His theory is general and can be applied to all continental regions, not only Asia. During winter intense cooling over the cold continents leads to the establishment of thermal high-pressure systems, while pressure remains relatively low in the warmer, lighter air over the oceans. The surface air flow therefore has a component from the highs over the land toward the lows over the ocean. During summer the land is warmer than the sea and a reverse current circulates from the relatively cool sea toward the heated land. The average sea-level pressure charts for the two extreme seasons show a reversal of pressure over Asia and its maritime surroundings. In winter the Siberian anticyclone accumulates subzero masses of air (−40°C to −60°C) at an equivalent mean sea-level pressure of between 1040 and 1060 mb, while in summer the torrid heat (about 40°C) reduces the pressure to 950 mb over northwest India. Modern explanations of the Indian monsoon are much more complex (see Lockwood, 1974; Lighthill and Pearce, 1981; Pant and Rupa Kumar, 1997), but follow the basic idea of Halley.

According to Miller and Keshavamurthy (1968), the southwest monsoon current in the lower 5 km near India consists of two main branches; the Bay of Bengal branch, influencing the weather over the northeastern part of India and Burma, and the Arabian Sea branch, dominating the weather over the western, central, and northwestern parts of India. The low-level flow across the equator during the southwest monsoon is not evenly distributed between latitudes 40°E and 80°E as was previously thought, but has been found by Findlater (1969, 1972) to take the form of low-level, high-speed southerly currents that are concentrated between about 38°E and 55°E. A particularly important feature of this flow is the strong southerly current with a mean wind speed of about 14 m/s, observed at the equator over eastern Africa from April to October. The strongest flow occurs near the 1.5 km level, but it often increases to more than 25 m/s and occasionally to more than 45 m/s at heights between 1.2 km and 2.4 km. According to Findlater this high-speed current flows intermittently during the southwest monsoon from the vicinity of Mauritius through Madagascar, Kenya, eastern Ethiopia, Somalia, and then across the Indian Ocean toward India.

When upper winds are taken into account, the Asian monsoon is a fairly complex system (Pant and Rupa Kumar, 1997). During the northern winter season (Figure A81), the subtropical

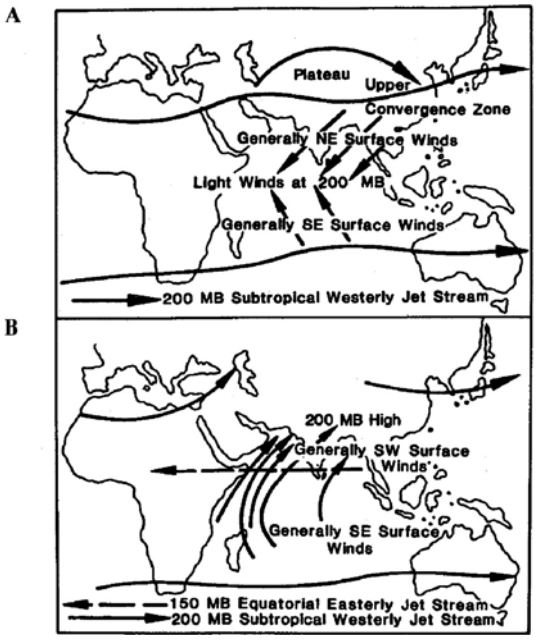

Figure A81 Schematic illustration of the major features of the Asian monsoon. **A:** northern winter; **B:** northern summer (after Lockwood, 1985).

westerly jet stream lies over southern Asia, with its core located at about 12 km altitude. It divides in the region of the Tibetan Plateau, with one branch flowing to the north of the plateau, and the other to the south. The two branches merge to the east of the plateau and form an immense upper convergence zone over China. In May and June the subtropical jet stream over northern India slowly weakens and disintegrates, causing the main westerly flow to move north into central Asia. While this is occurring, an easterly jet stream, mainly at about 14 km, builds up over the equatorial Indian Ocean and expands westward into Africa. The formation of the equatorial easterly jet stream is connected with the formation of an upper-level, high-pressure system over Tibet. In October the reverse process occurs; the equatorial easterly jet stream and the Tibetan high disintegrate, while the subtropical westerly jet stream reforms over northern India.

Middle and high latitude circulation patterns

The greatest atmospheric variability occurs in middle latitudes, from approximately 40–70°N and S, where large areas of the Earth's surface are affected by a succession of cyclones (depressions) and anticyclones or ridges. This is a region of strong thermal gradients with vigorous westerlies in the upper air, culminating in the polar-front jet stream near the base of the stratosphere. The zone of westerlies is permanently unstable and gives rise to a continuous stream of large-scale eddies near the surface, the cyclonic eddies moving poleward and the anticyclonic ones equatorward.

Compared to the Hadley cells, the middle-latitude atmosphere is highly disturbed and the suggested meridional circulation in Figure A77 is largely schematic. At the surface the predominant features are closed cyclonic and anticyclonic systems of irregular shape, while higher up, smooth wave-shaped patterns are the general rule. The dimensions of these upper waves are much larger than those of the surface cyclones and anticyclones which have dimensions of 1000–3000 km, and only rarely is there a one-to-one correspondence. In typical cases there are four or five major waves around the hemisphere, and superimposed on these are smaller waves that travel through the slowly moving train of larger waves. The major waves are called long waves or Rossby waves, after Rossby (1939, 1940, 1945), who first investigated their principal properties. These upper Rossby waves are important because they strongly influence the formation and subsequent evolution of the closed surface synoptic features.

Analyses of long time-series of climatogical data reveal large-scale correlations between fluctuations at remote locations. These fluctuations occur at the low frequency range of timescales, and they are called "teleconnections" to stress the correlation-at-a-distance aspect of their nature. The term "teleconnection" was introduced by Ångstrom (1935) in the context of patterns of climatic fluctuations; Bjerknes (1969) and Namias (1963, 1969) later used it to describe patterns of atmospheric responses to a remote surface forcing. Some teleconnections arise simply from natural preferred modes of the atmosphere associated with the mean climate state and the land–sea distribution, while several such as ENSO and the North Atlantic Oscillation are directly linked to sea surface changes.

In a simple atmosphere Rossby waves could arise anywhere in the middle latitude atmosphere, as is observed in the predominantly ocean-covered southern temperate latitudes. In contrast the northern temperate latitude Rossby waves tend to be locked in certain preferred locations. These preferred locations arise because the atmospheric circulation is influenced not only by the differing thermal properties of land and sea, but also by high mountain ranges and highlands in general. Influences on the propagation of Rossby waves through the atmosphere include zonal temperature asymmetries, transient synoptic weather systems and baroclinic effects.

Atmospheric thermal patterns

The basic thermal pattern of the lower half of the atmosphere in the temperate latitudes is partly controlled by prevailing mean surface temperatures. The mean thermal pattern may be usefully investigated by using the concept of thickness lines. The thickness of an atmospheric layer bounded by two fixed-pressure surfaces, 1000 mb and 500 mb, for example, is directly proportional to the mean temperature of the layer. Thus, low thickness values correspond to cold air and high thickness values to warm air. The geostrophic wind velocity at 500 mb is the vector sum of the 1000 mb geostrophic wind and the theoretical wind vector (the thermal wind) that blows parallel to the 1000–500-mb thickness lines with a velocity proportional to their gradient. This theoretical wind is known as the thermal wind and is shown in Figure A82.

The thermal wind is directed along the mean isotherms with lower temperature to the left in the northern hemisphere. Thus, in temperate latitudes the thermal wind will be westerly, and, since north–south horizontal temperature gradients are relatively steep, it will be strong. The upper winds are the vector sum of a rather weak surface wind field and a vigorous thermal wind field. This implies that, in the lower middle-latitude troposphere, winds will become increasingly westerly with altitude and that the upper wind field is strongly controlled by the thermal wind. Therefore, a parallel exists between the mean topography of the 500-mb level and the mean 1000–500-mb thickness patterns.

The mean January thickness patterns for the northern hemisphere show two dominant troughs near the eastern extremities of the two continental landmasses, while ridges lie over the eastern parts of the oceans. A third weak trough extends from northern Siberia to the eastern Mediterranean. Climatologically, the positions of the main troughs may be associated with cold air over the winter landmasses, and the positions of the ridges with relatively warm sea surfaces. As seen from Figure A83, the mean January 500-mb wind field, and therefore the mean Rossby wave locations, is similar to the thickness field.

In July the mean ridge in the thickness pattern found in January over the Pacific has moved about 25°W, and now lies over the warm North American continent, while there is a definite trough over the eastern Pacific. Patterns elsewhere are less marked, but a weak trough does appear over Europe, and may

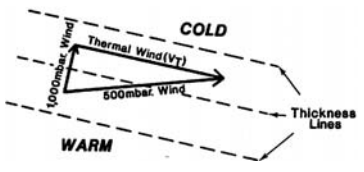

Figure A82 Definition of thermal wind. The thermal wind (VT) is the vector difference between the 1000-mb wind and the 500-mb wind.

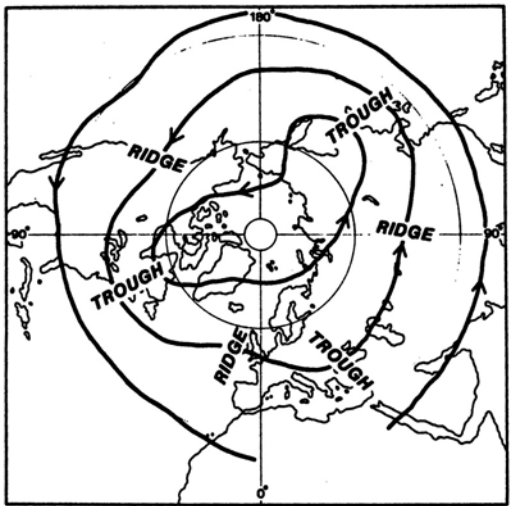

Figure A83 Selected mean contours of the 500-mb surface (about 5.5 km) in January. The upper winds blow along the contour lines.

perhaps be connected with the coolness of the North, Baltic, Mediterranean, and Black seas.

North Atlantic Oscillation

A major source of interannual variability in the atmospheric circulation over the North Atlantic and western Europe is the so-called North Atlantic Oscillation (NOA), which is associated with changes in the strength of the oceanic surface westerlies (Marshall et al., 2001). Its influence extends across much of the North Atlantic and well into Europe, and it is usually defined through the regional sea-level pressure field, although it is readily apparent in mid-troposphere height fields. The NAO's amplitude and phase vary over a range of time scales from intraseasonal to inter-decadal. The NAO is profoundly linked to the leading mode of variability of the whole northern hemisphere circulation, the annular mode or Arctic Oscillation. This suggests that Atlantic effects are more far-reaching and significant than previously thought (Marshall et al., 2001).

The NAO is often indexed by the standardized difference of December to February sea-level atmospheric pressure between Ponta Delgado, Azores (37.8°N, 25.5°W) or Lisbon, Portugal (38.8°N, 9.1°W) and Stkkisholmur, Iceland (65.18°N, 22.7°W) (Hurrell, 1995). Statistical analysis reveals that the NAO is the dominant mode of variability of the surface atmospheric circulation in the Atlantic and accounts for more than 36% of the variance of the mean December to March sea-level pressure field over the region from 20° to 80°N and 90°W to 40°E, during 1899 through to 1994. Marked differences are observed between winters with high and low values of the NAO. Typically, when the index is high the Icelandic low is strong, which increases the influence of cold Arctic airmasses on the northeastern seaboard of North America and enhances westerlies carrying warmer, moister airmasses into western Europe (Hurrell, 1995). During high NAO winters the westerlies directed onto northern Britain and southern Scandinavia are over 8 m/s stronger than during low NAO winters, with higher than normal pressures south of 55°N and a broad region of anomalously low pressure across the Arctic. In winter, western Europe has a negative radiation balance and mild temperature levels are maintained by the advection of warm air from the Atlantic. Thus strong westerlies are associated with anomalously warm winters, weak westerlies with anomalously cold winters, and NAO anomalies are related to downstream wintertime temperature and precipitation anomalies across Europe, Russia and Siberia (Hurrell, 1995; Hurrell and van Loon, 1996).

Overlying the interannual variability there have been four main phases of the NAO index during the historical record: prior to the 1900s the index was close to zero; between 1900 and 1930 strong positive anomalies were evident; between the 1930s and 1960s the index was low; and since the 1980s the index has been strongly positive. The recent persistent high positive phase of the NAO index, extending from about 1973 to 1995, is the most persistent and highest of the historical record. During each positive phase higher than normal winter temperatures prevail over much of Europe, culminating in the unprecedented strongly positive NAO index values and mild winters of 1989 and 1990. During high NAO index winters drier conditions also prevail over much of central and southern Europe and the Mediterranean, whilst enhanced rainfall occurs over the northwestern European seaboard (Hurrell, 1995).

Pacific atmospheric circulation oscillations

Interannual climate variability over the Pacific Ocean is dominated by ENSO (Salinger et al., 2001). This has the strongest SST signals of one sign along the equator over the central and eastern Pacific and a boomerang-shaped pattern of weaker SST signals of opposite sign extending over the middle latitudes of both hemispheres in the north and south Pacific. Salinger et al., (2001) comment that recently "ENSO-like" features in the climate system that operate on decadal to multidecadal time scales have been identified.

A recently identified pattern of longer-term variability is the Pacific Decadal oscillation (PDO) described by Mantua et al. (1997), which may be defined in terms of changes in Pacific sea-surface temperature north of 20°N latitude. Like the warm El Niño phase of ENSO, the warm or positive phase of PDO warms the Pacific near the equator and cools it at northern mid-latitudes; but unlike ENSO, PDO effects are stronger in the central and northern Pacific than near the equator, and it has an irregular period of several decades. It has been found that, during epochs in which the PDO is in its positive polarity, coastal central Alaska tends to experience an enhanced cyclonic flow of warm moist air which is consistent with heavier than normal precipitation. In these winters the mid-latitude depression track tends to split, with one branch carrying storms south to California and the other north to Alaska. The PDO was in its cool or negative phase from the first sea-surface temperature records in 1900 until 1925, then in warm or positive phase until 1945, cool again until 1977, and in warm phase until the 1990s.

An Inter-decadal Pacific Oscillation (IPO) has also been described by Power et al. (1998, 1999) and Folland et al. (1999), the time-series of which is broadly similar to the inter-decadal part of the North Pacific PDO index of Mantua et al. (1997). When the IPO is in a positive phase, SST over a large area of the southwest Pacific is cold, as is SST over the extra-tropical northwest Pacific. SST over the central tropical Pacific is warm, but unlike the ENSO situation it is less obviously warm over the equatorial far eastern Pacific. Also in contrast to

ENSO, warmth extends into the tropical west Pacific. Like the PDO the IPO shows three major phases this century: positive from 1922 to 1946 and from 1978 to at least 1998, with a negative phase between 1947 and 1976. A general reduction in sea-level pressure over the extra-tropical North Pacific Ocean during the winter (November to March) after about 1976 has been particularly evident. This appears as a deeper-than-normal Aleutian low-pressure system, accompanied by stronger-than-normal westerly winds across the central North Pacific and enhanced southerly to southwesterly flow along the west coast of North America.

Polar regions

Both polar regions are located in areas of general atmospheric subsidence, though the climate is not particularly anticyclonic; nor are the winds necessarily easterly. The moisture content of the air is low because of the intense cold, and horizontal thermal gradients are normally weak, with the result that energy sources for major atmospheric disturbances do not exist and are rarely observed. Vowinckel and Orvig (1970) suggest that the Arctic atmosphere can be defined as the hemispheric cap of fairly low kinetic energy circulation lying north of the main course of the planetary westerlies, which places it roughly north of 70°N. The situation over the south polar regions is more complex and the boundary of the Antarctic is not so clear.

John G. Lockwood

Bibliography

Ångstrom, A., 1935. Teleconnections of climate changes in present time. *Geography Annals*, **17**: 242–258.

Barry, R.G., and Carleton, A.M., 2001. *Synoptic and Dynamic Climatology*. London: Routledge.

Barry, R.G., and Chorley, R.J., 1976. *Atmosphere, Weather and Climate*. London: Methuen.

Berlage, H.P., 1966. The southern oscillation and world weather. *K. Meteorol. Inst.* (The Hague) Med. Verhand., **88**: 134.

Bjerknes, J., 1969. Atmospheric teleconnections from the equatorial Pacific. *Monthly Weather Review*, **97**: 163–72.

Corby, G.A., 1970. *The Global Circulation of the Atmosphere*. London: Royal Meteorological Society.

Crowe, P.R., 1971. *Concepts in Climatology*. London: Longman.

Diaz, H.F., Hoerling, M.P., and Eischeid, J.K., 2001. ENSO variability, teleconnections and climate change. *International Journal of Climatology*, **21**: 1845–1862.

Dietrich, G., and Kalle, K., 1957. *Allgemeine Meereskunde*. Berlin: Gebruder Borntraeger.

Findlater, J., 1969. A major low-level air current near the Indian Ocean during the northern summer. *Quarterly Journal of the Royal Meteorological Society*, **95**: 362–380.

Findlater, J., 1972. Aerial explorations of the low-level cross-equatorial current over eastern Africa. *Quarterly Journal of the Royal Meteorological Society*, **98**: 274–289.

Folland, C.K., Parker, D.E., Colman, A.W., and Washington, R., 1999. Large scale modes of ocean surface temperature since the late nineteenth century. In Navarra, A., ed., *Beyond El Niño: Decadal and Interdecadal Climate Variability*. Berlin: Springer, pp. 73–102.

Glantz, M.H., 1996. *Currents of Change: El Niño's Impact on Climate and society*. Cambridge: Cambridge University Press.

Hadley, G., 1735. Concerning the cause of the general trade-winds. *Royal Society of London Philosophical Transactions*, **29**: 58–62.

Halley, E., 1686. An historical account of trade-winds and monsoons observable in the seas between and near the tropics with an attempt to assign the physical causes of the said winds. *Royal Society of London Philosophical Transactions*, **26**: 153–168.

Houghton, J., 2002. *The Physics of Atmospheres*, 3rd edn. Cambridge: Cambridge University Press.

Hurrell, J.W., 1995. Decadal trends in the North Atlantic Oscillation: regional temperature and precipitation. *Science*, **269**: 676–679.

Hurrell, J.W., and van Loon, H., 1996. Decadal variations in climate associated with the North Atlantic Oscillation. *Climate Change*, **36**: 301–326.

Lamb, H.H., 1959. The southern westerlies. *Quarterly Journal of the Royal Meteorological Society*, **85**: 1–23.

Lamb, H.H., 1972. *Climate: Present, Past and Future*, vol. 1. London: Methuen.

Lighthill, J., and Pearce, R.P., 1981. *Monsoon Dynamics*. Cambridge: Cambridge University Press.

Lockwood, J.G., 1974. *World Climatology*. London: Edward Arnold.

Lockwood, J.G., 1979. *Causes of Climate*. London: Edward Arnold.

Lockwood, J.G., 1985. *World Climatic Systems*. London: Edward Arnold.

Lorenz, E.N., 1967. *The Nature and Theory of the General Circulation of the Atmosphere*. Geneva: World Meteorological Organization.

Lutgens, F.K., and Tarbuck, E.J., 1979. *The Atmosphere.* Englewood Cliffs, NJ: Prentice-Hall.

Mantua, N.J., Hare, S.R., Zhang, Y., Wallace, J.M., and Francis, R.C., 1997. A Pacific interdecadel climate oscillation with impacts on salmon production. *Bulletin of the American Meteorological Society*, **78**: 1069–1079.

Marshall, J., Kushnir, Y., Battisti, D., Chang, P., et al. 2001. North Atlantic climate variability: phenomena, impacts and mechanisms. *International Journal of Climatology*, **21**: 1863–1898.

McGregor, G.R., and Nieuwolt, S., 1998. *Tropical Climatology: An Introduction to the Climates of the Low Latitudes.* Chichester: Wiley.

Miller, F.R., and Keshavamurthy, R.N., 1968. *Structure of an Arabian Sea Summer Monsoon System*. Honolulu: East-West Center Press.

Namias, J., 1963. Interactions of circulation and weather between hemispheres. *Monthly Weather Review*, **91**: 482–486.

Namias, J., 1969. Seasonal interactions between the North Pacific and the atmosphere during the 1960s. *Monthly Weather Review*, **97**: 173–192.

Neiburger, M., Edinger, J.G., and Bonner, W.D., 1982. *Understanding Our Atmospheric Environment.* San Francisco: Freeman.

Nieuwolt, S., 1977. *Tropical Climatology.* New York: Wiley.

Pant, G.B., and Rupa Kumar, K., 1997. *Climates of South Asia.* Chichester: Wiley.

Piazzi-Smyth, C., 1858. An astronomical experiment on the Peak of Teneriffe. *Royal Society of London Philosophical Transactions*, **148**: 465–534.

Power, S., Tseitkin, F., Torok, S., Lavery, B., Dahni, R., and McAvaney, B., 1998. Australian temperature, Australian rainfall and the Southern Oscillation. 1910–1992: coherent variability and recent changes. *Australian Meteorological Magazine*, **47**: 85–101.

Power, S., Casey, T., Folland, C., Colman, A., and Mehta, V., 1999. Inter-decadal modulation of the impact of ENSO on Australia. *Climate Dynamics*, **15**: 319–324.

Riehl, H., 1962. The tropical circulation. *Science*, **135**: 13–22.

Riehl, H., 1969. On the role of the tropics in the general circulation of the atmosphere. *Weather*, **24**: 288–308.

Riehl, H., 1978. *Introduction to the Atmosphere*. New York: McGraw-Hill.

Riehl, H., 1979. *Climate and Weather in the Tropics*. London: Academic Press.

Rossby, C.G., 1939. Relation between variations in the intensity of the zonal circulation of the atmosphere and the displacements of the semipermanent centres of action. *Journal of Marine Research,* **2**: 38–55.

Rossby, C.G., 1940. Planetary flow patterns in the atmosphere. *Quarterly Journal of the Royal Meteorological Society*, **66**: 68–87.

Rossby, C.G., 1945. On the propagation and energy in certain types of oceanic and atmospheric waves. *Journal of Meteorology*, **2**: 187–204.

Salinger, M.J., Renwick, J.A., and Mullan, A.B., 2001. Interdecadal Pacific Oscillation and South Pacific Climate. *International Journal of Climatology*, **21**: 1705–1721.

Troup, A.J., 1965. The southern oscillation. *Quarterly Journal of the Royal Meteorological Society*, **91**: 490–506.

Vowinckel, E., and Orvig, S., 1970. The climate of the north polar basin, In Orvig, S., ed., *Climates of the Polar Regions*. Amsterdam: Elsevier, pp. 129–252.

Walker, G.T., and Bliss, E.W., 1932. World weather V. *Royal Meteorological Society Memoirs*, **4**(36): 53–84.

Cross-references

Blocking
Centers of Action
Coriolis Effect
Hadley Cell
Jet Streams
Rossby Wave/Rossby Number
Trade Winds and the Trade Wind Inversion

ATMOSPHERIC NOMENCLATURE

Vertical temperature distribution is the most common criterion used in defining atmospheric regions. Three popular systems of nomenclature are based on the thermal stratification of the atmosphere. Figure A84 displays these three classification schemes and the vertical temperature structure of the atmosphere up to 110 km.

Chapman (1950) was the first to suggest the common four-layer division of the atmosphere. He classified the atmosphere into troposphere, stratosphere, mesosphere, and thermosphere. The upper boundary of each layer is given the suffix "pause"; for example, the upper boundary of the troposphere is referred to as the tropopause. Chapman's subdivisions of the mesosphere into the mesoincline, mesodecline, and mesopeak were based on the temperature maximum occurring near 50 km.

In 1954 Goody devised a different classification of the upper atmosphere, replacing Chapman's mesosphere. Goody suggested that Chapman's mesosphere should be called upper stratosphere, and the region above 80 km should be called ionosphere rather than thermosphere.

In 1960 the International Union of Geodesy and Geophysics recommended a nomenclature in an attempt to standardize terminology. In this classification the troposphere is the lowest 10–20 km of the atmosphere where temperature generally declines with height. The lower stratosphere is the relatively isothermal region immediately above the tropopause, and the upper stratosphere extends from the lower stratosphere to the maximum temperature level at 40–50 km (stratopause). The mesosphere is the region bounded by the stratopause and the temperature minimum occurring at 70–80 km (mesopause). The thermosphere is the region above the mesopause where temperature increases with height. Additionally, atmospheric physicists commonly often refer to the region from 15 km to 95 km as the middle atmosphere while the region above that is referred to as the upper atmosphere.

As opposed to thermal stratification, physical and/or chemical processes are also used to delineate discrete layers of the atmosphere. Today the term ionosphere is often restricted to the region around 70–80 km, where the existence of free electrons becomes significant. This region has importance in the transmission of radio signals over long distances. Conversely, the neutrosphere refers to the un-ionized region between the surface and the ionosphere. The ozonosphere, a subdivision of the neutrosphere based on appreciable ozone concentration, is located from 10 km to 50 km.

Other criteria have been suggested for classification of atmospheric layers. For example, the exosphere has been defined as the region near the top of the atmosphere where particles can move in free orbits, subject only to the Earth's gravitation. Another criterion, based on composition, defines the homosphere as the region from the surface to 80–90 km, where

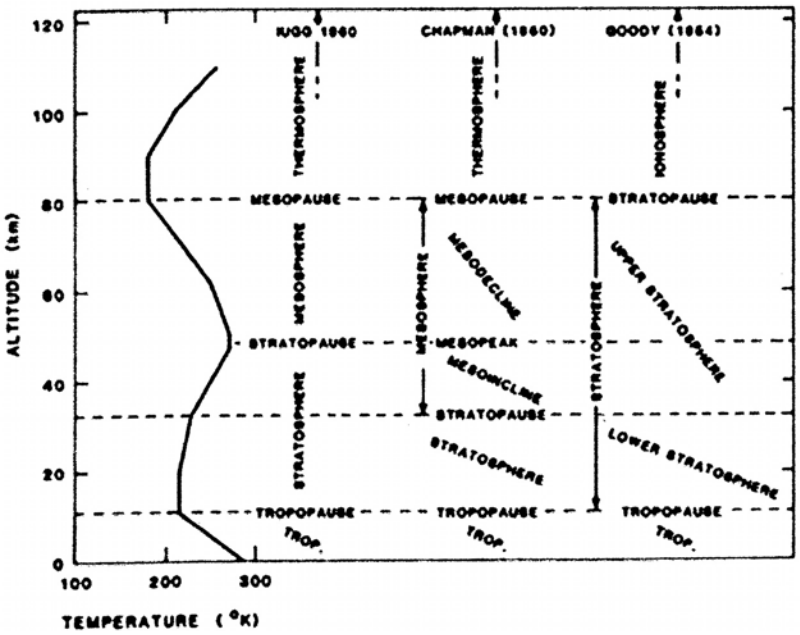

Figure A84 Vertical distribution of temperature up to 100 km, according to the US standard atmosphere, 1962, and three common systems of nomenclature (after Craig, 1965).

little photodissociation or gravitation separation occurs, and the heterosphere is the region above this, where atmospheric composition is not constant. The magnetosphere is defined as the region of the Earth's magnetic field which extends from the top of the ionosphere and is shaped by the solar wind. These and other variations in nomenclature have arisen in response to the needs of the various specialties in the atmospheric sciences.

Randall S. Cerveny

Bibliography

Brasseur, G., and Solomon, S., 1984. *Aeronomy of the Middle Atmosphere: chemistry and physics in the stratosphere and mesosphere*. Dordrecht, Holland: D. Reidel.

Chapman, S., 1950. Upper atmospheric nomenclature, *American Meteorological Society Bulletin*, **31**: 288–290.

Craig, R.A., 1965. *The Upper Atmosphere*. New York: Academic Press.

Goody, R.M., 1954. *The Physics of the Stratosphere*. London: Cambridge University Press.

Gordon, C.W., and Canuto, V., (eds), 1978: *The Earth, 1: The upper atmosphere, ionosphere and magnetosphere*. New York: Gordon & Breach.

Cross-references

Atmosphere
Inversion
Lapse Rate
Troposphere

ATMOSPHERIC NUCLEI AND DUST

Almost a century ago it was found that cloud and fog droplets form by condensation of water vapor from the atmosphere on small particles, so-called condensation nuclei. They were more systematically studied by Aitken toward the end of the nineteenth century. Condensation nuclei form part of the atmospheric aerosol content. These particles, aside from acting as condensation nuclei, also have an effect on the optical properties of the atmosphere and play an important role in atmospheric electricity. The light-scattering properties of these particles provided much information about their concentration and size distribution, especially in the early periods of investigation.

Nucleation process

In 1897 it was found that when a reasonably dust-free air sample, which was saturated with water vapor, was rapidly expanded so that adiabatic cooling occurred, droplet cloud formation would occur only if the expansion ratio was high enough to produce several hundred percent supersaturation. In the absence of nuclei a transition from the water-vapor phase to the liquid phase can occur only if the probability for aggregation of molecule clusters is high enough and supersaturation and temperature are adequate for such embryos to remain in equilibrium with their environment. However, if foreign particles are present in the air, condensation can occur at much lower supersaturations. The water-vapor molecules will attach themselves much more easily to such nuclei, thereby initiating the droplet-forming process. The effectiveness of a particle as a condensation nucleus largely depends on whether it is hygroscopic or hydrophobic (water attractive or repellent, respectively). Therefore, in the presence of condensation nuclei, condensation can occur at supersaturations on the order of a few tenths of a percent. This is in agreement with atmospheric observations. Similar observations apply to the formation of ice crystals. Small water droplets can be supercooled to temperatures as low as 40°C without freezing. At still lower temperatures, sudden formation of ice crystals occurs, i.e. spontaneous nucleation takes place. In the presence of freezing and sublimation nuclei, formation of ice crystals occurs at much warmer temperatures (−10°C or −15°C). The relative importance of freezing and sublimation nuclei remains to be determined. The term sublimation nucleus assumes that the transition from the vapor to the solid phase occurs directly by sublimation of molecules on the nucleus; in the case of freezing nuclei it is thought that the transition goes through the liquid water phase.

Properties and composition of atmospheric nuclei

Not all airborne particles (aerosol particles) act equally well either as condensation nuclei or as ice-forming nuclei. In the case of condensation nuclei, water affinity is an important factor in their efficiency. Supersaturation required to sustain a growing droplet is a function of the particle size; the smaller the particle (i.e. the greater the curvature of its surface), the higher the required saturation. From this consideration it follows that larger particles are more apt to act as condensation nuclei than small ones. In the case of freezing nuclei, particles whose crystal structure is similar to that of ice (pseudomorphic particles) are most likely to act as a base for building on the ice crystal lattice, and therefore form good freezing or sublimation nuclei. This concept does not seem to be in complete agreement with experimental evidence, however. For instance, quartz dust is not a good freezing nucleus; silver iodide is a good artificial freezing nucleus (cloud seeding).

Several conclusions may be drawn from this diagram: (a) In an isolated population of droplets containing equal masses of solute, the very small droplets must grow at the expense of the larger droplets. (b) Beyond a critical size the larger droplets may grow at the expense of the smaller. (c) If supersaturation of the vapor with respect to a flat surface is limited, say to about 0.1%, droplets must contain more than 10–15 gram of NaCl (or other similar solute) in order to reach critical size. (d) Small droplets may exist in equilibrium with moist air of relative humidity far below 100%.

According to Junge (1963), the size distribution of natural aerosols can be described by an inverse power law, according to which the number of particles is inversely proportional to the third or fourth power of their radius, although considerable deviations may occur in individual cases. Junge also defines three size groups, the Aitken particles (10^{-7} to 10^{-5} cm or 10^{-3} to 10^{-1} m radius); large particles (10^{-4} to 10^{-3} cm; see Table A43). Particles smaller than a few hundredths of a micron become unstable because their tendency to coagulate increases. Particles much larger than a few microns become more and more affected by gravitational forces and fall out more rapidly than smaller ones.

It can be concluded that approximately 60% in mass of the natural aerosol consists of inorganic, water-soluble material;

Table A43 Ranges of sizes of condensation nuclei and kerns occurring in the atmosphere[a]

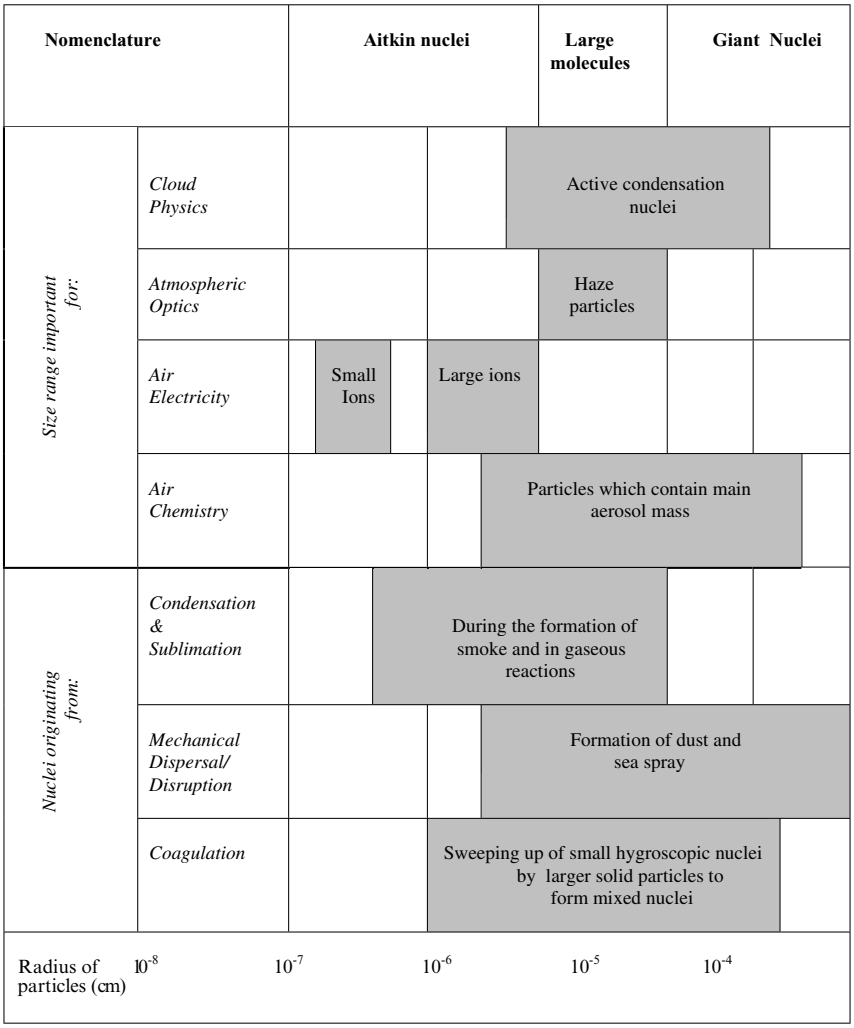

[a] Shading indicates size range at which labeled characteristics occur.

15% of organic material; and 25% of inorganic water-soluble material. The great majority of particles are mixed. In maritime airmasses, sea-salt particles are a major component in the natural aerosols. Such hygroscopic salt particles can act as excellent condensation nuclei. The continental aerosol originates partially from the ground itself (dust), but also from gaseous components. The inorganic nuclei seem to be formed to a large extent by the oxidation of sulfur gases (e.g. H_2S, SO_2) to sulfate compounds such as ammonium sulfate, etc. There are strong indications that a considerable portion of the nuclei in the size range below about 0.5 μm consists of organic materials and that these particles are extremely unstable. It is assumed that these are mostly particles formed from organic compounds with low vapor pressure. The vapors originate from certain types of vegetation and are changed to liquid or solid particles by photo-oxidation.

A group of cloud physicists believe that a correlation exists between the occurrence of meteor showers and precipitation. They assume the extraterrestrial meteors, by entering the atmosphere, disintegrate into fine dust particles that act as ice nuclei in the formation of cloud and precipitation particles.

Since 1947, when Vonnegut discovered that silver iodide crystals act as freezing nuclei at temperatures below about −4°C, much research has been done on artificial nuclei. It appears that nature, with few exceptions, provides enough nuclei for condensation and/or freezing. Adding artificial nuclei may change the size spectrum of cloud particles, leading to an increase in precipitation, but it may also result in a decrease (overseeding).

Robert W. Fenn

Bibliography

Aitken, L., 1888–1892. Related papers on the development and use of the dust counter. *Collected Scientific Papers (1923)*, pp. 187, 207, 236, 284.

Barry, R.G., and Chorley, R.J., 1992. *Atmosphere, Weather, and Climate*. New York: Methuen.
Eagleman, J.R., 1983. *Severe and Unusual Weather*. New York: Van Nostrand Reinhold.
Fleagle, R.G., and Businger, J.A., 1963. *An Introduction to Atmospheric Physics*. New York: Academic Press.
Goody, R., 1995. *Principles of Atmospheric Physics and Chemistry.* New York: Oxford University Press.
Junge, C.E., 1958. *Atmospheric Chemistry*. In *Advances in Geophysics*, **4**: 1–108.
Junge, C.E., 1963. *Air Chemistry and Radioactivity*. New York: Academic Press.
Ludlam, F.H., 1980. *Clouds and Storms.* State College, PA: Pennsylvania State University Press.
Meszaros, E., 1981. *Atmospheric Chemistry: Fundamental Aspects*. New York: Elsevier.
Peixoto, J.P., and Oort, A.H., 1992. *Physics of Climate*. New York: American Institute of Physics.
Roll, H.U., 1965. *Physics of the Marine Atmosphere*. New York: Academic Press.
Vonnegut, B., 1947. The nucleation of ice formation by silver iodide. *Journal of Applied Physics*, **18**: 593.
Woodcock, A.H., 1953. Salt nuclei of marine air as a function of altitude and wind force. *Journal of Meteorology*, **10**: 362–371.

Cross-references

Aerosols
Albedo and Reflectivity
Cloud Climatology
Fog and Mist
Precipitation
Radiation Laws

AUSTRALIA AND NEW ZEALAND, CLIMATE OF

The climates of Australia and New Zealand are strongly influenced by general circulation patterns prevalent in the SW Pacific. Critical to the strength of this circulation is the temperature gradient between Antarctica and the SE Asian tropics, and between Antarctica and the Australian continent. The ocean plays a key role, since there are no major land masses between the South island of New Zealand and Antarctica. More regional circulations, such as El Niño Southern Oscillation, affect the climate patterns in this region. The classic reference, which provides the first detailed summary of the climates of Australia and New Zealand, is Gentilli (1971).

Climates of Australia

Australia's climate depends on four major factors. First, the size and shape of Australia determine how the general circulation affects the continent. Australia covers 7 682 300 km^2, stretching from 10°41′S to 43°39′S and 113°09′E to 153°39′E at the extremes. Its greater longitudinal distance (4000 km) allows considerable airmass modification and a strong degree of continentality. Its limited latitudinal span creates moderate changes on a seasonal basis compared to larger continents such as North America.

Second, Australia's topography does little to obstruct air moving over the continent. The average altitude of the land mass is only 300 m, with 87% of the continent less than 500 m and 99.5% less than 1000 m. Only the eastern mountains, which extend north to south, have any major influence on synoptic flow.

Third, Australia is completely surrounded by water. Polar air originates from the Antarctic Ocean, and is basically cool and moist. The major influence of the ocean is coastal, and there is no significant upwelling of cold water. Australia's climate can be generally described as moderately continental with important ocean influences.

Fourth, Australia's geographical location places it under the global subtropical high-pressure zone. Much of Australia is under the influence of dry subsiding air and can be considered arid or semiarid, although not as dry as the west coasts of the other southern hemisphere continents. Particularly in summer, Australia experiences high sun angles and intense solar radiation under mostly clear skies. With the exception of Tasmania and much of the east coast, most of the continent receives over 3000 hours of sunshine per year, almost 70% of that possible (Bureau of Meteorology, 1988a).

Synoptic circulation patterns

In general, Australia is affected by midlatitude westerlies on the southern fringe, tropical convergence on the northern fringe in summer, and stable subsiding air under the subtropical anticyclone belt in between. The synoptic circulation patterns can best be described by comparing summer and winter seasons.

(a) Winter (May–October) (Figure A85)

The subtropical anticyclone belt covers the northern two-thirds of the continent. Dry stable SE trades dominate Australia north of 20°S, with greater than 50% frequency. This air originates over the Pacific, often loses some of its moisture due to orographic precipitation on the eastern highlands, and cools and stabilizes as it passes over the continental interior.

Frontal activity. South of 20°S the continent is under the influence of alternating anticyclones and cold fronts, associated with the northern edge of the midlatitude westerlies. Troughs and fronts from these systems extend into southern Australia (Figure A86), separating migratory anticyclones in 4–8-day intervals. These fronts move at an average speed of 35 km h^{-1} and can be divided into two types (Sturman and Tapper, 1996). Ana-fronts are more active and are associated with convection in the frontal zone. Kata-fronts are less active and are linked to subsiding air from anticyclones.

The impact of these fronts on the main continent is not usually strong, and only in spring extends into the northern half of the country (Smith et al., 1995). Tasmania is most severely affected, being closest in location to the midlatitude depressions. There is a striking absence of warm fronts because the frontal systems form well to the west of Australia and the warm front has swung south before the system reaches the continent.

Precipitation associated with winter frontal systems often occurs from the Northwest Australian cloud band (Sturman and Tapper, 1996), a source of moisture and deep convection which can stretch for distances of up to 5000 km between the Indian Ocean and S to SE Australia. Eighty percent of these cloud bands occur between April and September, with an average of about two per month.

Occasionally, secondary depressions or cut-off lows moving toward low latitudes can initiate severe storm situations.

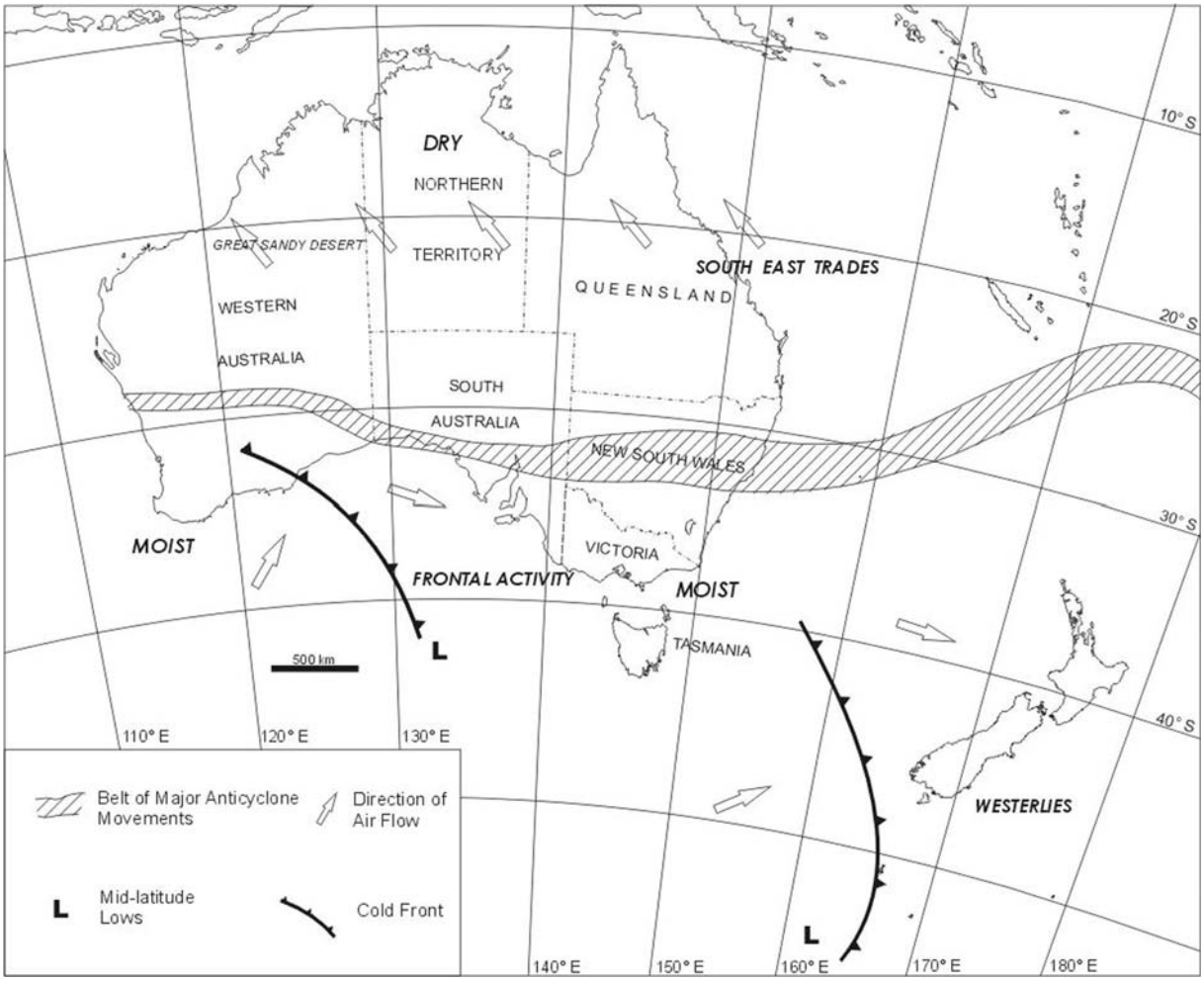

Figure A85 Simplified synoptic climatology of Australia, July surface circulation (Bridgman, 1987).

Development is better on the SE coast of Australia rather than on the SW. A slow-moving deep low-pressure system results, bringing strong winds and heavy precipitation for periods of 0.5–10 days (Tapper and Hurry, 1993). Such systems are more likely to develop in spring or fall (October–November or April–May) because the thermal gradient between airmasses is strongest. The cause is either the remnants of a tropical storm, or intense cyclonic development in an easterly dip in the isobaric pattern.

The interaction of the Indian Ocean air and the cooler maritime air south of the continent brings winter rains to S and SW Australia. In early winter these rains can be extensive and are related to mid-tropical convection and the strength of the westerlies. In late winter more showery precipitation occurs, associated with topographic and coastal convergence influences, and not with the general circulation (Allen and Haylock, 1993).

Winter anticyclones. Anticyclones dominate much of the continent in winter. On average, 40 anticyclones move over Australia in a year, with slightly less in fall–winter than spring–summer. Anticyclones enter the continent at about 115°E and 27°S on the west coast, dip to 35°S in S Australia, and exit about 30°S off the east coast (Figure A85). The mean anticyclonic track is furthest north in June–July except on the east coast of the continent, where the lag in ocean heating defers the maximum northward extent to August–September (Gentilli, 1971; Tapper and Hurry, 1993).

Over the continent the strength and persistence of the anticyclones can be intensified by wintertime cooling of the land. Anticyclones may remain stationary in the interior for several days, particularly if the high develops a meridional (longitudinal) orientation. This creates blocking, and is much more common east of 150°E, in the Tasman Sea. Eastward movement of weather systems is retarded and the convective motion associated with depressions is countered (Baines, 1990; Sturman and Tapper, 1996). Duration is up to 12 days, bringing dry, fine weather.

The presence of anticyclones in the winter enhances the effects of local topography on the continent, encouraging mesoscale inversions and cold air drainage to occur. It is not unusual to see nighttime floodplain temperatures 4–5°C cooler than those on the adjoining hilltop, caused by the downslope movement of cold air, and widespread frost and/or fog.

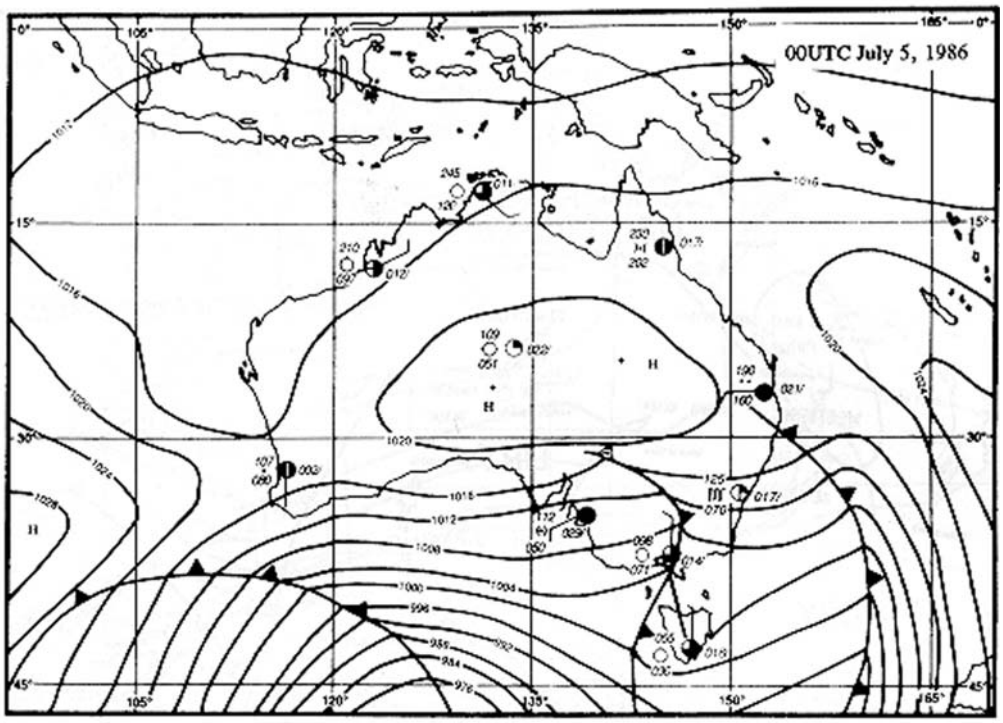

Figure A86 Representative synoptic meteorological situation in winter. Cold fronts parade across the southern third of the continent bringing cool cloudy weather and a light to moderate rainfall. Dry, cool conditions dominate the interior, with overnight frosts likely in many locations (Tapper and Hurry, 1983).

The subtropical jet stream. The trajectory and speed of movement of both anticyclones and fronts are strongly influenced by the subtropical jet stream, which is strongest over the southern part of the continent near 200–300 mb (10 000 m altitude) in the winter (Bridgman, 1998; Sturman and Tapper, 1996). The mean latitude of the jet is 26–32°S, but varies considerably from season to season and year to year. In winter its mean core speed is 70 m s^{-1} and northerly meandering from about 25°S is most apparent. In summer the jet is much weaker (30 m s^{-1}), with its mean axis position around 31°S. The jet is associated with the formation of upper air troughs and depressions which, when linked with a lower-level unstable airflow, can bring considerable rain to large areas of the southern half of the continent. Such troughs also provide the major medium for tropical moisture to reach the southern parts of the continent through the northwest cloud band. The strongest jets are also associated with strong cyclogenesis in the west Tasman Sea. It is not unusual in winter on the SE coast for a shallow surface anticyclone with surface pressures near 1020 mb to exist, with steady rain falling through the system from a mid-tropospheric trough.

When the jet is located between 20°S and 25°S it has a significant influence on rainfall systems occurring in late fall. Storms can bring strong rain and flooding to parts of the continental interior. They appear erratically in the general area from Geraldton–Port Hedland in Western Australia to Carpenteria–NE New South Wales in eastern Australia, providing secondary and sometimes primary rainfall maxima for some individual stations (Bridgman, 1998).

Anticyclonic shape and movements relate strongly to the area of upper tropospheric convergence on the equatorial side of the jet. If the jet meanders considerably across the continent, the anticyclones will be elongated longitudinally and will be slow-moving. If the jet has a strong zonal (east–west) component, the anticyclones will be zonally elongated and may move across the continent with considerable speed.

(b) Summer (November–April) (Figure A87)

Summer anticyclones. In summer the circulation systems are 5–8° further south, changing the climatic regimes affecting the northern and southern edge of the continent. Subsiding air from the subtropical high-pressure belt, now located poleward of Australia between 35°S and 45°S, covers most of the continent except for the northern tropical fringe and southern Tasmania. The descending air, originating at 10 000 m, warms adiabatically and subdivides into a series of traveling anticyclones (5–6 days periodicity) separated by troughs (Gentilli, 1971). The longitudinal extent of these anticyclones (Figure A88) is of the order of 2000–3000 km and the latitudinal extent 1000–2000 km. The counterclockwise circulation around the high during its passage ensures dry air from the hot interior moves coastward, limiting rainfall periods to troughs between anticyclonic systems or to onshore easterlies along the east coast of the continent. The pressure in the centre of the anticyclonic cells usually reaches 1030 mb, and falls to about 1005 mb in the trough between.

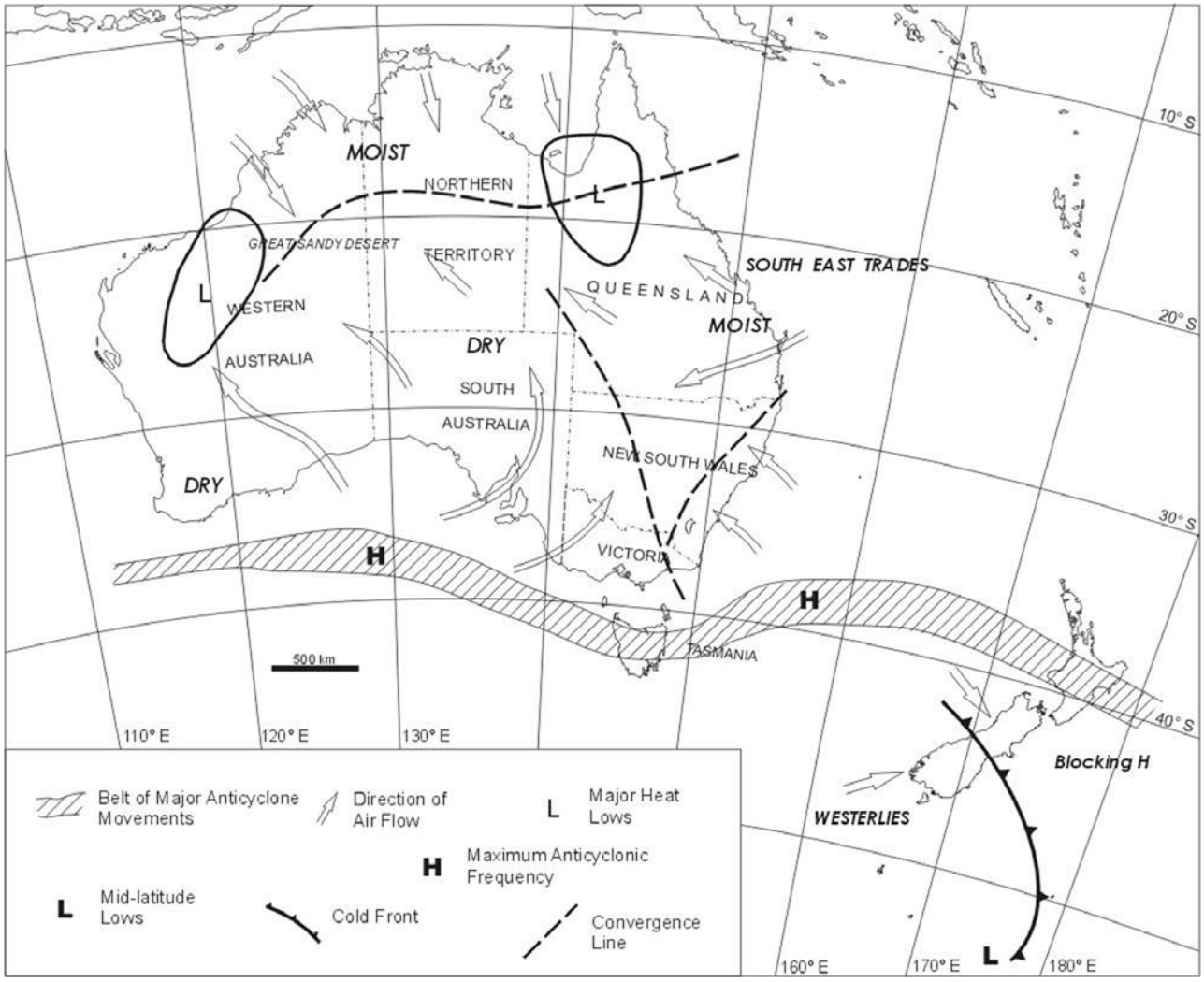

Figure A87 Simplified synoptic climatology of Australia, January surface circulation (Bridgman, 1987).

A typical weekly synoptic pattern for the southern half of Australia might be cooler S winds in the east side of a high, changing to E, NE and then NW winds as the high passes. Along the coasts, temperatures might warm from 22–24°C in the cooler Pacific maritime air to 36–38°C or higher in the continental air from the interior. The situation remains extremely hot and dry until the trough, or cool change between anticyclones, brings relief.

The summer cool change. In Western Australia the cool change is weak, often dry, and is mainly a change in temperature and wind direction (Reeder and Smith, 1992). It forms in the Cape Leeuwin–Kalgoorlie area as an incursion of Indian Ocean air, and is mainly controlled by the warm to hot air ahead, rather than the weak, cooler air behind. The change will often be sudden, bringing relief from exceedingly hot conditions, dropping temperatures by 10–15°C in the space of less than half an hour.

Cool changes, or Southerly Busters, reaching SE Australia, are often much stronger, with gusty winds and occasional rain, as they move east along the Victorian coast and then north along the NSW coast. They occur between November and March, and are channeled by the topography of the eastern highlands (Reeder and Smith, 1992; McInnis, 1993). Since the depth of the change is only about 3–5 km, this change in orientation is not reflected at 500 mb, but the buster may be associated with weak troughs at this level. The majority of the busters occur between 1300 and 2100, since their speed of movement strength is enhanced by a sea breeze. About half the cool changes are dry, but the change may be heralded by a roll cloud, gusty, squally winds (gusts up to 30 m s^{-1}) and thunderstorms. At passage a temperature drop of 10°C in a few minutes and up to 22°C in 24 hours may occur.

On occasion cool changes are associated with prefrontal troughs, which can bring severe weather, heavy precipitation, and flash floods. From 1957 to 1990, 69 meso-scale severe storms occurred in the Sydney region between November and

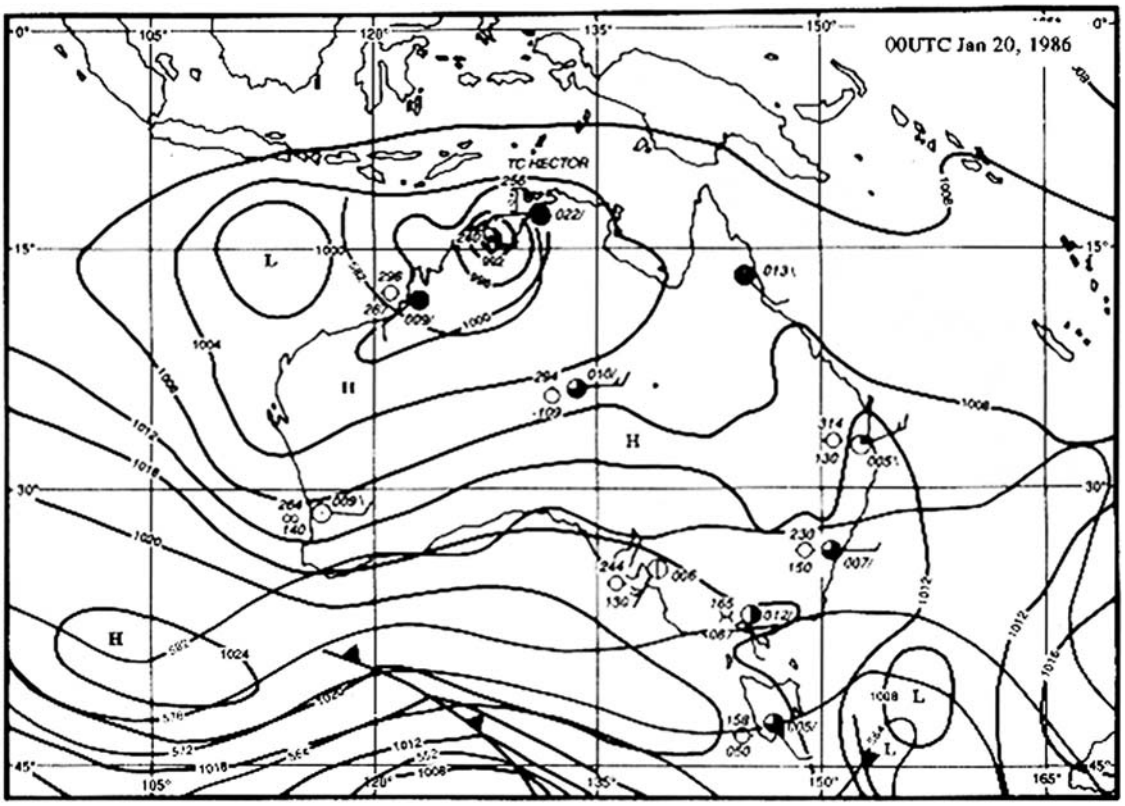

Figure A88 Representative synoptic meteorological situation in summer. A cool change separates an elongated high-pressure ridge. Hot NW winds from the continental interior invade SW Australia. Onshore SE winds affect the E coast, bringing cool, cloudy, and showery conditions. A tropical cycle (Hector) enters the continent near Darwin (Tapper and Hurry, 1993).

March (Speer and Geerts, 1994). The majority occurred between noon and 6 pm.

Regional and local circulations. The west coast trough develops between two strong highs centered south of the continent, as a dip in the isobaric pattern. The trough encourages hot strong NE winds from the interior to the coast, which continue until the trough moves inland and weakens (Tapper and Hurry, 1993).

The sea breeze brings cooling to the coast on summer days, as well as on occasional winter afternoons (Abbs and Physick, 1992). Established under clear skies and weak synoptic airflow, through land–water temperature contrasts of more than 7–8°C, the sea breeze can penetrate 80–90 km inland on average, depending on topography. A well-developed sea breeze may blow for 2–7 hours, depending on distance from the shore. Sea breezes are more strongly developed on the W and SW coasts than on the E coast. Bringing temperature relief of up to 15°C on a hot day, these breezes occur with daily frequencies of about 60% on the coast in summer. They often carry appropriate local names such as the Fremantle Doctor (Western Australia).

The morning glory is a spectacular wave structure that appears over the Gulf of Carpenteria just ahead of the wet season in Australia's north, created by a clash between two opposing sea breezes. It heralds strong wind squalls, long narrow roll clouds, and a pressure jump, but precipitation is rare (Collis and Whitaker, 1996).

The northern Australia rainy season, or monsoon. In northern Australia the shift of the subtropical high-pressure belts and subtropical jet allows a dynamically active low to form over the northern part of the continent (Figure A87). These encourage the entry of the intertropical convergence zone (ITCZ). The result is a moist NW air flow which meets the SE trades along a line approximately from Port Hedland (Western Australia) to Cairns (Queensland), which is commonly described as a monsoon (Joseph et al., 1991; Suppiah, 1992; Cook and Heedegen, 2001). Table A44 presents the range of dates of onset of the monsoon, illustrating the high variability in monsoon dynamics. There is a strong correlation with the previous season's monsoon rain in India, with

Table A44 Range of dates of onset and length of the North Australian summer monsoon (Suppiah, 1992)

	Minimum	Mean	Maximum	St Dev (days)
Onset	23 Nov.	24 Dec.	27 Jan.	15
Finish	1 Jan.	7 Mar.	6 Apr.	18
Length	11	74	119	25

below-normal rain creating a delay in monsoon onset in Australia.

The monsoonal flow generally extends to about 15°S, and is better developed east of 100°E. It brings the rainy season to northern Australia. Its onset can be abrupt, producing violent thunderstorms and tropical depressions during active phases. Rainfall is heaviest along the coast, decreasing quite rapidly inland. About 20% of the monsoon period consists of breaks, where moist humid air in the NW airstream is not triggered into precipitation (Sturman and Tapper, 1996).

To the south and east of the monsoonal trough SE winds dominate the eastern third of the continent. Low-level moisture from the Pacific Ocean is, to a large part, expended on the eastern highlands, but often reaches the interior. Convective and orographic activity results in rain through instability and thunderstorms, occasionally enhanced by an upper-level trough. The best rains occur when a mid-tropospheric trough extends southward from central Queensland, interacting with the unstable easterly flow (Tapper and Hurry, 1993).

Tropical cyclones. Australia is the only continent with the same incidence of tropical cyclones reaching either the W or E coast, due to the availability of warm seas to enhance formation and to the shape of the coastline. Ninety-five percent of tropical cyclones form in the latitudinal zone 9–19°S, in the shear line between the monsoon westerlies and the trade winds (Sturman and Tapper, 1996). The tropical cyclones season occurs between late November and early May. On average, eight to 10 cyclones form off the Australian coast every year, but there is considerable variation in frequency. About three on average reach NE Queensland each year, two or three reach Western Australia, and one reaches the Northern Territory (Figure A89). Landfall most often occurs around Port Hedland on the west coast, near Townsville on the east coast, and Wyndham, on the northeast coast of Western Australia. February and March are the months of highest frequency, particularly between 15°S and 20°S. The timing of the strongest tropical cyclones is linked to the active phases of the monsoon (Suppiah, 1992).

Tropical cyclones bring high winds and heavy rain to both coasts with considerable destruction potential. Flooding in much of Central Queensland and in Western Australia is inevitable if the cyclone moves inland. Much of the area is sparsely inhabited, however, and rains from tropical cyclones are often the main source of moisture for crops and grassland. Only on rare occasions does a tropica1 cyclone strike a heavily inhabited area. The most famous Australian cyclone is Tracy, which passed through Darwin on Christmas evening, 1974 and destroyed more than half the city.

Links to El Niño/Southern Oscillation. Tropical cyclones, the monsoonal flow, and precipitation in eastern Australia in general is very strongly influenced by the El Niño/Southern Oscillation (ENSO) circulation variations (Allen, 1988; Drosdowsky and Williams, 1991; Joseph et al., 1991), and the associated changes in sea-surface temperature, especially in spring and early summer. There is a significant correlation between the Southern Oscillation Index (SOI) and variations in precipitation, cloud cover, and the diurnal range of temperature. Lower SOI brings less rain (and often drought), lower cloud amounts, and greater diurnal temperature ranges. A positive SOI brings higher than average rainfall, deeper incursions of the monsoon into central Australia, and potential floods. Correlations (r) between precipitation and SOI reach 0.6 in western NSW, and are generally 0.4 over much of the eastern half of Australia (Sturman and Tapper, 1996). Correlations diminish greatly toward the SW of the continent.

The climatic elements

Tables A45 and A46 present means of various climatic elements for January and July and some climatic extremes. Two elements are of major concern to Australia: temperature and moisture.

Temperature

The range of annual average air temperature is from 28°C on the Kimberly coast (NW Western Australia) to about 4°C in the alpine mountain areas (>1500 m) in SE Australia. In January (summer) the average daily minimum is virtually equivalent to the annual average air temperature. In July (winter) minimums decrease from 21°C in the Darwin area to −20°C in the SE Australian mountains. Particularly in winter, the minimums are tempered on the coast by the ocean. Local cold air drainage and topography eliminates any regularity of pattern in the eastern highlands.

Maximum temperatures are much more important. Australia is known for its heat extremes rather than its cold (Bureau of Meteorology, 1988a, 1989). In January, 35°C is exceeded over most of the interior and 40°C regularly in NW Western Australia. Towns in this area, such as Marble Bar, exceed maxima of 40°C for several weeks at a time. Maxima drop to less than 20°C in Tasmania and in the higher altitudes of the SE Australian mountains. The coastal sea breezes create maximum temperature gradients in all directions from the interior, with the south and east coasts having maxima in the mid and upper 20s and the north and west coasts in the lower 30s. The maximum for single days under one synoptic system has reached 47.6°C in Adelaide, 46°C Melbourne, and 45.3°C in Sydney (11–14 January 1939).

In July, except for the eastern highlands, maximum temperatures follow a latitudinal pattern, decreasing from 30°C near Darwin and on the Cape York peninsula to 12°C on the south and Tasmanian coasts. July maxima in the mountains do not usually reach 5°C.

The sun and seasonal extent of cloud cover determines the month of highest temperature. Most of northern Australia, equatorward of 20°S, has highest maximum temperatures in November just before the onset of the monsoon, with some areas near Darwin and in the NW having the highest maximum in October. Just south of this area, to a line from Geraldton (W.A.) to Tennant Creek (N.T.) to Cooktown (Qld.), the highest maxima occur in December. Most of the interior and the NE coast has highest maxima in January, and the west and east coasts in February, due to the lag in ocean temperatures.

A combination of hot dry climatic conditions and strong winds from the center to the coast can create serious bushfire problems, particularly in late spring and early summer. Bushfires are enhanced when a blocking summer anticyclone occurs in the Tasman Sea and there is slow approach of a trough or depression from the southwest. Bushfire behavior is controlled by fuel availability, topography, pressure tendency and wind direction. Cumulative antecedent rainfall, or the total rainfall over several previous months or seasons, correlates strongly with bushfire frequency (Love and Downey, 1986). The region of highest fire hazard is the coastal zone of E Victoria and S

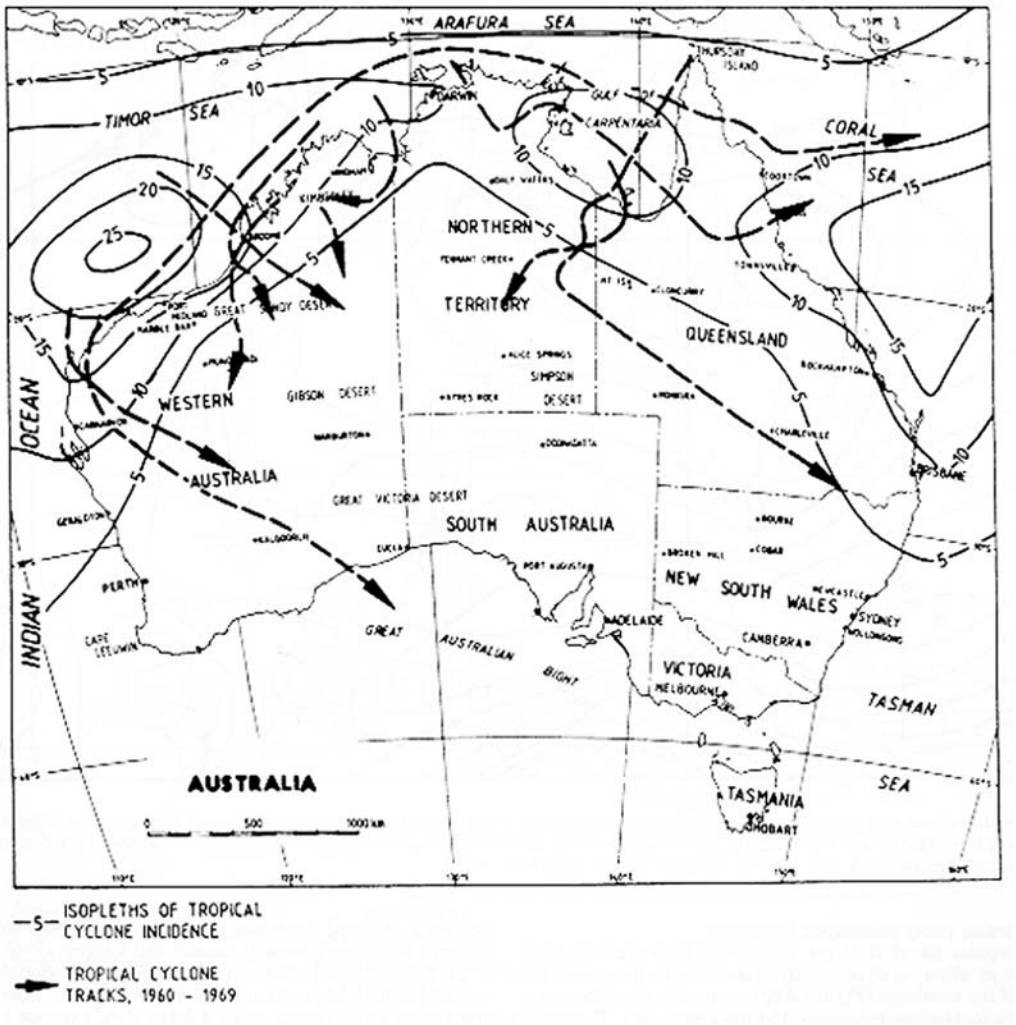

Figure A89 Average decadal incidence of tropical cyclone formation. Tropical cyclone tracks crossing the coast are shown to indicate representative storm paths (after Bridgman, 1998; Collis and Whitaker, 1996).

Table A45 Extreme weather events in Australia

Weather event	Location	Period	Value
Rainfall			
Hourly total	Deeral, Qld	13 Mar. 1936	330 mm
Daily total	Beerwah, Qld	3 Feb. 1893	907 mm
Monthly total	Bellanden Kerr, Qld Bellanden	Jan. 1979	5387 mm
Annual total	Kerr, Qld	1979	11251 mm
Highest annual mean	Babinda, Qld	32 years	4537 mm
Lowest annual mean	Troudaninna, SA	42 years	105 mm
Temperature			
Highest maximum	Cloncurry, Qld	16 Jan. 1889	53.1°C
Lowest minimum	Charlotte's Pass, NSW	29 Jun. 1994	−23°C
Longest heat wave[a]	Marble Bar, WA	30 Oct.−7 Apr. 1924	161 Days
Maximum annual average	Wyndham, WA	−	35.5°C
Wind			
Maximum gust	Mardie, WA	19 Feb. 1975	259 km/hr

[a] Defined as the number of days in a row the maximum temperature exceeded 37.8°C.
Data courtesy of the National Climate Centre, Australian Bureau of Meteorology.

Table A46 Mean climatic data for selected Australian capital cities, January and July

City (Lat./long.)	MSL alt (m)	Years of data	Pressure (hpa)	Wind speed (m/s)	Prevailing wind direction		Evap (mm)	Daily cloud (8ths)	Max. temp. (°C)	Min. temp. (°C)	Mean temp. (°C)	Hours of sunshine	9 a.m. relative humidity	Precipitation (mm) (days)	Fog days	Solar energy (MJ/m^2 per day)
					9 a.m.	3 p.m.										
Perth, WA (31°57′S/115°51′E)	19.5	42														
January			1012.6	4.9	E	SSW	280	2.3	31.5	16.7	23.5	10.5	51	7(3)	0.2	27.3
July			1018.8	3.9	NNE	W	58	4.5	17.7	9.0	13.2	5.3	76	164(18)	1.6	9.4
Darwin, NT (12°25′S/130°52′E)	31.0	45														
January			1006.2	2.6	W	NW	225	5.9	31.7	24.7	28.6	5.9	81	409(21)	0.0	18.4
July			1012.8	3.4	SE	E	229	1.3	30.3	19.2	25.1	9.8	62	1(1)	1.1	19.3
Sydney, NSW (33°56′S/151°10′E)	6.0	47														
January			1012.7	3.4	NE	NE	217	4.7	25.7	18.5	22.0	7.2	68	102(12)	0.3	22.5
July			1018.5	3.2	W	WSW	95	3.5	16.0	7.9	11.8	6.2	74	100(10)	2.1	10.4
Canberra, ACT (35°19′S/149°12′E)	571.0	47														
January			1012.0	1.8	NW	NW	251	4.1	27.7	12.9	20.3	8.9	60	60(8)	1.0	25.9
July			1020.2	1.2	NW	NW	54	4.4	11.0	-0.3	5.4	5.2	84	39(10)	7.9	9.5
Melbourne, Victoria (37°41′S/144°51′E)	132	16														
January			1012.8	3.6	S	S	228	4.1	26.0	13.4	19.9	8.1	68	42(8)	0.1	24.9
July			1202.2	3.6	N	N	47	5.2	12.8	4.9	9.5	3.7	81	33(14)	4.3	6.3
Hobart, Tasmonia (42°55′S/147°20′E)	4.0	28														
January			1010.6	3.5	NNW	SW	167	5.0	18.6	11.5	16.5	7.9	58	69(14)	0.3	23.2
July			1014.0	3.0	NNW	NNW	26	4.8	11.1	6.1	7.9	4.3	78	95(21)	1.4	5.5
Alice Spring, NT (23°49′S/133°53′E)	545	38														
January			1007.0	ND	ESE	SE	397	2.3	36.6	22.2	28.0	11.0	36	43(ND)	ND	26.7
July			1018.0	ND	ESE	SE	121	0.7	19.3	4.5	12.0	9.3	61	11(ND)	ND	16.0

After Bridgman (1987); Bureau of Meteorology (1988b).

New South Wales, where, due to the regular availability of good fuel grown during wet periods, large bushfires during dry periods occur every third year. In an area roughly from SE South Australia through Victoria and W New South Wales to the S Queensland coast, including S Tasmania near Hobart, one big fire occurs approximately every 10 years. Recent severe fires include the Ash Wednesday fires in Victoria and Southern Australia in February 1983, where 75 people were killed, more than 2000 houses destroyed, and property damage was $430 million (Tapper and Hurry, 1993); the east coast fires in the Sydney/Newcastle New South Wales area in January 1994; and the 2002 bushfires which created major destruction of houses in E New South Wales, and the Mt Stromolo astronomical observatory in Canberra.

Moisture (Figure A90). Australia is a dry continent with certain localized exceptions, and has periods of extreme rainfall variability (Haylock and Nicholls, 2000). Vapor pressure and atmospheric water vapor do not change much diurnally (or in the interior seasonally) except along the coast or where there is a significant rainy season. Potential evaporation regularly overshadows precipitation. Fifty percent of the continent has a median rainfall less than 300 mm y^{-1}, and 80% less than 600 mm y^{-1}. Highest rainfall occurs on the NE and N coasts, reaching 3800 mm y^{-1} in the eastern highlands, and lowest in the Simpson Desert (<150 mm y^{-1}) (Bureau of Meteorology, 1988a). Seventy-Five percent of the continent has an annual evaporation (class A pans) of greater than 2500 mm yr^{-1}. In the central and northwest sections of the continent, potential evaporation reaches 4500 mm yr^{-1}, more than 20 times the annual rainfall.

Rain days per year decrease from over 100 around Darwin and 120 or more on the NE Queensland coast, to less than 20 in the interior. In the area affected by the midlatitude westerlies, for example SW Tasmania, more than 150 rain days per year can occur.

Precipitation can be strongly seasonal, depending on location. Five main precipitation regimes dominate the continent (Bureau of Meteorology, 1988a, 1989; Stern et al., 2000) allowing an analysis by climatic zones (Figure A90):

1. In Northern Australia the monsoonal season (October to April) is markedly wet and the winter very dry. Most stations have more than 20 times the rainfall in summer compared to winter. The NE Queensland Coast has the highest annual rainfall in the country.

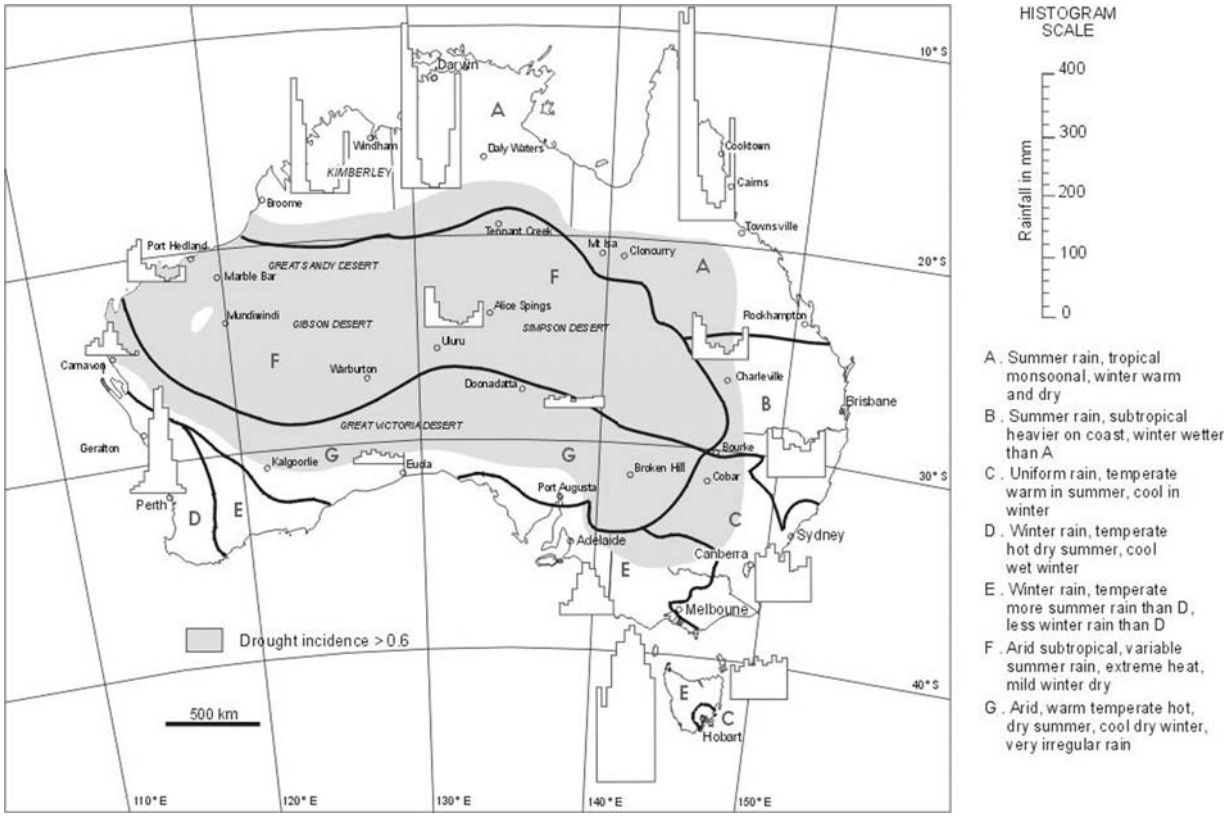

Figure A90 Representative monthly precipitation histograms (January begins at the left) for various parts of Australia. The data are averaged for meteorological districts and not representative of single stations. Included are climatic districts based on temperature and precipitation. The region of high to excessive drought incidence is shaded (Bridgman, 1998). A more detailed classification can be found in Stern et al. (2000).

2. In SE Queensland and NE New South Wales, summer is wet and winter is dry, but the difference between seasons is much less marked than under monsoon conditions. There is a tendency for a secondary peak in midwinter.
3. In SE Australia, including most of Victoria, E New South Wales and Tasmania, a relatively uniform precipitation regime exists. Victoria and Tasmania receive slightly more rain in winter than summer, and New South Wales the reverse, with the difference becoming greater closer to the equator.
4. SW Western Australia is winter wet (May to October), summer dry, the Mediterranean climate caused by the seasonal shifting of the subtropical high-pressure belt and the midlatitude westerlies. Climate here is strongly affected by changing conditions in the Indian Ocean (Smith et al., 2000).
5. More than half the continent, from NW Western Australia to the Great Australian Bight, is semiarid to arid, with a weak summer seasonal rainfall distribution in the west and north. This is the area of greatest rainfall variability, with heaviest rains associated with occasional tropical cyclones and severe local thunderstorms.

On a more local scale, severe thunderstorms associated with fronts and other convective triggers create flooding and damage (Kuleshov et al., 2002). Some of the strongest thunderstorms spawn tornadoes, particularly under extremely unstable conditions in the mid and upper troposphere. Tornadoes occur especially in the uplands of eastern Queensland and in the SW of Western Australia (Sturman and Tapper, 1996). The frequency of tornadoes may be 100–200 per year over the continent, occurring mainly outside the dry interior. In the northern half of the country, tornadoes are relatively rare and only develop in summer, as a result of strong local convection related to the wet season or sometimes associated with tropical cyclones. In the southern half, tornadoes in summer occur under convective activity associated with weak lows or troughs. In winter a secondary maximum occurs associated with cold fronts emanating from deep depressions in the midlatitude westerlies.

Tornado formation is strongly influenced by upper atmospheric airflow, the subtropical jet, and upper air trough location. Most occur within 6° latitude of the jet stream or within 14° longitude of an upper air trough. Diurnally tornadoes occur most often between 1530 and 1830. Winds occasionally exceed $50\,m\,s^{-1}$.

Snow, associated with winter cold fronts passing over elevated areas, is mainly confined to the mountains in SE Australia, particularly just south of Canberra, and on Tasmania's Central Plateau and uplands.

The lack of consistent rainfall over most of the continent creates one of Australia's most serious climatic problems, drought. Drought can be defined as a severe water shortage depending on the amount of water needed, or by the failure of rains at specific places. Where seasonal rainfall is critical, drought is defined as the failure of the wet season. The Australian Bureau of Meteorology (www.bom.gov.au) defines an index of drought to establish the concept of drought potential: 50th percentile of rainfall minus 10th percentile divided by the 30th percentile. High indexes (greater than 0.6) mean a strong potential for drought. More than two-thirds of Australia has high to extreme drought indexes (see Figure A90). The only areas escaping are the N, S and E coast and Tasmania.

Table A47 Annual average cost of weather-related disasters in Australia (Sturman and Tapper, 1996)

Type of disaster	Annual cost ($ million, 1989)	Percent of cost
Drought	303	24
Bushfire	68	5
Storm	202	16
Flood	386	31
Tropical cyclone	258	21
Other	33	3
Total	1250	100

Table A47 shows that drought, along with flood and tropical cyclones, create the highest cost from weather disasters in the country. The table emphasizes the importance of extreme weather to Australia.

New Zealand climates

New Zealand consists of two main islands and a number of smaller islands, located approximately 2500 km east of Australia. The country covers an area of 267 000 km^2, and is aligned north to south between latitudes 34°S and 47°S (Figure A91a). The distance north to south is approximately 1930 km, but the width of New Zealand reaches a maximum of only 400 km. New Zealand's size, location, orientation, and dominance by mountains (especially on the South Island), create a very different climatic regime than Australia.

Four major physical factors dominate New Zealand's climate. First, the ocean surrounding on all sides strongly defines the type of air that reaches the country. Important airmasses include tropical maritime air from the Pacific, with warm temperatures, 18–21°C, and considerable moisture; and polar maritime air from the southern ocean, with temperatures approximately 7–13°C. Thus New Zealand is consistently under the influence of moist air masses, allowing considerable rainfall. The ocean influences bring cool summers and mild winters, although cold air advection from the Antarctic Ocean can bring snow and frosts.

Second, the mountain ranges on the western sides of the two main islands create a considerable influence on atmospheric circulation (see Figure A91a). Dynamically, the mountains block upstream airflow, creating orographic uplift and vertical mixing, which leads to lee troughs on the downwind side. Very large spatial differences in precipitation can occur over the short distance between the windward mountain slopes and the rainshadows a few kilometers to the east. The mountains also act as channels for winds, and have significant influences on local airflows.

Third, New Zealand's geographic position places most of the country in the westerly circumpolar wind belt. Subtropical influences only occur irregularly, in the northern part of the North Island in summer.

Fourth, the much larger Australian continent exerts a seasonal influence. In winter considerable surface cooling under clear skies creates stabilization in the lower atmosphere. This effect extends eastward in the circulation pattern, helping weaken the westerly airflows over New Zealand. In summer the

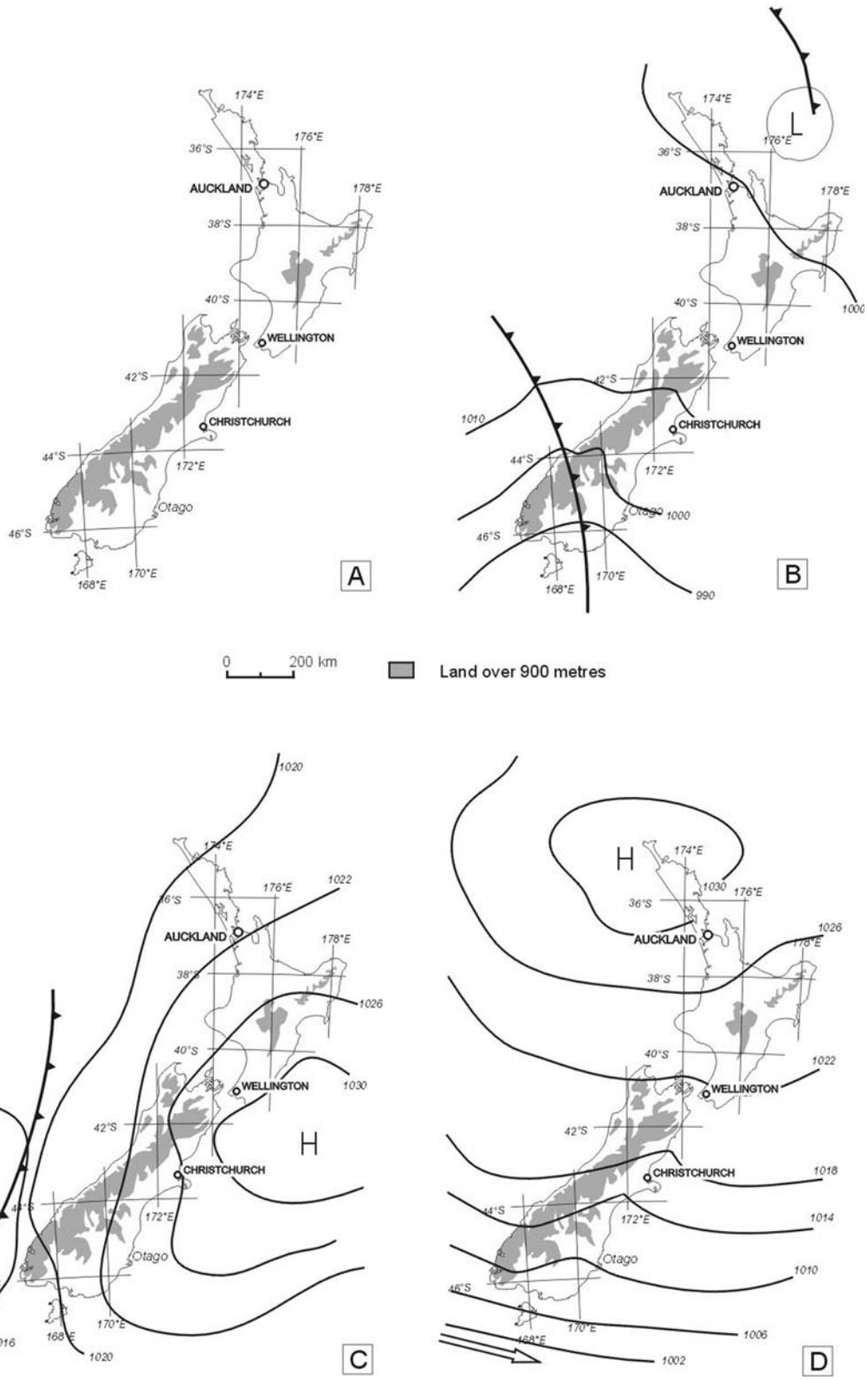

Figure A91 (**a**) New Zealand's physical features; (**b**) typical cold frontal passage over New Zealand; (**c**) typical blocking high situation to the east of New Zealand; (**d**) strong zonal circulation with high pressure to the north.

intense heating under clear skies over Australia creates a more convective atmosphere, which upon reaching New Zealand assists in creating stronger and more persistent westerly airflows.

The combination of these four factors has major influences on surface energy and water budgets. Unlike Australia, which has a water deficit over most of the continent and during most of the year, New Zealand's water budgets are generally positive. Latent heat has a greater influence than sensible heat, especially during daylight hours. The highly irregular terrain creates major spatial and temporal changes in the energy budget structure. For example, in the mountains, albedos can range from around 15% for alpine vegetation, to more than 60% for snow cover, over very small distances.

Synoptic circulation patterns

Figure A85 shows New Zealand's climatic circulation pattern in winter. The major band of anticyclonic movements extends to the north of the country. The westerlies, transporting fronts and depressions alternating with high-pressure systems, dominate. During this season the temperature gradient between Antarctica and locations further north is weakest, and therefore the strength of westerly circulation remains relatively weak.

In summer, as shown in Figure A87, the major belt of anticyclones now extends over most of the North Island. Here subsidence brings clear skies or extensive stratocumulus cloud sheets, over several days. The South Island remains under the influence of the westerlies. In spring and early summer the temperature gradient between Antarctica and the tropics, as well as the Australian continent, is strong. This is the season of strong winds and gales in the westerlies over southern New Zealand.

A more detailed evaluation of circulation in the New Zealand area reveals that three broad climate features provide the greatest influences:

1. *Troughs and depressions.* These are linked to cold frontal passages, occur regularly (approximately 40% of the time) during the year, although less frequently in fall. Depressions come from two main areas; those from the Southern Ocean are generally strong and move in a well-defined manner, guided by the westerly circulation. More infrequently, depressions form in the Tasman Sea. These can move slowly and erratically. Figure A91b shows a typical cold frontal passage. The isobaric pattern can be strongly deformed by the mountains. Frontal structure can be retarded or lost, and then re-formed once the system passes through the mountain area. Approximately half the fronts dissipate before reaching Cook Straight, the body of water between the two islands. Winds preceding the trough are generally northwesterly, and after frontal passage change to southwesterly. Higher elevations have a significant influence, causing wind direction deviations. Winds coming from a direction west of 220° can be prevented from reaching the eastern half of the country. The result is often heavy cloud and rain on the western sides of both islands, but partially cloudy to clear conditions to the east. Overall, precipitation is above average, but there is considerable spatial variation depending on geographical location.

   Troughs, depressions and fronts are usually steered by jet streams. In winter the jet stream is located between 25°S and 35°S, and can reach speeds of over 40 m s^{-1}. In summer the jet shifts to 45–50°S and is considerably weaker. There is considerable day-to-day variation.
2. *Anticyclonic or Blocking High.* Such conditions occur most frequently in summer and fall. Figure A91c presents an example. The frequency of blocking highs in this location is the highest in the southern hemisphere, and is linked to a split in the jet stream. Most frequently, blocking highs occur just to the east of New Zealand, and extend their influence over most of the country. They bring warmer temperatures than average over most of the country, higher precipitation to the northeast and lower precipitation to the southwest.

   Blocking highs bring settled weather, with light winds and mainly clear or partially cloudy skies. This encourages more local airflows to develop, such as sea breezes and katabatic winds (see discussion below). Fog can be prevalent inland.
3. Strong *zonal circulation* to the south with an anticyclone to the north is the third circulation regime. Figure A91d provides an example. This pattern creates drier and warmer than average conditions to the north, but higher rainfall to the

Table A48 Circulation periods affecting New Zealand climate during the twentieth century and impacts (after Salinger and Mullan, 1999; Salinger and Griffiths, 2001)

Period	Circulation	Temperature	Rainfall
1930–1950	More S to SW airflows	Lower over most of country; fewer days >25°C except NE North Island	Wetter to NE of South Island; drier in N and W of South Island
1951–1975	More E and NE airflow (higher frequency of blocking highs)	Higher over most of country; more days >25°C	Wetter in north of North Island; drier to SE of South Island
1976–1994	More W to SW airflows (more ENSO events)	Little change on average; fewer days >25°C except NE North Island	Wetter over South Island; drier in N of North Island

southwest. The enhanced westerlies to the south may result in somewhat milder conditions, especially in winter. This type of circulation regime is less frequent in summer than in other seasons of the year.

During the twentieth century there were changes in the circulation pattern which can be roughly classified into two-decade periods (Salinger and Mullan, 1999). Between 1930 and 1950 anomalously high frequencies of S and SW airflow occurred compared to the overall average. From 1951 to 1976 E and NE airflows were more frequent. From 1976 to 1998 the circulation reverted to more W and SW airflows. Table A48 summarizes the impacts of these three periods on New Zealand's climate.

Western Pacific regional influences on New Zealand circulation

There are three major interacting influences in the western Pacific that affect New Zealand's circulation pattern, and therefore climate variability (Kidson and Renwick, 2002). The enhancement of convection in the tropics in locations around the dateline decreases frequency of blocking and enhances zonal circulation. If convection is enhanced over the Indonesian area, blocking frequency near New Zealand is also enhanced, and zonal circulation reduced. The frequency and movements of troughs and depressions are not significantly affected.

Shifts in the location of the South Pacific Convergence Zone (SPCZ) affect the precipitation regime over New Zealand (Sturman and Tapper, 1996). When the SPCZ shifts eastward, circulation leading to drier conditions occurs over most of New Zealand except for the W and SW, where enhanced westerlies can bring more precipitation. A westward shift in the SPCZ creates the opposite effect, enhancing precipitation over most of the country except the W and SW coasts. These variations can be subtle and difficult to detect.

Both the strength and location of convection, and the location of the SPCZ, depend strongly on the Southern Oscillation, and whether an El Niño (ENSO) or La Niña (LNSO) event is occurring (Griffiths et al., 2003). During ENSO the SPCZ is shifted toward the NE, and convection is enhanced near the dateline. ENSO encourages high pressure with drought conditions in the north, with a stronger winter anticyclone. Enhanced meridional circulation leads to anomalous strength and frequency of southerly changes. During LNSO the SPCZ is shifted toward the SW, and convection is enhanced over the Indonesia area. Zonal circulation is enhanced, creating more rapidly moving troughs and depressions. NE airflow occurs at the expense of westerlies.

Local circulations

The interaction of the mountain terrain with synoptic circulation can create significant local airflows that affect New Zealand climate. The mountains both block airflow from more westerly sources and act to channel the airflow. The result is often a Foehn wind, which blows over the eastern parts of the country, creating warm dry conditions (Sturman and Tapper, 1996). On South Island a local name for this wind is the "Canterbury Northwester". Foehn winds are strong and gusty downslope winds from the lee of the mountain ranges, which warm through adiabatic compression. They often occur just before a cold frontal passage. Their strength and location depend on the atmospheric conditions to the windward of the mountain ranges, especially the vertical structure of the atmosphere. Foehn winds can create desiccation, very high temperatures, and damage to buildings, livestock and crops.

The Cook Straight acts a wind tunnel to encourage strong and gusty local wind passage from west to east of the country. These winds can recurve quite sharply, creating NE airflow on the E side of South Island.

Higher terrain can also create katabatic winds overnight over much of the eastern parts of New Zealand, when the synoptic situation is dominated by high pressure. The irregularity of the terrain creates complex downslope airflows, which eventually spill out over the glaciers, river valleys and plains. Low-level temperature inversions are common, especially in the winter, trapping air pollutants. A good example is wood smoke from home heating in the winter atmosphere in Christchurch, which creates highly elevated concentrations of fine particulate matter overnight.

Despite the narrowness of the islands, sea breezes occur on all coasts, especially in the summer. While these create some welcome relief from warm temperatures, their penetration inland is very much dependent on the terrain. Over very narrow areas, such as the very north of North Island, and in Auckland, sea breezes from both the Pacific Ocean and Tasman Sea can meet and interact together. Sea breeze depth ranges from 200 to 2000 m, and wind speeds can reach $15\,m\,s^{-1}$. They normally start in late morning and can extend into late evening (Sturman and Tapper, 1996).

Climatic elements (see Table A49)

The circulation variations over New Zealand, associated with changes affecting the circulation of the southwest Pacific region, significantly influence the temperature and precipitation distributions from year to year.

Temperature

Figure A92a shows the annual average temperature distribution. In summer the average temperatures range from about 18°C along the north coast of North Island to 14°C along the south coast of South Island. Particularly in South Island, the isotherm distribution is very strongly influenced by the terrain. Winter average temperatures range from 11°C in the very north of North Island to 4°C in the higher elevations below 45° latitude. Table A48 lists general changes from this average pattern as circulation periods change.

During ENSO periods the temperatures tend to be cooler over most of the country, affected by the increases in SW airflow. North Island is affected more strongly. Seasonally, this influence is weakest in summer (Kidson and Renwick, 2002). During LNSO periods the temperatures are generally milder in all areas, although the impact is less consistent on South Island. The S and W coasts are often cooler, associated with the stronger SW winds. Correlations between the South Oscillation and temperatures over New Zealand can reach 0.6 in the northern part of North Island, falling to below 0.4 along the south coast of the country and are significant.

Since 1950 the average temperatures over New Zealand have increased by about 0.5°C, in line with global increases

Table A49 Mean climatic data for selected New Zealand cities, January and July

City (Lat./long.)	Alt. (m)	Years of data	Max. temp. (°C)	Min. temp. (°C)	Mean temp. (°C)	Relative humidity 0900 (%)	Precipitation (mm)	Frost days	Daily sunshine (h)	Solar energy (MJ/m^2 per day)
Auckland (36.9°S/174.7°E)	41	25								
January			23.3	15.3	9.3	77.1	75	0	229	23.1
July			14.5	7.1	10.8	88.5	146	4	140	7.9
Wellington (41.3°S/174.8°E)	125	30								
January			20.3	13.8	16.9	80.3	72	0	246	23.6
July			11.4	6.3	7.5	86.3	136	3	117	5.7
Christchurch (43.5°S/172.6°E)	7	26								
January			22.5	12.2	17.4	72.9	42	0	230	21.9
July			11.3	1.9	6.6	87.3	79	16	124	5.1
Dunedin (45.9°S/170.5°E)	2	26								
January			18.9	11.5	15.2	73.1	72	0	178	18.5
July			9.8	3.2	6.5	80.2	69	16	101	4.5
Invercargill (46.5°S/168.3°E)	44	23								
January			18.6	9.4	14.0	80.8	114	1	180	20.4
July			9.5	0.9	5.2	88.9	88	18	93	4.3

Data from www.niwa.co.nz.

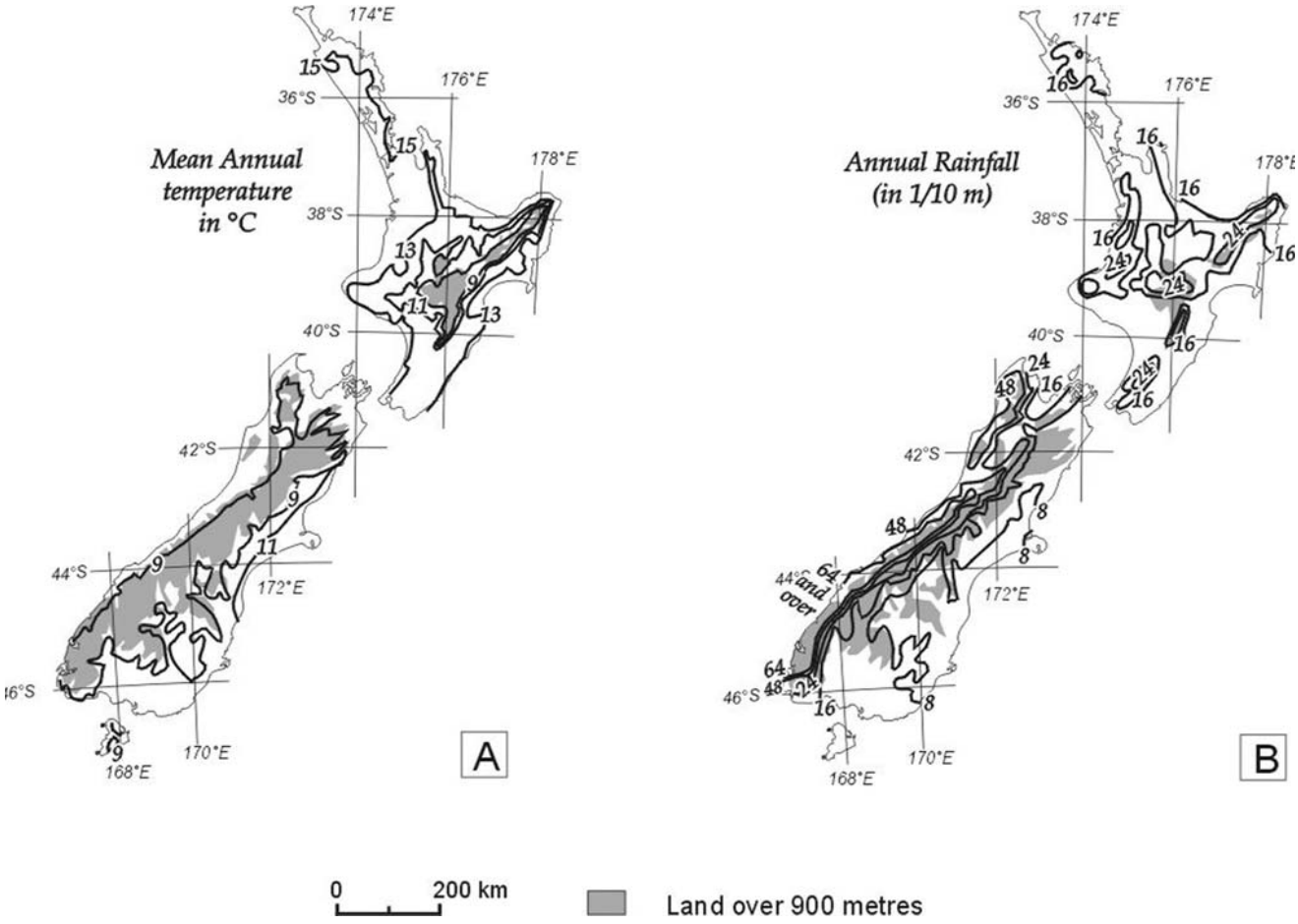

Figure A92 (**a**) New Zealand average yearly temperature distribution (°C); (**b**) New Zealand average yearly rainfall (cm divided by 10) (after Kirkpatrick, 1999).

associated with **greenhouse warming** (Salinger and Griffiths, 2001). There is little evidence of change in maximum temperatures or extremes, but minimum temperatures have increased significantly. There has been a decrease in the frequency of extremely cold nights. Between 1976 and 1998 the number of days with frost was lower by an average five to 15 in each year, compared to earlier periods.

Precipitation

The precipitation distribution pattern over New Zealand is highly irregular (Figure A92b), mainly due to terrain influences. Precipitation can range from more that 12 000 mm y^{-1} on the mountain tops of South Island to less than 600 mm y^{-1} on the eastern plains, for example the Canterbury area. Particularly on South Island, snow is an important component, covering 35% of the area on average but with high variability from year to year.

The greatest source of rainfall is fronts and troughs, particularly if they are associated with cold pools of air in the mid-to-upper troposphere. These can bring severe storms and create very heavy rain. Such storms are more likely to occur in winter and spring than in summer.

Overall, increased rainfall on a seasonal or yearly basis is associated with a higher frequency of N airflows, and thus linked to LNSO. Under this pattern rainfall to the S and W is often reduced, associated with weaker westerly circulation. This varies, depending on the time of year and the strength of the LNSO event.

ENSO periods bring drier weather to the N and E, and, compared to Australia, occasional much shorter periods of drought. Droughts rarely last more than 3 weeks. Increased westerlies during this period bring higher rainfall than average to the W and S coasts of especially South Island. The SOI does not correlate significantly with rainfall over New Zealand (TPE, 2001).

Changes in rainfall associated with the major changes in circulation in 1950 and 1976 are less well defined than for temperature (Salinger and Griffiths, 2001). The eastern part of South Island and the central area in North Island show significant decreases, by 15–25%. Increases occur on the south and west sides of both islands. Otherwise, there are no significant changes in rainfall distributions. The length of dry spells over New Zealand has been reduced by 1.5 to 4.5 days since 1950.

Table A50 Extreme weather events in New Zealand

Weather event	Location	Period	Value
Rainfall (mm)			
Hourly Total	Whenuapai	16 Feb 1966	107
Daily Total	Colliers Creek (S.I.)	21–22 Jan 1994	682
Monthly Total	Cropp River (S.I.)	Dec 1995	2927
Annual Total	Cropp River (S.I.)	1998	16617
Lowest Annual Total	Alexandra (S.I.)	Nov 1963–Oct 1964	167
Temperature (°C)			
Highest Maximum (N.I.)	Ruatoria	7 Feb 1973	39.2
Highest Maximum (S.I)	Rangiora & Jordan	7 Feb 1973	42.4
Lowest Minimum (N.I.)	Chateau Tongariro	7 Jul 1937	−13.6
Lowest Minimum (S.I.)	Ophir	3 Jul 1995	−21.6
Wind Gusts (km/h)			
Highest, North Island	Hawkins Hill	6 Nov 1959	248
Lowest, South Island	Mt John	18 Apr 1970	250

Data from http://www.metservice.co.nz
N.I. – North Island; S.I. – South Island.

Other climate elements

Thunderstorms are most often linked with fronts and troughs, and are higher in frequency on the west side of the islands, associated with orographic forcing. On the east coast of the islands, diurnal variations are typically a maximum in the afternoon and early evening, associated with a summertime peak in frequency and a thermal (convective) origin. On the west coast a higher frequency occurs at night, with an erratic seasonality pattern. Here wintertime thunderstorms occur more regularly, associated with friction and orographic effects. Along a north–south transect through the center of both islands, thunderstorm frequencies peak in the afternoon and early evening, but a secondary peak overnight is evident.

Hail frequencies increase from north to south, associated with the deep convection in cold fronts and troughs. New Zealand has approximately 25 tornadoes per year. North Island has an approximately three times higher frequency than South Island. Most tornadoes are relatively small by world standards, and are more frequent in the afternoon. Wind speeds can reach 190 km/h (Sturman and Tapper, 1996).

Tropical cyclones affect New Zealand rarely, creating strong winds, and heavy rain can occur on the northern and northeastern parts of North Island.

Table A50 lists extreme weather events for New Zealand. The maximum temperatures for both North and South Island are associated with a strong Foehn event, which occurred just before a cold frontal passage. Subsequently, the temperature then rapidly dropped to around 22°C. The lowest minimum temperatures occurred in snowfield stations in the winter. Short-term, high-rainfall events are associated with severe storms, and longer-term records with the higher altitudes on the western slopes of South Island mountain ranges. The lowest annual rainfall occurs at Alexandra on South Island, in the rainshadow east of the mountain ranges. In comparison with Australia (Table A45), New Zealand extremes show higher rainfall amounts but lower maximum and higher minimum temperatures.

By global standards New Zealand is basically one Köppen climate type, Cf (warm temperate climate with sufficient precipitation during all months). On a more detailed regional scale, however, a simplified climate classification of New Zealand produces eight categories, as shown in Figure A93.

Near-future climate change in Australia and New Zealand

The climate is varying continuously, and there are concerns about near-future changes associated with greenhouse warming in Australia and New Zealand. A series of reports focusing on the results of meteorological network measurements in both countries, and global and regional climate modeling, suggest the following scenario is likely for Australia and New Zealand (www.dar.csiro.com; www.niwa.co.nz).

Higher temperatures in general across Australia are probable, 0.4–2.0°C by 2030 and 1–6°C by 2070. The extra heat capacity of the oceans will delay and minimize warming along the coast. Most of the change will most likely occur in the minimum temperature, decreasing the overall daily temperature range. Evidence that this has already been occurring comes from Queensland (Lough, 1995) and other parts of the country (Bureau of Meteorology 2003). Warmer minimum temperatures would decrease the number of days below 0°C (by up to six per year) and less snow cover would exist. However, an increase in the number of extremely hot days in summer is expected, particularly in the desert areas of Western Australia.

Rainfall zones are likely to shift southwards, leading to lower rainfall in the south and east, especially in winter and spring, but higher rainfall in summer. Winter rainfall may increase slightly in central Australia, but decrease or remain the same in most other parts of the country. There has been a downward trend in rainfall in the SW since the mid-1960s (Allen and Haylock, 1993), which may continue. The climate record already shows an increase in Australian cloud cover during this century (Jones, 1991). There may be greater frequencies of high-rainfall events, and decreased numbers of low-rainfall events, as well as increased frequencies of drought, bushfires, and fine weather (Sturman and Tapper, 1996). Potential

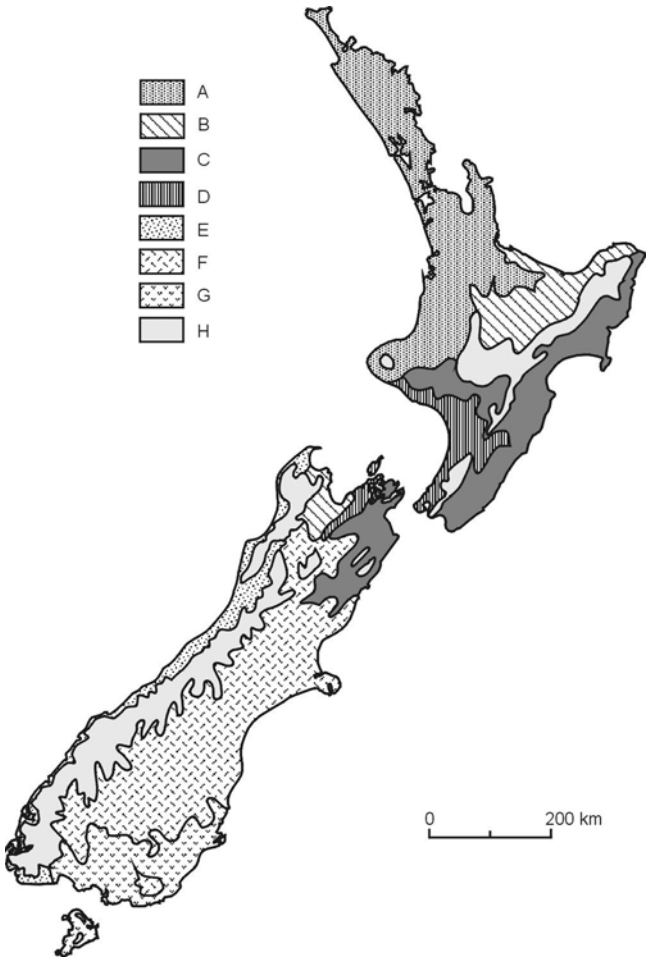

Figure A93 Simplified climate classification for New Zealand (modified from Sturman and Tapper, 1996). **A**, mild winter, warm moist summers, annual rainfall 1000–2500 mm, winter rainfall maximum, prevailing SW winds, occasional storms from E or NE. **B**, annual rainfall 1000–2000 mm, winter maximum, mild winters (but frequent frost), very warm summers, heavy rain from N or NE. **C**, very warm summers (strong Foehn effect), cool to moderate winters, annual rainfall 600–1500 mm (heavier in isolated places), winter maximum, lower and more unreliable summer rain. **D**, winds dominant from W and NW, frequent gales throughout year, annual rainfall 900–2000 mm, cooler temperatures. **E**, cool annual temperatures, range is small, prevailing SW winds, strong mountain influence on rainfall distribution (increase with altitude). **F**, cool winters, warm summers, frequent frosts, occasional snow (especially inland), annual rainfall 500–1500 mm, NE winds prevail along coast, NW winds inland. **G**, cool winters, warm summers, annual rainfall 500–1300 mm, slight winter maximum. **H**, extreme rainfall variations in mountains, cool to cold temperatures.

evaporation will increase. A greater intensity in extreme rainfall events and tropical cyclones is expected.

For New Zealand, the summer increase in temperature by the latter two decades of the 21st century may range from 1°C in the S to 1.8°C in the N. Winter increases are slightly higher, ranging from 1.6°C in the S to 2.2°C in the N. Model results suggest decreases in precipitation of around 5% on the east coast of both islands, and an increase of up to 15% on the west coasts. Winter precipitation may change quite dramatically, with reductions of 10–15% on the east coasts and increases of more than 30% in the mountains of the South Island. These changes reflect the increasing frequency and strength of SW and W airflows.

Readers are referred to the following Bibliography for further information on the climate of Australia and New Zealand.

Howard A. Bridgman

Bibliography

Abbs, D.J., and Physick, W.L., 1992. Sea-breeze observations and modelling, *Australian Meteorological Magazine*, **41**: 7–20.

Allen, R.J., 1988. El Niño Southern Oscillation influences in the Australasian region. *Progress in Physical Geography*, **12**: 313–348.

Allen, R.J., and Haylock, M.R., 1993. Circulation features associated with winter rainfall decrease in southwestern Australia. *Journal of Climate*, **6**: 1356–1367.

Baines, P.G., 1990. What's interesting and different about Australian meteorology?, *Australian Meteorological Magazine*, **38**: 123–146.

Bridgman, H.A., 1998. Australia's Climate and Water Resources. In Herschy, R., ed., *Encyclopaedia of Hydrology and Water Resources*. London: Chapman & Hall, pp. 98–109.

Bureau of Meteorology, 1988a. *Climatic Atlas of Australia*. Canberra: Department of Administrative Services, 67 pp.

Bureau of Meteorology, 1988b. *Climatic Averages, Australia*. Brisbane: Watson Ferguson.

Bureau of Meteorology, 1989. *Climate of Australia*. Canberra, Australian Government Publishing Service.

Bureau of Meteorology, 2003. *The Greenhouse Effect and Climate Change*. Melbourne: Commonwealth Bureau of Meteorology, Melbourne.

Castles, I., 1995. *Year Book Australia 1995*. Canberra: Australian Bureau of Statistics.

Collis, K., and Whitaker, R., 1996. *The Australian Weather Book*. Sydney: National Book Distributors.

Cook, G., and Heedegen, R., 2001, Spatial variation in the duration of the rainy season in monsoonal Australia, *International Journal of Climatology*, **21**: 1723–1732.

Drosdowsky, W., and Williams, M., 1991. The Southern Oscillation in the Australian region. Part I: anomalies at the extremes of the oscillation. *Journal of Climate*, **4**: 619–638.

Gentilli, J., 1971. Climates of Australia and New Zealand. In Landsberg, H., ed., *World Survey of Climatology*. Amsterdam: Elsevier.

Gentilli, J., 1972. *Australian Climatic Patterns*, Adelaide: Thomas Nelson.

Griffiths, G., Salinger, M., and Leleu, I., 2003. Trends in extreme daily rainfall across the South Pacific and relationship to the South Pacific Convergence Zone. *International Journal of Climatology* **23**: 847–869.

Haylock, M., and Nicholls, N., 2000. Trends in extreme rainfall indices for an updated high quality data set for Australia, 1910–1998. *International Journal of Climatology*, **20**: 1533–1542.

Hess, G.D., and Spillane, K.T., 1990. Characteristics of dust devils in Australia. *Journal of Applied Meteorology*, **29**: 498–507.

Hobbs, J., 1998. Present climates of Australia and New Zealand. In Hobbs, J., Lindesay, J., and Bridgman, H., eds., *Climates of the Southern Hemisphere Continents Past Present and Future*. Chichester: Wiley, pp. 63–106.

Holland, G.J., Lynch, A.H., and Leske, L.M., 1987. Australian east-coast cyclones. Part I. Synoptic overview and case study. *Monthly Weather Review*, **115**: 3024–3036.

Jones, P.A., 1991. Historical records of cloud cover and climate for Australia. *Australian Meteorological Magazine*, **39**: 181–190.

Joseph, P.V., Liebmann, B., and Hindon, H.H., 1991. Interannual variability of the Australian summer monsoon onset: possible influences of the Indian summer monsoon and El Niño, *Journal of Climate*, **4**: 529–538.

Kidson, J., 2000. An analysis of New Zealnad synoptic types and their use in defining weather regimes. *International Journal of Climatology*, **20**: 299–316.
Kidson, J. and Renwick, J., 2002. Patterns of convection in the tropical Pacific and their influence on New Zealand weather. *International Journal of Climatology*, **22**: 151–174.
Kirkpatrick, R., 1999. *Contemporary Atlas of New Zealand*. Auckland: Bateman.
Kuleshov, Y., deHoedt, G., Wright, W., and Brewster, A., 2002. Thunderstorm distribution and frequency in Australia. *Australian Meteorological Magazine*, **51**: 145–154.
Lough, J.M., 1995. Temperature variations in a tropical–subtropical environment: Queensland, Australia, 1910–1987. *International Journal of Climatology*, **15**: 77–96.
Love, G., and Downey, A., 1986. A prediction of bushfires in central Australia. *Australian Meteorological Magazine*, **34**: 93–102.
McInnis, K.L., 1993. Australian southerly busters. Part III: the physical mechanism and synoptic conditions contributing to development, *Monthly Weather Review*, **121**: 3261–3281.
Reeder, M.J., and Smith, R.K., 1992. Australian spring and summer cold fronts. *Australian Meteorological Magazine*, **41**: 101–123.
Salinger, M. and Griffiths, G., 2001. Trends in New Zealand daily temperature and rainfall extremes. *International Journal of Climatology*, **21**: 1437–1452.
Salinger, M., and Mullan, A., 1999. New Zealand climate: temperature and precipitation variations and their links with atmospheric circulation, 1930–1984. *International Journal of Climatology*, **19**: 1049–1072.
Salinger, M., Renwick, J., and Mullan, A., 2001, Interdecadal Pacific Oscillation and South Pacific climate. *International Journal of Climatology*, **21**: 1705–1723.
Smith, I., McIntosh, P., Ansell, T., Reason, C., and McInnes, K., 2000. Southwest Western Australian winter rainfall and its association with Indian Ocean climate variability. *International Journal of Climatology*, **20**: 1913–1930.
Smith, R.K., Reeder, M.J., Tapper, N.J., and Christie, D.R., 1995. Central Australian cold fronts, *Monthly Weather Review*, **123**: 16–28.
Speer, M., and Geerts, B., 1994. A synoptic-mesoalpha-scale climatology of flash-floods in the Sydney metropolitan area. *Australian Meteorological Magazine*, **43**: 87–103.
Stern, H., deHoedt, G., and Ernst, J., 2000. Objective classification of Australian climates. *Australian Meteorological Magazine*, **49**: 87–98.
Sturman, A.P., and Tapper, N.J., 1996. *The Weather and Climate of Australia and New Zealand*. Melbourne: Oxford University Press.
Suppiah, R., 1992. The Australian summer monsoon: a review. *Progress in Physical Geography*, **16**: 283–318.
Tapper, N., and Hurry, L., 1993. *Australia's Weather Patterns: An Introductory Guide*. Mt Waverly (Victoria): Dellastra.
TPE, 2001. (Sturman, A., and Spronken-Smith, R., eds.) *The Physical Environment A New Zealand Perspective*. Melbourne: Oxford University Press.

Cross-references

AirMass Climatology
Climate Classification
Drought
El Niño
Southern Oscillation
Synoptic Climatology
Vegetation and Climate

Web sites of interest

Australian Bureau of Meteorology, www.bom.gov.au
New Zealand Meteorological Bureau, www.metservice.co.nz
Division of Atmospheric Research, Commonwealth Scientific and Industrial Research Organisation, Australia, www.dar.csiro.au
National Institute of Water and Atmospheric Research (NIWA), www.niwa.co.nz/atmos/

AZORES (BERMUDA) HIGH

This is one of seven regions of year-round relatively high pressure where barometric values are typically higher than adjacent areas and where the air is drier, skies clearer, and surface wind speeds slower. The other six regions are the Siberian (Asiatic), Pacific (Hawaiian), and North American (Canadian) Highs in the northern hemisphere, and the Indian Ocean, South Atlantic (St Helena), and South Pacific Highs in the southern hemisphere.

The Azores (or Bermuda) High is a large subtropical anticyclone centered between 25°N and 35°N in the Atlantic Ocean. The high often extends westward as far as Bermuda; when this occurs it is known in North America as the Bermuda High. It extends to great elevations, with deep tropical easterlies on its equatorward side and midlatitude westerlies on its poleward side. This very persistent and quasistationary feature of the atmosphere's circulation is elongated in an east–west direction, with its center of highest pressure located over the eastern portion of the subtropical Atlantic in the general vicinity of the Azores. It is most pronounced in the summer, when land–water temperature contrasts are substantial, and has an extreme summertime position of about 34–38°N. The expanding high often gets large enough to affect hurricane trajectories, moving the storms westward toward the West Indies and the southeastern United States. In winter it is less pronounced and is located at somewhat lower latitudes.

Within the heart of the Azores High, winds are light and variable, and the high is characterized by divergence, subsidence, and fair weather. However, there is a marked contrast between the eastern and western portions of the high. The eastern side is characterized by strong subsidence and a dry climate, whereas the western side has little or no subsidence and a wetter climate. This contrast corresponds to the moisture and stability differences between the east and west sides of the oceanic trade winds.

The cause of this contrast is not clear. The longer trajectory of air over the warm waters of the subtropical Atlantic contributes to a more humid west-side climate. This circulation pattern results in hot and humid weather for the central and eastern United States in the summer. The ultimate cause is probably related to the inherent distribution of continents and oceans. Large east–west circulations exist in heating between subtropical continents and oceans. The strongly subsiding eastern portions of the Azores High coincide with the sinking branches of these east–west cells, whereas the western portion of the high is near the rising branch of the circulation cell.

The relative strength of the high is used as one variable to determine the North Atlantic Oscillation and its derived index.

Robert M. Hordon and Mark Binkley

Bibliography

Ahrens, C.D., 2003. *Meteorology Today: An Introduction to Weather, Climate, and the Environment*, 7th edn. Brooks/Cole (Thomson Learning).

Curry, J.A., and Webster, P.J., 1999. *Thermodynamics of Atmospheres and Oceans*. San Diego, CA: Academic Press.
Hartmann, D.L., 1994. *Global Physical Climatology.* San Diego, CA: Academic Press.
Lutgens, F.K., and Tarbuck, E.J., 2004. *The Atmosphere: An Introduction to Meteorology*, 9th edn. Upper Saddle River, New Jersey: Pearson Prentice Hall.
Nese, J.M., and Grenci, L.M., 1998. *A World of Weather: fundamentals of meteorology*, 2nd edn. Dubuque, IO: Kendall/Hunt.
Oliver, J.E., and Hidore, J.J., 2002. *Climatology: An Atmospheric Science*, 2nd edn. Upper Saddle River, New Jersey: Pearson Prentice Hall.
Robinson, P.J., and Henderson-Sellers, A., 1999. *Contemporary Climatology*, 2nd edn. Harlow: Longman.
Wallace, J.M., and Hobbs, P.V., 1997. *Atmospheric Science: an introductory survey*. San Diego, CA: Academic Press.

Cross-references

Airmass Climatology
Atmospheric Circulation, Global
Centers of Action
North Atlantic Oscillation
Oscillations
Pacific (Hawaiian) High
Zonal Index